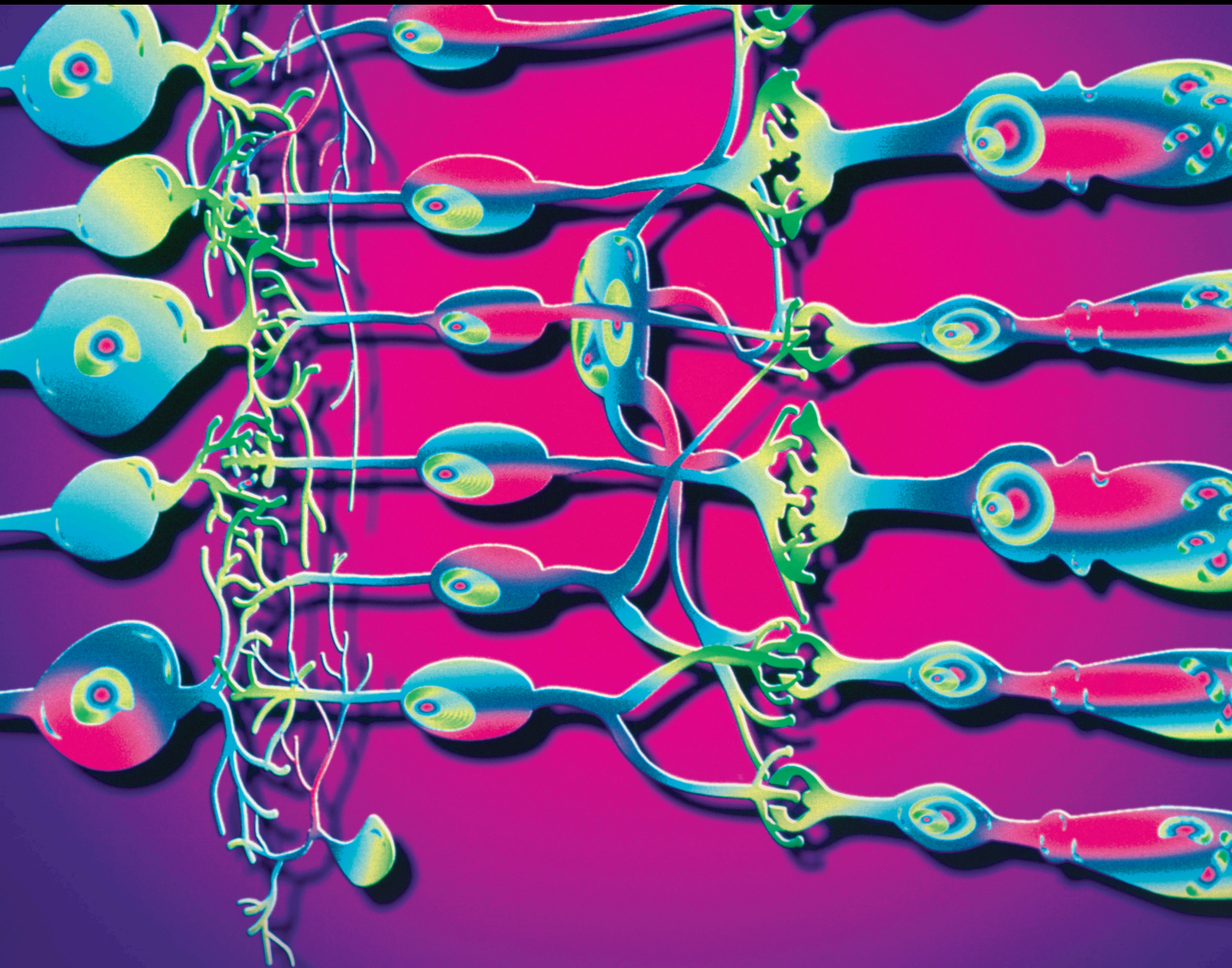


Advances and Clinical Applications of Anterior Segment Imaging Techniques 2020

Lead Guest Editor: Sang Beom Han

Guest Editors: Jodhbir S. Mehta, Yu-chi Liu, and Karim Mohamed-Noriega





**Advances and Clinical Applications of Anterior
Segment Imaging Techniques 2020**

Journal of Ophthalmology

**Advances and Clinical Applications of
Anterior Segment Imaging Techniques
2020**

Lead Guest Editor: Sang Beom Han

Guest Editors: Jodhbir S. Mehta, Yu-chi Liu, and
Karim Mohamed-Noriega



Copyright © 2021 Hindawi Limited. All rights reserved.

This is a special issue published in "Journal of Ophthalmology." All articles are open access articles distributed under the Creative Commons Attribution License, which permits unrestricted use, distribution, and reproduction in any medium, provided the original work is properly cited.

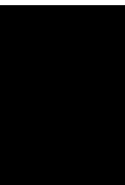
Chief Editor

Steven F. Abcouwer, USA

Editorial Board

Steven F. Abcouwer, USA
Monica L. Acosta, New Zealand
Aniruddha Agarwal, USA
Hamid Ahmadi, Iran
Hee B. Ahn, Republic of Korea
Siamak Ansari-Shahrezaei, Austria
Taras Ardan, Czech Republic
Francisco Arnalich-Montiel, Spain
Kofi Asiedu, Ghana
Takayuki Baba, Japan
Stefano Baiocchi, Italy
Paul Baird, Australia
Angelo Balestrazzi, Italy
Antonio Benito, Spain
Mehmet Borazan, Prof. MD, Turkey
Vincent M. Borderie, France
Lorenza Brescia, Italy
Carlo Cagini, Italy
Gonzalo Carracedo, Spain
Arturo Carta, Italy
Alejandro Cerviño, Spain
Colin Clement, Australia
Inés Contreras, Spain
Miguel Cordero-Coma, Spain
Ciro Costagliola, Italy
Roberto dell'Omo, Italy
Priyanka P. Doctor, India
Manuel S. Falcão, Portugal
Bao Jian Fan, USA
Paulo Fernandes, Portugal
Giulio Ferrari, Italy
Michele Figus, Italy
Paolo Fogagnolo, Italy
Maria-Andreea Gamulescu, Germany
Santiago García-Lázaro, Spain
Zisis Gatziofias, Switzerland
Jose M. González-Meijome, Portugal
Vlassis Grigoropoulos, Greece
Carl Peter Herbort, Switzerland
Shigeru Honda, Japan
Pierluigi Iacono, Italy
Takeshi Iwase, Japan
Vishal Jhanji, USA
Takashi Kojima, Japan

Naoshi Kondo, Japan
Toshihide Kurihara, Japan
Sentaro Kusuhara, Japan
George Kymionis, Greece
Prof. Dr. Achim Langenbucher, Germany
Achim Langenbucher, Germany
Van C. Lansingh, Mexico
Paolo Lanzetta, Italy
Theodore Leng, USA
Hong LIANG, France
Su-Ho Lim, Republic of Korea
Marco Lombardo, Italy
Antonio Longo, Italy
Norberto López-Gil, Spain
Andrea Lucisano, Italy
Angel Luis Ortega, Spain
Marco Lupidi, Italy
Tamer A. Macky, Egypt
Edward Manche, USA
Leonardo Mastropasqua, Italy
Cosimo Mazzotta, Italy
Colm McAlinden, United Kingdom
Alessandro Meduri, Italy
Enrique Mencía-Gutiérrez, Spain
Marcel Menke, Switzerland
Carsten H. Meyer, Switzerland
Elad Moisseiev, Israel
Mário Monteiro, Brazil
Paolo Mora, Italy
Majid M. Moshirfar, USA
Marco Mura, USA
Jean-Claude Mwanza, USA
Carlo Nucci, Italy
Akio Oishi, Japan
Giovanni William Oliverio, Italy
Neville Osborne, United Kingdom
Ji-jing Pang, USA
Mohit Parekh, United Kingdom
Sudhir Patel, Scotland
Enrico Peiretti, Italy
Marco Pellegrini, Italy
Grazia Pertile, Italy
David P. Piñero, Spain
Eli Pradhan, Nepal



Eli Pradhan, Nepal
Antonio Queiros, Portugal
Miguel Rechichi, Italy
Anthony G. Robson, United Kingdom
Mario R. Romano, Italy
Marta Sacchetti, Italy
Wataru Saito, Japan
Juan A. Sanchis-Gimeno, Spain
Dirk Sandner, Germany
Ana Raquel Santiago, Portugal
Rehman Siddiqui, Pakistan
Bartosz Sikorski, Poland
Shivalingappa K. Swamynathan, USA
Nóra Szentmáry, Hungary
Masaru Takeuchi, Japan
Suphi Taneri, Germany
Christoph Tappeiner, Switzerland
Stephen Charn Beng Teoh, Singapore
Miguel Teus, Spain
Biju B. Thomas, USA
Oren Tomkins-Netzer, United Kingdom
Lisa Toto, Italy
Giacinto Triolo, Italy
Giacinto Triolo, Italy
Maurizio Uva, Italy
Manuel Vidal-Sanz, Spain
Paolo Vinciguerra, Italy
Tsutomu Yasukawa, Japan
Vicente Zanon-Moreno, Spain
Tomasz Zarnowski, Poland

Contents

Advances and Clinical Applications of Anterior Segment Imaging Techniques 2020

Sang Beom Han , Jodhbir S. Mehta , Yu-Chi Liu , and Karim Mohamed Noriega 
Editorial (2 pages), Article ID 9808071, Volume 2021 (2021)

Effect of Topical Brimonidine 0.15% on Conjunctival Injection after Strabismus Surgery in Children

Dong Hyun Kim , Hee Kyung Yang , Sang Beom Han , and Jeong-Min Hwang 
Research Article (5 pages), Article ID 5574194, Volume 2021 (2021)

Advances in Imaging Technology of Anterior Segment of the Eye

Sang Beom Han, Yu-Chi Liu, Karim Mohamed-Noriega, and Jodhbir S. Mehta 
Review Article (9 pages), Article ID 9539765, Volume 2021 (2021)

Comparison of the Stability of Two Intraocular Lenses in Primary Angle-Closure Glaucoma after Phacoemulsification

Chang Zhang, Meng Zhang , Bing Zhang , Shanhong Wang , and Yuhong Wang 
Research Article (5 pages), Article ID 9284245, Volume 2020 (2020)

Tear Lipid Layer Thickness in Children after Short-Term Overnight Orthokeratology Contact Lens Wear

Li Zeng , Zhi Chen , Dan Fu, Jiaqi Zhou , and Xingtao Zhou 
Research Article (9 pages), Article ID 3602653, Volume 2020 (2020)

Eyes of Aniso-Axial Length Individuals Share Generally Similar Corneal Biometrics with Normal Eyes in Cataract Population

Min Zhang , Tianhui Chen , Michael Deng , Jiahui Chen , Qinghe Jing , and Yongxiang Jiang 
Research Article (9 pages), Article ID 4760978, Volume 2020 (2020)

Keratoconus Diagnosis: Validation of a Novel Parameter Set Derived from IOP-Matched Scenario

Dan Lin , Lei Tian , Shu Zhang , Like Wang , Ying Jie , and Yongjin Zhou 
Research Article (6 pages), Article ID 6530279, Volume 2020 (2020)

Bleb Morphology Using Anterior-Segment Optical Coherence Tomography after Ahmed Glaucoma Valve Surgery with Tenon Capsule Resection

Fariad M. Wagdy 
Research Article (11 pages), Article ID 8386135, Volume 2020 (2020)

Assessment of Scleral and Conjunctival Thickness of the Eye after Ultrasound Ciliary Plasty

Bartłomiej Bolek , Adam Wylęgała, and Edward Wylęgała
Research Article (10 pages), Article ID 9659014, Volume 2020 (2020)

Intraoperative Optical Coherence Tomography Imaging in Corneal Surgery: A Literature Review and Proposal of Novel Applications

Hiroshi Eguchi , Fumika Hotta, Shunji Kusaka, and Yoshikazu Shimomura
Research Article (10 pages), Article ID 1497089, Volume 2020 (2020)

Intraoperative Optical Coherence Tomography Analysis of Clear Corneal Incision: Effect of the Lateral Stromal Hydration

Jiri Cendelin, Stepan Rusnak , and Lenka Hecova

Research Article (8 pages), Article ID 8490181, Volume 2020 (2020)

Function and Morphology of the Meibomian Glands Using a LipiView Interferometer in Rotating Shift Medical Staff

Jing Zhang , Zhengzheng Wu, Liangnan Sun, and Xin-hua Liu 

Research Article (6 pages), Article ID 3275143, Volume 2020 (2020)

Comparison of Different Types of Corneal Foreign Bodies Using Anterior Segment Optical Coherence Tomography: A Prospective Observational Study

Tao Wang, Lei Zhong, Shiyi Yin, Tiancheng Bao, Jiezheng Yang, Ting Wang, and Shiqi Ling 

Clinical Study (7 pages), Article ID 9108317, Volume 2020 (2020)

Objective Imaging Diagnostics for Dry Eye Disease

Sang Beom Han , Yu-Chi Liu , Karim Mohamed-Noriega , Louis Tong , and Jodhbir S. Mehta 

Review Article (11 pages), Article ID 3509064, Volume 2020 (2020)

Observation of Gonio Structures during Microhook Ab Interno Trabeculotomy Using a Novel Digital Microscope with Integrated Intraoperative Optical Coherence Tomography

Akiko Ishida, Kazunobu Sugihara, Tomoki Shirakami, Aika Tsutsui, Kaoru Manabe, and Masaki Tanito 

Research Article (5 pages), Article ID 9024241, Volume 2020 (2020)

The Effectiveness of Ultrasound Biomicroscopic and Anterior Segment Optical Coherence Tomography in the Assessment of Anterior Segment Tumors: Long-Term Follow-Up

Joanna Konopińska , Łukasz Lisowski , Ewa Wasiluk, Zofia Mariak , and Iwona Obuchowska 

Clinical Study (8 pages), Article ID 9053737, Volume 2020 (2020)

Endothelial Plaques as Sign of Hyphae Infiltration of Descemet's Membrane in Fungal Keratitis

Xiaolin Qi, Ting Liu, Man Du, and Hua Gao 

Research Article (6 pages), Article ID 6083854, Volume 2020 (2020)

Changes in Corneal Volume at Different Areas and Its Correlation with Corneal Biomechanics after SMILE and FS-LASIK Surgery

Pinghui Wei , George PM Cheng , Jiamei Zhang , Alex LK Ng , Tommy CY Chan , Vishal

Jhanji , and Yan Wang 

Research Article (7 pages), Article ID 1713979, Volume 2020 (2020)

Editorial

Advances and Clinical Applications of Anterior Segment Imaging Techniques 2020

Sang Beom Han ¹, **Jodhbir S. Mehta** ^{2,3,4}, **Yu-Chi Liu** ^{2,3,4}
and **Karim Mohamed Noriega** ⁵

¹Department of Ophthalmology, Kangwon National University School of Medicine, Kangwon National University Hospital, Chuncheon, Republic of Korea

²Singapore National Eye Centre, Singapore

³Singapore Eye Research Institute, Singapore

⁴Department of Ophthalmology, Yong Loo Lin School of Medicine, National University of Singapore, Singapore

⁵Department of Ophthalmology, University Hospital, Faculty of Medicine, Autonomous University of Nuevo Leon, Monterrey, Mexico

Correspondence should be addressed to Sang Beom Han; m.sangbeom.han@gmail.com

Received 19 July 2021; Accepted 19 July 2021; Published 26 August 2021

Copyright © 2021 Sang Beom Han et al. This is an open access article distributed under the Creative Commons Attribution License, which permits unrestricted use, distribution, and reproduction in any medium, provided the original work is properly cited.

The rapid advancement of anterior segment imaging technologies in recent years has allowed for precise visualization and accurate assessment of the anterior segment structures. Therefore, these devices have become necessary for better diagnosis and treatment of anterior segment disorders, i.e., corneal diseases, cataract, glaucoma, and disorders of the eyelid and lacrimal system.

As we have mentioned in the call for papers, the published manuscripts cover the topics of anterior segment imaging techniques including corneal topography, confocal microscopy, anterior segment optical coherence tomography (OCT), specular microscopy, and ultrasound biomicroscopy (UBM). In addition to the application of these anterior segment imaging devices in research as well as in the diagnosis and monitoring of anterior segment disorders, particular interest was also placed on novel technologies of anterior segment imaging and applications of artificial intelligence in anterior segment imaging. In this Special Issue, the authors contributed 14 original research papers and 3 review articles regarding newly developed technologies of anterior segment imaging and clinical application of novel imaging devices.

The authors have contributed their original research papers on various topics on anterior segment imaging, as follows: (1) Changes in Corneal Volume at Different Areas

and Its Correlation with Corneal Biomechanics after SMILE and FS-LASIK Surgery; (2) Endothelial Plaques as Sign of Hyphae Infiltration of Descemet's Membrane in Fungal Keratitis; (3) The Effectiveness of Ultrasound Biomicroscopic and Anterior Segment Optical Coherence Tomography in the Assessment of Anterior Segment Tumors: Long-Term Follow-Up; (4) Observation of Gonio Structures during Microhook Ab Interno Trabeculotomy Using a Novel Digital Microscope with Integrated Intraoperative Optical Coherence Tomography; (5) Comparison of Different Types of Corneal Foreign Bodies Using Anterior Segment Optical Coherence Tomography: A Prospective Observational Study; (6) Function and Morphology of the Meibomian Glands Using a LipiView Interferometer in Rotating Shift Medical Staff; (7) Intraoperative Optical Coherence Tomography Analysis of Clear Corneal Incision: Effect of the Lateral Stromal Hydration; (8) Assessment of Scleral and Conjunctival Thickness of the Eye after Ultrasound Ciliary Plasty; (9) Bleb Morphology Using Anterior-Segment Optical Coherence Tomography after Ahmed Glaucoma Valve Surgery with Tenon Capsule Resection; (10) Keratoconus Diagnosis: Validation of a Novel Parameter Set Derived from IOP-Matched Scenario; (11) Eyes of Aniso-Axial Length Individuals Share Generally Similar Corneal Biometrics with Normal Eyes in Cataract Population; (12)

Comparison of the Stability of Two Intraocular Lenses in Primary Angle-Closure Glaucoma after Phacoemulsification; (13) Tear Lipid Layer Thickness in Children after Short-Term Overnight Orthokeratology Contact Lens Wear; (14) Effect of Topical Brimonidine 0.15% on Conjunctival Injection after Strabismus Surgery in Children.

This Special Issue also includes review articles on the following topics: (1) Objective Imaging Diagnostics for Dry Eye Disease; (2) Intraoperative Optical Coherence Tomography Imaging in Corneal Surgery: A Literature Review and Proposal of Novel Applications; (3) Advances in Imaging Technology of the Anterior Segment of the Eye.

We hope these papers will provide readers with valuable clinical information on anterior segment imaging and new ideas for research on associated topics.

Conflicts of Interest

The Guest Editors declare that there are no conflicts of interest.

Acknowledgments

This work was supported by Bumsuk Academic Research Fund in 2020.

*Sang Beom Han
Jodhbir S. Mehta
Yu-Chi Liu
Karim Mohamed Noriega*

Research Article

Effect of Topical Brimonidine 0.15% on Conjunctival Injection after Strabismus Surgery in Children

Dong Hyun Kim ¹, Hee Kyung Yang ¹, Sang Beom Han ², and Jeong-Min Hwang ¹

¹Department of Ophthalmology, Seoul National University College of Medicine, Seoul National University Bundang Hospital, Seongnam, Republic of Korea

²Department of Ophthalmology, Kangwon National University College of Medicine, Kangwon National University Hospital, Chuncheon, Kangwon, Republic of Korea

Correspondence should be addressed to Sang Beom Han; m.sangbeom.han@gmail.com and Jeong-Min Hwang; hjm@snu.ac.kr

Received 8 January 2021; Revised 7 April 2021; Accepted 13 April 2021; Published 4 May 2021

Academic Editor: Alessandro Meduri

Copyright © 2021 Dong Hyun Kim et al. This is an open access article distributed under the Creative Commons Attribution License, which permits unrestricted use, distribution, and reproduction in any medium, provided the original work is properly cited.

Purpose. To investigate the effects of topical brimonidine 0.15% instillation on conjunctival injection after strabismus surgery in children. **Methods.** We retrospectively analyzed 63 Korean children who underwent strabismus surgery for intermittent exotropia. Patients received topical brimonidine 0.15% after surgery for up to 4 weeks. Conjunctival injection was objectively assessed using a software that automatically scored the region of interest from the image of the bulbar conjunctiva. Conjunctival injection scores were compared with those of the control group who were not prescribed topical brimonidine. **Results.** The mean scores of conjunctival injection after rectus muscle recession and resection were significantly lower in the brimonidine group than the controls at 4 weeks after surgery ($P = 0.008$ and 0.046 , respectively). There was no significant difference in intraocular pressure between the two groups. No adverse effects, such as dry mouth, fatigue/drowsiness, headache, sedation, hypotension, or bradycardia, were reported. **Conclusions.** Administration of topical brimonidine 0.15% after strabismus surgery is efficacious and safe in reducing postoperative conjunctival injection.

1. Introduction

Various complications may occur after strabismus surgery, including local issues such as conjunctival injection, scar formation, and inclusion cysts; however, severe problems such as cellulitis and endophthalmitis are rarely seen [1–3]. Conjunctival injection is by far one of the most common complications after strabismus surgery [2]. Although patients do not expect conjunctival injection to persist for a long time after surgery, it may cause anxiety, cosmetic problems, and disappointment, despite successful ocular alignment [4].

Brimonidine tartrate is a selective α_2 -adrenergic receptor agonist that has been widely used to lower intraocular pressure (IOP) [5, 6]. Alpha-adrenergic agonists bind to α -receptors on vascular smooth muscles and induce smooth muscle contraction and vasoconstriction [7]. Alpha-

adrenergic agonists have been widely used in the treatment of glaucoma because vasoconstriction limits blood flow to the ciliary muscle and reduces the production of aqueous humor [8]. As brimonidine affects vasoconstriction primarily via the α_2 -adrenergic receptor, it has been reported that the pre- and postoperative use of topical brimonidine can help reduce bleeding-related problems in ophthalmic surgery [9–11]. In addition, brimonidine has relatively lower systemic adverse effects than other vasoconstrictors such as phenylephrine, and the safety of brimonidine has been confirmed in children over 2 years of age [12].

A few studies have assessed the effect of prophylactic topical brimonidine in reducing intraoperative bleeding in strabismus surgery [13–15]. However, to the best of our knowledge, no studies have reported the effect of postoperative use of topical brimonidine in reducing conjunctival injection after surgery. Therefore, we performed this study to

evaluate the effect of brimonidine on conjunctival injection after strabismus surgery in children.

2. Methods

2.1. Patients. A retrospective study was performed on consecutive children between 7 and 12 years of age with exotropia who underwent unilateral lateral rectus recession with medial rectus resection (RR) by the same surgeon (J-M. H.). A limbal conjunctival incision was made in all operations, and all surgical incisions were repaired with a minimal number of sutures with absorbable 8-0 polyglactin sutures (8-0 Polysorb; Covidien, Mansfield, MA, USA). All patients underwent complete ophthalmological examination before surgery. Data were collected on demographics and clinical characteristics, including age, sex, preoperative angle of deviation, dosage of surgery, and cycloplegic refractive errors. Patients were excluded if they had other possible causes of inflammatory diseases of the anterior segment, including conjunctivitis, keratitis, and uveitis, a history of prior strabismus surgery, simultaneous oblique or vertical muscle surgery, simultaneous vertical transposition surgery, adjustable surgery, use of biodegradable collagen matrix implant, ocular disease other than strabismus, systemic disorders such as congenital anomalies, neurological disorders, and connective tissue disease, or if they did not comply with postoperative anterior segment photographs. This study was approved by the Institutional Review Board (IRB) of the Seoul National University Bundang Hospital.

After surgery, all patients received gatifloxacin 0.3% (Gatiflo; Handok, Inc., Chungbuk, Korea), topical fluorometholone 0.1% (Fluvin; Taejoon Pharmaceutical, Seoul, Korea), and topical bromfenac 0.1% (Bronuck; Taejoon Pharmaceutical, Seoul, Korea) for 4 weeks. In addition, patients who were prescribed topical brimonidine tartrate 0.15% (Alphagan P; Allergan, Inc., Irvine, CA, USA) twice a day for 4 weeks were defined as the brimonidine group. The control group was defined as those who did not receive topical brimonidine.

2.2. IOP Measurement. IOP was measured using noncontact tonometry (ICT-900, KOWA, Japan) 4 weeks after surgery. IOP measurements were repeated until three measurements differed by ≤ 1 mm Hg, and the average of these three readings was recorded.

2.3. Conjunctival Injection. Conjunctival injection was measured by an objective method using software that automatically scores the region of interest from the image of the bulbar conjunctiva [16–18]. A masked observer measured each anterior segment photograph of the conjunctiva using the contrast-limited adaptive histogram equalization algorithm, and the results were converted into numeric values ranging from 0 to 100 (Figure 1). The nasal and temporal quadrants of the conjunctiva were analyzed separately. Extensive subconjunctival hemorrhage was not included in the region of interest. Postoperative conjunctival injection scores were assessed at 4 weeks after surgery and

were calibrated as the amount of increase in numeric values compared with preoperative values.

2.4. Statistical Analysis. Statistical analysis was performed using SPSS version 22.0 for Windows (SPSS, Inc., Chicago). Independent t-test and chi-square test were used to compare the groups. Linear regression was used to analyze the relationship between conjunctival injection scores and age, cycloplegic refraction, angle of deviation, and surgical dosage. Statistical significance was set at $P < 0.05$. All continuous variables were reported as mean \pm standard deviation (range, min, and max) values.

3. Results

A total of 63 consecutive patients (36 boys and 27 girls) who underwent RR surgery were included in the study. The mean age was 9.1 ± 1.0 years (range, 7.6–11.8 years). A comparison of clinical characteristics and surgical details between the two groups showed no statistically significant differences (Table 1). No cases of postoperative infection or abnormal bleeding occurred. No known adverse effects of brimonidine were reported, including dry mouth, fatigue/drowsiness, headache, sedation, hypotension, or bradycardia [19, 20].

3.1. Conjunctival Injection. Figure 2 compares the differences in conjunctival injection scores between the two groups. The mean scores of postoperative conjunctival injection after rectus muscle recession and resection were significantly lower in the brimonidine group than the control group at 4 weeks after surgery ($P = 0.008$ and 0.046 , respectively). In linear regression analysis, no linear correlation was observed between the surgical dosage, age, axial length, or the degree of conjunctival injection.

3.2. Intraocular Pressure. The mean intraocular pressure at 4 weeks after surgery was 11.7 ± 3.3 (range, 7–20) mmHg in the brimonidine group and 12.4 ± 3.0 (range, 8–19) mmHg in the control group ($P = 0.418$).

4. Discussion

In this study, we evaluated the safety and efficacy of treatment with 0.15% brimonidine tartrate ophthalmic solution for reducing conjunctival injection after strabismus surgery in children. These data demonstrate that the postoperative administration of topical brimonidine 0.15% can significantly reduce conjunctival injection after strabismus surgery.

Conjunctival injection is an important cosmetic problem after strabismus surgery. Escardo-Paton and Harrad [4] reported that the median duration of conjunctival injection following surgery was approximately 10 weeks. In addition, a few patients had persistent postoperative conjunctival injection beyond 24 weeks. Although postoperative conjunctival injection does not cause severe ophthalmological problems, it may be a cosmetic concern and cause psychosocial stress that affects social activities over several

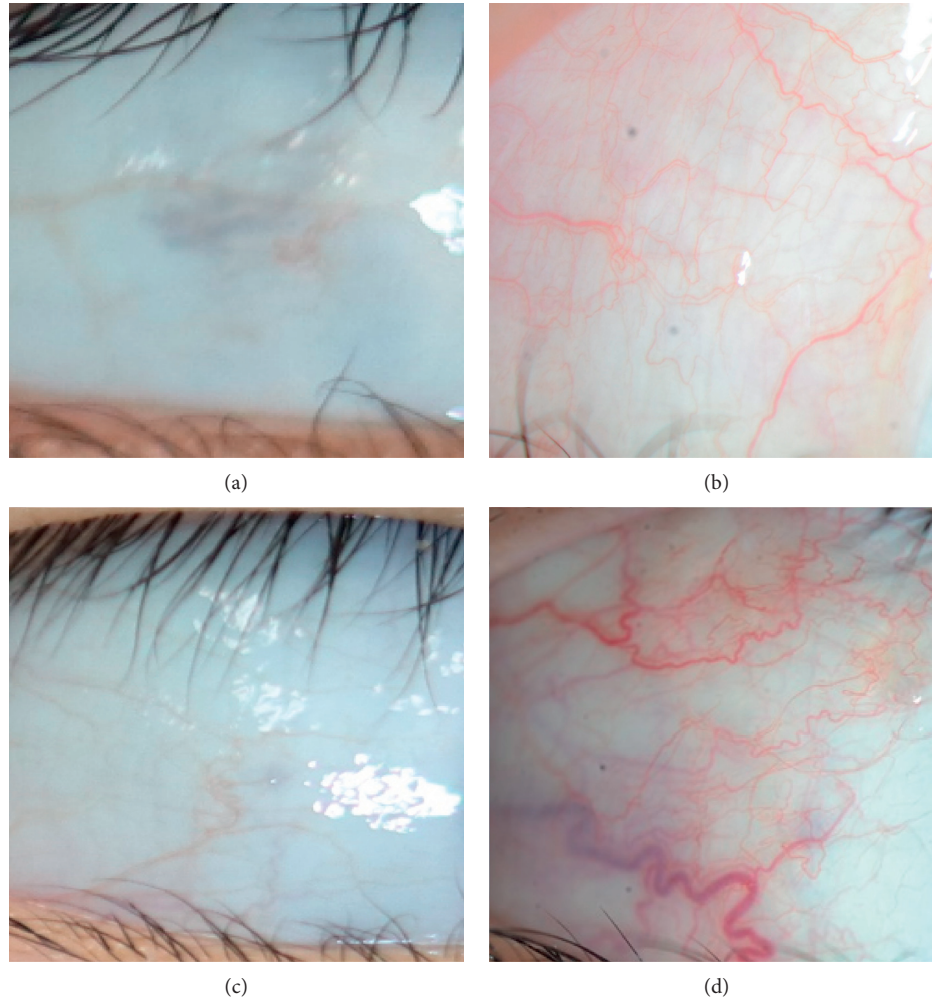


FIGURE 1: Anterior segment photographs of conjunctival injection before and after strabismus surgery in the brimonidine group ((a), (b)) and control group ((c), (d)). Conjunctival injection increased after strabismus surgery in both groups, while the amount of increase was less in the brimonidine group. Based on the preoperative conjunctival injection score, (b) scored 6.4 and (d) scored 33.3.

TABLE 1: Baseline characteristics of patients receiving topical brimonidine 0.15% and the control group.

Characteristics	Brimonidine ($n = 32$)	Control ($n = 31$)	Total ($n = 63$)	P value
Sex (M:F)	18:14	18:13	36:27	0.884*
Laterality (R:L)	15:17	17:14	32:31	0.527*
Mean age (years)	9.2 ± 1.1 (7.7–11.8)	9.0 ± 1.0 (7.6–11.6)	9.1 ± 1.0 (7.6–11.8)	0.549 [†]
Cycloplegic refraction (D)	-1.30 ± 1.61 (-5.25–+2.25)	-1.34 ± 1.82 (-6.50–+1.25)	-1.32 ± 1.70 (-6.50–+2.25)	0.916 [†]
Angle of deviation (PD)				
Distance	23.2 ± 7.4 (12–45)	22.8 ± 7.2 (12–45)	23.0 ± 7.2 (12–45)	0.824 [†]
Near	29.9 ± 8.3 (15–45)	27.0 ± 8.6 (12–40)	28.5 ± 8.5 (12–45)	0.177 [†]
Surgical dosage (mm)				
Medial rectus muscle	6.1 ± 0.9 (4.0–7.0)	5.7 ± 1.2 (3.5–7.0)	5.9 ± 1.0 (3.5–7.0)	0.168 [†]
Lateral rectus muscle	5.6 ± 1.2 (4.0–8.5)	5.4 ± 1.2 (3.5–8.5)	5.5 ± 1.2 (3.5–8.5)	0.605 [†]

M = male; F = female; R = right; L = left; D = diopters; PD = prism diopters. * P value by Pearson's χ^2 test. [†] P value by independent t-test.

weeks or months, as would be required for the injection to subside [21].

Currently, the most widely used ophthalmic vasoconstrictors, such as phenylephrine, are α_1 - or mixed α_1/α_2 -adrenergic receptor agonists. However, α_1 -adrenergic

agonists are associated with cardiovascular adverse effects, and rebound conjunctival injection may occur when discontinued, which restricts their long-term use. [22–24] Conversely, since brimonidine affects vasoconstriction through the α_2 -adrenergic receptor, the possibility of

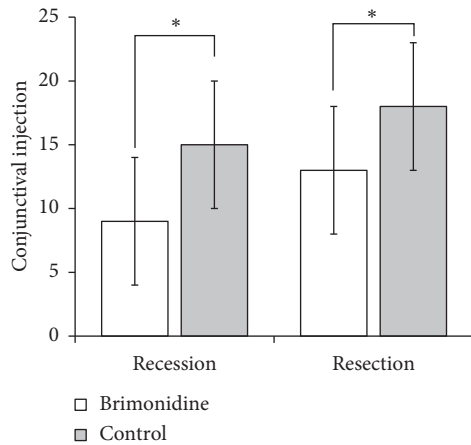


FIGURE 2: Comparison of conjunctival injection between the brimonidine group and control group. The mean score of injection at the temporal bulbar conjunctiva overlaying an area of the previous lateral rectus recession was significantly lower in the brimonidine group, 9.1 ± 9.9 in the brimonidine group and 15.9 ± 9.8 in the control group ($p = 0.008$). At the nasal bulbar conjunctiva overlaying an area of the previous medial rectus resection, the mean score of conjunctival injection was significantly lower in the brimonidine group, 13.0 ± 11.1 in the brimonidine group and 18.6 ± 10.5 in the control group ($p = 0.046$).

cardiovascular events or rebound conjunctival injection is relatively low. Therefore, brimonidine can be safely used to reduce conjunctival injection after strabismus surgery. However, the overall safety profile of brimonidine in children under 2 years of age remains uncertain. [12] In our study, brimonidine was not prescribed for patients under 2 years of age.

Several studies have reported the efficacy of brimonidine in reducing bleeding-related problems in strabismus surgery [13–15]. Two previous studies prophylactically administered topical brimonidine or phenylephrine in patients with strabismus before surgery [13, 15]. Those studies reported that both drugs can reduce intraoperative bleeding and postoperative subconjunctival hemorrhage compared with sodium hyaluronate when assessed by a subjective scoring system [13, 15]. Dahlmann-Noor et al. [14]. analyzed video images up to 20 minutes after instilling brimonidine or apraclonidine at the beginning of adjustable strabismus surgery in 10 adults. They quantified the surface area of the anterior ocular blood vessels on video images with ImageJ (open source, public domain software) and reported that brimonidine reduced the surface area of blood vessels by 69.2% and this persisted for 20 minutes. In our study, we evaluated the efficacy of postoperative topical brimonidine 0.15% instillation for a prolonged period of 4 weeks in children using the contrast-limited adaptive histogram equalization (CLAHE) algorithm that automatically extracts vasculature and scores the degree of vascularity in numeric values ranging from 0 to 100, as performed in the previous studies [16–18]. We chose the CLAHE algorithm to determine postoperative conjunctival injection because it is theoretically most suitable for the quantification of vascularization, as shown in the previous studies [16–18, 25–27].

Our study is significant in that it has objectively proved the effect of brimonidine on conjunctival injection after strabismus surgery.

Topical brimonidine prescription has other benefits besides reducing conjunctival injection. Topical corticosteroids are generally used to control postoperative inflammation after strabismus surgery. However, there are concerns regarding IOP elevation associated with the use of steroids [17, 18, 28–31]. In particular, there have been several reports of increases in IOP by up to 82% due to topical steroids after strabismus surgery in children [30, 31]. Even fluorometholone, which causes lesser IOP elevation than other steroids, significantly induced IOP elevation after strabismus surgery in children, and 23% of patients reported an increase of ≥ 10 mm Hg compared with the baseline IOP [17]. The next-generation corticosteroid, loteprednol, can also cause IOP elevation after strabismus surgery, especially in young children ≤ 8 years of age [18]. Therefore, postoperative brimonidine can be a prophylactic measure in patients with steroid-induced IOP elevation.

Our study objectively confirmed that topical brimonidine can be used to control conjunctival injection after strabismus surgery in children aged 7 years or older. Furthermore, we found that brimonidine did not cause serious systemic complications in children. Brimonidine can also alleviate IOP elevation that may occur with topical steroid application after strabismus surgery.

There are some limitations that must be considered. First, our study was a nonrandomized retrospective study; therefore, there may be a selection bias. However, to exclude this bias, we included all patients who underwent RR surgery between September 2019 and April 2020. Second, since conjunctival injection was assessed at 4 weeks after using brimonidine, the long-term effect after stopping the drug remains to be elucidated.

In conclusion, administration of topical brimonidine 0.15% after strabismus surgery is efficacious and safe in reducing postoperative conjunctival injection. However, further research will be needed to determine the long-term effect of topical brimonidine on postoperative conjunctival injection after discontinuation of the drug.

Data Availability

The Institutional Review Board of Seoul National University Bundang Hospital/Ethics Committee has placed ethical restrictions to protect patient identities. However, the data are available to anyone who is interested without restriction. The minimal dataset will be available upon request. For data requests, please contact the SNUBH IRB office at 82-31-787-8804, 98614@snuh.org.

Conflicts of Interest

The authors have no conflicts of interest to disclose.

Authors' Contributions

Dong Hyun Kim and Hee Kyung Yang are co-first authors.

Acknowledgments

This study has been conducted with the support of the Basic Science Research Program through the National Research Foundation of Korea (NRF) funded by the Ministry of Education (Grant no. NRF-2017R1D1A1B03029983) and the Korean government Ministry of Science and ICT(MSIT) (No. 2019R1F1A1061433).

References

- [1] J. A. Bradbury and R. H. Taylor, "Severe complications of strabismus surgery," *Journal of American Association for Pediatric Ophthalmology and Strabismus*, vol. 17, no. 1, pp. 59–63, 2013.
- [2] M. J. Wan and D. G. Hunter, "Complications of strabismus surgery: incidence and risk factors," *Semin Ophthalmol*, vol. 29, no. 5-6, pp. 421–428, 2014.
- [3] S. Olitsky and D. Coats, "Complications of strabismus surgery," *Middle East African Journal of Ophthalmology*, vol. 22, no. 3, pp. 271–278, 2015.
- [4] J. A. Escardó-Paton and R. A. Harrad, "Duration of conjunctival redness following adult strabismus surgery," *Journal of American Association for Pediatric Ophthalmology and Strabismus*, vol. 13, no. 6, pp. 583–586, 2009.
- [5] J. C. Adkins and J. A. Balfour, "Brimonidine," *Drugs & Aging*, vol. 12, no. 3, pp. 225–241, 1998.
- [6] S. Baiocchi, C. Mazzotta, A. Sgheri et al., "In vivo confocal microscopy: qualitative investigation of the conjunctival and corneal surface in open angle glaucomatous patients undergoing the XEN-Gel implant, trabeculectomy or medical therapy," *Eye and Vision (Lond)*, vol. 7, p. 15, 2020.
- [7] R. M. Graham, D. M. Perez, J. Hwa, and M. T. Piascik, "α1-Adrenergic receptor subtypes," *Circulation Research*, vol. 78, no. 5, pp. 737–749, 1996.
- [8] S. Arthur and L. B. Cantor, "Update on the role of alpha-agonists in glaucoma management," *Experimental Eye Research*, vol. 93, no. 3, pp. 271–283, 2011.
- [9] R. A. Norden, "Effect of prophylactic brimonidine on bleeding complications and flap adherence after laser in situ keratomileusis," *Journal of Refractive Surgery*, vol. 18, no. 4, pp. 468–471, 2002.
- [10] M. C. Desco, A. Navea, E. Ferrer, and J. L. Menezo, "Effect of prophylactic brimonidine on bleeding complications after cataract surgery," *European Journal of Ophthalmology*, vol. 15, no. 2, pp. 228–232, 2005.
- [11] C. S. Kim, K. Y. Nam, and J. Y. Kim, "Effect of prophylactic topical brimonidine (0.15%) administration on the development of subconjunctival hemorrhage after intravitreal injection," *Retina*, vol. 31, no. 2, pp. 389–392, 2011.
- [12] G. P. Daubert, "Is brimonidine ophthalmic a safe therapy for infants?" *Journal of Clinical Pharmacy and Therapeutics*, vol. 31, no. 3, pp. 289–292, 2006.
- [13] S. Hong, C. Y. Kim, G. J. Seong, and S.-H. Han, "Effect of prophylactic brimonidine instillation on bleeding during strabismus surgery in adults," *American Journal of Ophthalmology*, vol. 144, no. 3, pp. 469–470, 2007.
- [14] A. H. Dahlmann-Noor, E. Cosgrave, S. Lowe, M. Bailly, and A. J. Vivian, "Brimonidine and apraclonidine as vasoconstrictors in adjustable strabismus surgery," *Journal of American Association for Pediatric Ophthalmology and Strabismus*, vol. 13, no. 2, pp. 123–126, 2009.
- [15] A. Gupta, R. Kekunnaya, V. Sachdeva, and H. L. Rao, "Strabismus surgery hemostasis," *Ophthalmology*, vol. 119, no. 3, pp. 649–650, 2012.
- [16] I. K. Park, Y. S. Chun, K. G. Kim, H. K. Yang, and J.-M. Hwang, "New clinical grading scales and objective measurement for conjunctival injection," *Investigative Ophthalmology & Visual Science*, vol. 54, no. 8, pp. 5249–5257, 2013.
- [17] H. K. Yang, S. B. Han, and J.-M. Hwang, "Diclofenac versus fluorometholone after strabismus surgery in children," *British Journal of Ophthalmology*, vol. 98, no. 6, pp. 734–738, 2014.
- [18] Y. J. Yoo, H. K. Yang, and J. M. Hwang, "Efficacy and safety of loteprednol 0.5% and fluorometholone 0.1% after strabismus surgery in children," *Journal of Ocular Pharmacology and Therapeutics*, vol. 34, no. 6, pp. 468–476, 2018.
- [19] R. J. Bowman, J. Cope, and K. K. Nischal, "Ocular and systemic side effects of brimonidine 0.2% eye drops (Alphagan) in children," *Eye (London, England)*, vol. 18, no. 1, pp. 24–26, 2004 Jan.
- [20] Y. Levy and D. Zadok, "Systemic side effects of ophthalmic drops," *Clinical Pediatrics*, vol. 43, no. 1, pp. 99–101, 2004.
- [21] J. Fishbaugh, "Subconjunctival hemorrhage—something more you should know," *Insight*, vol. 20, no. 1, pp. 20–21, 1995.
- [22] C. N. S. Soparkar, K. R. Wilhelmus, D. D. Koch, G. W. Wallace, and D. B. Jones, "Acute and chronic conjunctivitis due to over-the-counter ophthalmic decongestants," *Archives of Ophthalmology*, vol. 115, no. 1, pp. 34–38, 1997.
- [23] C. Tappeiner, G.-M. Sarra, and M. Abegg, "Abuse of vasoconstrictive eyedrops mimicking an ocular pemphigoid," *European Journal of Ophthalmology*, vol. 19, no. 1, pp. 129–132, 2009.
- [24] F. W. Fraunfelder, F. T. Fraunfelder, and B. Jensvold, "Adverse systemic effects from pledgets of topical ocular phenylephrine 10%," *American Journal of Ophthalmology*, vol. 134, no. 4, pp. 624–625, 2002.
- [25] S. B. Han, H. S. Jeon, M. Kim et al., "Risk factors for recurrence after pterygium surgery," *Cornea*, vol. 35, no. 8, pp. 1097–1103, 2016.
- [26] S. B. Han, H. S. Jeon, M. Kim et al., "Quantification of astigmatism induced by pterygium using automated image analysis," *Cornea*, vol. 35, no. 3, pp. 370–376, 2016.
- [27] H. K. Yang, Y. J. Lee, J. Y. Hyon, K. G. Kim, and S. B. Han, "Efficacy of bevacizumab injection after pterygium excision and limbal conjunctival autograft with limbal fixation suture," *Graefe's Archive for Clinical and Experimental Ophthalmology*, vol. 258, no. 7, pp. 1451–1457, 2020.
- [28] M. F. Armaly, "Effect of corticosteroids on intraocular pressure and fluid dynamics," *Archives of Ophthalmology*, vol. 70, no. 4, pp. 482–491, 1963.
- [29] C. N. McGhee, "Pharmacokinetics of ophthalmic corticosteroids," *British Journal of Ophthalmology*, vol. 76, no. 11, pp. 681–684, 1992.
- [30] M. Ohji, S. Kinoshita, E. Ohmi, and Y. Kuwayama, "Marked intraocular pressure response to instillation of corticosteroids in children," *American Journal of Ophthalmology*, vol. 112, no. 4, pp. 450–454, 1991.
- [31] A. K. Kwok, D. S. Lam, J. S. Ng, D. S. Fan, S. J. Chew, and M. O. Tso, "Ocular-hypertensive response to topical steroids in children," *Ophthalmology*, vol. 104, no. 12, pp. 2112–2116, 1997.

Review Article

Advances in Imaging Technology of Anterior Segment of the Eye

Sang Beom Han,¹ Yu-Chi Liu,^{2,3,4} Karim Mohamed-Noriega,⁵ and Jodhbir S. Mehta^{2,3,4} 

¹Department of Ophthalmology, Kangwon National University School of Medicine, Kangwon National University Hospital, Chuncheon, Republic of Korea

²Singapore National Eye Centre, Singapore, Singapore

³Singapore Eye Research Institute, Singapore, Singapore

⁴Department of Ophthalmology, Yong Loo Lin School of Medicine, National University of Singapore, Singapore, Singapore

⁵Department of Ophthalmology, University Hospital, Faculty of Medicine, Autonomous University of Nuevo Leon, Monterrey, Mexico

Correspondence should be addressed to Jodhbir S. Mehta; jodmehta@gmail.com

Received 22 June 2020; Revised 5 February 2021; Accepted 16 February 2021; Published 23 February 2021

Academic Editor: Achim Langenbacher

Copyright © 2021 Sang Beom Han et al. This is an open access article distributed under the Creative Commons Attribution License, which permits unrestricted use, distribution, and reproduction in any medium, provided the original work is properly cited.

Advances in imaging technology and computer science have allowed the development of newer assessment of the anterior segment, including Corvis ST, Brillouin microscopy, ultrahigh-resolution optical coherence tomography, and artificial intelligence. They enable accurate and precise assessment of structural and biomechanical alterations associated with anterior segment disorders. This review will focus on these 4 new techniques, and a brief overview of these modalities will be introduced. The authors will also discuss the recent advances in research regarding these techniques and potential application of these techniques in clinical practice. Many studies on these modalities have reported promising results, indicating the potential for more detailed comprehensive understanding of the anterior segment tissues.

1. Introduction

Direct visualization of ocular surface tissue using conventional techniques, e.g., slit-lamp biomicroscopy, still remains the primary examination tool for anterior segment diseases [1]. Development of devices for anterior segment imaging, such as anterior segment optical coherence tomography (OCT), corneal topography, specular microscopy, confocal microscopy, ultrasound biomicroscopy, and ocular response analyzer, has enabled detailed objective observations of anterior segment structures that can contribute to improved anatomical and visual outcome after cornea, cataract, and refractive surgeries [2].

Development of newer technologies, such as corneal visualization Scheimpflug Technology (Corvis ST), Brillouin microscopy, and ultrahigh-resolution OCT (UHR-OCT), is expected to allow even more detailed visualization of anterior segment structures, which would allow even more understanding of anterior segment pathology. Artificial

intelligence may also be useful for providing optimal diagnostic and treatment protocols by integrating findings obtained using various imaging modalities.

In this review, we aim to provide an overview of these 4 newer techniques and discuss the research advances and potential clinical application of these modalities.

1.1. Corneal Biomechanical Assessment Using Ultrahigh-Speed Imaging and Special Analytical Methods. The Corvis ST (OCULUS Optikgeräte GmbH, Wetzlar, Germany) is the integration of two measurements modalities, i.e., a non-contact tonometer with a collimated high-intensity air pulse and an ultrafast Scheimpflug camera, that is used for the assessment of biomechanical properties of the cornea [3–9].

In the device, a fixed pressure air pulse causes corneal deformation, while passing through two applanation moments; the corneal movement during the deformation process is recorded using an ultrafast Scheimpflug camera at

a speed of 4330 frames/s [10]. In each examination, a series of 140 images with width of 8.5 mm is obtained in 33 ms [3, 10]. As the Corvis ST is capable of analyzing the whole process of dynamic corneal deformation, it enables calculation of various dynamic corneal response (DCR) parameters [3, 11, 12]. Parameters including “deformation” are calculated without compensating for whole eye movement (WEM), while the parameters including “deflection” compensate for the WEM [13].

As the air pulse is triggered, the cornea deforms inward through the moment of first corneal applanation (A1), [3] at which the length of the applanated cornea (A1 length), the velocity of the corneal apex (A1 velocity), time from the measurement beginning (A1 time), and corneal deflection amplitude (A1 DeflAmp), defined as the displacement of the corneal apex without the WEM, are measured [3].

Just prior to A1, deformation amplitude ratio (DA ratio) at 1 or 2 mm, i.e., central deformation divided by an average of the deformation 1 or 2 mm from center with maximum value, is measured, and deflection amplitude ratio (DefA ratio) at 1 or 2 mm can be calculated after compensation for WEM [3].

Initially, the moment during the cornea highest concavity (HC), parameters including radius of corneal curvature (HC radius), time from beginning to the moment of HC (HC time), maximum deformation amplitude (DA), corneal deflection area (HCDeflArea), corneal deflection amplitude (HCDeflAmp), delta arc length of the outer corneal edge between initial state and HC (HCdArclength), and distance between two corneal peaks at HC (peak distance) are measured [3, 9, 13]. The radius of corneal curvature at HC (curvature radius HC) and the maximum value of the integrated inverse of the corneal radius HC (InvRadMax) are also determined [3, 9, 13].

At the moment of the second applanation (A2), the time for the A2 (A2 time), length of the flattened cornea (A2 length), and the velocity of the corneal apex (A2 velocity) are measured [3]. The value of corneal displacement before and after deformation (WEMax; maximum WEM) can also be determined [14, 15]. Corneal thickness over the entire cornea including central corneal thickness (CCT) and intraocular pressure (IOP) data, including uncorrected and biomechanically corrected IOP (bIOP), were also assessed [16]. As IOP values have strong association with the age, CCT, and DCR parameters, [17] bIOP was calculated based on an algorithm designed to compensate for the effects of these factors [18]. Stiffness parameters (SP) can be calculated by dividing the loading (air pressure—bIOP) on the cornea by the displacement of the corneal apex at A1 (SP-A1) and HC (SP-HC), respectively [3]. Several studies have demonstrated that Corvis ST had high repeatability and reproducibility for measurement of CCT, IOP, bIOP, and DCR parameters [10, 14, 15].

DCR parameters were shown to be helpful for the detection of corneal ectasia (Figure 1) [19, 20]. Keratoconus is associated with an increase in DA [21, 22]. A larger curvature radius HC and lower InvRadMax were related to increased corneal stiffness and higher resistance to deformation. [13].

For early and accurate diagnosis of corneal ectasia, several indices have been developed [6, 23]. Vinciguerra et al. [6] proposed the Corvis Biomechanical Index (CBI) by combining DCR parameters including the DA ratio at 2 mm, InvRadMax, and SP-A1 and corneal thickness data expressed as Ambrósio’s Relational Thickness in the horizontal profile (ARTh) [23]. CBI with a cut-off value of 0.5 successfully detected 98.2% of corneal ectasia with 100% specificity, suggesting its potential value for early detection of keratoconus [6]. In a subsequent study, they presented 12 cases with subclinical keratoconus detected using CBI cut-off value of 0.5 in which topography and tomography were all normal [24].

In 2017, Ambrosio et al. [23] introduced the tomographic biomechanical index (TBI) by integrating Scheimpflug-based corneal tomographic and biomechanical data to improve accuracy for detection of corneal ectasia (Figure 2) [23]. The TBI cut-off value of 0.79 provided 100% sensitivity and 100% specificity for detecting clinical corneal ectasia [23]. They also showed that TBI was significantly more accurate than CBI or Belin-Ambrosio Deviation display (BAD-D) for detecting corneal ectasia [23]. Steinberg et al. [25] also demonstrated that TBI was superior to CBI and BAD-D in keratoconus screening in topographical and tomographical normal fellow eyes of clinically ectatic eyes, although all the three indices were excellent for discriminating advanced keratoconus from normal eyes. Ferreira-Mendes et al. [26] revealed that the TBI was more accurate than BAD-D and CBI for detecting subclinical ectasia amongst topographically normal eyes in patients with asymmetric ectasia, indicating that the index might identify an intrinsic susceptibility for ectasia progression [26]. Other studies have also shown that TBI was the most accurate amongst the various indices developed so far for discriminating subclinical keratoconus from normal eyes [20,27]. Kataria et al. [20] reported that, among indices including CBI, TBI, BAD-D, and SP-A1, TBI showed the weakest correlation with biomechanical confounding factors. However, the cut-off value of TBI for detecting eyes with ectasia susceptibility varied amongst the studies, and no consensus regarding the cut-off value has been established yet [28]. Koh et al. [29] showed that 40% of cases with clinical ectasia in one eye and a fellow eye with normal topography were classified as normal by BAD-D, CBI, and TBI. These findings suggest that further studies are necessary for further development of indices and guidelines for discriminating eyes with ectasia susceptibility [29].

Corvis ST can also be helpful in monitoring changes in cornea after collagen cross-linking (CXL) treatment [30, 31]. CXL treatment was associated with increase in A2V and DA as well as decrease in A2L in eyes with keratoconus [31]. The difference between the A1L and A2L was reliable in discriminating cross-linked keratoconic corneas from untreated keratoconic or healthy corneas [31]. Hashemi et al. [30] showed that Corvis ST showed DCR changes suggesting corneal strengthening, such as decreased DA 2 mm and increased SP-A1, indicating that the device can provide biomechanical evidence of the efficacy of corneal CXL [30].

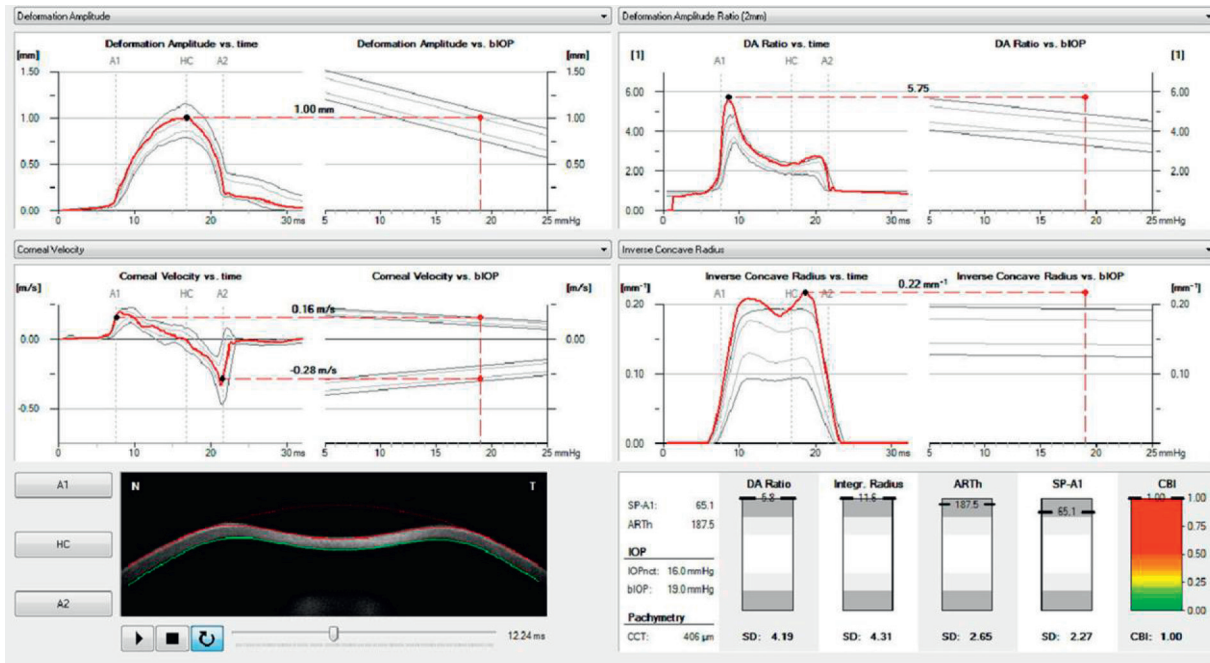


FIGURE 1: Vinciguerra screening report displays DCR parameters of a patient with keratoconus in comparison with normative values. The ARTh and SP-A1 are lower, and the DA ratio, integrated radius, and CBI are higher in keratoconus compared to normal subjects.

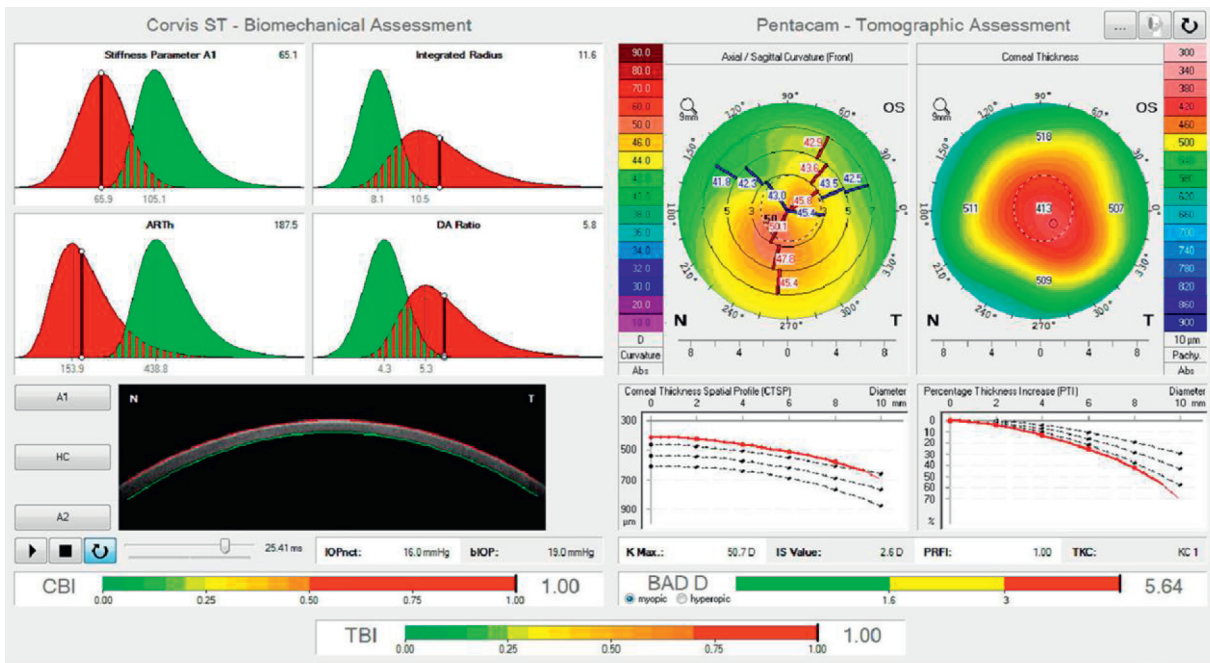


FIGURE 2: Corvis ST biomechanical/tomographic assessment of a keratoconic eye. Biomechanical assessment shows increase in DA ratio and integrated radius, and decrease in ARTh and SP-A1 (top left). Tomographic assessment shows central corneal thinning with an asymmetric bow tie pattern (top right). The percentage of thickness increase (PTI) graph shows an inferior escape from the normal mean. CBI, TBI, and BAD are all increased (bottom).

Corvis ST is also expected to be useful for evaluation of changes in corneal biomechanical properties associated with refractive errors and keratorefractive surgery [32–34]. Tubtimthong et al. [35] demonstrated that high myopia was associated with higher DA and smaller curvature radius,

indicating that the condition might have reduced corneal stiffness and decreased stability. Hashemi et al. [34] showed that laser-assisted in situ keratomileusis (LASIK) led to more substantial changes in corneal biomechanical properties than photorefractive keratectomy (PRK) in high myopia,

although both procedures caused significant biomechanical changes in the cornea. Corvis ST has shown that both LASIK and small incision lenticule extraction (SMILE) cause remarkable changes in corneal biomechanical parameters [32, 33, 36]. However, SMILE was associated with reduced change in DA and better recovery of corneal biomechanical strength [32, 33]. Khamar et al. [36] reported that creation of a LASIK flap caused greater acute biomechanical weakening intraoperatively in comparison to a SMILE cap, although both resulted in similar biomechanical changes after wound healing.

Cataract surgery was associated with decreased SP-A1 and increased DA even at 3 months postoperatively, suggesting decreased corneal stiffness [37, 38]. As the reduction in corneal stiffness was associated with falsely low IOP measurements, care should be taken particularly when evaluating glaucoma patients after cataract surgery [37].

Corvis ST is also expected to be a potential biomarker in thyroid orbitopathy [39, 40]. Thyroid orbitopathy was associated with a decrease in WEM, which had a correlation with increase in cross-sectional area of the extraocular muscles [40]. Leszczynska et al. [39] also demonstrated biomechanical alterations including decreased WEM length and time, increased bIOP, and higher SP, indicating reduced orbital compliance in association with thyroid orbitopathy [39].

With the development of OCT technology, swept source (SS) OCT combined with air puff applanation is also expected to enable accurate and precise evaluation of corneal biomechanical properties [41, 42]. Several studies have shown the efficacy of SS-OCT with an air puff in assessment of dynamic response of cornea to air pulse, suggesting it as a potential option for the *in vivo* assessment of corneal mechanical properties, particularly due to its high resolution [43, 44].

2. Brillouin Microscopy

Brillouin microscopy is a recently introduced modality to measure the viscoelastic property of the cornea *in vivo* [45]. In Brillouin microscopy, a low-power, near-infrared laser beam is focused into the corneal tissue and it interacts with intrinsic acoustic waves, which leads to a Brillouin frequency shift of scattered light reflected from the modulation of the focus [45, 46]. The Brillouin frequency shift is proportional to the acoustic propagation speed of tissue at the focus, which is proportional to the square of the longitudinal modulus; thus, assessment of the Brillouin frequency shift provides a determination of longitudinal modulus or mechanical compressibility, which is the inverse of the longitudinal modulus, of the target tissue [45].

Brillouin microscopy is advantageous due to its non-contact nature and ability to generate 3D mapping of the spatial variation of longitudinal modulus using high-resolution confocal spectrometer and is expected to be widely used for practice and research on anterior segment disorders [45, 46].

Clinical studies using Brillouin microscopy have demonstrated significant alteration in corneal elastic properties

in keratoconus, suggesting the potential applicability of the device for detection of cornea with ectasia susceptibility [47, 48]. Brillouin frequency shift in the cone region is significantly reduced in keratoconic corneas compared to normal ones [47–49]. In keratoconus, the cone region has substantially decreased Brillouin frequency shift, compared to the peripheral regions [47–49]. Shao et al. [47] also demonstrated that asymmetry of Brillouin frequency shifts between the right and left cone regions is significantly higher in eyes with early keratoconus compared with normal eyes, indicating that bilateral symmetry of Brillouin value might have a value for detection of early-stage KC.

The modality may also be useful in evaluation of corneal CXL protocols [50, 51]. Brillouin analyses revealed that accelerated CXL protocols were especially ineffective in the deeper portions of the cornea [50], and the stiffening effect of localized-CXL extended to regions surrounding the localized irradiated area [51].

Brillouin microscopy can be useful in the management of corneal endothelial disorders and monitoring the disease severity [52, 53]. Brillouin frequency shift was shown to have negative correlation with corneal hydration, [52] which might be helpful in evaluating abnormal hydration change associated with endothelial dysfunction. Eltony et al. [53] revealed that patients with Fuchs' endothelial dystrophy showed a centralized reduction in Brillouin shift, which was consistent with central corneal edema. Brillouin microscopy also detected substantially reduced corneal hydration after Descemet membrane endothelial keratoplasty (DMEK) [53].

The technique is also expected to be useful for the evaluation of corneal biomechanical change associated with cornea, refractive, and cataract surgery [45, 54]. LASIK flap creation resulted in significantly reduced Brillouin frequency shift, due to reduced corneal stiffness [54]. As differences in biomechanical properties including corneal hydration might contribute to the variability in refractive outcome after cataract and refractive surgeries, [55, 56] Brillouin microscopy is expected to be helpful for establishment of individually tailored nomograms for optimal visual outcome [45, 55].

3. Ultrahigh Resolution OCT (UHR-OCT)

Although anterior segment time-domain OCT, which has been commercially utilized since the early 2000s, is capable of providing comprehensive images of anterior segment structure, it lacks the ability to show structural details due to the lower resolution [57, 58]. Advances in technology have enabled development of spectral-domain OCT with improved axial resolution of 4–7 μm and, subsequently, ultrahigh-resolution (UHR) OCT with axial resolution of 1–4 μm [58].

UHR-OCT uses a light source based on Ti:sapphire laser with a broad bandwidth of larger than 100 nm as well as an optical system specifically designed to deliver optimal performance [59], which results in a resolution of less than 5 μm [58, 59].

Enhanced axial resolution of UHR-OCT enabled precise delineation of all 5 corneal layers and thickness

measurement of each layer [59]. The device also allowed visualization of microstructures, such as limbal palisades of Vogt, limbal blood vessels, corneal nerve fiber bundles, and aqueous humor drainage pathway including intrascleral, episcleral, and conjunctival venous plexuses [59], which may be helpful for understanding the pathophysiology of various anterior segment disorders and glaucoma.

UHR-OCT also allows visualization of precorneal tear film and tear film lipid layer [60–62] and provides thickness data of tear film and lipid layer with excellent reproducibility [61, 62]. These findings suggest that the UHR-OCT can be a viable option for diagnosis and management of dry eye disease [59]. It also enabled precise evaluation of re-epithelialization after corneal injury by 3D mapping and observation of microarchitectural alterations in early phases of corneal wound healing [63, 64].

UHR-OCT was also shown to be a viable tool for detection, differential diagnosis, and monitoring of treatment response of ocular surface tumors including ocular surface squamous neoplasia and melanoma [58, 65, 66]. It can provide clear demarcation and information regarding depth, localization, and characteristics of various ocular surface lesions [67]. UHR-OCT findings of the lesions showed close correlation with histopathologic features [66, 67]. Shousha et al. [66] suggested that UHR-OCT can play a critical role in guiding the diagnosis in some cases, in which the optical signs obtained using the device indicated that the presumed clinical diagnosis might be incorrect and favored a diagnosis later confirmed by histopathologic examination [66]. These findings indicate that UHR-OCT may have potential for noninvasive options for confirming diagnosis and monitoring treatment response of ocular surface lesions [66, 67]. The modality also enables detection of subclinical ocular surface neoplasia that cannot be observed by slit-lamp examination [66, 68], which may be invaluable for surveillance for recurrent or residual tumors after treatment [58].

UHR-OCT can also be helpful for diagnosis and treatment of ocular surface infection. For instance, the device allows visualization of characteristic signs of *Acanthamoeba* keratitis, such as corneal nerve thickening reflecting radial keratoneuritis and highly reflective dots indicating the cysts [59].

The ability of the UHR-OCT to generate vertical thickness map and indices of the corneal epithelium and Bowman's layer can be helpful for discrimination of subclinical corneal ectasia [69, 70]. In 2019, Santos et al. [71] reported that a UHR-OCT combined with a deep learning algorithm called CorneaNet was capable of segmentation of both healthy and keratoconus images with high reliability, suggesting that the device can be a useful tool for early detection of keratoconus.

UHR-OCT allows in vivo high-resolution visualization of corneal endothelial cells and measurement of density of the cells [72], which can be beneficial for detection and monitoring of pathologic conditions in endothelium, e.g., endothelial guttata in Fuchs' endothelial dystrophy [68].

The device can also be helpful for management after corneal surgery, particularly after keratoplasty. UHR-OCT allows visualization of endothelial graft after DMEK [59],

which enables early detection of graft detachment. It can also detect a gap in the keratoprosthesis-cornea interface with absence of epithelial closure after implantation of artificial cornea [73], which is critical for prevention of complications, such as leakage, graft extrusion, and endophthalmitis [73].

As UHR-OCT technology has a potential for visualization of anterior segment structure at a microscopic level and assessment of ocular biometry with excellent accuracy, it is expected to further improve visual outcome after cataract and refractive surgery [2].

4. Artificial Intelligence

Artificial intelligence (AI) using machine learning and deep learning is expected to be helpful for diagnosis and treatment of anterior segment diseases, although the use of AI has already been extensively established for systemic associations with retinal findings [74, 75]. Machine learning algorithms including support vector machines or random forest models are programmed to adapt according to the input data and produce assumptions, e.g., determinations or predictions, based on the parameters of its algorithm [76]. Conventional machine learning might be sufficient for designing predictive algorithms using clinical data including medical records or population-based studies [77]. Deep learning refers to a subset of machine learning technique that involves neural networks comprising multiple neuron-like computational layers of algorithms, i.e., convolutional neural networks (CNNs) [76]. Deep learning has been widely used for the analysis of image-based data including anterior segment photographs, fundus photographs, or OCT images, due to its improved diagnostic performance [77].

Mahesh Kumar et al. [78] reported that a multiclass computer-aided system, based on machine learning using support vector machine by sequential minimal optimization algorithm, showed accuracy of 97% for diagnosing anterior segment eye abnormalities such as senile arcus or cataracts, suggesting the potential of ophthalmic image analysis using AI for clinical application.

AI has currently been useful for development of indices for discrimination of keratoconus [23,79]. The TBI developed using random forest model with leave-one-out cross-validation was shown to be superior to other indices, such as CBI and BAD-D, for differentiation between keratoconus and normal corneas [23, 26]. The Pentacam random forest index (PRFI), a random forest model generated using Pentacam HR (Oculus, Wetzlar, Germany) data, was also demonstrated to improve the accuracy of detection of ectasia susceptibility compared to BAD-D [79].

AI also allows rapid assessment of the corneal endothelium with good reliability [80–83]. A deep learning method called U-net was capable of substantially faster and more accurate segmentation compared to manual segmentation [80, 81]. Heinzelmann et al. [84] revealed that the endothelial cell counts measured using U-Net showed strong correlation with those obtained with the gold standard, suggesting the potential applicability of the AI model in the long-term assessment of corneal grafts. After DMEK, deep

learning model using CNN can also be useful for automated quantification of graft dislocation, which may enable early detection of graft [85].

AI enables rapid and accurate evaluation of corneal subbasal nerve plexus using in vivo confocal microscopy (IVCM) [86, 87]. Using neural network and random forest models, Chen et al. [86] generated an automated method for detection and quantification of nerve fibers in IVCM images with speed and repeatability superior to manual quantification. Al-Fahdawi et al. [88] introduced an automatic system using AI for nerve segmentation and assessment of parameters including nerve thickness, tortuosity, and length in IVCM images, which is expected to be useful for early detection of diabetic peripheral neuropathy. Williams et al. [87] also introduced a deep learning algorithm for the automated quantification of the corneal nerves, which showed rapid and excellent localization performance.

AI can be helpful for the diagnosis and management of ocular surface infection [89,90]. Xu et al. [89] revealed that an automatic hyphae detection method based on image recognition with adaptive robust binary pattern in IVCM images was more accurate than corneal smear examination, suggesting the potential applicability of AI for noninvasive diagnosis of fungal keratitis [89]. A system for automatic segmentation of corneal ulcer areas using a joint method of Otsu and Gaussian mixture modeling has also been proposed [90].

In dry eye disease, deep learning can be applied for the automatic segmentation of the anterior segment OCT image with a thresholding-based segmentation algorithm for the evaluation of the tear meniscus [91].

For iris tumor, Ouabida et al. [92] showed that an automatic method using the Vander Lugt correlator based active contour method and a *K*-means clustering model detected all iris tumors with an accuracy of 100% [92].

AI is also expected to be useful for screening of cataract [93–95]. Lin et al. [93] introduced an automatic detection protocol for pediatric cataracts using a deep learning algorithm using anterior segment photographs. Yang et al. [94] also developed an ensemble learning based method using support vector machine and back-propagation neural network, which showed good performance for detection and grading of cataract [94]. Wu et al. [95] reported that a universal AI platform integrated with a AI-based multilevel collaborative pattern showed excellent reliability for diagnosis of cataract and detection of referable cases, which might enable effective referral service for cataracts. Machine learning algorithms have also shown higher efficacy with comparable safety in nomogram prediction in SMILE compared with surgeon-developed normograms [96].

5. Conclusion

Novel techniques including Corvis ST, Brillouin microscopy, and UHR-OCT are expected to enable even more detailed assessment of anterior segment structures with high accuracy. AI can integrate the findings from these new modalities as well as from conventional imaging devices and

generate protocols for optimal diagnosis and treatment of various anterior segment disorders.

With further developments, these future techniques may allow comprehensive and precise evaluation of anatomical and functional alterations associated with various anterior segment diseases, which would be critical for enhanced diagnostic performance and treatment outcome.

Data Availability

The data supporting this systemic review are from previously reported studies and datasets, which have been cited in this article.

Conflicts of Interest

The authors declare no conflicts of interest.

Acknowledgments

This study was supported by a research grant of Kangwon Institute for Unification Studies, Kangwon National University, in 2019, and the Basic Science Research Program through the National Research Foundation of Korea (NRF) funded by the Ministry of Education (grant no. NRF-2017R1D1A1B03029983).

References

- [1] K. C. Shih, R. H. Tse, Y. T. Lau, and T. C. Chan, "Advances in corneal imaging: current Applications and beyond," *The Asia-Pacific Journal of Ophthalmology*, vol. 8, no. 2, 2019.
- [2] S. B. Han, J. S. Mehta, Y. C. Liu, and K. Mohamed-Noriega, "Advances and clinical applications of anterior segment imaging techniques," *Journal of Ophthalmology*, vol. 2016, Article ID 8529406, 2 pages, 2016.
- [3] M. Jedzierska and R. Koprowski, "Novel dynamic corneal response parameters in a practice use: a critical review," *BioMedical Engineering OnLine*, vol. 18, no. 1, 17 pages, 2019.
- [4] G. Nemeth, E. Szalai, Z. Hassan, A. Lipecz, Z. Flasko, and L. Modis, "Corneal biomechanical data and biometric parameters measured with scheinpluf-based devices on normal corneas," *International Journal of Ophthalmology*, vol. 10, no. 2, pp. 217–222, 2017.
- [5] M. Jedzierska, R. Koprowski, S. Wilczynski, and K. Kryszk, "A new method for detecting the outer corneal contour in images from an ultra-fast scheinpluf camera," *BioMedical Engineering OnLine*, vol. 18, no. 1, p. 115, 2019.
- [6] R. Vinciguerra, R. Ambrósio, A. Elsheikh et al., "Detection of keratoconus with a new biomechanical index," *Journal of Refractive Surgery*, vol. 32, no. 12, pp. 803–810, 2016.
- [7] R. Vinciguerra, R. Ambrósio, C. J. Roberts et al., "Should the corvis biomechanical index (CBI) include corneal thickness parameters?" *Journal of Refractive Surgery*, vol. 34, no. 3, pp. 213–216, 2018.
- [8] R. Vinciguerra, V. Romano, E. M. Arbabi et al., "In vivo early corneal biomechanical changes after corneal cross-linking in patients with progressive keratoconus," *Journal of Refractive Surgery*, vol. 33, no. 12, pp. 840–846, 2017.
- [9] R. Vinciguerra, A. Elsheikh, C. J. Roberts et al., "Influence of pachymetry and intraocular pressure on dynamic corneal response parameters in healthy patients," *Journal of Refractive Surgery*, vol. 32, no. 8, pp. 550–561, 2016.

- [10] J. Hong, J. Xu, A. Wei et al., "A new tonometer-the corvis ST tonometer: clinical comparison with noncontact and goldmann applanation tonometers," *Investigative Ophthalmology & Visual Science*, vol. 54, no. 1, pp. 659–665, 2013.
- [11] R. Koprowski, R. Ambrosio, and S. Reisdorf, "Scheimpflug camera in the quantitative assessment of reproducibility of high-speed corneal deformation during intraocular pressure measurement," *Journal of Biophotonics*, vol. 8, no. 11-12, pp. 968–978, 2015.
- [12] R. Koprowski, "Automatic method of analysis and measurement of additional parameters of corneal deformation in the Corvis tonometer," *BioMedical Engineering OnLine*, vol. 13, no. 1, p. 150, 2014.
- [13] L. P. G. Esporcatté, M. Q. Salomao, B. T. Lopes et al., "Biomechanical diagnostics of the cornea," *Eye and Vision (London)*, vol. 7, p. 9, 2020.
- [14] G. Nemeth, Z. Hassan, A. Csutak, E. Szalai, A. Berta, and L. Modis, "Repeatability of ocular biomechanical data measurements with a scheimpflug-based noncontact device on normal corneas," *Journal of Refractive Surgery*, vol. 29, no. 8, pp. 558–563, 2013.
- [15] A. Miki, N. Maeda, Y. Ikuno, T. Asai, C. Hara, and K. Nishida, "Factors associated with corneal deformation responses measured with a dynamic scheimpflug analyzer," *Investigative Ophthalmology & Visual Science*, vol. 58, no. 1, pp. 538–544, 2017.
- [16] D. P. Piñero and N. Alcón, "Corneal biomechanics: a review," *Clinical and Experimental Optometry*, vol. 98, no. 2, pp. 107–116, 2015.
- [17] H. Lee, C. J. Roberts, T.-i. Kim, R. Ambrósio, A. Elsheikh, and D. S. Y. Kang, "Changes in biomechanically corrected intraocular pressure and dynamic corneal response parameters before and after transepithelial photorefractive keratectomy and femtosecond laser-assisted laser in situ keratomileusis," *Journal of Cataract & Refractive Surgery*, vol. 43, no. 12, pp. 1495–1503, 2017.
- [18] A. Eliasy, K. J. Chen, R. Vinciguerra et al., "Determination of corneal biomechanical behavior in-vivo for healthy eyes using CorVis ST tonometry: stress-strain index," *Frontiers in Bioengineering and Biotechnology*, vol. 7, p. 105, 2019.
- [19] M.-R. Sedaghat, H. Momeni-Moghaddam, R. Ambrósio et al., "Diagnostic ability of corneal shape and biomechanical parameters for detecting frank keratoconus," *Cornea*, vol. 37, no. 8, pp. 1025–1034, 2018.
- [20] P. Kataria, P. Padmanabhan, A. Gopalakrishnan, V. Padmanaban, S. Mahadik, and R. Ambrósio, "Accuracy of scheimpflug-derived corneal biomechanical and tomographic indices for detecting subclinical and mild keratectasia in a South Asian population," *Journal of Cataract & Refractive Surgery*, vol. 45, no. 3, pp. 328–336, 2019.
- [21] C. Ji, J. Yu, T. Li et al., "Dynamic curvature topography for evaluating the anterior corneal surface change with Corvis ST," *BioMedical Engineering OnLine*, vol. 14, p. 53, 2015.
- [22] C. Ye, M. Yu, G. Lai, and V. Jhanji, "Variability of corneal deformation response in normal and keratoconic eyes," *Optometry and Vision Science*, vol. 92, no. 7, pp. e149–e153, 2015.
- [23] R. Ambrósio, B. T. Lopes, F. Faria-Correia et al., "Integration of scheimpflug-based corneal tomography and biomechanical assessments for enhancing ectasia detection," *Journal of Refractive Surgery*, vol. 33, no. 7, pp. 434–443, 2017.
- [24] R. Vinciguerra, R. Ambrósio, C. J. Roberts, C. Azzolini, and P. Vinciguerra, "Biomechanical characterization of subclinical keratoconus without topographic or tomographic abnormalities," *Journal of Refractive Surgery*, vol. 33, no. 6, pp. 399–407, 2017.
- [25] J. Steinberg, M. Siebert, T. Katz et al., "Tomographic and biomechanical scheimpflug imaging for keratoconus characterization: a validation of current indices," *Journal of Refractive Surgery*, vol. 34, no. 12, pp. 840–847, 2018.
- [26] J. Ferreira-Mendes, B. T. Lopes, F. Faria-Correia, M. Q. Salomão, S. Rodrigues-Barros, and R. Ambrósio, "Enhanced ectasia detection using corneal tomography and biomechanics," *American Journal of Ophthalmology*, vol. 197, pp. 7–16, 2019.
- [27] L. Tian, Y. F. Huang, L. Q. Wang et al., "Corneal biomechanical assessment using corneal visualization scheimpflug technology in keratoconic and normal eyes," *Journal of Ophthalmology*, vol. 2014, Article ID 147516, 8 pages, 2014.
- [28] J. Fernández, M. Rodríguez-Vallejo, and D. P. Piñero, "Tomographic and biomechanical index (TBI) for screening in laser refractive surgery," *Journal of Refractive Surgery*, vol. 35, no. 6, p. 398, 2019.
- [29] S. Koh, R. Ambrósio, R. Inoue, N. Maeda, A. Miki, and K. Nishida, "Detection of subclinical corneal ectasia using corneal tomographic and biomechanical assessments in a Japanese population," *Journal of Refractive Surgery*, vol. 35, no. 6, pp. 383–390, 2019.
- [30] H. Hashemi, R. Ambrósio, R. Vinciguerra et al., "Two-year changes in corneal stiffness parameters after accelerated corneal cross-linking," *Journal of Biomechanics*, vol. 93, pp. 209–212, 2019.
- [31] T. A. Fuchsluger, S. Brettel, G. Geerling, W. Kaisers, and P. Franko Zeitz, "Biomechanical assessment of healthy and keratoconic corneas (with/without crosslinking) using dynamic ultrahigh-speed scheimpflug technology and the relevance of the parameter (A1L–A2L)," *British Journal of Ophthalmology*, vol. 103, no. 4, pp. 558–564, 2019.
- [32] R. Shetty, M. Francis, R. Shroff et al., "Corneal biomechanical changes and tissue remodeling after SMILE and LASIK," *Investigative Ophthalmology & Visual Science*, vol. 58, no. 13, pp. 5703–5712, 2017.
- [33] I. M. Osman, H. A. Helaly, M. Abdalla, and M. A. Shousha, "Corneal biomechanical changes in eyes with small incision lenticule extraction and laser assisted in situ keratomileusis," *BMC Ophthalmology*, vol. 16, p. 123, 2016.
- [34] H. Hashemi, S. Asgari, M. Mortazavi, and R. Ghaffari, "Evaluation of corneal biomechanics after excimer laser corneal refractive surgery in high myopic patients using dynamic scheimpflug technology," *Eye & Contact Lens: Science & Clinical Practice*, vol. 43, no. 6, pp. 371–377, 2017.
- [35] A. Tubtimthong, S. Chansangpetch, N. Ratprasatporn et al., "Comparison of corneal biomechanical properties among axial myopic, nonaxial myopic, and nonmyopic eyes," *BioMed Research International*, vol. 2020, Article ID 8618615, 7 pages, 2020.
- [36] P. Khamar, R. Shetty, R. Vaishnav, M. Francis, R. M. M. A. Nuijts, and A. Sinha Roy, "Biomechanics of LASIK flap and SMILE cap: a prospective, clinical study," *Journal of Refractive Surgery*, vol. 35, no. 5, pp. 324–332, 2019.
- [37] H. B. Wallace, S. L. Misra, S. S. Li, and J. McKelvie, "Biomechanical changes in the cornea following cataract surgery: a prospective assessment with the corneal visualisation scheimpflug Technology," *Clinical & Experimental Ophthalmology*, vol. 47, no. 4, pp. 461–468, 2019.
- [38] K. Hirasawa, S. Nakakura, Y. Nakao et al., "Changes in corneal biomechanics and intraocular pressure following cataract

- surgery," *American Journal of Ophthalmology*, vol. 195, pp. 26–35, 2018.
- [39] A. Leszczynska, K. Moehler, E. Spoerl et al., "Measurement of orbital biomechanical properties in patients with thyroid orbitopathy using the dynamic scheimpflug analyzer (Corvis ST)," *Current Eye Research*, vol. 43, no. 3, pp. 289–292, 2018.
- [40] H. S. Hwang, E. C. Kim, M. S. Kim, and S. W. Yang, "A novel method for quantifying the biomechanical parameters of orbital soft tissue using a corneal dynamic scheimpflug analyser: a retrospective study," *BMC Ophthalmology*, vol. 19, no. 1, p. 53, 2019.
- [41] C. Dorrnsoro, D. Pascual, P. Pérez-Merino, S. Kling, and S. Marcos, "Dynamic OCT measurement of corneal deformation by an air puff in normal and cross-linked corneas," *Biomedical Optics Express*, vol. 3, no. 3, pp. 473–487, 2012.
- [42] D. Alonso-Caneiro, K. Karnowski, B. J. Kaluzny, A. Kowalczyk, and M. Wojtkowski, "Assessment of corneal dynamics with high-speed swept source optical coherence tomography combined with an air puff system," *Optics Express*, vol. 19, no. 15, pp. 14188–14199, 2011.
- [43] E. Maczynska, K. Karnowski, K. Szulzycki et al., "Assessment of the influence of viscoelasticity of cornea in animal ex vivo model using air-puff optical coherence tomography and corneal hysteresis," *Journal of Biophotonics*, vol. 12, no. 2, Article ID e201800154, 2019.
- [44] E. Maczynska, J. Rzeszewska-Zamiara, A. Jimenez Villar, M. Wojtkowski, B. J. Kaluzny, and I. Grulkowski, "Air-puff-Induced dynamics of ocular components measured with optical biometry," *Investigative Ophthalmology & Visual Science*, vol. 60, no. 6, pp. 1979–1986, 2019.
- [45] S. H. Yun and D. Chernyak, "Brillouin microscopy," *Current Opinion in Ophthalmology*, vol. 29, no. 4, pp. 299–305, 2018.
- [46] G. Scarcelli and S. H. Yun, "Confocal Brillouin microscopy for three-dimensional mechanical imaging," *Nature Photonics*, vol. 2, no. 1, pp. 39–43, 2008.
- [47] P. Shao, A. M. Eltony, T. G. Seiler et al., "Spatially-resolved Brillouin spectroscopy reveals biomechanical abnormalities in mild to advanced keratoconus in vivo," *Scientific Reports*, vol. 9, no. 1, p. 7467, 2019.
- [48] G. Scarcelli, S. Besner, R. Pineda, P. Kalout, and S. H. Yun, "In vivo biomechanical mapping of normal and keratoconus corneas," *JAMA Ophthalmology*, vol. 133, no. 4, pp. 480–482, 2015.
- [49] T. G. Seiler, P. Shao, A. Eltony, T. Seiler, and S.-H. Yun, "Brillouin spectroscopy of normal and keratoconus corneas," *American Journal of Ophthalmology*, vol. 202, pp. 118–125, 2019.
- [50] J. N. Webb, J. P. Su, and G. Scarcelli, "Mechanical outcome of accelerated corneal crosslinking evaluated by Brillouin microscopy," *Journal of Cataract & Refractive Surgery*, vol. 43, no. 11, pp. 1458–1463, 2017.
- [51] J. N. Webb, E. Langille, F. Hafezi, J. B. Randleman, and G. Scarcelli, "Biomechanical impact of localized corneal cross-linking beyond the irradiated treatment area," *Journal of Refractive Surgery*, vol. 35, no. 4, pp. 253–260, 2019.
- [52] P. Shao, T. G. Seiler, A. M. Eltony et al., "Effects of corneal hydration on Brillouin microscopy in vivo," *Investigative Ophthalmology & Visual Science*, vol. 59, no. 7, pp. 3020–3027, 2018.
- [53] A. M. Eltony, F. Clouser, P. Shao, R. Pineda, and S.-H. Yun, "Brillouin microscopy visualizes centralized corneal edema in Fuchs endothelial dystrophy," *Cornea*, vol. 39, no. 2, pp. 168–171, 2020.
- [54] J. B. Randleman, J. P. Su, and G. Scarcelli, "Biomechanical changes after LASIK flap creation combined with rapid cross-linking measured with Brillouin microscopy," *Journal of Refractive Surgery*, vol. 33, no. 6, pp. 408–414, 2017.
- [55] A. Denoyer, X. Ricaud, C. Van Went, A. Labbé, and C. Baudouin, "Influence of corneal biomechanical properties on surgically induced astigmatism in cataract surgery," *Journal of Cataract & Refractive Surgery*, vol. 39, no. 8, pp. 1204–1210, 2013.
- [56] W.-S. Kim and J.-M. Jo, "Corneal hydration affects ablation during laser in situ keratomileusis surgery," *Cornea*, vol. 20, no. 4, pp. 394–397, 2001.
- [57] J. L. B. Ramos, Y. Li, and D. Huang, "Clinical and research applications of anterior segment optical coherence tomography - a review," *Clinical & Experimental Ophthalmology*, vol. 37, no. 1, pp. 81–89, 2009.
- [58] B. J. Thomas, A. Galor, A. A. Nanji et al., "Ultra high-resolution anterior segment optical coherence tomography in the diagnosis and management of ocular surface squamous neoplasia," *The Ocular Surface*, vol. 12, no. 1, pp. 46–58, 2014.
- [59] R. M. Werkmeister, S. Sapeta, D. Schmidl et al., "Ultrahigh-resolution OCT imaging of the human cornea," *Biomedical Optics Express*, vol. 8, no. 2, pp. 1221–1239, 2017.
- [60] R. M. Werkmeister, A. Alex, S. Kaya et al., "Measurement of tear film thickness using ultrahigh-resolution optical coherence tomography," *Investigative Ophthalmology & Visual Science*, vol. 54, no. 8, pp. 5578–5583, 2013.
- [61] V. Aranha Dos Santos, L. Schmetterer, M. Gröschl et al., "In vivo tear film thickness measurement and tear film dynamics visualization using spectral domain optical coherence tomography," *Optics Express*, vol. 23, no. 16, pp. 21043–21063, 2015.
- [62] V. A. Dos Santos, L. Schmetterer, G. J. Triggs et al., "Super-resolved thickness maps of thin film phantoms and in vivo visualization of tear film lipid layer using OCT," *Biomedical Optics Express*, vol. 7, no. 7, pp. 2650–2670, 2016.
- [63] A. M. Bata, K. J. Witkowska, P. A. Wozniak et al., "Effect of a matrix therapy agent on corneal epithelial healing after standard collagen cross-linking in patients with keratoconus," *JAMA Ophthalmology*, vol. 134, no. 10, pp. 1169–1176, 2016.
- [64] A. Pantalon, M. Pfister, V. Aranha Dos Santos et al., "Ultrahigh-resolution anterior segment optical coherence tomography for analysis of corneal microarchitecture during wound healing," *Acta Ophthalmologica*, vol. 97, no. 5, pp. e761–e771, 2019.
- [65] C. A. Medina, T. Plesec, and A. D. Singh, "Optical coherence tomography imaging of ocular and periocular tumours," *British Journal of Ophthalmology*, vol. 98, no. 2, pp. ii40–ii46, 2014.
- [66] M. A. Shousha, C. L. Karp, A. P. Canto et al., "Diagnosis of ocular surface lesions using ultra-high-resolution optical coherence tomography," *Ophthalmology*, vol. 120, no. 5, pp. 883–891, 2013.
- [67] L. M. Vajzovic, C. L. Karp, P. Haft et al., "Ultra high-resolution anterior segment optical coherence tomography in the evaluation of anterior corneal dystrophies and degenerations," *Ophthalmology*, vol. 118, no. 7, pp. 1291–1296, 2011.
- [68] M. A. Shousha, V. L. Perez, J. Wang et al., "Use of ultra-high-resolution optical coherence tomography to detect in vivo characteristics of descemet's membrane in fuchs' dystrophy," *Ophthalmology*, vol. 117, no. 6, pp. 1220–1227, 2010.
- [69] Z. Xu, J. Jiang, C. Yang et al., "Value of corneal epithelial and bowman's layer vertical thickness profiles generated by

- UHR-OCT for sub-clinical keratoconus diagnosis,” *Scientific Reports*, vol. 6, p. 31550, 2016.
- [70] R. Yadav, R. Kottaiyan, K. Ahmad, and G. Yoon, “Epithelium and bowman’s layer thickness and light scatter in keratoconic cornea evaluated using ultrahigh resolution optical coherence tomography,” *Journal of Biomedical Optics*, vol. 17, no. 11, Article ID 116010, 2012.
- [71] V. A. d. Santos, L. Schmetterer, H. Stegmann et al., “CorneaNet: fast segmentation of cornea OCT scans of healthy and keratoconic eyes using deep learning,” *Biomedical Optics Express*, vol. 10, no. 2, pp. 622–641, 2019.
- [72] X. Yao, K. Devarajan, R. M. Werkmeister et al., “In vivo corneal endothelium imaging using ultrahigh resolution OCT,” *Biomedical Optics Express*, vol. 10, no. 11, pp. 5675–5686, 2019.
- [73] S. Zarei-Ghanavati, C. Betancurt, A. M. Mas et al., “Ultra high resolution optical coherence tomography in boston type I keratoprosthesis,” *Journal of Ophthalmic & Vision Research*, vol. 10, no. 1, pp. 26–32, 2015.
- [74] S. K. Wagner, D. J. Fu, L. Faes et al., “Insights into systemic disease through retinal imaging-based oculomics,” *Translational Vision Science & Technology*, vol. 9, no. 2, 2020.
- [75] U. Schmidt-Erfurth, A. Sadeghipour, B. S. Gerendas, S. M. Waldstein, and H. Bogunović, “Artificial intelligence in retina,” *Progress in Retinal and Eye Research*, vol. 67, pp. 1–29, 2018.
- [76] R. Kapoor, S. P. Walters, and L. A. Al-Aswad, “The current state of artificial intelligence in ophthalmology,” *Survey of Ophthalmology*, vol. 64, no. 2, pp. 233–240, 2019.
- [77] D. S. W. Ting, A. Y. Lee, and T. Y. Wong, “An ophthalmologist’s guide to deciphering studies in artificial intelligence,” *Ophthalmology*, vol. 126, no. 11, pp. 1475–1479, 2019.
- [78] R. G. Mahesh Kumar, “Computer-aided diagnosis of anterior segment eye abnormalities using visible wavelength image analysis based machine learning,” *Journal of Medical Systems*, vol. 42, no. 7, p. 128, 2018.
- [79] B. T. Lopes, I. C. Ramos, M. Q. Salomão et al., “Enhanced tomographic assessment to detect corneal ectasia based on artificial intelligence,” *American Journal of Ophthalmology*, vol. 195, pp. 223–232, 2018.
- [80] N. Joseph, C. Kolluru, B. A. M. Benetz et al., “Quantitative and qualitative evaluation of deep learning automatic segmentations of corneal endothelial cell images of reduced image quality obtained following cornea transplant,” *Journal of Medical Imaging (Bellingham)*, vol. 7, no. 1, Article ID 014503, 2020.
- [81] C. Kolluru, B. A. Benetz, N. Joseph, H. J. Menegay, J. H. Lass, and D. Wilson, “Machine learning for segmenting cells in corneal endothelium images,” *Proceedings of SPIE-The International Society for Optical Engineering*, vol. 10950, 2019.
- [82] J. P. Viguera-Guillen, E.-R. Andrinopoulou, A. Engel et al., “Corneal endothelial cell segmentation by classifier-driven merging of oversegmented images,” *IEEE Transactions on Medical Imaging*, vol. 37, no. 10, pp. 2278–2289, 2018.
- [83] J. P. Viguera-Guillen, J. van Rooij, H. G. Lemij et al., “Convolutional neural network-based regression for biomarker estimation in corneal endothelium microscopy images,” *IEEE Engineering in Medicine and Biology Society*, vol. 2019, pp. 876–881, 2019.
- [84] S. Heinzelmann, M. C. Daniel, P. C. Maier, T. Reinhard, and D. Böhringer, “Automatisierte zellzählung in spenderhornhäuten aus organkultur mittels, “Deep Learning” erreicht hohe Präzision und Genauigkeit,” *Klinische Monatsblätter für Augenheilkunde*, vol. 236, no. 12, pp. 1407–1412, 2019.
- [85] M. Treder, J. L. Laueremann, M. Alnawaiseh, and N. Eter, “Using deep learning in automated detection of graft detachment in Descemet membrane endothelial keratoplasty: a pilot study,” *Cornea*, vol. 38, no. 2, pp. 157–161, 2019.
- [86] X. Chen, J. Graham, M. A. Dabbah, I. N. Petropoulos, M. Tavakoli, and R. A. Malik, “An automatic tool for quantification of nerve fibers in corneal confocal microscopy images,” *IEEE Transactions on Biomedical Engineering*, vol. 64, no. 4, pp. 786–794, 2017.
- [87] B. M. Williams, D. Borroni, R. Liu et al., “An artificial intelligence-based deep learning algorithm for the diagnosis of diabetic neuropathy using corneal confocal microscopy: a development and validation study,” *Diabetologia*, vol. 63, no. 2, pp. 419–430, 2020.
- [88] S. Al-Fahdawi, R. Qahwaji, A. S. Al-Waisy et al., “A fully automatic nerve segmentation and morphometric parameter quantification system for early diagnosis of diabetic neuropathy in corneal images,” *Computer Methods and Programs in Biomedicine*, vol. 135, pp. 151–166, 2016.
- [89] X. Wu, Y. Tao, Q. Qiu, and X. Wu, “Application of image recognition-based automatic hyphae detection in fungal keratitis,” *Australasian Physical & Engineering Sciences in Medicine*, vol. 41, no. 1, pp. 95–103, 2018.
- [90] Z. Liu, Y. Shi, P. Zhan et al., “Automatic corneal ulcer segmentation combining Gaussian mixture modeling and Otsu method,” *IEEE Engineering in Medicine and Biology Society*, vol. 2019, pp. 6298–6301, 2019.
- [91] H. Stegmann, R. M. Werkmeister, M. Pfister, G. Garhöfer, L. Schmetterer, and V. A. dos Santos, “Deep learning segmentation for optical coherence tomography measurements of the lower tear meniscus,” *Biomedical Optics Express*, vol. 11, no. 3, pp. 1539–1554, 2020.
- [92] E. Ouabida, A. Essadique, and A. Bouzid, “Automated segmentation of ophthalmological images by an optical based approach for early detection of eye tumor growing,” *Physica Medica*, vol. 48, pp. 37–46, 2018.
- [93] X. Liu, J. Jiang, K. Zhang et al., “Localization and diagnosis framework for pediatric cataracts based on slit-lamp images using deep features of a convolutional neural network,” *PLoS One*, vol. 12, no. 3, Article ID e0168606, 2017.
- [94] J.-J. Yang, J. Li, R. Shen et al., “Exploiting ensemble learning for automatic cataract detection and grading,” *Computer Methods and Programs in Biomedicine*, vol. 124, pp. 45–57, 2016.
- [95] X. Wu, Y. Huang, Z. Liu et al., “Universal artificial intelligence platform for collaborative management of cataracts,” *The British Journal of Ophthalmology*, vol. 103, no. 11, pp. 1553–1560, 2019.
- [96] T. Cui, Y. Wang, S. Ji et al., “Applying machine learning techniques in nomogram prediction and analysis for SMILE treatment,” *American Journal of Ophthalmology*, vol. 210, pp. 71–77, 2020.

Research Article

Comparison of the Stability of Two Intraocular Lenses in Primary Angle-Closure Glaucoma after Phacoemulsification

Chang Zhang,¹ Meng Zhang ,² Bing Zhang ,¹ Shanhong Wang ,¹ and Yuhong Wang ³

¹Eye Department, Tongde Hospital of Zhejiang Province, No. 234 Gucai Road, Hangzhou, Zhejiang Province, China

²Glaucoma Department, Eye Hospital of Zhejiang Province, No. 270 West College Road, Lucheng District, Wenzhou, Zhejiang Province, China

³Xiamen University Affiliated Xiamen Eye Center, 336 Xiahe Road, Siming District, Xiamen, Fujian Province, China

Correspondence should be addressed to Yuhong Wang; wangyuhong654@163.com

Received 1 May 2020; Revised 20 October 2020; Accepted 3 November 2020; Published 16 November 2020

Academic Editor: Karim Mohamed Noriega

Copyright © 2020 Chang Zhang et al. This is an open access article distributed under the Creative Commons Attribution License, which permits unrestricted use, distribution, and reproduction in any medium, provided the original work is properly cited.

Objective. To observe the stability of intraocular lenses (IOLs) in primary angle-closure glaucoma by ultralong scan depth spectral-domain optical coherence tomography (UL-OCT) after phacoemulsification. **Methods.** A prospective, randomized study. 73 patients (82 eyes) with primary closed-angle glaucoma and age-related cataract were included in the study. 42 eyes were implanted with ZCB00, while 40 eyes were implanted with Softec HD after phacoemulsification. The tilt, decentration, and space between IOL and posterior capsule (IOL-PC space) were analyzed using UL-OCT at 1 week, 1 month, and 3 months after surgery. The intergroup difference was compared with the paired *t*-test. **Result.** The difference of decentration and tilt was not statistically significant (both $P > 0.05$) both in the horizontal and vertical positions at 1 week, 1 month, and 3 months postoperatively. The horizontal IOL-PC space is $0.111 \pm 0.091 \text{ mm}^2$, $0.044 \pm 0.066 \text{ mm}^2$, and $0.055 \pm 0.055 \text{ mm}^2$ in the Softec HD group and $0.458 \pm 0.488 \text{ mm}^2$, $0.497 \pm 0.363 \text{ mm}^2$, and $0.492 \pm 0.441 \text{ mm}^2$ in the ZCB00 group. The vertical IOL-PC space is $0.102 \pm 0.061 \text{ mm}^2$, $0.037 \pm 0.052 \text{ mm}^2$, and $0.053 \pm 0.079 \text{ mm}^2$ in the Softec HD group and $0.692 \pm 0.815 \text{ mm}^2$, $0.510 \pm 0.415 \text{ mm}^2$, and $0.691 \pm 0.635 \text{ mm}^2$ in the ZCB00 group. The difference was statistically significant ($P < 0.05$) both in the horizontal and vertical positions except for the first week on the horizon. The Softec HD group is smaller than the ZCB00 group. **Conclusion.** There is no difference in the stability of the IOL although the IOL-PC space is different. The thickness of IOL may affect the IOL-PC space.

1. Introduction

Primary angle-closure glaucoma (PACG) is the most common type of glaucoma in the clinic. The anatomical structures such as shortness of the axial eye length, shallow anterior chamber, increased thickness, and curvature of the crystalline lens were different from cataract [1]. Most of the patients are combined with cataract and phacoemulsification which can relieve pupillary block. At present, there is no intraocular lens designed for glaucoma patients and no report on the selection of IOL in relevant research. However, the stability of IOL in the capsular bag is crucial for patients in visual quality [2]. The application of ultralong scan depth

spectral-domain optical coherence tomography (UL-OCT) makes the state of IOL in the capsular bag clear. In this study, UL-OCT was used to measure the decentration, tilt, and IOL-PC space of IOL and analyze the factors for the better selection of IOL in the clinic.

2. Materials and Methods

A total of 82 eyes (73 patients) with PACG were randomly divided into 2 groups. Randomization was done using computer-generated tables (Microsoft Excel; Microsoft Corporation, Redmond, Washington). ZCB00 was performed in 42 eyes (37 patients), and Softec HD was

performed in 40 eyes (36 patients) of patients who visited the Eye Hospital, Wenzhou Medical University, from May 2017 to May 2019 (Table 1).

Each patient has undergone a complete ophthalmological evaluation. Patients with other eye and systemic diseases, such as high myopia, uveitis, retinal diseases, corneal disease, and previous corneal or intraocular surgery, were excluded from the study. The study protocol was approved by the Zhejiang Eye Hospital Ethics Committee (another name of Zhejiang Eye Hospital is Eye Hospital, Wen Zhou Medical University) and adhered to the Declaration of Helsinki. All of the participants signed an informed consent form.

The Softec HD group was implanted with one-piece aspherical IOL (Softec HD, Lenstec, USA), which is a one-piece, biaspheric, square edge, 12 mm diameter, hydrophilic acrylic IOL. The ZCB00 group was implanted with one-piece aspherical IOL (ZCB00, AMO, USA), which is a plate-haptic, aspheric surface, 13 mm diameter, square edge hydrophobic acrylate IOL.

Phacoemulsification was performed by one experienced surgeon under topical anesthesia with a 3.2 mm clear corneal incision. A 4.5 mm capsulorhexis, centered on the dilated pupil, was performed with the aid of capsulorhexis forceps. The incision of the right eyes was on the temporal side while the left eyes on the paranasal side. The residual viscoelastic was absorbed completely.

A custom spectrometer with a unique design was developed to achieve an experimental scan depth of 7.2 mm in air based on the technology of spectral-domain OCT. The modification includes a transmission grating and a line scan CCD camera (Aviiva SM2 CL 2010, 2048 pixels; Atmel, San Jose, CA). X - Y cross-aiming was applied to align the UL-OCT scanning position necessary to image the entire IOL in the capsule and the posterior capsule (PC). The UL-OCT has an approximately 6- μ m axial resolution and a scan width up to 20 mm. The accuracy and repeatability of the instrument have been confirmed in previous works [3, 4]. The ZCB00 IOL and Softec HD IOL are shown in Figure 1.

Follow-up assessments were performed at 1 week and 1 and 3 months postoperatively. The horizontal and vertical position of IOL was performed. Then, using Image-pro plus version 6.0, the OCT images were analyzed. The tilt angle and decentration length were measured according to the method by Alberto de Castro et al. [5, 6]. The method was based on the Scheimpflug system: IOL decentration is obtained from the distance between the IOL center and the pupillary axis. Total decentration, determined by trigonometry analysis, shows the magnitude of the result vector of horizontal and vertical decentration [7]. The tilt was calculated by dividing the slope of IOL by the slope of the limbus [8]. The OCT images were taken as in Figure 1, the curve of the surface of the IOL and the PC was drawn, and then it was substituted into the two-dimensional coordinate plane to get the scatter plot as in Figure 2. The area between the IOL and posterior capsular region was evaluated through the function of the software [9].

Statistical analyses were performed to compare the differences in the biometric data between the ZCB00 group

TABLE 1: The age and gender distribution.

	Softec HD group	ZCB00 group	<i>P</i> value
Age (year)	65.34 \pm 11.32	68.25 \pm 10.68	> 0.05
Gender (M:F)	13:24	11:25	> 0.05

and the Softec HD group using SPSS 19.0. The Kolmogorov-Smirnov test was used to confirm the normal distribution. The tilt and decentration were compared with the paired t -test. The IOL-PC space was compared with the rank sum test. Differences were considered statistically significant when the P value was less than 0.05.

3. Results

Table 2 shows the postoperative visual acuity results in the two IOL groups. At the 3-month visit, no significant difference was found in corrected-distance visual acuity (CDVA), uncorrected-distance visual acuity (UDVA), and axial length between the groups. The thickness of IOL was significantly different between the two groups. Softec HD was thicker than ZCB00.

The total decentration is 0.182 \pm 0.054 mm, 0.232 \pm 0.081 mm, and 0.183 \pm 0.089 mm in the Softec HD group and 0.311 \pm 0.212 mm, 0.214 \pm 0.111 mm, and 0.228 \pm 0.156 mm in the ZCB00 group at 1 week, 1 month, and 3 months postoperatively. The difference was not statistically significant.

The horizontal tilt is 1.65 \pm 6.23°, 0.45 \pm 4.29°, and -1.76 \pm 7.37° in the Softec HD group and 0.05 \pm 6.21°, 0.34 \pm 8.51°, and -0.17 \pm 6.30° in the ZCB00 group at 1 week, 1 month, and 3 months postoperatively. The vertical tilt is 3.67 \pm 6.61°, -0.94 \pm 4.73°, and 0.54 \pm 9.51° in the Softec HD group and -0.73 \pm 7.33°, 0.32 \pm 7.20°, and 0.07 \pm 5.52° in the ZCB00 group. The difference was not statistically significant both in the horizontal and vertical positions.

Table 3 shows the horizontal IOL-PC space in the two study groups. The difference was statistically significant ($P < 0.05$) except for the first week. Table 4 shows the vertical IOL-PC space. The difference was statistically significant ($P < 0.05$). The IOL-PC space in the Softec HD group is smaller than the space in the ZCB00 group (Figure 3).

4. Discussion

The quality of visual acuity will be improved without decentration and tilt [10]. However, a previous study had reported that IOL tilt was more extensive in the eyes with glaucoma than normal cataract [11]. The increased thickness, curvature of the crystalline lens, and a more anterior lens position indicate that lens capsule configuration is also abnormal in eyes with angle-closure glaucoma. It is therefore reasonable to conclude that the implanted IOL is apt to be tilted or decentered in eyes with CAG. Another study found AL is negatively correlated with crystalline lens tilt, which means IOLs are more prone to tilt in patients with a short AL [12]. The possible explanation is that the crystalline lens is more likely to tilt in the crowded intraocular space. In addition, Chen et al. [13] have found that the thicker lens was

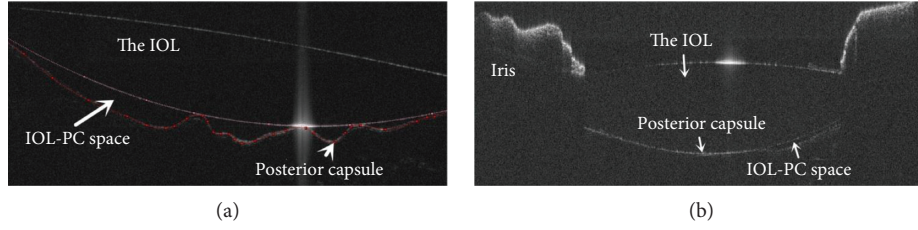


FIGURE 1: The UL-OCT detects the boundaries of intraocular lens (IOL), posterior capsule (PC), and the space between IOL and posterior capsule (IOL-PC space). (a) The ZCB00 IOL. (b) The Softec HD IOL. UL-OCT =ultralong scan depth spectral-domain optical coherence tomography.

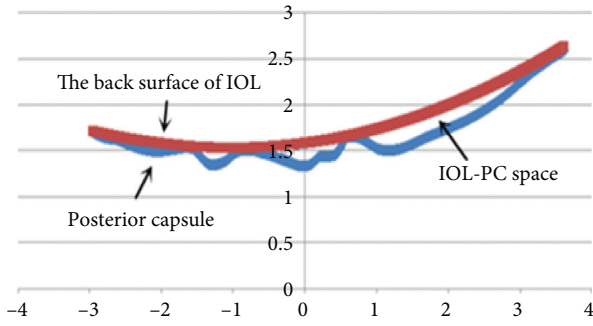


FIGURE 2: The scatter plot.

TABLE 2: Postoperative results in the two study groups.

	Softec HD	ZCB00	<i>P</i>
UDVA (logMAR)	0.18 ± 0.13	0.21 ± 0.09	0.28
CDVA (logMAR)	0.10 ± 0.09	0.13 ± 0.12	0.24
Axial length (mm)	22.84 ± 1.92	22.92 ± 2.11	0.32
Thickness of IOL (mm)	1.47 ± 0.355	1.19 ± 0.287	0.03

CDVA = corrected-distance visual acuity; UDVA = uncorrected-distance visual acuity; logMAR = logarithm of the minimum angle of resolution.

TABLE 3: Horizontal IOL-PC space (mm^2) postoperative.

	1 week	1 month	3 months	<i>P</i> value
Softec (mm^2)	0.11 ± 0.091	0.044 ± 0.066	0.055 ± 0.055	0.189
ZCB00 (mm^2)	0.458 ± 0.488	0.497 ± 0.363	0.492 ± 0.441	0.823
<i>P</i> value	0.15	0.002	0.001	

TABLE 4: Vertical IOL-PC space (mm^2) postoperative.

	1 week	1 month	3 months	<i>P</i> value
Softec (mm^2)	0.102 ± 0.061	0.037 ± 0.052	0.053 ± 0.079	0.035
ZCB00 (mm^2)	0.692 ± 0.815	0.510 ± 0.415	0.691 ± 0.635	0.997
<i>P</i> value	0.013	0.001	0.006	

strongly correlated with larger decentration. Therefore, the decentration and tilt in PACG may be different from cataract, so the research may have a reference value for the choice of IOL in clinical work.

We have found that the IOL-PC space of Softec HD, which is constituted by hydrophilic acrylate, is significantly smaller than that of ZCB00 made of hydrophobic acrylate material. The finding is different from some research: hydrophobic acrylates have better biocompatibility, which can make the optical part of IOL close to the posterior capsule and reduce the incidence of posterior cataract and the shrinkage of the capsule. However, the hydrophilic acrylate material could not be closely attached to the posterior capsule, which provided space for LECs growth and proliferation [9]. The reasons may be as follows: the thickness of IOL is determined by the material and the diopter. In this experiment, the average thickness of Softec HD is 1.47 ± 0.355 mm and ZCB00 is 1.19 ± 0.287 mm. The difference is statistically significant. If the IOL is assumed to be a standard ellipsoid, according to the ellipse volume formula $V = 4/3\pi abc$ (a , b , and c , respectively, represent half of each axis), where the length of a and b takes the radius of the optical surface and c takes half of the thickness, then it can be inferred that the volume of Softec HD is about 50.87 ± 12.28 mm^3 and ZCB00 is about 44.83 ± 10.81 mm^3 . Takuhei et al. have reported that the lens thickness is positively correlated with axial length [14]. Another study found that equatorial capsular bag diameter is correlated with axial length [15]. A significant difference in axial length was not found between the study groups, which means a difference in capsular bag size is not a likely reason for the larger IOL-PC space observed in the ZCB00 group. Then, we can speculate that Softec HD with a larger volume fills the capsular bag better. As a result, the IOL-PC space in Softec HD is smaller than ZCB00.

The IOL-PC space on visual function is in agreement with the concept “no space, no cell, no PCO” [16]. Studies have reported that, with increasing severity of PCO, visual acuity and stray light deteriorate [17]. In our study, a thicker IOL could promote the elimination of IOL-PC space. So, we can infer that the incidence of posterior cataract is reduced and vision will be maintained better with a thicker IOL.

There was no statistical difference between the tilt and decentration although the IOL-PC space was significantly different. The result is similar to the research of Katayama et al. [18]: decentration and tilt did not change significantly although the posterior capsular opacity (PCO) value in the hydrophilic group increased significantly with time and was statistically significantly higher than in the hydrophobic group at 18 and 24 months postoperatively in either group.

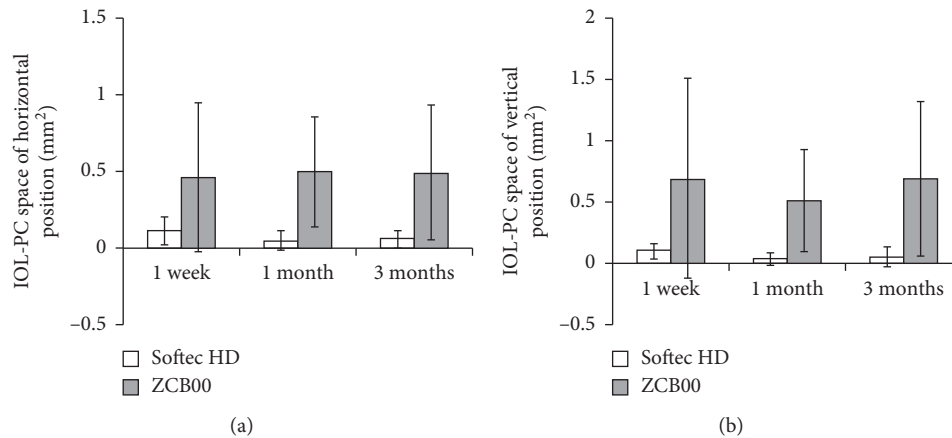


FIGURE 3: Postoperative IOL-PC space (SD) at different time points. Significant difference was found between the horizontal and vertical positions when compared at 1 week, 1 month, and 3 months postoperatively ($P < 0.05$) except for the first week on the horizon.

The reasons may be as follows: first, Modesti et al. [19] considered that the maximum diameter of the lens capsule at any time after cataract surgery was < 12.0 mm, which was smaller than that of the IOLs in this study (12 mm in Softec HD and 13 mm in ZCB00). But, the lens capsule is thicker than the intraocular lens, so the IOL is stuck in the center of the capsule without bound to the posterior capsule tightly. As a result, haptic provides most of the strength for the stability of the IOL. This finding explains that IOLs with a diameter greater than 12 mm were more stable than IOLs with a diameter less than 12 mm [20]. Besides, the two IOL's haptics are made of acrylate, which is soft and firm. When the capsule is contracted, the soft haptic can be compressed independently without transmitting this force to the IOL optics. Therefore, in the case of different IOL-PC space, stability is less affected.

The limitations of this trial were that it was limited by clinical work and only followed up for 3 months. PCO begins three months after surgery, and the long-term stability of IOL in patients with PACG remains unknown. Besides, studies have shown that mathematics can be used based on cross-sectional and sagittal images. Modeling restores the 3D stereo image of the IOL to accurately calculate the maximum tilt and decentration of the IOL [21]. But in clinical work, mathematical modeling requires a lot of time and effort.

In summary, by using UL-OCT, we could clearly observe the IOL and posterior capsule. The objective quantification of thickness demonstrated a correlation with IOL-PC space. Maybe the haptic and diameter of IOL length play a more important role in stability than IOL-PC space. These results suggested that UL-OCT could be used as a powerful method to evaluate the IOL-PC space and the tilt and decentration of IOL.

Data Availability

The data that support the findings of this study are available from the corresponding author upon reasonable request.

Disclosure

The authors alone are responsible for the content and writing of the paper.

Conflicts of Interest

The authors report no conflicts of interest.

Acknowledgments

This work was funded by the Key Laboratory of Myopia, Health Commission, Fudan University.

References

- [1] R. F. Loew, "Aetiology of the anatomical basis for primary angle-closure glaucoma. Biometrical comparisons between normal eyes and eyes with primary angle-closure glaucoma," *British Journal of Ophthalmology*, vol. 54, no. 3, pp. 161–169, 1970.
- [2] R. N. McNeely, E. Pazo, A. Spence et al., "Visual quality and performance comparison between 2 refractive rotationally asymmetric multifocal intraocular lenses," *Journal of Cataract and Refractive Surgery*, vol. 43, no. 8, pp. 1020–1026, 2017.
- [3] M. Shen, L. Cui, M. Li, D. Zhu et al., "Extended scan depth optical coherence tomography for evaluating ocular surface shape," *Journal of Biomedical Optics*, vol. 16, no. 5, Article ID 056007, 2011.
- [4] M. Shen, L. Cui, C. Riley, M. R. Wang, and J. Wang, "Characterization of soft contact lens edge fitting using ultra-high resolution and ultra-thin scan depth optical coherence tomography," *Investigative Ophthalmology and Visual Science*, vol. 52, no. 7, pp. 4091–4097, 2011.
- [5] P.-Y. Chang, C.-Y. Lian, J.-K. Wang, P.-Y. Su, J.-Y. Wang, and S.-W. Chang, "Surgical approach affects intraocular lens decentration," *Journal of the Formosan Medical Association*, vol. 116, no. 3, pp. 177–184, 2017.
- [6] A. D. Castro, P. Rosales, and S. Marcos, "Tilt and decentration of intraocular lenses in vivo from Purkinie and Scheimpflug imaging Validation study," *Journal of Cataract and Refractive Surgery*, vol. 33, no. 3, pp. 418–429, 2007.
- [7] K. Kránitz, K. Miháltz, G. L. Sándor, A. Takacs, M. C. Knorz, and Z. Z. Nagy, "Intraocular lens tilt and decentration

- measured by Scheimpflug camera following manual or femtosecond laser-created continuous circular capsulotomy,” *Journal of Refractive Surgery*, vol. 28, no. 4, pp. 259–263, 2012.
- [8] D. A. Kumar, A. Agarwal, G. Prakash, S. Jacob, Y. Saravanan, and A. Agarwal, “Evaluation of intraocular lens tilt with anterior segment optical coherence tomography,” *American Journal of Ophthalmology*, vol. 151, no. 3, pp. 406–412, 2011.
- [9] S. Yu, C. Lu, and X. Tang, “Application of spectral domain optical coherence tomography to objectively evaluate posterior capsular opacity in vivo,” *Journal of Ophthalmology*, vol. 2018, Article ID 5461784, 9 pages, 2018.
- [10] T. Lawu, K. Mukai, H. Matsushima, and T. Senoo, “Effects of decentration and tilt on the optical performance of 6 aspheric intraocular lens designs in a model eye,” *Journal of Cataract and Refractive Surgery*, vol. 45, no. 5, pp. 662–668, 2019.
- [11] K. Hayashi, H. Hayashi, F. Nakao, and F. Hayashi, “Intraocular lens tilt and decentration after implantation in eyes with glaucoma,” *Journal of Cataract and Refractive Surgery*, vol. 25, no. 11, pp. 1515–1520, 1999.
- [12] L. Wang, R. G. De Souza, M. P. Weikert, and D. D. Koch, “Evaluation of crystalline lens and intraocular lens tilt using a swept-source optical coherence tomography biometer,” *Journal of Cataract and Refractive Surgery*, vol. 45, no. 1, pp. 35–40, 2019.
- [13] X. Chen, X. Gu, W. Wang et al., “Characteristics and factors associated with intraocular lens tilt and decentration after cataract surgery,” *Journal of Cataract and Refractive Surgery*, vol. 46, no. 8, pp. 1126–1131, 2020.
- [14] T. Shoji, N. Kato, S. Ishikawa et al., “Association between axial length and in vivo human crystalline lens biometry during accommodation: a swept-source optical coherence tomography study,” *Japanese Journal of Ophthalmology*, vol. 64, no. 1, pp. 93–101, 2020.
- [15] M. Tehrani, B. H. Dick, F. Krummenauer, G. Pfirrmann, T. Boyle, and B. M. Stoffelns, “Capsule measuring ring to predict capsular bag diameter and follow its course after foldable intraocular lens implantation,” *Journal of Cataract and Refractive Surgery*, vol. 29, no. 11, pp. 2127–2134, 2003.
- [16] D. J. Apple, K. D. Solomon, M. R. Tetz et al., “Posterior capsule opacification,” *Survey of Ophthalmology*, vol. 37, no. 2, pp. 73–116, 1992.
- [17] M. C. J. van Bree, T. J. T. P. van den Berg, and B. L. M. Zijlmans, “Posterior capsule opacification severity, assessed with straylight measurement, as main indicator of early visual function deterioration,” *Ophthalmology*, vol. 120, no. 1, pp. 20–33, 2013.
- [18] Y. Katayama, S. Kobayakawa, H. Yanagawa, and T. Tochikubo, “The relationship between the adhesion characteristics of acrylic intraocular lens materials and posterior capsule opacification,” *Ophthalmic Research*, vol. 39, no. 5, pp. 276–281, 2007.
- [19] M. Modesti, G. Pasqualitto, R. I. Appolloni, and P. Sourdille, “Preoperative and postoperative size and movements of the lens capsular bag: ultrasound biomicroscopy analysis,” *Journal of Cataract and Refractive Surgery*, vol. 37, no. 10, pp. 1775–1784, 2011.
- [20] B. C. Pecorella, R. Khoramnia, L. F. Weber, T. Tandogan, and G. U. Auffarth, “Rotation and decentration of an undersized plate-haptic trifocal toric intraocular lens in an eye with moderate myopia,” *Journal of Cataract and Refractive Surgery*, vol. 42, no. 3, pp. 489–493, 2016.
- [21] L. Lin, W. Ke, Y. Yan et al., “Calculate method of the IOL tilt and decentration based on surface fitting,” *Beijing Biomedical Engineering*, vol. 32, no. 2, pp. 164–168, 2013.

Research Article

Tear Lipid Layer Thickness in Children after Short-Term Overnight Orthokeratology Contact Lens Wear

Li Zeng ^{1,2,3} Zhi Chen ^{1,2,3} Dan Fu,^{1,2,3} Jiaqi Zhou ^{1,2,3} and Xingtao Zhou ^{1,2,3}

¹Department of Ophthalmology and Optometry, Eye and ENT Hospital, Fudan University, Shanghai, China

²NHC Key Laboratory of Myopia, Fudan University, Shanghai, China

³Shanghai Research Center of Ophthalmology and Optometry, Shanghai, China

Correspondence should be addressed to Xingtao Zhou; doctzhouxingtao@163.com

Received 26 June 2020; Revised 5 October 2020; Accepted 15 October 2020; Published 16 November 2020

Academic Editor: Yu Chi Liu

Copyright © 2020 Li Zeng et al. This is an open access article distributed under the Creative Commons Attribution License, which permits unrestricted use, distribution, and reproduction in any medium, provided the original work is properly cited.

Meibomian gland lipid secretion is important to the stability of the tear film and ocular surface comfort. Changes in the tear film's lipid layer thickness (LLT) after orthokeratology treatment may reflect underlying changes to the meibomian gland function. The purpose of this study was to investigate the features of the tear lipid layer in normal children and the effects of short-term orthokeratology treatment. Altogether, 163 myopic children (age: 10.7 ± 1.9 years, 8–15 years; 71 males) with no contact lens use history were enrolled in this study, of whom 56 were successfully fitted with orthokeratology lenses and completed the 1-month study. The tear film's LLT (average, maximum, and minimum) and blinking pattern were measured by a LipiView® interferometer in 163 participants at baseline and in 56 orthokeratology participants at 1 week and 1 month after overnight lens wear. Results show that LLT (average) was 58.09 ± 21.66 nm in Chinese normal children. LLT was significantly correlated with rate of partial blinks at every follow-up (all $p < 0.05$). Compared to baseline, the LLT (average and minimum) and partial blinks (number and rate) at 1 week and 1 month after orthokeratology treatment both significantly increased, and the increase of LLT was correlated with elevation of rate of partial blinks. In conclusion, LLT was shown to be elevated after short-term overnight orthokeratology treatment and was related to change in rate of partial blinks. Further studies are needed to clarify the long-term effect and the underlying mechanism.

1. Introduction

Orthokeratology has been used worldwide since the advent of rigid, gas permeable lens material in the 1990s [1]. The high-Dk lens material combined with a paracentral reverse geometry design has made overnight wear possible and provides wearers with good visual acuity in the daytime [2, 3]. A previous study of over 29,500 contact lens fittings revealed that orthokeratology was gaining popularity over the past decade [4], and another study showed that over 25% of prescribed rigid contact lenses were orthokeratology lenses for children and adolescents, and 47% were for younger children (6–12 years old) [5].

The *Implementation Plan for the Comprehensive Prevention and Control of Childhood and Adolescent Myopia*, issued by the Chinese government in 2018, has made

orthokeratology, amongst other myopia control modalities, even more well-established in China [6]. Therefore, the safety issues associated with the popularity of orthokeratology lens fitting have recently received unprecedented attention.

As the first and foremost protection measure for the cornea, the tear film plays an important role in maintaining safety in contact lens wear by nourishing the cornea with oxygen, clearing the debris accumulated behind the lens, rewetting the ocular surface, and decreasing friction during blinking, etc. Compared with daily wear contact lenses, overnight orthokeratology has an advantage of inducing less disturbance to tear volume during a closed-eye condition by reducing evaporation [7]. Additionally, orthokeratology has been reported to increase daily eye comfort, especially in late afternoon, as compared to soft contact lenses [8]. The impact

of orthokeratology on the tear breakup time, tear volume, and meibomian gland morphology in children after long-term orthokeratology treatment suggested the common safety of orthokeratology for ocular surface health [7, 9]. However, the change in corneal shape following orthokeratology lens wear and its closed-eye wearing modality may impact the tear dynamics and biochemistry accordingly. For example, changes in tear osmolarity, composition, inflammatory mediators, and corneal nerve density after orthokeratology have been reported [10–13]. Considering these mechanical, chemical, or biological impacts, potential change in meibomian gland function in lipid secretion could occur.

Recent development of LipiView® interferometer has enabled us to directly measure lipid layer thickness (LLT) with reasonable accuracy and repeatability, both in normal and dry eye patients [14, 15]. To our knowledge, few studies have investigated the influence of orthokeratology lenses on tear LLT; however, it appears that the average level of LLT in children needs to be considered independently from adults [16, 17]. The current study aimed at evaluating the LLT in a group of normal Chinese children, and the changes in LLT after short-term orthokeratology treatment.

2. Methods

This study was performed with approval from the hospital's institutional review board (trial number: 2015013–3). Informed consent was obtained from all subjects. The whole study was performed in accordance with the Declaration of Helsinki.

This study included two parts. In the first stage, we measured LLT (average, minimum, and maximum) and blinking pattern in 163 asymptomatic participants. In the second stage, 56 of 163 participants accepted orthokeratology treatment, and LLT and blinking pattern in 56 participants were followed up to 1 week and 1 month.

2.1. Participants. Between October 1, 2017, and September 30, 2019, 163 children (71 males, 92 females; age range: 8–15 years; mean age: 10.7 ± 1.9 years) consulting the myopia control clinic of the Fudan University Eye and ENT Hospital, Shanghai, China, were enrolled in this study. No participant had previous contact lens history, dry eye symptoms, or significant meibomian gland dysfunction. They had no systemic diseases or other eye diseases affecting ocular surface health.

2.2. Collection of Ocular Biometrics of 163 Participants at Baseline. Demographic and ocular biometrics data of participants at baseline were collected. It was obtained by reviewing records of participants at regular clinic within 1 month before baseline, including slit lamp examination, spherical and cylindrical refractive error, best corrected distance visual acuity, axial length (IOLmaster 500, Carl Zeiss, Germany), thinnest corneal thickness (Pentacam, Oculus Optikgerate, Wetzlar, Germany), corneal curvature

along the flat meridian (K1), and the steep meridian (K2) (NIDEK RT-5100, Japan).

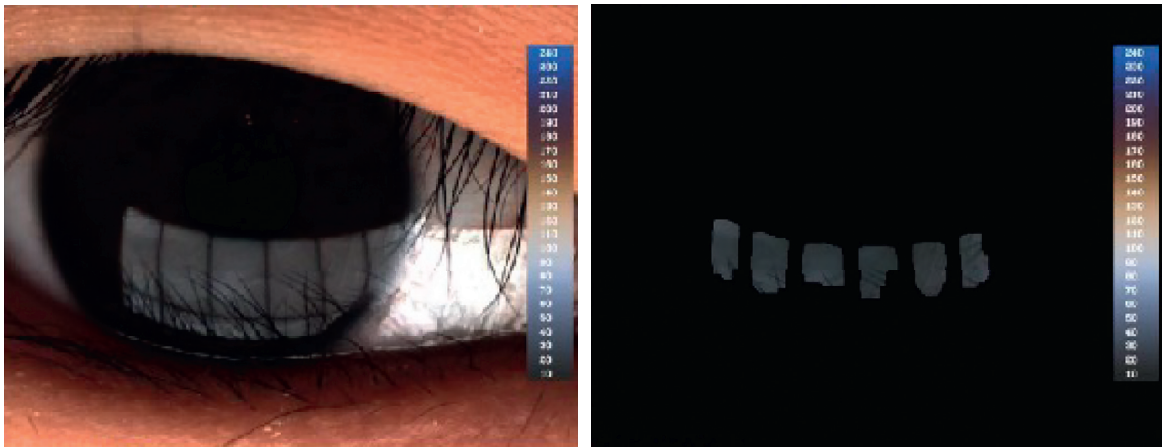
2.3. Orthokeratology Lens Fitting and Wearing of 56 Participants. Among the 163 participants in the clinic, 56 accepted orthokeratology treatment. All orthokeratology lenses were fitted in accordance with the manufacturer's recommendation, demonstrated adequate movement on blink and showed good centration under slit lamp microscope and corneal topography during the trial lens fitting period. Over refraction was then performed with a refractive target being plano. Participants were requested to insert orthokeratology lenses before going to sleep, with a minimum of 8 hours of lens wear each night. Children and their guardians received instructions on how to safely insert and remove the lenses, along with the lens care regimen. Participants in this study did not use additional artificial tears other than routine drops for lens wearing and taking off.

2.4. Follow-Up of Lipid Layer Thickness and Blinks. The LipiView® interferometer (Johnson & Johnson, USA), which measures the LLT (average, minimum, and max) during natural blinking in a noninvasive manner with satisfactory repeatability, was used to evaluate the LLT and blinking pattern (number of blinks, number of partial blinks, and rate of partial blinks). First, 163 normal participants were enrolled. Next, among 163 participants, LLT and blinking pattern of 56 undergoing orthokeratology treatment were followed up to 1 week and 1 month.

All measurements were made in both eyes, and data of the right eye were included for analysis in this study. Duration of measurement on LipiView was 19.1 seconds per round. In this time window, LLT (average, minimum and maximum) was calculated automatically, and the number of blinks and partial blinks were also automatically counted and displayed on the screen (Figure 1). The ambient temperature was controlled between 25 to 30°C, and relative humidity between 50% and 65%. After adjusting the position of the chin and forehead, the participants were instructed to fixate on the internal target, and the camera was then adjusted until the inferior tear meniscus area was clearly in focus. Image capture was obtained with participants blinking naturally. Reliability index (CFactor on-screen) was requested to exceed 0.7, otherwise the measurements would be repeated. The results were output as interferometric color units (ICU), which was equivalent to nanometers (nm). The LipiView® interferometer had an upper cutoff of 100 nm in the measurement of LLT.

2.5. Statistical Analysis. For data of 163 normal participants at baseline, Pearson and Spearman correlation analyses were conducted to investigate the correlation between LLT (average, min, and max) and blink pattern (number of complete blinks, number of partial blinks, and rate of partial blinks). Rate of partial blinks was calculated as follows: number of partial blinks/number of blinks. Correlation of LLT and other parameters including age, sex, spherical and

Eye: OD - capture date: 11/4/2017 8:46:37 AM - lipiview® serial number: 00385



Average LLT: 56 nm
 Maximum LLT: 76 nm @ frame 238
 Minimum LLT: 42 nm @ frame 531

Partial blinks: 14/14
 CFactor: 0.97
 Standard dev: 5

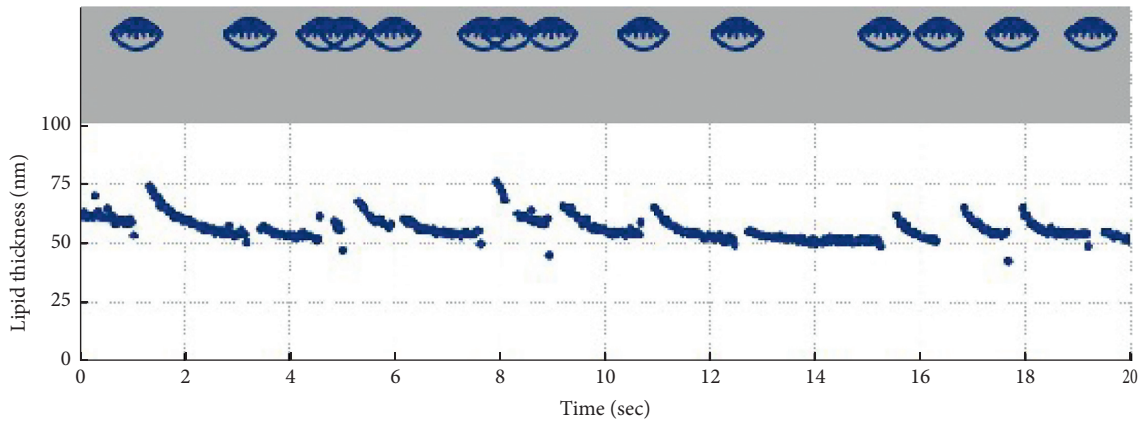


FIGURE 1: Display of LLT and blinking pattern on-screen of LipiView® interferometer. The result of LLT (average, minimum, and max) of a participant on the screen of LipiView. CFactor: reliability index, which needs to be above 0.7. Partial blinks: before slash is number of partial blinks, and after slash is number of all blinks during 19.1 s.

cylindrical refractive error, cylindrical axis, axial length, thinnest corneal thickness, and corneal curvature at the flat meridian (K1) and steep meridian (K2) was also analyzed.

Correlation analysis of lipid layer thickness and blinking pattern was conducted for data of 56 participants undergoing orthokeratology treatment at every follow-up. Single-factor repeated measure ANOVA was used to analyze the change in lipid layer thickness (average, minimum, and max) and blinking pattern (number of blinks, number of partial blinks, and rate of partial blinks) 1 week and 1 month after orthokeratology treatment. Repeated measure correlation (rmcorr) was used to analyze the correlation between change in lipid layer thickness and change in blinking pattern after orthokeratology treatment [18].

Statistical significance was defined as a p value < 0.05 . SPSS software 22.0 (IBM Corp., Armonk, NY, USA) and R (4.0.2) were used.

3. Results

3.1. LLT of 163 Participants and the Correlation between LLT and Other Variables. At baseline (baseline data of participants are presented in Tables 1 and 2), the average tear LLT (average, max, and min) of 163 participants was 58.09 ± 21.66 nm ($n = 163$), 82.14 ± 20.12 nm ($n = 154$), and 46.37 ± 20.04 nm ($n = 154$), respectively.

Correlation analysis of LLT and blinking pattern is presented in Table 1. Number of partial blinks and rate of partial blinks were correlated with LLT (average, maximum, and minimum).

The results revealed that the tear LLT (average) was significantly correlated with age ($r = 0.17$, $p = 0.03$), axial length ($r = 0.18$, $p = 0.02$), thinnest corneal thickness ($r = -0.21$, $p = 0.01$), K1 ($r = -0.20$, $p = 0.01$), and K2 ($r = -0.19$, $p = 0.02$) (Table 2).

TABLE 1: LLT (average, minimal, and max) and blinking pattern of 163 eyes at baseline.

	LLT average (nm) 58.09 ± 21.66, n = 163	LLT max (nm) 82.14 ± 20.12, n = 154	LLT min (nm) 46.37 ± 20.04, n = 154
Blinks 10.13 ± 4.50, n = 154	r = -0.05, p = 0.52, n = 154	r = -0.16, p = 0.84, n = 154	r = -0.15, p = 0.07, n = 154
Partial blinks 5.55 ± 4.36, n = 154	r = 0.18*, p = 0.027, n = 154	r = 0.22*, p = 0.006, n = 154	r = 0.19*, p = 0.02, n = 154
Rate of partial blinks 0.55 ± 0.33, n = 154	r = 0.26*, p = 0.001, n = 154	r = 0.29*, p < 0.001, n = 154	r = 0.32*, p < 0.001, n = 154

LLT: lipid layer thickness. LLT average: average value of LLT during 19.1-second measurement. LLT max: maximum value of LLT during 19.1-second measurement. LLT min: minimum value of LLT during 19.1-second measurement. Blink: number of blinks during 19.1s. Partial blink: number of partial blinks during 19.1s. r: relative coefficient. P: significance. n: number.

TABLE 2: Correlation of LLT (average) and other clinical variables of 163 eyes at baseline.

	LLT average (nm)	Age (years)	Sex	Sph (D)	Cylin (D)	Axis	BCDVA (logMAR)	Axial length (mm)	K1 (D)	K2 (D)	TCT (um)
Number of cases (n)	163	163	163	155	155	106	116	157	153	154	149
Average	58.09	10.67	—	-2.86	-0.35	79.15	1.06	24.77	42.70	43.82	544.89
Standard deviation	21.66	1.89	—	1.18	0.47	83.89	0.10	0.83	1.27	1.41	28.07
Association with LLT average (nm)	r	0.17*	-0.08	-0.00	-0.05	0.04	0.03	0.18*	0.20*	-0.19*	-0.21*
	p	0.03	0.33	0.97	0.53	0.66	0.76	0.02	0.02	0.02	0.01
	n	163	163	155	155	106	116	157	153	154	149

LLT average: average value of LLT during 19.1-second measurement. Sph: spherical power. Cylin: cylindrical power. BCDVA: best corrected distance visual acuity. K1: flat corneal curvature. K2: steep corneal curvature. TCT: thinnest corneal thickness. Blink: number of blinks during 19.1 s. Partial blink: number of partial blinks during 19.1 s. r: relative coefficient. P: significance. n: number.

3.2. Follow-Up of LLT and Blinking in 56 Participants after Orthokeratology Treatment. All 56 participants who underwent orthokeratology treatment showed an uneventful course, with daily uncorrected visual acuity higher than 0.8 on Snellen chart and SE being ±0.5D of plano. All 56 participants finished both the 1-week and 1-month follow-up visits. Grade one or less corneal staining was found at 1-week follow-up. No complications were observed during the 1-month follow-up.

3.2.1. Correlation between LLT and Blinking Pattern at Every Follow-Up. LLT and blinking pattern of 56 participants at every follow-up are presented in Table 3. Correlation between LLT and blinking pattern at baseline, 1 week, and 1 month was analyzed, respectively (Table 3). Correlation analysis of LLT and other clinical variables of 56 OK participants at baseline are presented in Table 4.

3.2.2. Change of LLT after Orthokeratology Treatment. ANOVA results of LLT (average, minimum, and maximum) at baseline, 1 week, and 1 month are presented in Table 5 and Figure 2.

LLT (average) significantly changed over time ($p = 0.028$), with pairwise comparison showing a significant difference between 1 week and baseline ($p = 0.017$) and between 1 month and baseline ($p = 0.025$). No statistical difference was detected between the 1-week and 1-month follow-up visits ($p = 0.699$) (Table 5, Figure 2).

LLT (minimum) also significantly changed over time ($p = 0.024$), with pairwise comparison showing a significant difference between 1 week and baseline ($p = 0.022$) and

between 1 month and baseline ($p = 0.012$). No statistical difference was detected between the 1-week and 1-month follow-up visits ($p = 0.864$) (Table 5, Figure 2).

No significant change of LLT (maximum) at 1 week or 1 month was detected ($p = 0.447$) (Table 5, Figure 2).

LLT: lipid layer thickness. average: average value of LLT. min: minimum value of LLT. max: maximum value of LLT. ANOVA: single-factor repeated measure analysis of variance. LSD: LSD paired *t*-test. n: number. P: significance.

3.2.3. Change of Blinking Pattern after Orthokeratology Treatment. ANOVA results of blinking pattern (number of blinks, number of partial blinks, and rate of partial blinks) at baseline, 1 week, and 1 month are presented in Table 6 and Figure 3.

No significant change of number of blinks was detected over time ($p = 0.727$), with pairwise comparison showing no significant difference in any pair (Table 6, Figure 3).

Partial blinks significantly changed over time ($p = 0.037$), with pairwise comparison showing a significant difference between 1 week and baseline ($p = 0.012$). No statistical difference was detected between 1 month and baseline ($p = 0.417$) or between the 1-week and 1-month follow-up visits ($p = 0.094$) (Table 6, Figure 3).

Rate of partial blinks significantly changed over time ($p = 0.008$), with pairwise comparison showing a significant difference between 1 week and baseline ($p < 0.001$). No statistical difference was detected between 1 month and baseline ($p = 0.056$) or between the 1-week and 1-month follow-up visits ($p = 0.366$) (Table 6, Figure 3).

TABLE 3: LLT (average, minimal, and max) and blinking pattern of 56 OK eyes at baseline.

	Baseline		
	LLT average (nm) 54.29 ± 22.13, n = 56	LLT max (nm) 80.36 ± 20.47, n = 56	LLT min (nm) 42.30 ± 19.66, n = 56
Blinks 10.89 ± 4.79, n = 56	r = -0.14, p = 0.45, n = 56	r = -0.10, p = 0.45, n = 56	r = -0.18, p = 0.19, n = 56
Partial blinks 5.70 ± 5.06, n = 56	r = 0.18, p = 0.19, n = 56	r = 0.13, p = 0.35, n = 56	r = 0.17, p = 0.20, n = 56
Rate of partial blinks 0.51 ± 0.33, n = 56	r = 0.28*, p = 0.04, n = 56	r = 0.23, p = 0.09, n = 56	r = 0.30*, p = 0.02, n = 56
1 week			
	LLT average (nm) 62.41 ± 23.08, n = 56	LLT max (nm) 83.86 ± 18.93, n = 56	LLT min (nm) 49.96 ± 22.94, n = 56
Blinks 11.23 ± 4.90, n = 56	r = 0.25, p = 0.07, n = 56	r = 0.22, p = 0.11, n = 56	r = 0.18, p = 0.19, n = 56
Partial blinks 7.59 ± 5.72, n = 56	r = 0.45*, p = 0.001, n = 56	r = 0.48*, p < 0.001, n = 56	r = 0.45*, p < 0.001, n = 56
Rate of partial blinks 0.65 ± 0.34, n = 56	r = 0.48*, p < 0.001, n = 56	r = 0.54*, p < 0.001, n = 56	r = 0.53*, p < 0.001, n = 56
1 month			
	LLT average (nm) 61.39 ± 24.36, n = 56	LLT max (nm) 82.43 ± 18.98, n = 56	LLT min (nm) 50.57 ± 25.17, n = 56
Blinks 10.46 ± 4.49, n = 54	r = -0.33, p = 0.81, n = 54	r = 0.08, p = 0.55, n = 54	r = -0.04, p = 0.77, n = 54
Partial blinks 6.37 ± 4.71, n = 54	r = 0.23, p = 0.10, n = 54	r = 0.36*, p = 0.007, n = 54	r = 0.27, p = 0.05, n = 56
Rate of partial blinks 0.60 ± 0.36, n = 54	r = 0.37*, p = 0.005, n = 54	r = 0.43*, p = 0.001, n = 54	r = 0.44*, p = 0.001, n = 56

LLT: lipid layer thickness. LLT average: average value of LLT during 19.1-second measurement. LLT max: maximum value of LLT during 19.1-second measurement. LLT min: minimum value of LLT during 19.1-second measurement. Blink: number of blinks during 19.1s. Partial blink: number of partial blinks during 19.1s. r: relative coefficient. P: significance. n: number.

TABLE 4: Association of LLT average and other variables of 56 orthokeratology eyes at baseline.

	LLT average (nm)	Age (years)	Sex	Sph (D)	Cylin (D)	Axis	BCDVA logMAR	Axial length(mm)	K1 (D)	K2 (D)	TCT (um)
Number of cases (n)	56	56	56	56	56	56	56	56	56	56	56
Average	54.29	10.30	—	-2.90	-0.42	95.95	-0.02	24.82	42.77	43.91	550.79
Standard deviation	22.13	1.75	—	1.12	0.48	83.81	0.04	0.70	1.07	1.12	26.16
Association with LLT average	r	-0.03	-0.38*	0.07	0.06	0.34*	0.04	0.03	-0.74	-0.67	-0.21
	P	0.82	0.00	0.63	0.66	0.04	0.76	0.82	0.59	0.621	0.12
	n	56	56	56	56	37	56	56	56	56	56

LLT: lipid layer thickness. Sph: spherical power. Cylin: cylindrical power. BCDVA: best corrected distance visual acuity. K1: flat corneal curvature. K2: steep corneal curvature. TCT: thinnest corneal thickness. Blink: number of blinks during 19.5 s. Partial blink: number of partial blinks during 19.5 s.

TABLE 5: Short-term change of LLT (average, minimum, and max) after orthokeratology.

	n	LLT average	Standard deviation	ANOVA	Baseline (LSD)	1 week (LSD)	1 month (LSD)
LLT (average)							
Baseline	56	54.29	22.13	p = 0.028* n = 56	—	P = 0.017* n = 56	p = 0.025* n = 56
1 week	56	62.41	23.08		p = 0.017* n = 56	—	p = 0.699 n = 56
1 month	56	61.10	24.41		p = 0.025* n = 56	p = 0.699 n = 56	—
LLT (min)							
Baseline	56	42.30	19.66	p = 0.024* n = 56	—	p = 0.022* n = 56	p = 0.012* n = 56
1 week	56	49.96	22.74		p = 0.022* n = 56	—	p = 0.864 n = 56
1 month	56	50.57	24.94		p = 0.012* n = 56	p = 0.864 n = 56	—
LLT (max)							
Baseline	56	80.36	20.47	p = 0.447 n = 56	—	p = 0.265 n = 56	p = 0.436 n = 56
1 week	56	83.86	18.76		p = 0.265 n = 56	—	p = 0.572 n = 56
1 month	56	82.43	18.81		p = 0.436 n = 56	p = 0.572 n = 56	—

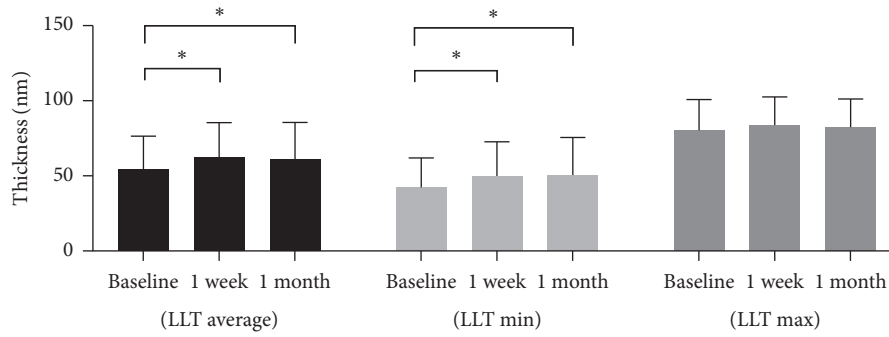


FIGURE 2: Lipid layer thickness (average, minimum and max) after orthokeratology lens wear. The average lipid layer thickness (average, minimum, and max) of the 56 patients at baseline, 1 week, and 1 month after orthokeratology treatment. * denotes $p < 0.05$.

TABLE 6: Short-term change of blinking pattern after orthokeratology.

	<i>n</i>	Average	Standard deviation	ANOVA	Baseline(LSD)	1 week (LSD)	1 month (LSD)
Blinks							
Baseline	54	10.89	4.74	$p = 0.727$ $n = 54$	—	$p = 0.660$ $n = 54$	$p = 0.907$ $n = 54$
1 week	54	11.23	4.86		$p = 0.660$ $n = 54$	—	$p = 0.454$ $n = 54$
1 month	54	10.49	4.49		$p = 0.907$ $n = 54$	$p = 0.454$ $n = 54$	—
Partial blinks							
Baseline	54	5.70	5.01	$p = 0.037^*$ $n = 54$	—	$p = 0.012^*$ $n = 54$	$p = 0.417$ $n = 54$
1 week	54	7.59	5.67		$P = 0.012^*$ $n = 54$	—	$p = 0.094$ $n = 54$
1 month	54	6.37	4.66		$p = 0.417$ $n = 54$	$p = 0.094$ $n = 54$	—
Rate of partial blinks							
Baseline	54	0.51	0.33	$p = 0.008$ $n = 54$	—	$p < 0.001^*$ $n = 54$	$p = 0.056$ $n = 54$
1 week	54	0.65	0.33		$p < 0.001^*$ $n = 54$	—	$p = 0.366$ $n = 54$
1 month	54	0.61	0.35		$p = 0.056$ $n = 54$	$p = 0.366$ $n = 54$	—

ANOVA: single-factor repeated measure analysis of variance. LSD: LSD paired *t*-test. *n*: number. *P*: significance.

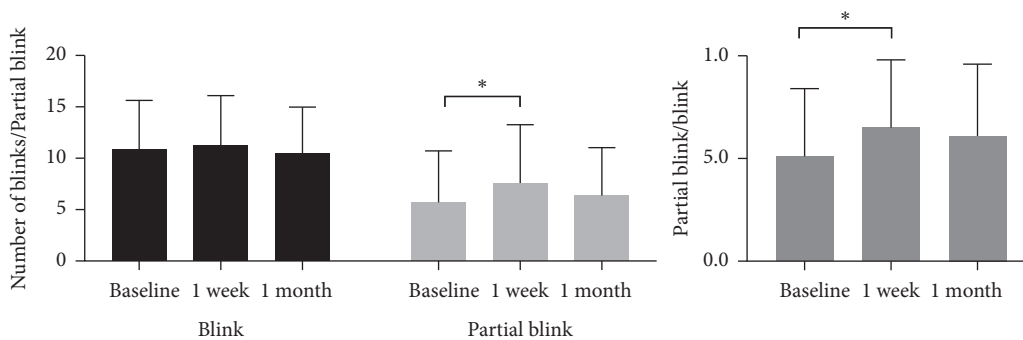


FIGURE 3: Blinks, partial blinks, and rate of partial blinks after orthokeratology lens wear. The number of blinks, the number of partial blinks, and rate of partial blinks of the 56 patients at baseline, 1 week, and 1 month after orthokeratology treatment. * denotes $p < 0.05$.

3.2.4. Association between Change of LLT and Change of Blinking Pattern. Rmcorr analysis showed significant association between rate of partial blinks and LLT (average, minimum, and max) with $p = 0.003$, 0.001 , and 0.014 , respectively (Table 7).

4. Discussion

In this study, we used a noninvasive LipiView® interferometer to observe features of the LLT in normal children and

found that a number of ocular biometrics were associated with LLT. We also measured LLT in children undergoing orthokeratology treatment and found that even short-term lens wear had an impact on LLT.

LipiView has been used for dry eye evaluation in adults. However, LLT is complicated by the presence and category of dry eye, which is common among this population. A thicker LLT of 80 (20–100) nm could be found in group where 79% were diagnosed with meibomian gland dysfunction [14], while another study found that dry eye

TABLE 7: Correlation of change in LLT and blinking pattern after orthokeratology.

	LLT ave	LLT min	LLT max
Blink	$r = 0.04, p = 0.677, n = 56$	$r = -0.05, p = 0.612, n = 56$	$r = 0.04, p = 0.649, n = 56$
Partial blink	$r = 0.18, p = 0.055, n = 56$	$r = 0.12, p = 0.217, n = 56$	$r = 0.18, p = 0.055, n = 56$
Partial blink/blink	$r = 0.28, p = 0.003, n = 56$	$r = 0.31, p = 0.001, n = 56$	$r = 0.23, p = 0.014, n = 56$

LLT: lipid layer thickness. ave: average. min: minimum.

symptom scores were higher in participants with LLT lower than 60 nm [19]. These results were even higher than normal children in our study showing 58.09 ± 21.66 nm ($n = 163$, aged 10.7 ± 1.9 years), combining with previous study revealing different composition of lipid in meibum from varied populations [20], indicating that LLT in children needs to be evaluated with different standards.

When focusing on children and adolescents, we found that the average value of 58.09 ± 21.66 nm in our study was close to that in a previous study, being 58.1 ± 20.0 nm in asymptomatic children aged 10.8 ± 1.8 years [16]. Both studies together offered the normal range of LLT in children at age of myopia progression. Another study reported a higher average LLT of 68.7 ± 23.1 nm in elder children aged 15 years with a healthy ocular surface [17]. Combining previous studies and the current study, it is tentative to conclude that tear LLT varies in younger children, adolescents, and adults. The threshold value of LLT for the diagnosis of dry eye also needs to be differently defined at various ages.

Further analysis found that LLT was positively associated with age ($r = 0.193, p = 0.013$) in the present study. Although r value close to 0.2 revealed weak power of the test, when combined the facts mentioned above, it suggested age to be a factor of LLT. It is acknowledged that even 1-month-old infants already have morphologically complete meibomian glands which are distributed across the whole tarsal plates of both the upper and lower eyelids [21]. After infancy, meibomian gland loss begins, causing MG deficiency to become more prevalent into childhood and adolescence [16]. Meibomian glands decrease with age in normal subjects ranging from 4 to 98 years old [22]. However, LLT was observed to increase with age in normal children in our study. We speculate that the volume of lipid is dependent on the secretory function of every gland duct rather than the number of meibomian gland. During childhood and adolescents, potential increase in secretory function of meibomian glands might compensate for the decrease in gland tubes. The percent area of the meibomian gland acini in the eyelid was shown to be significantly higher in adolescents than in children [23]. Moreover, the composition of lipids has been shown to be related to age, suggesting another potential functional change of glands over time [20]. These above-mentioned facts helped explain the potential mechanism of positive association between LLT and age in normal children in the current study.

Our results indicated that LLT was positively correlated with axial length and negatively correlated with corneal curvatures and thinnest corneal thickness in 163 participants. However, these correlations were weak with r value

near 0.2, and the correlation was no longer significant in analysis of 56 OK participants at baseline. Previous studies focusing on association of dry eye and axial length in populations with different degree of myopia also got different results [24, 25], indicating further studies are needed for clarification of correlation of LLT and other variables. It is well acknowledged that the axial length elongates and corneal flattens with age in childhood [26]; therefore, age-matched design will be necessary in studies.

Blinking helps to distribute lipid over ocular surface, being beneficial to stabilize tear film and improve dry eye disease [27], and therefore, a concerned factor in ocular surface health. Especially, in Asian population, incomplete blinks are more observed due to anatomic features of eye lids [28], which were reported to be correlated with dry eye disease [29], although the causality has not been clearly clarified. These suggested us that blinking pattern in Chinese children was an important factor of LLT. In our study, number of blinks had no significant change at 1-week or 1-month follow-up, while number of partial blinks and rate of partial blinks increased significantly after orthokeratology treatment. Ocular surface disease index and corneal sensitivity showed changes after orthokeratology in previous studies [7]. Lum et al. found a decrease in corneal sensitivity and nerve fiber density after orthokeratology lens wear [13], and these changes had already occurred after one month of orthokeratology wear [30], which could potentially change blinking pattern.

In this study, children who have undergone orthokeratology treatment showed an increase in LLT even in the short term of one week and lasted till one month. We speculated that the interaction of the orthokeratology contact lens and the ocular surface, especially between the lens edge and the tarsal plate, could have yielded an elevation in lipid secretion during blinking. In our study, rate of partial blinks was significantly correlated with LLT at every follow-up. Notably, rmcrr analysis confirmed that increase in rate of partial blinks was associated with increase of LLT (average, max, and minimum) after orthokeratology lens wear. However, being different with other studies indicating that partial blinks were associated with dry eye disease and poorer lipid layer quality [29, 31, 32], increase of rate of partial blinks in our study was accompanied with elevation in LLT value. Since this is a short-term observation study and advent of dry eye is a chronic process, we could not conclude that the increase in LLT was “good” sign for ocular surface health. It might be temporary, or a kind of stimulus response. Interestingly, similar 1-month change of incomplete blinking was observed after corneal refractive surgeries; however, it was accompanied with decreased LLT [33]. The

mechanism under the difference change of LLT needs further study.

Considering other factors of LLT change, studies have shown that tear composition including ascorbate, sIgA, albumin, and lactate dehydrogenase changed dramatically after one night of orthokeratology lens wear, which could be an “irritation” caused by short-term orthokeratology treatment [11]. Also, composition change of tear might have influence on detection of thickness of the lipid layer. Moreover, changed corneal curvature of reshaped cornea could influence the dynamics of tear. In terms of long-term effects of orthokeratology lens wear on ocular surface, a previous study showed an insignificant decrease in tear breakup time and no change in meibomian glands after three years of overnight orthokeratology treatment [7]. These studies combined suggested that despite a short-term interruption, orthokeratology is generally safe in the long run with minimal influence on ocular surface.

There are limitations of this study. Morphology of meibomian glands was not quantitatively analyzed. Data such as refraction and corneal curvature after orthokeratology were missing. Further studies in the future will help better understand the lipid layer quality, in addition to quantity, after orthokeratology.

5. Conclusion

LLT in Chinese normal children was different with LLT in adults reported previously. Significant correlation between LLT and rate of partial blinks was found. LLT increased in children undergoing orthokeratology in the short term and the change was associated with increase in rate of partial blinks. A long-term study incorporating LLT and other tear composition parameters is needed to elucidate the long-term impact of orthokeratology on ocular surface and the underlying mechanism.

Data Availability

The datasets of the current study are available upon request from the co-first authors Li Zeng and Zhi Chen.

Ethical Approval

This study was performed in accordance with the Declaration of Helsinki and was approved by the Ethics Committee of the Eye and ENT Hospital, Shanghai, China.

Consent

Written informed consent, after the aims and nature of the study were explained, was obtained from the participants for publication of this article and any accompanying images and data.

Disclosure

Li Zeng and Zhi Chen should be considered as equal first authors.

Conflicts of Interest

The authors declare that they have no conflicts interest.

Authors' Contributions

Li Zeng, Zhi Chen, and Xingtao Zhou were responsible for study concept and design. Li Zeng, Zhi Chen, Dan Fu, and Jiaqi Zhou carried out data collection. Li Zeng conducted analysis and interpretation of data. Li Zeng and Zhi Chen were involved in drafting and critical revision of the manuscript. Xingtao Zhou was responsible for supervision. All authors have read and approved the whole manuscript and the publication. Li Zeng and Zhi Chen contributed equally to this work.

Acknowledgments

This work was supported by the following funds in collection, analysis, and interpretation of data, and in writing the manuscript: National Natural Science Foundation of China (grant no. 81770955), Joint Research Project of New Frontier Technology in Municipal Hospitals (grant no. SHDC12018103), Project of Shanghai Science and Technology (grant no.20410710100), and National Natural Science Foundation of China for Young Scholars (grant no. 81700870).

References

- [1] A. Alharbi, D. La Hood, and H. A. Swarbrick, “Overnight orthokeratology lens wear can inhibit the central stromal edema response,” *Investigative Ophthalmology & Visual Science*, vol. 46, no. 7, pp. 2334–2340, 2005.
- [2] E. Lum and S. Ha, “Lens Dk/t influences the clinical response in overnight orthokeratology,” *Optometry And Vision Science: Official Publication of the American Academy of Optometry*, vol. 88, pp. 469–475, 2011.
- [3] M. J. Rah, J. M. Jackson, L. A. Jones, H. J. Marsden, M. D. Bailey, and A. J. T. Barr, “Overnight orthokeratology: preliminary results of the lenses and overnight orthokeratology (LOOK) study,” *Optometry and Vision Science*, vol. 79, no. 9, pp. 598–605, 2002.
- [4] P. B. Morgan, N. Efron, C. A. Woods, and J. Santodomingo-Rubido, “International survey of orthokeratology contact lens fitting,” *Contact Lens and Anterior Eye*, vol. 42, no. 4, pp. 450–454, 2019.
- [5] N. Efron, P. B. Morgan, and C. A. Woods, “Survey of contact lens prescribing to infants, children, and teenagers,” *Optometry and Vision Science*, vol. 88, no. 4, pp. 461–468, 2011.
- [6] J. S. Wolffsohn, A. Calossi, P. Cho et al., “Global trends in myopia management attitudes and strategies in clinical practice - 2019 Update,” *Contact Lens and Anterior Eye*, vol. 43, no. 1, pp. 9–17, 2020.
- [7] K.-S. Na, Y.-S. Yoo, H. S. Hwang, J. W. Mok, H. S. Kim, and C.-K. Joo, “The influence of overnight orthokeratology on ocular surface and meibomian glands in children and adolescents,” *Eye & Contact Lens: Science & Clinical Practice*, vol. 42, no. 1, pp. 68–73, 2016.
- [8] N. García-Porta, L. Rico-Del-Viejo, A. Martín-Gil, G. Carracedo, J. Pintor, and J. M. González-Méijome, “Differences in dry eye questionnaire symptoms in two different

- modalities of contact lens wear: silicone-hydrogel in daily wear basis and overnight orthokeratology,” *BioMed Research International*, vol. 2016, p. 1242845, 2016.
- [9] J. Li, P. Dong, and H. Liu, “Effect of overnight wear orthokeratology lenses on corneal shape and tears,” *Eye & Contact Lens: Science & Clinical Practice*, vol. 44, no. 5, pp. 304–307, 2018.
 - [10] A. Nieto-Bona, M. Nombela-Palomo, G. Felipe-Márquez, and M. A. Teus, “Tear film osmolarity in response to long-term orthokeratology treatment,” *Eye & Contact Lens: Science & Clinical Practice*, vol. 44, no. 2, pp. 85–90, 2018.
 - [11] C. K. M. Choy, P. Cho, I. F. F. Benzie, and V. Ng, “Effect of one overnight wear of orthokeratology lenses on tear composition,” *Optometry and Vision Science*, vol. 81, no. 6, pp. 414–420, 2004.
 - [12] J. González-Pérez, C. Villa-Collar, J. M. González-Méijome, N. G. Porta, and M. Á. Parafita, “Long-term changes in corneal structure and tear inflammatory mediators after orthokeratology and LASIK,” *Investigative Ophthalmology & Visual Science*, vol. 53, no. 9, pp. 5301–5311, 2012.
 - [13] E. Lum, B. Golebiowski, and H. A. Swarbrick, “Reduced corneal sensitivity and sub-basal nerve density in long-term orthokeratology lens wear,” *Eye & Contact Lens: Science & Clinical Practice*, vol. 43, no. 4, pp. 218–224, 2017.
 - [14] J. W. Jung, S. Y. Park, J. S. Kim, E. K. Kim, K. Y. Seo, and T.-I. Kim, “Analysis of factors associated with the tear film lipid layer thickness in normal eyes and patients with dry eye syndrome,” *Investigative Ophthalmology & Visual Science*, vol. 57, no. 10, pp. 4076–4083, 2016.
 - [15] M. Markoulli, T. B. Duong, M. Lin, and E. Papas, “Imaging the tear film: a comparison between the subjective keeler tear-scope-plus and the objective Oculus keratograph 5M and lipi view interferometer,” *Current Eye Research*, vol. 43, no. 2, pp. 155–162, 2018.
 - [16] Y. Zhao, S. Chen, S. Wang et al., “The significance of meibomian gland changes in asymptomatic children,” *The Ocular Surface*, vol. 16, no. 3, pp. 301–305, 2018.
 - [17] T. Mizoguchi, R. Arita, S. Fukuoka, and N. Morishige, “Morphology and function of meibomian glands and other tear film parameters in junior high school students,” *Cornea*, vol. 36, no. 8, pp. 922–926, 2017.
 - [18] J. Z. Bakdash and L. R. Marusich, “Repeated measures correlation,” *Frontiers in Psychology*, vol. 8, p. 456, 2017.
 - [19] D. Finis, N. Pischel, S. Schrader, and G. Geerling, “Evaluation of lipid layer thickness measurement of the tear film as a diagnostic tool for meibomian gland dysfunction,” *Cornea*, vol. 32, no. 12, pp. 1549–1553, 2013.
 - [20] R. K. Shrestha, D. Borchman, G. N. Foulks, M. C. Yappert, and S. E. Milliner, “Analysis of the composition of lipid in human meibum from normal infants, children, adolescents, adults, and adults with meibomian gland dysfunction using 1H-nmr spectroscopy,” *Investigative Ophthalmology & Visual Science*, vol. 52, no. 10, pp. 7350–7358, 2011.
 - [21] R. Shirakawa, R. Arita, and S. Amano, “Meibomian gland morphology in japanese infants, children, and adults observed using a mobile pen-shaped infrared meibography device,” *American Journal of Ophthalmology*, vol. 155, no. 6, pp. 1099–1103, 2013.
 - [22] R. Arita, K. Itoh, K. Inoue, and S. Amano, “Noncontact infrared meibography to document age-related changes of the meibomian glands in a normal population,” *Ophthalmology*, vol. 115, no. 5, pp. 911–915, 2008.
 - [23] Y. Wu, H. Li, Y. Tang, and X. Yan, “Morphological evaluation of meibomian glands in children and adolescents using noncontact infrared meibography,” *Journal of Pediatric Ophthalmology & Strabismus*, vol. 54, no. 2, pp. 78–83, 2017.
 - [24] J. A. Sanchis-Gimeno, M. Herrera, F. Sánchez-del-Campo, and F. Martínez-Soriano, “Differences in ocular dimensions between normal and dry eyes,” *Surgical and Radiologic Anatomy*, vol. 28, no. 3, pp. 267–270, 2006.
 - [25] N. Ilhan, O. Ilhan, E. Ayhan Tuzcu et al., “Is there a relationship between pathologic myopia and dry eye syndrome?” *Cornea*, vol. 33, no. 2, pp. 169–171, 2014.
 - [26] T. L. Lu, J. F. Wu, X. Ye et al., “Axial length and associated factors in children: the shandong children eye study,” *Ophthalmologica*, vol. 235, no. 2, pp. 78–86, 2016.
 - [27] A. J. Bron, A. Tomlinson, G. N. Foulks et al., “Rethinking dry eye disease: a perspective on clinical implications,” *The Ocular Surface*, vol. 12, no. 2, pp. S1–S31, 2014.
 - [28] J. S. Kim, M. T. M. Wang, and J. P. Craig, “Exploring the Asian ethnic predisposition to dry eye disease in a pediatric population,” *The Ocular Surface*, vol. 17, no. 1, pp. 70–77, 2019.
 - [29] H. Pult, B. H. Riede-Pult, and P. J. Murphy, “The relation between blinking and conjunctival folds and dry eye symptoms,” *Optometry and Vision Science*, vol. 90, no. 10, pp. 1034–1039, 2013.
 - [30] E. Lum, B. Golebiowski, and H. A. Swarbrick, “Changes in corneal subbasal nerve morphology and sensitivity during orthokeratology: onset of change,” *The Ocular Surface*, vol. 15, no. 2, pp. 227–235, 2017.
 - [31] A. D. Kim, A. Muntz, J. Lee, M. T. M. Wang, and J. P. Craig, “Therapeutic benefits of blinking exercises in dry eye disease. Contact Lens & Anterior Eye,” *The Journal of the British Contact Lens Association*, vol. 11, 2020.
 - [32] M. T. M. Wang, L. Tien, A. Han et al., “Impact of blinking on ocular surface and tear film parameters,” *The Ocular Surface*, vol. 16, no. 4, pp. 424–429, 2018.
 - [33] Y. Li, S. Li, J. Zhou, C. Liu, and M. Xu, “Relationship between lipid layer thickness, incomplete blinking rate and tear film instability in patients with different myopia degrees after small-incision lenticule extraction,” *PloS One*, vol. 15, Article ID e0230119, 2020.

Research Article

Eyes of Aniso-Axial Length Individuals Share Generally Similar Corneal Biometrics with Normal Eyes in Cataract Population

Min Zhang ^{1,2} Tianhui Chen ^{1,2} Michael Deng ^{1,2} Jiahui Chen ^{1,2} Qinghe Jing ^{1,2}
and Yongxiang Jiang ^{1,2}

¹Department of Ophthalmology and Vision Science, Eye and ENT Hospital of Fudan University, Shanghai, China

²NHC Key Laboratory of Myopia (Fudan University), Key Laboratory of Myopia,

Chinese Academy of Medical Sciences and Key Laboratory of Visual Impairment and Restoration of Shanghai, Shanghai, China

Correspondence should be addressed to Yongxiang Jiang; yongxiang_jiang@163.com

Received 22 June 2020; Revised 1 October 2020; Accepted 14 October 2020; Published 30 October 2020

Academic Editor: Karim Mohamed Noriega

Copyright © 2020 Min Zhang et al. This is an open access article distributed under the Creative Commons Attribution License, which permits unrestricted use, distribution, and reproduction in any medium, provided the original work is properly cited.

Aims. To determine the characteristics of corneal biometrics in eyes from aniso-axial length cataract patients compared with eyes from non-aniso-axial length individuals. **Methods.** This is a retrospective case series. Cataract patients with preoperative binocular measurements were recruited. A binocular axial difference of ≥ 1 mm was considered to indicate aniso-axial length. The anterior segmental biometrics were measured using Pentacam HR (Oculus, Wetzlar, Germany) and IOLMaster 500 (Carl Zeiss Meditec, Jena, Germany). Comparisons of biometrics were made among 4 eye conditions: the longer eyes from aniso-axial length patients, the shorter eyes from aniso-axial length patients, the longer eyes from non-aniso-axial length patients, and the shorter eyes from non-aniso-axial length patients. The aniso-axial length eyes were also stratified into 8 subgroups with axial length (AL) increments of 1 mm, and the biometrics of the subgroups were compared. **Results.** There was smaller anterior corneal astigmatism in the shorter aniso-axial length group than those in the longer aniso-axial length group (1.01 ± 0.70 D vs 1.12 ± 0.76 D, $P = 0.031$). The longer aniso-axial length eyes had greater anterior corneal steep curvature (44.13 ± 1.69 D vs 43.87 ± 1.69 D, $P = 0.009$) and anterior corneal astigmatism (1.12 ± 0.76 D vs 1.02 ± 0.69 D, $P = 0.023$) compared with longer non-aniso-axial length subjects. Other corneal biometrics were similar between the aniso-axial length eyes and the non-aniso-axial length eyes. In the longer aniso-axial length group, the posterior corneal aberrations of eyes in the ≥ 5 mm subgroups were greater than those in the < 5 mm subgroups (0.879 ± 0.183 μm vs 0.768 ± 0.178 μm for total aberrations, $P < 0.001$; 0.228 ± 0.086 μm vs 0.196 ± 0.043 μm for high-order aberrations, $P = 0.036$; 0.847 ± 0.173 μm vs 0.741 ± 0.179 μm for low-order aberrations, $P = 0.001$). **Conclusion.** Eyes of aniso-axial length individuals share generally similar corneal biometrics with normal eyes in cataract population. Anterior corneal astigmatism of the longer eyes from the aniso-axial length cataract patients was higher than that of the longer eyes from the non-aniso-axial length individuals. Total posterior corneal aberrations of the longer aniso-axial length eyes increased when the binocular axial difference was over 5 mm.

1. Introduction

Anisometropia is a distinct condition of binocular asymmetry—both the eyes of an individual share an identical genetic background and similar environmental exposure but develop significantly different refractive status [1]. It is one of the leading causes of amblyopia, either alone or combined with strabismus [2, 3]. Anisometropia also follows amblyopia caused by either deprivation or strabismus. However,

the chronology and effects of anisometropia on ocular biometrics are unclear [4].

The well-accepted standard for anisometropia is a difference of > 1.00 diopter (D) of the spherical lens (DS) and/or 1.00 D of the cylinder lens [5, 6]. The comparison of binocular parameters in the anisometropic eye was studied previously, indicating that axial length (AL) was the most important factor in anisometropia [7]. Whether or not other anterior segmental parameters such as corneal power, lens

power, and anterior chamber resulting in or related to anisometropia is under debate [7–9].

On the one hand, previous studies have fully analyzed the general relationship between AL and corneal biometrics, indicating flatter cornea and smaller corneal curvature (K values) with AL elongation [10]. On the other hand, available anisometropia studies only focused on binocular parameter comparisons in the anisometropia patients rather than comparisons between normal and anisometropia eyes. As the etiology of anisometropia is still unclear and the binocular development is asymmetric in the anisometropic eyes, we are not sure if the anisometropic eyes and the normal eyes follow the same rule of AL- K value interactions. Here, we were supposed to figure out if the corneal biometrics in anisometropic eyes are different from that in nonanisometropic eyes following the AL elongation. We undertook to define the monocular characteristics of anisometropia patients by comparing the ocular biometrics of the asymmetrically developed eyes with those of the normal eyes in a large cohort of cataract patients.

Lens opacity also contributed to anisometropia diagnosis [8]. In cataract population, early asymmetric cataract development (especially nuclear sclerosis) in both eyes was reported to account for about 40% of anisometropia [11]. However, cataract patients have reduced fixation stability and visual acuity, along with the substantial degree of optometry variability [2], and measurement precision of cataract cases needs to be taken into account when diagnosing anisometropia. Also, lens-related factors contributing to anisometropia make no sense for them as a cataract is replaced by intraocular lens (IOL) after surgical treatment. Thus, the clinical significance of preoperative optometry in cataract patients is reduced.

Considering AL plays the most important role in anisometropia [7, 8, 12, 13], is independent of the cataract surgery itself, can be precisely measured in cataract patients [14], and has unparalleled status in IOL power calculation, we assume that “aniso-axial length” is synonymous with “anisometropia.” In this study, it is defined as an individual’s binocular axial difference of ≥ 1 mm. First, according to the Gullstrand eye model, the AL of the eye globe is 24.38 mm [15], and other modified schematic eyes and investigation results have shown this length to be around 24 mm [16, 17]. Second, eyes with AL ≥ 26 mm or with refractive errors more serious than -6.00 DS are equally considered high myopia [18]. Third, in children aged 6–7 or 12–13 years with anisometropia of ≥ 1 D, the mean asymmetry of the interocular AL was 0.40 ± 0.40 or 0.60 ± 0.50 mm, respectively [6]. Therefore, an increase in the AL of 1 mm can cause a change in the refractive error at the corneal surfaces of about -3.00 DS. Because other factors may compensate the anisometropia caused by aniso-axial length, we consider that an axial difference of ≥ 1 mm can be deemed anisometropia, or even serious anisometropia of about ≥ 3 DS.

Thus, we aimed to (1) compare the binocular corneal biometrics from cataract patients with an axial difference ≥ 1 mm; (2) compare the corneal biometrics of eyes from cataract patients with an axial difference ≥ 1 mm to those of

eyes from the cataract patients with symmetric binocular ALs; and (3) determine the characteristics of corneal biometrics in aniso-axial length cataract patients.

2. Materials and Methods

This was a retrospective case series conducted at the Eye and ENT Hospital of Fudan University, Shanghai, China. It was approved by the Human Research Ethics Committee of the Eye and ENT Hospital of Fudan University (no. 2020103) and complied with the tenets of the Declaration of Helsinki.

All patients were recruited, and the data were collected between September 29, 2016, and August 15, 2018, following the methods described before [19, 20]. In general, cataract patients with ocular comorbidities or history of ocular surgeries or contact lens within 2 weeks were excluded. A rotating Scheimpflug camera (Pentacam HR; Oculus, Wetzlar, Germany) and partial coherence interferometry (IOLMaster 500; Carl Zeiss Meditec, Jena, Germany) were used for data collection. Only patients in whom both eyes were examined were included. Written informed consent was obtained from each patient.

All patients were divided into the aniso-axial length group (binocular axial difference ≥ 1 mm) and the non-aniso-axial length group (binocular axial difference < 1 mm). The two eyes of each patient were separated into the longer one and the shorter one. Each eye from the aniso-axial length group in the longer set and the shorter set got the AL matched with one or two eyes from the non-aniso-axial length group in the longer set and the shorter set, respectively (see more details in Appendix Methods). Corneal astigmatism was defined as “with the rule” (WTR), “against the rule” (ATR), or “oblique,” according to the axis of the corneal steep meridian, as previously described [19].

All continuous data are shown as means \pm standard deviations (SD). The normality of continuous data was tested using the Kolmogorov–Smirnov test. All categorical data were compared using the chi-square test. Variables were compared among the longer aniso-axial length, the shorter aniso-axial length, the longer non-aniso-axial length, and the shorter non-aniso-axial length groups using analyses of variance (ANOVA) and a post hoc analysis with the LSD correction. Studied variables included the following: (1) anterior corneal curvature (flat and steep radius of curvature, r_1 and r_2), anterior and posterior corneal curvature values (flat and steep power of curvature, K_1 and K_2 ; average radius and power of curvature defined as the central radius of curvature in the steep direction/central radius of curvature in the flat direction using $n = 1.3375$, R_m and K_m), and astigmatism; (2) the root mean square of the anterior, posterior, and total corneal low-order aberrations (LOAs), high-order aberrations (HOAs), and total aberrations (TAs); (3) the anterior, posterior, and total corneal Zernike polynomial coefficients of the third-order aberrations (vertical coma, horizontal coma, vertical trefoil, and oblique trefoil) and the primary spherical aberrations (SAs); and (4) the central corneal thickness (CCT). Except for r_1 , r_2 and CCT reported using IOLMaster 500, others were obtained using Pentacam HR.

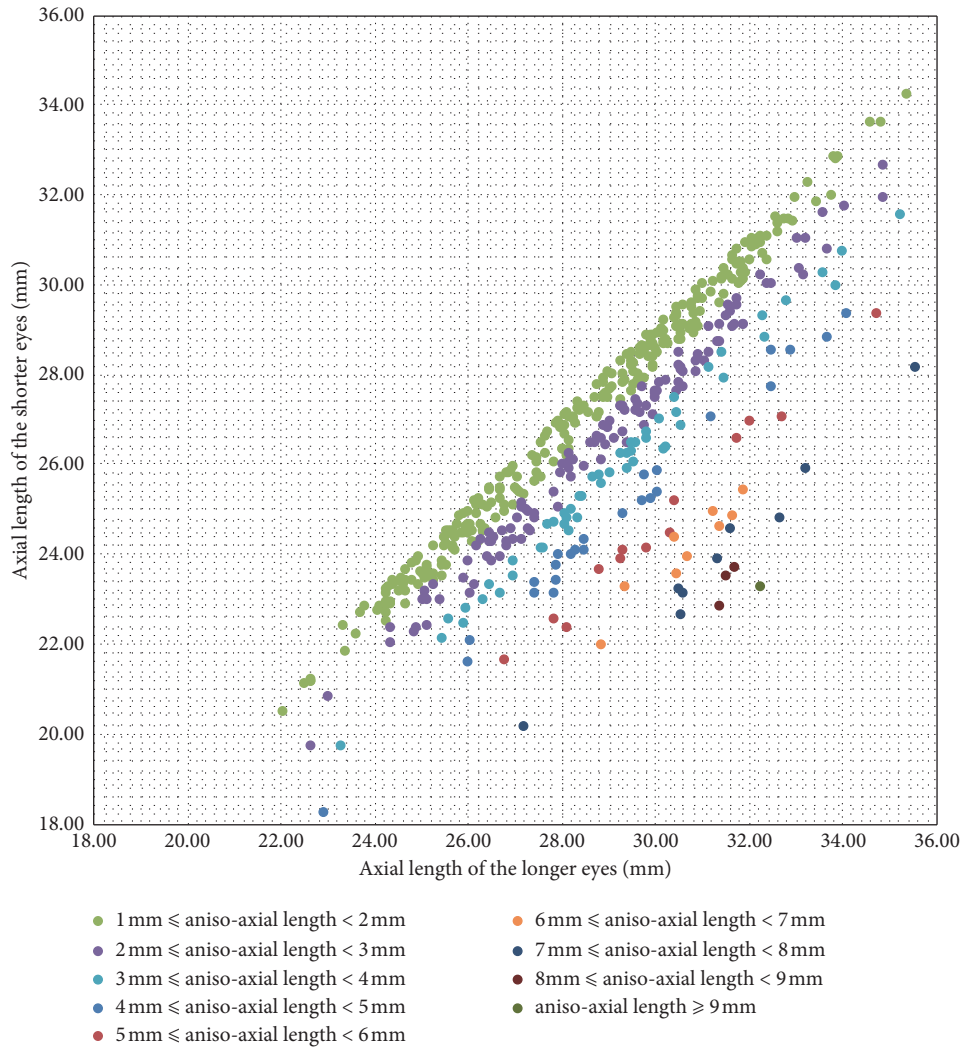


FIGURE 1: Distributions of the binocular axial lengths of 505 aniso-axial length patients. Every dot in the figure represents one person with a binocular axial difference ≥ 1 mm. The horizontal axis indicates the axial length of the relative longer eye in each patient, and the vertical axis indicates the axial length of the relative shorter eye.

All aniso-axial length eyes in both the shorter and longer sets were also divided into eight subgroups based on the axial difference in increments of 1 mm (1-2, 2-3, 3-4, 4-5, 5-6, 6-7, 7-8, and 8-9 mm, where a value of 1 mm is included in the 1-2 mm subgroup, and similarly for other values that fall at the boundary between two subgroups). The variables were compared again among all subgroups in the two sets with ANOVA and post hoc LSD correction, respectively. Data analyses were performed using SPSS 26.0 (SPSS, IBM Corp., Armonk, NY, USA). A P value < 0.05 was considered to indicate statistical significance.

3. Results

In total, anterior segmental biometrics of 10,094 eyes from 6747 cataract patients were available and 3347 patients had both eyes examined. Among them, 2842 patients had an absolute difference in the AL of < 1 mm between their two eyes. The distribution of the AL of the remaining 505

aniso-axial length patients is shown in Figure 1; among these patients, 16 were excluded because of their young age (< 20 years old). Ultimately, 489 aniso-axial length patients were recruited, together with 564 shorter non-aniso-axial length eyes and 597 longer non-aniso-axial length eyes (Table 1). The ≥ 9 mm subgroup had only one patient and was excluded in statistical analyses among subgroups.

Only one statistically significant difference between the shorter and longer eyes in the aniso-axial length group: anterior corneal astigmatism (1.01 ± 0.70 D vs 1.12 ± 0.76 D, $P = 0.031$) was detected. Anterior corneal $K2$ and astigmatism were higher in the longer aniso-axial length group compared with the longer non-aniso-axial length group (44.13 ± 1.69 D vs 43.87 ± 1.69 for the anterior corneal $K2$, $P = 0.009$; 1.12 ± 0.76 D vs 1.02 ± 0.69 D for the anterior corneal astigmatism, $P = 0.023$; Table 2 and Figure 2). The division of the total corneal astigmatism into WTR, ATR, or oblique astigmatism was similar ($P = 0.569$; Table 3).

TABLE 1: Demographic data of patients included in the study.

	Shorter set			Longer set			Total
	Non-aniso-axial length (N=564)	Aniso-axial length (N=489)	P value	Non-aniso-axial length (N=597)	Aniso-axial length (N=489)	P value	
Gender based on eyes (male/female)†	268/296	167/322	<0.001*	261/336	167/322	0.001*	863/1276
Age (years)	57.49 ± 10.28	58.01 ± 10.57	0.415	57.88 ± 10.41	58.01 ± 10.57	0.836	57.84 ± 10.44
Axial length (mm)	26.72 ± 2.71	26.56 ± 2.77	>0.999	28.68 ± 2.85	28.92 ± 2.71	0.890	27.73 ± 2.96

*P < 0.05. †Chi-square test.

TABLE 2: Comparisons of corneal biometrics between non-aniso-axial length and aniso-axial length patients in both the shorter and longer sets.

	Shorter set			Longer set			P value††
	Non-aniso-axial length	Aniso-axial length	P value†	Non-aniso-axial length	Aniso-axial length	P value†	
CCT (mm)	544.07 ± 31.88	539.48 ± 32.05	0.018*	543.51 ± 30.43	539.92 ± 31.29	0.061	0.028*
K2 F (D)	43.80 ± 1.63	44.02 ± 1.63	0.033*	43.87 ± 1.69	44.13 ± 1.69	0.009*	0.005*
r2 F (mm)	7.66 ± 0.29	7.62 ± 0.29	0.010*	7.64 ± 0.30	7.60 ± 0.28	0.007*	0.001*
K1 B (D)	-6.16 ± 0.26	-6.19 ± 0.26	0.025*	-6.16 ± 0.26	-6.19 ± 0.27	0.047*	0.029*
K2 B (D)	-6.44 ± 0.29	-6.49 ± 0.27	0.010*	-6.46 ± 0.29	-6.49 ± 0.28	0.054	0.013*
Rm B (mm)	6.36 ± 0.26	6.32 ± 0.25	0.015*	6.36 ± 0.27	6.32 ± 0.26	0.042*	0.017*
Km B (mm)	-6.30 ± 0.26	-6.34 ± 0.25	0.012*	-6.30 ± 0.27	-6.33 ± 0.26	0.051	0.017*
Astigmatism F (D)	0.94 ± 0.73	1.01 ± 0.70	0.110	1.02 ± 0.69	1.12 ± 0.76	0.023*	0.002*
TA F (μm)	2.30 ± 0.75	2.38 ± 0.68	0.103	2.33 ± 0.90	2.47 ± 0.78	0.002*	0.002*
LOA F (μm)	2.23 ± 0.74	2.30 ± 0.67	0.106	2.25 ± 0.88	2.40 ± 0.77	0.002*	0.002*
TA cornea (μm)	2.03 ± 0.72	2.10 ± 0.67	0.148	2.03 ± 0.88	2.18 ± 0.76	0.002*	0.005*
LOA cornea (μm)	1.95 ± 0.72	2.02 ± 0.65	0.151	1.95 ± 0.86	2.10 ± 0.75	0.002*	0.004*

†Post hoc LSD correction; ††analyses of variance. *P < 0.05. F = anterior corneal surface; B = posterior corneal surface; Corneal = total cornea; K1 = flat power of curvature in the center of anterior surface using $n = 1.3375$ on a ring in 15° around the corneal apex; K2 = steep power of curvature in the center of anterior surface using $n = 1.3375$ on a ring in 15° around the corneal apex; Rm = average radius of curvature (central radius of curvature in the steep direction/central radius of curvature in the flat direction); Km = average power of curvature using $n = 1.3375$; LOAs = low order aberrations; TAs = total aberrations. Only r2 and CCT were reported using IOLMaster 500, and others were obtained using Pentacam HR.

No significant differences were detected between longer or shorter eyes from aniso-axial length or non-aniso-axial length individuals in HOAs, coma, or trefoil. The SAs were slightly higher in the aniso-axial length group and highest in the shorter aniso-axial length group (ANOVA, all $P > 0.100$). The anterior corneal, posterior corneal, and total corneal SAs of the shorter aniso-axial length eyes were $0.34 \pm 0.12 \mu\text{m}$, $-0.13 \pm 0.03 \mu\text{m}$, and $0.31 \pm 0.12 \mu\text{m}$, respectively, and those of the longer aniso-axial length eyes were $0.33 \pm 0.12 \mu\text{m}$, $-0.13 \pm 0.03 \mu\text{m}$, and $0.30 \pm 0.12 \mu\text{m}$, respectively (Table 4). The anterior and posterior corneal SAs did not differ significantly among the four groups. We found wide distributions of SAs in the aniso-axial length groups and the non-aniso-axial length groups (Table 4). By the way, a total of 13 eyes with negative SAs were detected, 7 eyes from the non-aniso-axial length group and 6 eyes from the aniso-axial length group. Their specific corneal biometrics are presented in Appendix Table A1.

There were 266, 114, 50, 25, 13, 8, 9, and 3 aniso-axial length patients with axial differences of 1-2, 2-3, 3-4, 4-5, 5-6, 6-7, 7-8, and 8-9 mm, respectively. ANOVA of the corneal biometrics detected significant differences in the posterior corneal TAs ($P = 0.025$), posterior corneal HOAs ($P = 0.005$), posterior corneal LOAs ($P = 0.039$), and posterior corneal

oblique trefoil ($P = 0.040$) among subgroups in the longer set, whereas there were no significant difference among subgroups in the shorter set. The distributions of the variables in the eight subgroups of the longer set are shown in Figure 3. Post hoc analysis with LSD correction indicated an increase of posterior corneal TAs, HOAs, LOAs, and oblique trefoil at an axial difference of 5 mm ($P < 0.05$ of comparisons between the subgroups with an axial difference of <5 mm and ≥ 5 mm. Exact standard errors, mean differences, or P values were not shown) for all four variables. General comparisons in the longer set between eyes with an axial difference < 5 mm and ≥ 5 mm also indicated statistical significance in TAs ($0.879 \pm 0.183 \mu\text{m}$ vs $0.768 \pm 0.178 \mu\text{m}$, $P < 0.001$), HOAs ($0.228 \pm 0.086 \mu\text{m}$ vs $0.196 \pm 0.043 \mu\text{m}$, $P = 0.036$), and LOAs ($0.847 \pm 0.173 \mu\text{m}$ vs $0.741 \pm 0.179 \mu\text{m}$, $P = 0.001$). However, the same 5 mm cut-off was not found among subgroups in the analysis of ALs with ANOVA (Appendix Table A2).

4. Discussion

Anisometropia is the condition in which an individual's eyes have significant binocular refractive differences. Shapira et al. [21] found that the more myopic eye of anisometropic

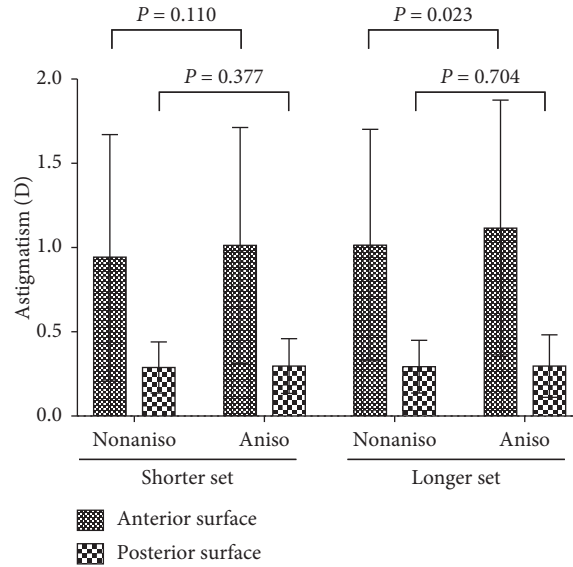


FIGURE 2: Comparison of astigmatism among the aniso-axial length groups and the non-aniso-axial length groups in the shorter set or the longer set. Non-aniso = non-aniso-axial length group, Aniso = aniso-axial length group. *P* values were reported by post hoc LSD correction.

TABLE 3: Distributions of total corneal astigmatism divisions in the non-aniso-axial length group and the aniso-axial length group of the two sets.

	Shorter set		Longer set		Total
	Non-aniso-axial length	Aniso-axial length	Non-aniso-axial length	Aniso-axial length	
WTR	297 (52.66%)	250 (51.12%)	308 (51.59%)	238 (48.67%)	1093
ATR	172 (30.50%)	156 (31.90%)	183 (30.65%)	170 (34.76%)	681
Oblique	95 (16.84%)	83 (16.97%)	106 (17.76%)	81 (16.56%)	365
Total	564 (100%)	489 (100%)	597 (100%)	489 (100%)	2139

WTR = with-the-rule astigmatism; ATR = against-the-rule astigmatism; oblique = oblique astigmatism. Percentages of astigmatism division in each group were shown in brackets. *P* > 0.05 using the chi-square test.

TABLE 4: Distributions of total, anterior, and posterior corneal SAs in different groups.

Groups	SAs	Minimum (μm)	Maximum (μm)	Mean ± SD (μm)
Aniso, longer (N = 489)	Total cornea	-0.118	0.742	0.303 ± 0.120
	Posterior corneal surface	-0.235	-0.016	-0.128 ± 0.034
	Anterior corneal surface	-0.102	0.768	0.334 ± 0.116
Non, longer (N = 597)	Total cornea	-0.133	0.687*	0.295 ± 0.151
	Posterior corneal surface	-0.229	-0.021	-0.132 ± 0.034
	Anterior corneal surface	-0.180	0.751*	0.331 ± 0.148
Aniso, shorter (N = 489)	Total cornea	-0.365	0.681	0.306 ± 0.125
	Posterior corneal surface	-0.224	-0.011	-0.128 ± 0.035
	Anterior corneal surface	-0.286	0.695	0.337 ± 0.118
Non, shorter (N = 564)	Total cornea	-0.154	0.702	0.293 ± 0.117
	Posterior corneal surface	-0.223	-0.018	-0.131 ± 0.035
	Anterior corneal surface	-0.099	0.698	0.328 ± 0.112

SAs = spherical aberrations; Aniso = aniso-axial length group; Non = non-aniso-axial length group; shorter = shorter set; longer = longer set; SD = standard deviation. The *P* values of total posterior and anterior corneal SAs with analyses of variance were >0.05 among the four groups. *One non-aniso-axial length eye in the longer set with anterior corneal SA = 2.767 μm, posterior corneal SA = -0.097 μm, and total corneal SA = 2.748 μm was considered abnormal and was not listed as the maximum.

patients before refractive surgery yielded lower predictability and accuracy in terms of surgical outcomes and tended to be overcorrected, whereas the less myopic eye had similar outcomes as the isometropic control eyes. This indicated that there were some unknown characteristics of anisometropic

eyes. We tried to address this problem with a cataract population in this study.

Patients in this study had unusually long axial length (26.56 ± 2.77 mm in the shorter aniso-axial length group and 28.92 ± 2.71 mm in the longer aniso-axial length group) and

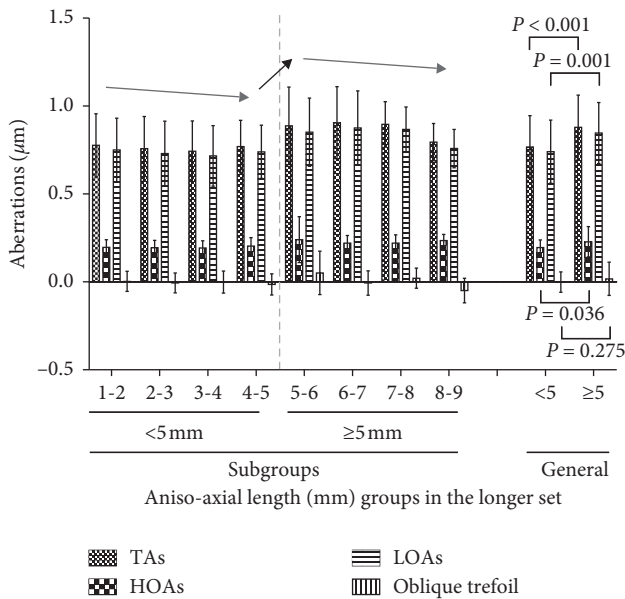


FIGURE 3: Distribution of posterior corneal aberrations among the eight subgroups in the longer set. TAs=total aberrations; HOAs=high-order aberrations; LOA=low-order aberrations. For the aniso-axial length subgroups, a value of 1 mm is included in the 1-2 mm subgroup and similarly for other values that fall at the boundary between two subgroups. The P values for TAs, HOAs, LOAs, and oblique trefoil with analyses of variance among the eight aniso-axial length subgroups in the longer set were 0.025, 0.005, 0.039, and 0.040, respectively. The P values for TAs, HOAs, LOAs, and oblique trefoil using independent Student's t test between aniso-axial length eyes in the longer set with and without AL ≥ 5 mm were <0.001 , 0.036, 0.001, and 0.275, respectively.

were incredibly young (58.01 ± 10.57 years old in the aniso-axial length group). This is consistent with our previous publication based on the same cataract population, reporting 26.65% patient with an AL >26 mm among 6747 eyes from 6747 patients [20]. There are two reasons for such a large proportion of high myopia in this population. First, urban China has a high prevalence of high myopia. In survey among university students in Shanghai, which is the most advanced area in China and the location of our hospital, the prevalence of high myopia was 19.5% in 2012 [22]. Second, instead of an epidemiological investigation, our study population is a retrospective hospital-based clinical research. Our hospital is one of the top specialized hospitals in ophthalmology in China, high-myopia patients come to our hospital in great numbers. Thus, the percentage of high myopia in our cataract patients rises to 25% in this study. As high-myopia patients tended to develop cataract early [23], it was reasonable to have relatively young cataract population compared with the general population.

In this study, using a definition of aniso-axial length/anisometropia as a binocular axial difference of 1 mm (about 3 D), the percentage of aniso-axial length patients was 15.09% (505/3347). Most aniso-axial length patients had 1-2 D asymmetry in AL between the two eyes (275/505 = 54.46% with no age limit; Figure 1). Deng et al. [24] reported a prevalence of anisometropia of $>20\%$ in elderly

patients of >1 D spherical refraction. Our comparatively lower fraction seems credible as stricter definition of aniso-axial length/anisometropia was applied.

Among all the aniso-axial length patients, we detected greater tendencies for female patients to develop aniso-axial length and for the right eye to be the longer one, which are consistent with the findings of Linke et al. [25] and Singh et al. [9], respectively. Many studies support the proposition that the dominant eye is the more myopic in patients with myopic anisometropia [26–29]. The dextrorality might contribute to the greater proportion of myopic right eyes and right dominance of eyes [30]. So, it is reasonable to find the right eyes as the longer ones in aniso-axial length individuals with the dextrorality of Chinese.

In this study, we found no significant differences in corneal biometrics between the two eyes of aniso-axial length patients, except anterior corneal astigmatism (1.01 ± 0.70 D in the shorter eyes vs 1.12 ± 0.76 D in the longer eyes, $P = 0.031$), and only slightly greater aberrations in the shorter eyes compared with the longer eyes of aniso-axial length patients (all $P > 0.05$ for anterior corneal, posterior, and total cornea; data not shown). These findings are roughly consistent with those of previous studies [1, 31] of anisomyopes, which have reported similar levels of aberrations between the two eyes or slightly higher levels in the less myopic eye.

The focus of this study was the comparison of the longer and shorter eyes of aniso-axial length patients with the AL-matched eyes of non-aniso-axial length patients. To our surprise, when examining the anterior corneal surface, only $K2$ differed between the aniso-axial length and non-aniso-axial length groups (44.13 ± 1.69 D vs 43.87 ± 1.69 D, $P = 0.009$). $K1$, $K2$, Rm , and Km of the posterior corneal surface in both the longer set and the shorter set had significant lower values (larger absolute values when negative) in the aniso-axial length group than in the non-aniso-axial length group (Table 2). This might make some compensation for the binocular refractive imbalance in aniso-axial length patients. Though the contribution of the posterior corneal curvature is small [32], its effects on total corneal refractive status should not be neglected casually, especially in aniso-axial length patients.

Because of the difference in the corneal curvature, we expected to find a difference in corneal astigmatism between eyes from the aniso-axial length and the non-aniso-axial length groups. Astigmatism was greater in the longer aniso-axial length group than those in the longer non-aniso-axial length group, but only significant in anterior corneal astigmatism (1.12 ± 0.76 D vs 1.02 ± 0.69 D for the anterior corneal surface, $P = 0.023$; and 0.30 ± 0.19 D vs 0.29 ± 0.16 D for the posterior corneal surface, $P = 0.377$; Figure 2). Though no difference in posterior corneal astigmatism may hold true in the means, it cannot be so in individuals, as posterior corneal curvatures ($K1$, $K2$, and Km) were smaller in the aniso-axial length group than those in the non-aniso-axial length group. Again, the contribution of posterior corneal surface to the total corneal refractive status should be paid attention to in aniso-axial length individuals.

Though statistically significant, the difference of anterior corneal astigmatism between the longer aniso-axial length and the non-aniso-axial length was only 0.10 D. This is partially consistent with previous studies that have shown that the asymmetry of the ocular refractive status does not seriously affect the cornea, while some have reported statistically significant effects [1, 8, 33, 34]. It also confirmed a smaller contribution of corneal astigmatism to the anisometropia compared with defocus (where AL plays an important role), supporting the rationale of defining aniso-axial length/anisometropia as AL asymmetry. As we matched these eyes from the aniso-axial length patients solely by AL to the eyes of other non-aniso-axial length patients, the mean corneal powers were also very similar and the difference in mean corneal astigmatism was small. And most of the other parameters are similar, which seems to indicate, a little indirectly, that axial length is the main thing that varies.

Of the SAs and other HOAs, the total corneal SA of the aniso-axial length eyes remained stable at $0.302 \pm 0.120 \mu\text{m}$ in the longer set and $0.306 \pm 0.125 \mu\text{m}$ in the shorter set and did not differ from those of the non-aniso-axial length patients (both $P > 0.050$). The tendency of SA to be lower in the shorter set than in the longer aniso-axial length group is consistent with our previous study [19] of 502 eyes with cataract and axially high myopia, and 1500 eyes with age-related cataracts ($0.281 \pm 0.207 \mu\text{m}$ vs $0.314 \pm 0.153 \mu\text{m}$ for total corneal SA, respectively, $P < 0.001$). The implantation of an aspheric IOL with $-0.20 \mu\text{m}$ to achieve an outcome of $+0.10 \mu\text{m}$ SA would be the preferred option, as described before [19]. The range of total corneal SAs in the non-aniso-axial length group was -0.154 to $0.702 \mu\text{m}$ (one abnormal case excluded), and the distribution of SAs of the aniso-axial length group (from -0.365 to $0.742 \mu\text{m}$) was wide. Therefore, customized SA correction may be the best option for the aniso-axial length cataract population. Although a negative ocular SA might lead to axial elongation, it seems that the incidence of negative corneal SA does not correlate with the monocular AL, regardless of whether there is a binocular axial difference (Appendix Table A1).

ANOVA with LSD post hoc correction of the corneal biometrics in the subgroups with various axial differences in the longer set indicated a clear cut-off at 5 mm for the posterior corneal TAs, HOAs, LOAs, and oblique trefoil (Figure 3). This is inconsistent with an axial cut-off at 5 or 7 mm in the longer set (Appendix Table A2). Our previous studies [19, 35] suggest that the corneal aberrations of highly myopic cataract patients and those with age-related cataract differed only slightly and these are insufficient to explain these results. More care must be taken in future clinical studies, and more attention should be paid to posterior corneal aberrations.

The first limitation of this study was its retrospective design without the inclusion of IOL formulae or postoperative refractive outcomes. However, this study is a foundational analysis for a later study, detecting potential differences in refraction-affecting anterior segmental biometrics. The second limitation was that no case with binocular astigmatism difference (especially total corneal

astigmatism) was studied because we focused on the asymmetry of AL. Further analyses based on binocular asymmetry of the total corneal astigmatism and inconsistencies its axis/division are required to provide general indications for toric IOL implantation in aniso-astigmatism patients.

In conclusion, eyes of aniso-axial length individuals share generally similar corneal biometrics with normal eyes in cataract population. Anterior corneal astigmatism of the longer eyes from the aniso-axial length cataract patients was higher than that of the longer eyes from the non-aniso-axial length individuals. Total posterior corneal aberrations of the longer aniso-axial length eyes increased when the binocular axial difference was over 5 mm.

Data Availability

Raw data were generated at the Eye and ENT Hospital of Fudan University, Shanghai, China. Derived data supporting the findings of this study are available from the corresponding author on request.

Additional Points

Synopsis. Eyes of aniso-axial length individuals share generally similar corneal biometrics with normal eyes in cataract population. Anterior corneal astigmatism of the longer eyes from the aniso-axial length cataract patients was higher than that of the longer eyes from the non-aniso-axial length individuals.

Conflicts of Interest

The authors declare no conflicts of interest.

Acknowledgments

The authors thank Dongjin Qian, PhD, of the Eye and ENT Hospital of Fudan University for data acquisition. This study was funded by the Scientific Innovation Project of Shanghai Science and Technology Commission (grant no. 18411965200) and the National Natural Science Foundation of China (grant no. 81770908).

Supplementary Materials

Appendix methods: axial length match. Appendix Table A1: patients with negative total corneal SAs in the advanced analysis. Appendix Table A2: comparison of axial lengths among the different binocular axial difference subgroups of the longer aniso-axial length set. (*Supplementary Materials*)

References

- [1] S. J. Vincent, M. J. Collins, S. A. Read, and L. G. Carney, "Myopic anisometropia: ocular characteristics and aetiological considerations," *Clinical and Experimental Optometry*, vol. 97, no. 4, pp. 291–307, 2014.

- [2] B. T. Barrett, A. Bradley, and T. R. Candy, "The relationship between anisometropia and amblyopia," *Progress in Retinal and Eye Research*, vol. 36, pp. 120–158, 2013.
- [3] A. Yekta, A. Fotouhi, H. Hashemi et al., "The prevalence of anisometropia, amblyopia and strabismus in schoolchildren of Shiraz, Iran," *Strabismus*, vol. 18, no. 3, pp. 104–110, 2010.
- [4] E. L. Smith 3rd., L.-F. Hung, B. Arumugam, J. M. Wensveen, Y. M. Chino, and R. S. Harwerth, "Observations on the relationship between anisometropia, amblyopia and strabismus," *Vision Research*, vol. 134, pp. 26–42, 2017.
- [5] S. R. Bharadwaj and T. R. Candy, "The effect of lens-induced anisometropia on accommodation and vergence during human visual development," *Investigative Ophthalmology & Visual Science*, vol. 52, no. 6, pp. 3595–3603, 2011.
- [6] L. O'Donoghue, J. F. McClelland, N. S. Logan, A. R. Rudnicka, C. G. Owen, and K. J. Saunders, "Profile of anisometropia and aniso-astigmatism in children: prevalence and association with age, ocular biometric measures, and refractive status," *Investigative Ophthalmology & Visual Science*, vol. 54, no. 1, pp. 602–608, 2013.
- [7] K. Tekin, V. Cankurtaran, M. Inanc, M. A. Sekeroglu, and P. Yilmazbas, "Effect of myopic anisometropia on anterior and posterior ocular segment parameters," *International Ophthalmology*, vol. 37, no. 2, pp. 377–384, 2017.
- [8] H. Hashemi, M. Khabazkhoob, M. H. Emamian, M. Shariati, T. Abdolahi-nia, and A. Fotouhi, "All biometric components are important in anisometropia, not just axial length," *British Journal of Ophthalmology*, vol. 97, no. 12, pp. 1586–1591, 2013.
- [9] N. Singh, J. Rohatgi, and V. Kumar, "A prospective study of anterior segment ocular parameters in anisometropia," *Korean Journal of Ophthalmology*, vol. 31, no. 2, pp. 165–171, 2017.
- [10] N. P. Brown, J. F. Koretz, and A. J. Bron, "The development and maintenance of emmetropia," *Eye (Lond)*, vol. 13, no. Pt 1, pp. 83–92, 1999.
- [11] G. Haegerstrom-Portnoy, M. E. Schneck, L. A. Lott, S. E. Hewlett, and J. A. Brabyn, "Longitudinal increase in anisometropia in older adults," *Optometry and Vision Science*, vol. 91, no. 1, pp. 60–67, 2014.
- [12] C. W. Lee, S. Y. Fang, D. C. Tsai et al., "Prevalence and association of refractive anisometropia with near work habits among young school children: the evidence from a population-based study," *PLoS One*, vol. 12, no. 3, Article ID e0173519, 2017.
- [13] O. Pärssinen, M. Kauppinen, J. Kaprio, and T. Rantanen, "Anisometropia of ocular refractive and biometric measures among 66- to 79-year-old female twins," *Acta Ophthalmologica*, vol. 94, no. 8, pp. 768–774, 2016.
- [14] M. Moshirfar, B. Buckner, Y. C. Ronquillo, and D. Hofstedt, "Biometry in cataract surgery," *Current Opinion in Ophthalmology*, vol. 30, no. 1, pp. 9–12, 2019.
- [15] P. G. Gobbi, F. Fasce, S. Bozza, and R. Brancato, "Optomechanical eye model with imaging capabilities for objective evaluation of intraocular lenses," *Journal of Cataract & Refractive Surgery*, vol. 32, no. 4, pp. 643–651, 2006.
- [16] B. Vojnikovic and E. Tamajo, "Gullstrand's optical schematic system of the eye—modified by Vojnikovic & Tamajo," *Collegium Antropologicum*, vol. 37, no. Suppl 1, pp. 41–45, 2013.
- [17] H.-L. Liou and N. A. Brennan, "Anatomically accurate, finite model eye for optical modeling," *Journal of the Optical Society of America A*, vol. 14, no. 8, pp. 1684–1695, 1997.
- [18] M. Zejmo, M. Formińska-Kapuścik, E. Pieczara et al., "Etiopathogenesis and management of high-degree myopia. Part I," *Medical Science Monitor: International Medical Journal of Experimental and Clinical Research*, vol. 15, no. 9, pp. RA199–202, 2009.
- [19] M. Zhang, D. Qian, Q. Jing, J. Chen, and Y. Jiang, "Analysis of corneal spherical aberrations in cataract patients with high myopia," *Scientific Reports*, vol. 9, no. 1, p. 1420, 2019.
- [20] M. Zhang, D. Qian, Q. Jing, J. Chen, M. Deng, and Y. Jiang, "Correlations of corneal spherical aberration with astigmatism and axial length in cataract patients," *Journal of Ophthalmology*, vol. 2019, p. 7, Article ID 4101256, 2019.
- [21] Y. Shapira, I. Vainer, M. Mimouni et al., "Effect of anisometropia on the predictability and accuracy of refractive surgery," *Cornea*, vol. 35, no. 11, pp. 1410–1415, 2016.
- [22] J. Sun, J. Zhou, P. Zhao et al., "High prevalence of myopia and high myopia in 5060 Chinese university students in Shanghai," *Investigative Ophthalmology & Visual Science*, vol. 53, no. 12, pp. 7504–7509, 2012.
- [23] X. Wang, D. Li, Y. Du, W. He, and Y. Lu, "DNA hypermethylation-mediated downregulation of antioxidant genes contributes to the early onset of cataracts in highly myopic eyes," *Redox Biology*, vol. 19, pp. 179–189, 2018.
- [24] L. Deng, J. Gwiazda, R. E. Manny et al., "Limited change in anisometropia and aniso-axial length over 13 years in myopic children enrolled in the correction of myopia evaluation trial," *Investigative Ophthalmology & Visual Science*, vol. 55, no. 4, pp. 2097–2105, 2014.
- [25] S. J. Linke, G. Richard, and T. Katz, "Prevalence and associations of anisometropia with spherical ametropia, cylindrical power, age, and sex in refractive surgery candidates," *Investigative Ophthalmology & Visual Science*, vol. 52, no. 10, pp. 7538–7547, 2011.
- [26] S. J. Vincent, M. J. Collins, S. A. Read, L. G. Carney, and M. K. Yap, "Interocular symmetry in myopic anisometropia," *Optometry and Vision Science: Official Publication of the American Academy of Optometry*, vol. 88, no. 12, pp. 1454–1462, 2011.
- [27] Q. Wang, Y. Wu, W. Liu, and L. Gao, "Dominant eye and visual evoked potential of patients with myopic anisometropia," *Biomed Research International*, vol. 2016, Article ID 5064892, 6 pages, 2016.
- [28] S. J. Linke, J. Baviera, G. Richard, and T. Katz, "Association between ocular dominance and spherical/astigmatic anisometropia, age, and sex: analysis of 1274 hyperopic individuals," *Investigative Ophthalmology & Visual Science*, vol. 53, no. 9, pp. 5362–5369, 2012.
- [29] S. J. Linke, J. Baviera, G. Munzer, J. Steinberg, G. Richard, and T. Katz, "Association between ocular dominance and spherical/astigmatic anisometropia, age, and sex: analysis of 10,264 myopic individuals," *Investigative Ophthalmology & Visual Science*, vol. 52, no. 12, pp. 9166–9173, 2011.
- [30] S. Jiang, Z. Chen, H. Bi et al., "Elucidation of the more myopic eye in anisometropia: the interplay of laterality, ocular dominance, and anisometropic magnitude," *Scientific Reports*, vol. 9, no. 1, p. 9598, 2019.
- [31] A. Hartwig, D. A. Atchison, and H. Radhakrishnan, "Higher-order aberrations and anisometropia," *Current Eye Research*, vol. 38, no. 1, pp. 215–219, 2013.
- [32] Y. Y. Jin, Z. Zhou, X. Y. Yuan, H. Song, and X. Tang, "Effect of the posterior corneal surface on total corneal astigmatism in patients with age-related cataract," *International Journal of Ophthalmology*, vol. 11, no. 6, pp. 958–965, 2018.
- [33] E. Mohammadi, H. Hashemi, M. Khabazkhoob, M. H. Emamian, M. Shariati, and A. Fotouhi, "The prevalence of anisometropia and its associated factors in an adult

population from Shahroud, Iran,” *Clinical and Experimental Optometry*, vol. 96, no. 5, pp. 455–459, 2013.

- [34] Z. Jiang, M. Shen, R. Xie, J. Qu, A. Xue, and F. Lu, “Interocular evaluation of axial length and retinal thickness in people with myopic anisometropia,” *Eye & Contact Lens: Science & Clinical Practice*, vol. 39, no. 4, pp. 277–282, 2013.
- [35] M. Zhang, Q. Jing, J. Chen, and Y. Jiang, “Analysis of corneal higher-order aberrations in cataract patients with high myopia,” *Journal of Cataract & Refractive Surgery*, vol. 44, no. 12, pp. 1482–1490, 2018.

Research Article

Keratoconus Diagnosis: Validation of a Novel Parameter Set Derived from IOP-Matched Scenario

Dan Lin ¹, Lei Tian ^{2,3,4}, Shu Zhang ¹, Like Wang ¹, Ying Jie ² and Yongjin Zhou ¹

¹Shenzhen University, Health Science Center, School of Biomedical Engineering, Xueyuan Avenue 1066, Shenzhen 518055, China

²Beijing Institute of Ophthalmology, Beijing Tongren Eye Center, Beijing Tongren Hospital, Capital Medical University, Beijing, China

³Beijing Ophthalmology & Visual Sciences Key Laboratory, National Engineering Research Center for Ophthalmology, Beijing 100730, China

⁴Beijing Advanced Innovation Center for Big Data-Based Precision Medicine, Beihang University and Capital Medical University, Beijing Tongren Hospital, Beijing 100730, China

Correspondence should be addressed to Ying Jie; jie_yingcn@aliyun.com and Yongjin Zhou; yjzhou@szu.edu.cn

Received 25 June 2020; Revised 28 August 2020; Accepted 3 October 2020; Published 28 October 2020

Academic Editor: Yu Chi Liu

Copyright © 2020 Dan Lin et al. This is an open access article distributed under the Creative Commons Attribution License, which permits unrestricted use, distribution, and reproduction in any medium, provided the original work is properly cited.

Purpose. Considering that intraocular pressure (IOP) is an important confounding factor in corneal biomechanical evaluation, the notion of matching IOP should be introduced to eliminate any potential bias. This study aimed to assess the capability of a novel parameter set (NPS) derived from IOP-matched scenario to diagnose keratoconus. **Methods.** Seventy samples (training set; 35 keratoconus and 35 normal corneas; pairwise matching for IOP) were used to determine NPS by forward logistic regression. A large validation dataset comprising 62 matching samples (31 keratoconus and 31 normal corneas) and 203 unmatched samples (112 keratoconus and 91 normal corneas) was used to evaluate its clinical significance. To further assess its diagnosis capability, NPS was compared with the other two prior biomechanical indexes. **Results.** NPS was comprised of three biomechanical parameters, namely, DA Ratio Max 1 mm (DRM1), the first applanation time (AT1), and an energy loading parameter (Eload). NPS was successfully applied to the validation dataset, with a higher accuracy of 96.8% and 95.6% in the IOP-matched and -unmatched scenarios, respectively. More surprisingly, accuracy of NPS was 95.5% in the combined validation, an improvement compared to the two prior biomechanical indexes. **Conclusions.** This is the first study taking IOP bias into consideration to determine a biomechanical parameter set. Our study shows that NPS indeed offers comparable performance in keratoconus diagnosis. **Translational Relevance.** Determining a parameter set after eliminating the influence from IOP is useful in revealing the essential differences between keratoconus and normal corneas and possibly facilitating further progress in keratoconus diagnosis.

1. Introduction

The clinical diagnosis of keratoconus remains a significant challenge, especially before the appearance of any signs or symptoms. It has been well documented that the changes in the biomechanical properties of keratoconus are postulated to occur before the disease becomes tomographically apparent [1–4]. These changes can be certainly attributed to the abnormalities in stromal collagen [1–4]. Therefore, it is becoming increasingly popular to detect keratoconus with the biomechanical parameters derived from Corneal

Visualization Scheimpflug Technology (Corvis ST, Oculus, Germany).

Corvis ST is a relatively new device that induces corneal deformation with an air puff and allows the real-time monitoring of the entire deformation process using an ultra-high-speed Scheimpflug camera [5, 6]. During the dynamic process of corneal deformation, Corvis ST can be used to simultaneously measure the corneal biomechanical parameters and intraocular pressure (IOP). More recently, IOP has been gradually accepted as a biasing factor for corneal biomechanical evaluation [7, 8], and thus it is supposed to be

excluded to ensure an unbiased analysis. Unfortunately, in the field of keratoconus diagnosis, there is a lack of studies that determine the combined biomechanical parameters from the perspective of IOP matching. Additionally, plethora of new and important biomechanical parameters [5, 9] is catching up, but prior studies [10–12] have not considered them yet.

To make matters more precise and comprehensive, it is our job to develop a novel parameter set (NPS) taking IOP bias and new biomechanical parameters into consideration. As we will show later, adopting this new parameter set allows clinicians to diagnose keratoconus better and easier.

2. Patients and Methods

2.1. Patients. A total of 335 corneal samples were included in this study, which are divided into two groups: keratoconus group ($n = 178$) and normal cornea group ($n = 157$). Among them, 132 corneal samples (66 keratoconic corneas and 66 normal corneas) were pairwise matched for IOP, while the remaining 203 eyes (112 keratoconic corneas and 91 normal corneas) were not matched for IOP. The maximum IOP difference between the pairs was 0.6 mm Hg. 70 corneas with IOP-matched scenario were randomly selected for the assessment of parameter set. Moreover, 62 and 203 corneas with IOP-matched and IOP-unmatched scenarios, respectively, were used to assess the performance of the parameter set. For patients diagnosed with keratoconus in only one eye, the particular eye was selected for measurement. Meanwhile, one eye was randomly selected from normal controls and patients with keratoconus in both eyes.

All patients underwent a complete ophthalmic examination, including a detailed assessment of uncorrected distance visual acuity, corrected distance visual acuity, slit-lamp microscopy and fundus examination, corneal topography (Allegro Topolyzer; WaveLight Laser Technologie AG, Erlangen, Germany), corneal tomography (Pentacam; Oculus Optikgeräte GmbH), ocular biomechanics, and IOP measurement (Corvis ST). All measurements were performed by two experienced ophthalmologists in a single visit. A diagnosis of keratoconus was carried out if the eye had (i) an irregular cornea, determined by distorted keratometry mires or distortion of the retinoscopic or ophthalmoscopic red reflex, and (ii) at least one of the following slit-lamp signs: Vogt's striae, Fleischer's ring with an arc >2 mm, or corneal scarring consistent with keratoconus [13–15].

Potential subjects were excluded from this study if they (i) had previously undergone corneal or ocular surgery, (ii) had ocular pathology other than keratoconus, and/or (iii) had systemic diseases that affect their eye. All participants were asked to remove soft contact lenses for at least 2 weeks and rigid contact lenses for at least 1 month prior to the examination. Clinical data were collected in 2018 at the Beijing Institute of Ophthalmology, Beijing Tongren Hospital, Beijing, China. All participants signed a written informed consent form, in accordance with the ethical principles stated in the Declaration of Helsinki.

2.2. Collection of Parameters. A total of 21 biomechanical parameters were extracted, including 11 parameters from the Corvis ST software, 9 parameters proposed by our group previously, and 1 parameter defined by other scholars.

Corvis ST allows the noninvasive imaging of the cornea's dynamic deformation in response to an air puff. A high-speed Scheimpflug camera records the movements of the cornea and then displays them on the built-in control panel in a slow motion. During the deformation response, a precisely metered air pulse causes the cornea to move inward or flatten (the phenomena of corneal applanation), which is known as the first applanation (A1). The cornea continues to move inward until reaching a point with highest concavity. After that, it rebounds from this concavity to another point of applanation (A2) and then returns to its normal convex curvature. After completing the deformation process, several output measurements are generated from Corvis ST. All these parameters and their details are listed in Table 1.

Our research team has proposed several new parameters to measure the biomechanical behavior of corneas [9]. For instance, maximum area of deformation (MA) is used to describe the maximum corneal deformation area within the two knees. Maximum area–time of deformation (MA-time) represents the time from the beginning of deformation to the occurrence of maximum deformation area. Corneal contour deformation (CCD) describes a distance between the original contour and the contour with the highest concavity. Maximum corneal inward/outward velocity (V_{inmax}/V_{outmax}) represents the maximum corneal inward/outward deformation velocity at centerline. In 2016, we subsequently proposed energy absorbed area ($A_{absorbed}$) and Tangent stiffness coefficient (S_{TSC}) to indicate the corneal viscosity and elasticity, respectively [5]. Additionally, the corneal viscoelasticity is defined by both energy loading (Eload) and energy return (Ereturn) of cornea during the air puff indentation.

Stiffness parameter (SP-A1) is a parameter associated with corneal stiffness [16], which has been defined as resultant pressure (Pr) divided by the amplitude of deformation at A1. Pr is defined as the adjusted pressure at A1 (adj-AP1) minus a biomechanically corrected IOP (bIOP) [17]. The computational formula is as follows: $SP-A1 = (adj-AP1 - bIOP)/\text{deformation amplitude at A1}$.

2.3. Statistical Analysis. Statistical analyses were performed using R (RStudio 3.4.0). The Kolmogorov–Smirnov test was used to assess the normality of data. Both Welch's modified Student's two-sample t -test and Mann–Whitney U test were applied to compare the difference of biomechanical parameters between keratoconus and normal groups. P values less than 0.05 were considered statistically significant.

Forward logistic regression was performed to determine NPS based on all the biomechanical parameters in IOP-matched scenario. Area under the Curve of ROC (AUC), F1 score, sensitivity, specificity, and accuracy were calculated to evaluate the discriminative ability of parameter sets. The values closer to 1 indicate a greater performance.

TABLE 1: Biomechanical parameters derived from the Corvis ST software and their corresponding definitions.

Parameters	Abbreviation	Definitions
The time of the first applanation (ms)	AT1	The length of time from the initiation of air puff to the first applanation
The time of the second applanation (ms)	AT2	The length of time from the initiation of air puff to the second applanation
The length of the first applanation (mm)	AL1	The lengths of flattened cornea at the first applanation
The length of the second applanation (mm)	AL2	The lengths of flattened cornea at the second applanation
The velocity of the first applanation (m/s)	V_{in}	Speed of corneal apex at the first applanation
The velocity of the second applanation (m/s)	V_{out}	Speed of corneal apex at the second applanation
The time of highest concavity (ms)	HC-time	Time from the initiation of air puff until the highest concavity of the cornea
DA Ratio Max 1 mm	DRM1	Maximum ratios of corneal deformation at the apex divided by the average deformation 1 mm to either side of the apex
Peak distance (mm)	PD	Distance of the two knees at highest concavity
Deformation amplitude (mm)	DA	Maximum deformation amplitude at highest concavity
The highest radius of concavity (mm)	HC-radius	Corneal concave curvature at its highest concavity

TABLE 2: The comparison of bIOP, CCT, and the three biomechanical parameters of NPS with IOP-matched scenario between keratoconus group ($n=35$) and normal cornea group ($n=35$).

Parameters	Keratoconus ($n=35$)	Normal ($n=35$)	P
bIOP [17]	13.89 ± 1.23	13.45 ± 1.02	0.142*
Age	23.49 ± 7.05	23.66 ± 4.21	0.902#
CCT	489.20 ± 27.66	532.92 ± 26.64	0.000*
AT1	6.30 ± 0.34	6.90 ± 0.32	0.000*
DRM1	1.18 ± 0.02	1.17 ± 0.01	0.012*
Eload	108.50 ± 9.13	90.71 ± 6.67	0.000#

[17] IOP from Corvis ST was corrected based on finite element modeling. Pairwise matching was performed for bIOP. *Two-tailed Student's t -test. #Mann-Whitney U test.

3. Results

In the present study, bIOP was used to correct IOP based on the finite element modeling [17]. As shown in Table 2, all parameters were significantly different between keratoconus and normal cornea groups ($P < 0.05$), except for bIOP and age.

As a consequence, the three significantly differential parameters, namely, DRM1, AT1, and Eload, were selected for NPS. The equations are presented as follows:

$$\text{Beta} = ((A1 * \text{DRM1}) + (A2 * \text{AT1}) + (A3 * \text{Eload}) + A4),$$

$$\text{Possibility} = \frac{\exp(\text{Beta})}{(1 + \exp(\text{Beta}))} \quad (1)$$

The impact of each NPS parameter was evaluated, as demonstrated in Figure 1. When Eload was included in the logistic regression model, the AUC of NPS was found to be 96.8%, with a sensitivity of 91.4% and specificity of 88.6%. Following the addition of AT1, the AUC and specificity of

NPS were improved to 97.7% and 91.4%, respectively. Lastly, after the inclusion of DRM1, NPS exhibited the highest AUC, accuracy, sensitivity, and specificity of 98.5%, 94.3%, 94.3%, and 94.3%, respectively, at the optimal cut-off point of 0.5.

The performance of NPS in both training set and validation set was illustrated in Figure 2. Interestingly, NPS performed better in the validation set (accuracy = 96.8% and 95.6% in IOP-matched and -unmatched validation, respectively) than in the training set (accuracy = 94.3%). More notably, in both training set and validation set, NPS exhibited the same score of three evaluation indicators at the best cut-off point of 0.5.

Likewise, in the combined validation, NPS showed a comparable diagnosis capability compared to two reported parameter sets, namely, adjusted Corvis Biomechanical Index (aCBI) [11] and Dynamic Corneal Response Index (DCR) [12]; see Figure 3. The AUC of NPS (98.0%) was slightly higher than the other two parameter sets (aCBI: 97.3%; DCR: 93.2%). At the optimal cut-off point of 0.5, the accuracy of NPS reached 95.5%, while it reached 93.6% for aCBI and 86.0% for DCR.

4. Discussion

With the confounding influence of IOP being discovered gradually, how are we supposed to diagnose keratoconus using biomechanical parameters from Corvis ST videos? Vinciguerra et al. [10] have reported that the parameter set determined from IOP-unmatched dataset and validated with IOP-matched scenario [11] can result in decreased accuracy. From our point of view, this decline is attributed not only to the matching of central corneal thickness (CCT) as presumed by the authors [11], but also to the fact that the parameter set is established from the IOP-unmatched dataset. Therefore, in this study, a dataset independent of IOP was deliberately used to determine the parameter set with no biasing effect of IOP. Moreover, two additional datasets of both IOP-influenced and IOP-

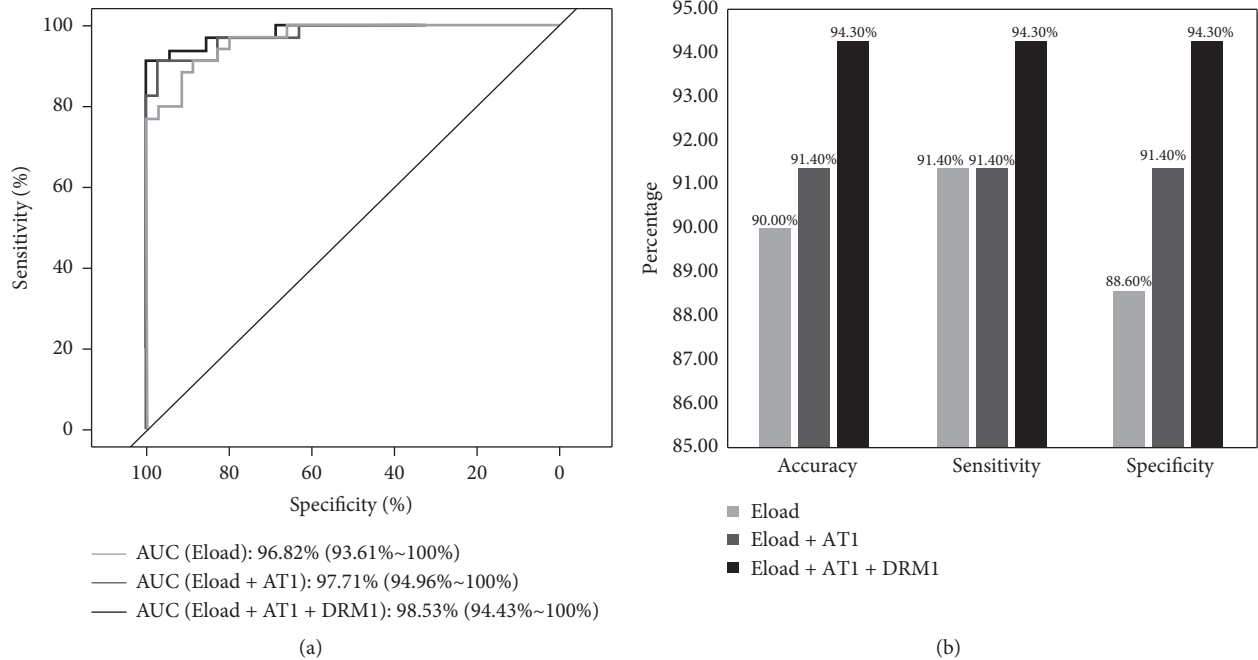


FIGURE 1: (a) Receiver operator characteristic curve for each step of the forward logistic regression in IOP-matched scenario (35 keratoconus and 35 normal eyes). (b) Gain in sensitivity and specificity with each step of the logistics regression to establish the novel NPS with IOP-matched scenario (35 keratoconus and 35 normal eyes; best cut-off point = 0.5).

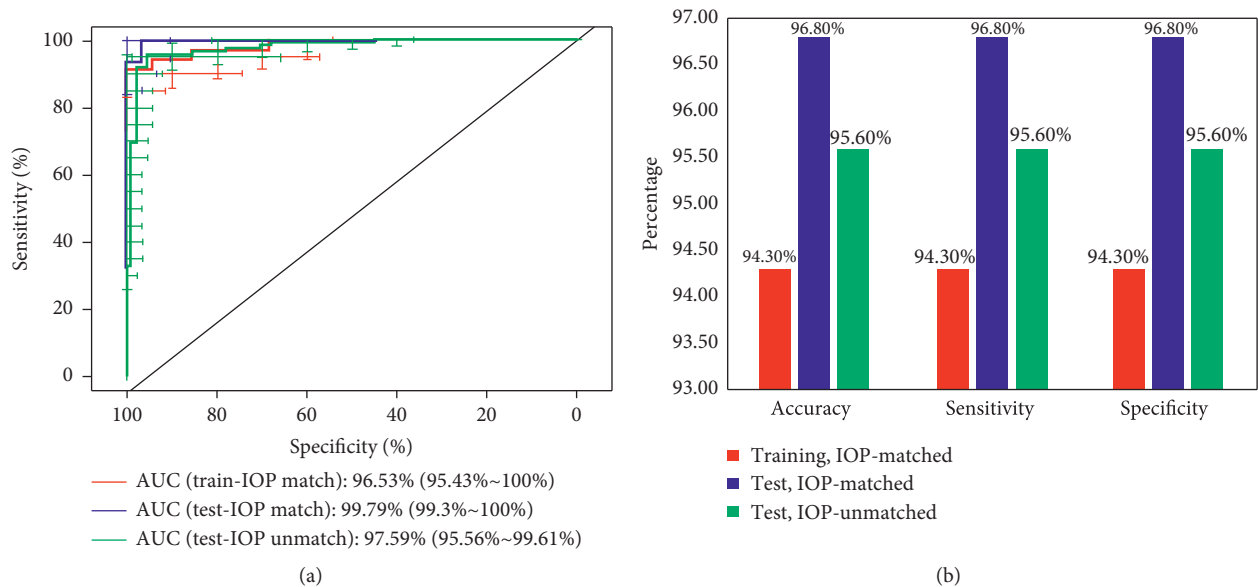


FIGURE 2: Representative graphs for ROC curves (a) and three evaluation indicators (accuracy, sensitivity, and specificity) (b) for NPS in both IOP-matched training set (35 keratoconus and 35 normal eyes), and IOP-matched (31 keratoconus and 31 normal eyes) and IOP-unmatched (112 keratoconus and 91 normal eyes) validation.

uninfluenced were used to validate the discriminative ability of NPS. Interestingly, the results demonstrated a slightly improved accuracy as well as the balanced indicators of NPS (Figure 2) during the validation step, which in turn confirmed the strategy of this study.

It has been noted that the biomechanical parameters reported in prior studies [10–12] are limited to those

available from Corvis ST software. In the present study, we incorporated more parameters from different sources [5, 9] to enable a comprehensive analysis. As presented in Figure 1, only 3 parameters (i.e., DRM1, Eload, AT1) were ultimately selected in IOP-matched group, in which Eload is obtained from an external data source [5]. This result indicated that new biomechanical parameters should be paid more

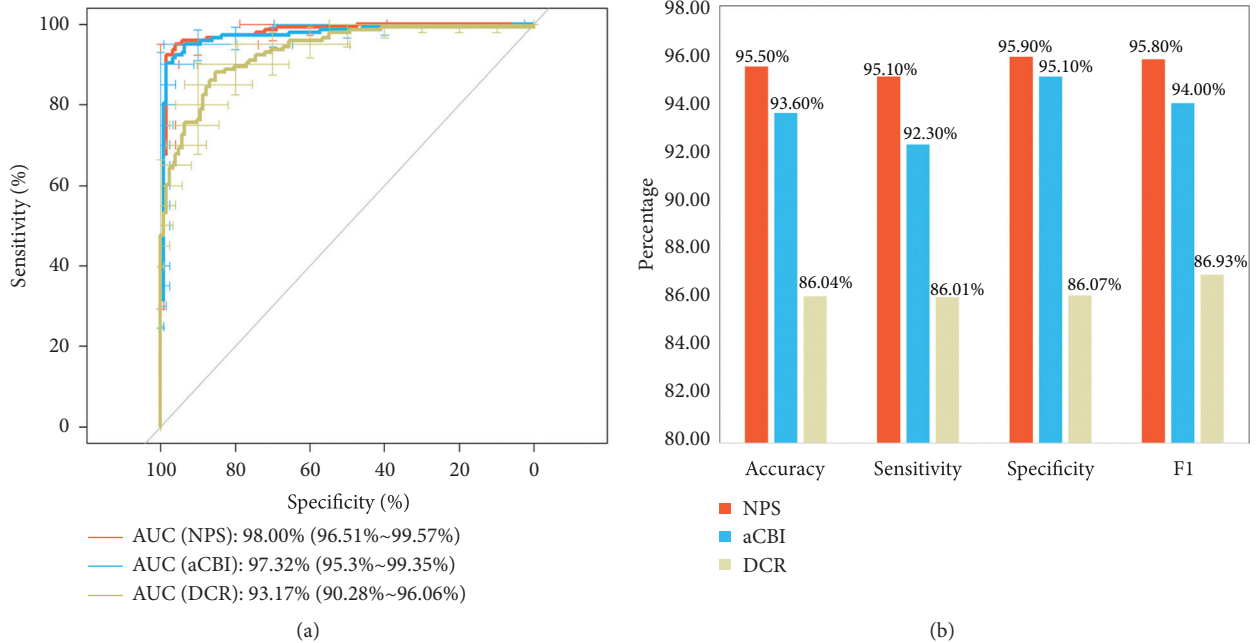


FIGURE 3: Representative graphs for ROC curves (a) and four evaluation indicators (accuracy, sensitivity, specificity, and F1) (b) of NPS, aCBI, and DCR in combined (145 keratoconus and 122 normal eyes) validation.

attention as they may provide valuable knowledge in terms of keratoconus detection.

As the main goal of our study was to validate whether a parameter set derived from IOP-matched scenario can exhibit its clinical significance in keratoconus diagnosis, comparing it with the established biomechanical indexes can help to achieve this goal. The results showed that NPS exhibited similar or better performance in the validation set (Figure 3). In our opinions, these may be primarily caused by the following four reasons. First, NPS incorporates a new biomechanical parameter, namely, Eload [5]. As a parameter describing energy loading during corneal deformation, Eload reflects the viscoelasticity, a significant biomechanical property of corneal tissues, thereby playing a big role in the diagnosis. Second, DRM1 is a well-known biomechanical parameter representing the ability of deformation. It makes an impact on keratoconus screening, which is consistent with prior studies [10–12]. Third, in general, the simpler the model, the greater the robustness. NPS contains only 3 parameters, which is less than aCBI or DCR, making it practical to adjust to each new dataset. Finally, the biomechanical parameters of NPS are chosen on the basis of IOP-matched scenario and hence are naturally stable and can be used to reveal the true difference between keratoconus and normal corneas. Given all these reasons, findings from this study could be interpreted to some extent.

It is worth noting that we deliberately did not match CCT, another confounding factor in corneal biomechanics [7], because we believed that, as an important part in the pathogenesis of keratoconus, corneal thinning should be included to reveal the resulting changes in biomechanical stability. Nevertheless, the potential limitation of this study is the lack of gold standard for measuring IOP as well as the appropriate statistical test for

evaluating indicators of these three biomechanical indexes (Figure 3). While there are signs of improvement, the results should be interpreted cautiously.

In conclusion, this study indicated that the parameter set (NPS) derived from IOP-matched scenario can effectively differentiate keratoconus from normal corneas. Using this parameter set prevents us from unnecessarily considering the confounding influence from IOP. It will lead to the ease of use in the clinical practice and the follow-up diagnosis success at earlier stages of keratoconus. Further research is warranted to further elucidate its potential use.

Data Availability

The data used to support the findings of this study are available from the corresponding author upon request.

Conflicts of Interest

All authors declare no conflicts of interest regarding the publication of this paper.

Authors' Contributions

Dan Lin and Lei Tian contributed equally to this work and should be considered as equal first authors.

Acknowledgments

This research was supported by the National Key R&D Program of China (2016YFC0104700); National Natural Science Foundation of China (31600758, 81471735, and 61427806); Beijing Natural Science Foundation (7174287);

Beijing Nova Program (Z181100006218099); the Open Research Fund from Beijing Advanced Innovation Center for Big Data-Based Precision Medicine, Beijing Tongren Hospital, Beihang University & Capital Medical University (BHTR-KFJJ-202001).

References

- [1] H. R. Vellara and D. V. Patel, "Biomechanical properties of the keratoconic cornea: a review," *Clinical and Experimental Optometry*, vol. 98, no. 1, pp. 31–38, 2015.
- [2] A. R. Jr, R. S. Alonso, A. Luz, and L. G. C. Velarde, "Corneal-thickness spatial profile and corneal-volume distribution: tomographic indices to detect keratoconus," *Journal of Cataract & Refractive Surgery*, vol. 32, no. 11, pp. 1851–1859, 2006.
- [3] A. Konstantopoulos, P. Hossain, and D. F. Anderson, "Recent advances in ophthalmic anterior segment imaging: a new era for ophthalmic diagnosis?" *British Journal of Ophthalmology*, vol. 91, no. 4, pp. 551–557, 2007.
- [4] V. Kozobolis, H. Sideroudi, A. Giarmoukakis, M. Gkika, and G. Labiris, "Corneal biomechanical properties and anterior segment parameters in forme fruste keratoconus," *European Journal of Ophthalmology*, vol. 22, no. 6, pp. 920–930, 2012.
- [5] L. K. Wang, L. Tian, and Y. P. Zheng, "Determining in vivo elasticity and viscosity with dynamic Scheimpflug imaging analysis in keratoconic and healthy eyes," *Journal of Biophotonics*, vol. 9, no. 5, pp. 54–463, 2016.
- [6] Y. Hon and A. K. C. Lam, "Corneal deformation measurement using Scheimpflug noncontact tonometry," *Optometry and Vision Science*, vol. 90, no. 1, pp. E1–E8, 2013.
- [7] R. Vinciguerra, A. Elsheikh, C. J. Roberts et al., "Influence of pachymetry and intraocular pressure on dynamic corneal response parameters in healthy patients," *Journal of Refractive Surgery*, vol. 32, no. 8, pp. 550–561, 2016.
- [8] T. Huseynova, G. O. Waring, C. Roberts, R. R. Krueger, and M. Tomita, "Corneal biomechanics as a function of intraocular pressure and pachymetry by dynamic infrared signal and Scheimpflug imaging analysis in normal eyes," *American Journal of Ophthalmology*, vol. 157, no. 4, pp. 885–893, 2014.
- [9] L. Tian, M. W. L. Ko, L.-k. Wang et al., "Assessment of ocular biomechanics using dynamic ultra high-speed Scheimpflug imaging in keratoconic and normal eyes," *Journal of Refractive Surgery*, vol. 30, no. 11, pp. 785–791, 2014.
- [10] R. Vinciguerra, R. Ambrósio, A. Elsheikh et al., "Detection of keratoconus with a new biomechanical index," *Journal of Refractive Surgery*, vol. 32, no. 12, pp. 803–810, 2016.
- [11] J. Steinberg, N. E. Amirabadi, A. Frings, J. Mehlan, T. Katz, and S. J. Linke, "Keratoconus screening with dynamic biomechanical in vivo Scheimpflug analyses: a proof-of-concept study," *Journal of Refractive Surgery*, vol. 33, no. 11, pp. 773–778, 2017.
- [12] R. N. Mercer, G. O. Waring, C. J. Roberts et al., "Comparison of corneal deformation parameters in keratoconic and normal eyes using a non-contact tonometer with a dynamic ultra-high-speed Scheimpflug camera," *Journal of Refractive Surgery*, vol. 33, no. 9, pp. 625–631, 2017.
- [13] U. D. Sanctics, C. Loiacono, L. Richiardi et al., "Sensitivity and specificity of posterior corneal elevation measured by pentacam in discriminating keratoconus/subclinical keratoconus," *Ophthalmology*, vol. 115, no. 9, pp. 1534–1539, 2008.
- [14] Ö. Ö. Uçakhan, V. Çetinkor, M. Özkan, and A. Kanpolat, "Evaluation of Scheimpflug imaging parameters in subclinical keratoconus, keratoconus, and normal eyes," *Journal of Cataract & Refractive Surgery*, vol. 37, no. 6, pp. 1116–1124, 2011.
- [15] K. Zadnik, J. T. Barr, T. B. Edrington et al., "Baseline findings in the collaborative longitudinal evaluation of keratoconus (CLEK) study," *Investigative Ophthalmology & Visual Science*, vol. 39, no. 13, pp. 2537–2546, 1998.
- [16] C. J. Roberts, A. M. Mahmoud, J. Bons et al., "A new stiffness parameter in air puff induced corneal deformation analysis," *Investigative Ophthalmology & Visual Science*, vol. 57, 2016.
- [17] A. A. Joda, M. M. S. Shervin, D. Kook, and A. Elsheikh, "Development and validation of a correction equation for corvis tonometry," *Computer Methods in Biomechanics and Biomedical Engineering*, vol. 19, no. 9, pp. 943–953, 2016.

Research Article

Bleb Morphology Using Anterior-Segment Optical Coherence Tomography after Ahmed Glaucoma Valve Surgery with Tenon Capsule Resection

Faried M. Wagdy 

Ophthalmology Department, Faculty of Medicine, Menofia University, Shebeen El-Kom, Egypt

Correspondence should be addressed to Faried M. Wagdy; fariedwagdy1976@gmail.com

Received 24 June 2020; Revised 1 October 2020; Accepted 5 October 2020; Published 23 October 2020

Academic Editor: Karim Mohamed Noriega

Copyright © 2020 Faried M. Wagdy. This is an open access article distributed under the Creative Commons Attribution License, which permits unrestricted use, distribution, and reproduction in any medium, provided the original work is properly cited.

Objectives. To evaluate the internal morphology of blebs using anterior-segment optical coherence tomography (AS-OCT) and the surgical outcomes of Ahmed glaucoma valve (AGV) surgery with Tenon capsule resection compared to conventional AGV surgery in patients with refractory glaucoma. **Patients and Methods.** This randomised prospective study included 30 eyes from 30 patients (age range: 42–55 y) with refractory glaucoma from March 2018 to February 2020. The study included two groups: AGV with the Tenon capsule resection group ($n = 15$) and the conventional AGV surgery group ($n = 15$). Follow-up continued until 6 months after surgery. The primary outcome was intraocular pressure (IOP) and its association with the number of postoperative glaucoma medications, best corrected visual acuity, visual field, and postoperative complications. The internal morphology of the blebs in both groups was evaluated at 1-day, 1-week, 1-month, 3-month, and 6-month follow-up using AS-OCT in terms of the consequent changes in bleb wall thickness, bleb wall reflectivity, and bleb cavity morphology throughout the 6-month follow-up period. **Results.** A significant reduction in IOP was found in both groups, with a greater reduction in group I, where the mean IOP decreased from 32.73 ± 2.12 mmHg in the preoperative period to 13.33 ± 1.59 mmHg after 6 months, whereas in group II, the mean IOP decreased from 33.2 ± 2.21 mmHg in the preoperative period to 14.27 ± 1.44 mmHg after 6 months (p value < 0.05). The difference between the 2 groups in terms of the decrease in IOP was insignificant except at 1 and 3 months, where there was a significant difference (p value = 0.016 and 0.01 at 1 and 3 months, respectively). The bleb analysis revealed a significant reduction in the wall thickness in both groups at 1 and 3 months, which was mostly associated with the hypertensive phase. In group I, the bleb wall thickness decreased from 754.67 ± 53.93 μ m in the first postoperative day to 684 ± 81.66 μ m and 671.6 ± 69.48 μ m at 1 and 3 months, respectively, while in group II, the bleb wall thickness decreased from 707.13 ± 31.7 μ m in the first postoperative day to 499.53 ± 99.1 μ m and 506 ± 76.91 μ m at 1 and 3 months, respectively. There was a significant reduction in AS-OCT, and bleb reflectivity was insignificant throughout the follow-up period (p value > 0.05). Regarding postoperative complications, the hypertensive phase occurred more frequently in group II (6 eyes, 40%) than in group I (2 eyes, 13.3%). Other complications were also reported more frequently in group II such as hypotony, shallow anterior chamber (AC), and tube exposure. **Conclusion.** AS-OCT was beneficial in the analysis of bleb morphology after AGV surgery where there were more diffuse functioning multicystic blebs and less thinning in the bleb wall thickness during the hypertensive phase after resection of the Tenon capsule, which might be related to the less incidence of fibrosis around the surgical site.

1. Introduction

Glaucoma drainage devices are important therapeutic tools for the management of refractory glaucoma with high success rates [1]. Ahmed glaucoma valve (AGV) is a glaucoma drainage shunt that is performed in refractory

glaucoma, especially after the failure of previous conventional surgeries. It allows the aqueous to flow directly through the valve tube and lowers the complications related to this technique [2–4]. Following AGV surgery, the bleb is subjected to two stages. The early hypotensive phase is followed by a hypertensive phase that tends to often occur at

1 month, and often stabilises at 6 months after the AGV implantation. The cause is still poorly understood [5]. The hypertensive phase occurred in 82% of the cases after Ahmed valve implantation. Partial intraoperative Tenon capsule resection using the Mitomycin C adjunctive may be effective in developing thin avascular blebs if performed during the Ahmed glaucoma valve surgery [6].

A novel technique of Tenon capsule resection combined with an AGV implantation was developed to clarify the effectiveness and the safety of the Tenon capsule resection, when it is performed during an AGV surgery, bringing a relatively low incidence of tube exposure and the hypertensive phase [7].

AS-OCT is a noncontact diagnostic method that presents a cross-sectional, three-dimensional, and high-resolution image of the anterior segment of the eye, with an axial resolution that ranges from 3 to 20 μm . There are two AS-OCT devices that are currently available: Visante-OCT (Carl Zeiss Meditec; USA) and slit-lamp OCT (SL-OCT; Heidelberg Engineering GmbH, Germany) [8, 9]. AS-OCT provides qualitative and quantitative assessments of the most important structures related to AGV surgery and can be used to assess the position of the tube in the anterior chamber (AC) and to determine the bleb characteristics and function. Although bleb imaging is usually performed by ultrasound biomicroscopy (UBM) [10, 11], AS-OCT can be useful to assess the bleb morphology and function and to differentiate between functioning and nonfunctioning blebs [12]. AS-OCT also can measure the maximum bleb wall thickness and the maximum bleb wall reflectivity after AGV surgery, which are usually affected by subsequent fibrosis in the bleb after surgery and are therefore used as indicators for the success of the surgery [13].

The present study was aimed to evaluate the internal bleb morphology of blebs using AS-OCT and the surgical outcomes of Ahmed glaucoma valve (AGV) surgery with Tenon capsule resection as compared to conventional AGV surgery in patients with refractory glaucoma.

2. Patients and Methods

Thirty eyes with refractory glaucoma, in spite of the maximally tolerated medication after previous trabeculectomy surgery, were included in a prospective, randomised, controlled clinical study that used a computer-generated random number table. This study was conducted in Menofia University Hospital between March 2018 and February 2020. Institutional research board committee approval was obtained. Two groups were studied: group I for the AGV surgery with Tenon capsule resection ($n = 15$ eyes) and group II for the conventional AGV surgery ($n = 15$ eyes). Preoperatively, all the patients were subjected to IOP measurement using the Goldman applanation tonometer, visual acuity assessment (VA) using Snellen E chart, visual field analysis (VF) by Humphrey visual field analyser, Angle examination by gonioscope, optic disc examination by Volk+90 lens, slit lamp examination for the assessment of the corneal clarity, and any corneal touch with the tube and anterior chamber depth. All the patients had peribulbar anaesthesia by the same surgeon.

3. Surgical Technique

3.1. Operative Technique in Group II (Conventional AGV Surgery). The AGV device should be primed before the surgery. Priming is performed using a 26G cannula, injecting 1 cc of balanced salt solution (BSS). The superior-temporal conjunctiva was incised and appropriately cauterised. Mitomycin C (MMC) at a concentration of 0.2 mg/ml was applied using 3 sponges soaked with MMC that were placed over the sclera and left for 2 minutes, followed by irrigation using a balanced salt solution, and the valve body plate was placed approximately 10 mm posterior to the corneal limbus and fixed to the underlying sclera with Nylon 10-0 sutures. A two-third thickness longitudinal scleral flap (2 mm \times 6 mm) was created, and the tube was then inserted for 2-3 mm into the AC parallel to the iris plane. The flap was closed tightly with Nylon sutures to avoid leakage around the tube. The tube was ligated to the underlying sclera with an 8-0 Vicryl. Conjunctiva and Tenon capsule were sutured with Nylon 10-0.

3.1.1. Operative Technique in Group I (AGV Surgery with Tenon Capsule Resection). The same steps were performed for the conventional AGV surgery, the difference being that the Tenon capsule was dissected from the limbus up to the posterior border of the AGV body plate. Finally, the conjunctiva was closed with nylon sutures.

3.1.2. Postoperative Management. Postoperative treatment included combined antibiotic and steroid eye drops every four hours in the first week with a gradual tapering after 2 weeks.

The surgical outcomes were evaluated based on the following:

- (i) IOP and the number of glaucoma medications: a complete success was defined as an IOP lower than 21 mmHg without treatment, a qualified success was defined as an IOP lower than 21 mmHg with medical treatment, failure was defined as an IOP more than 21 mmHg during any time throughout the follow-up period with medical treatment. The hypertensive phase was defined as an elevated IOP more than 21 mmHg during the first 3 months after surgery. If the hypertensive phase could not be lowered with medications, it would be considered a failure. Patients were divided into two categories: the hypertensive and the nonhypertensive categories. Hypotony was defined as an IOP < 6 mmHg. The number of postoperative antiglaucomatous medications was identified.
- (ii) Visual acuity: visual acuity assessment (VA) using the Snellen E chart was performed. The final postoperative BCVA changes were classified as "worsened", "stable", or "improved" when compared to the preoperative BCVA. A change of one line of Snellen visual acuity or less was defined as stable, whereas greater changes were defined as worsened or improved accordingly.

- (iii) Visual field: visual field assessment was based on Brusini Classification based on Mean Deviation (MD) and Corrected Pattern Standard Deviation (CPSD) Values:

Stage 0: both MD and CPSD within normal limits.

Stage 1: MD between -3 and -5 dB and CPSD ≤ 3 dB, or MD < -3 dB and CPSD between 3 and 5 dB, or both MD and CPSD between -3 and -5 dB.

Stage 2: MD > -5 and < -8 dB and CPSD < -8 dB, or MD < -3 dB and CPSD > 5 and < 8 dB.

Stage 3: MD between -8 and -12 dB, or CPSD ≥ 8 dB.

Stage 4: MD ≥ -12 dB and < -20 dB.

Stage 5: MD ≥ -20 dB [14].

- (iv) Postoperative complications: all intraoperative and postoperative complications were recorded.
- (v) Anterior segment OCT assessment: a Spectralis OCT (Heidelberg Engineering, Heidelberg, Germany) was performed to visualise the postoperative blebs at 1 week, 1 month, 3 months, and 6 months. AS-OCT was performed in a room with a constant and minimal degree of room illumination. Patients were initially asked to fixate their eyes at an inferonasal position to facilitate the imaging of the superotemporal bleb and the nearby angle and AC. Automatic real-time of eight frames and 41 sections with a $139 \mu\text{m}$ interval were used for imaging the cross section of the bleb. The maximal bleb wall thickness was calculated by measuring in micrometres the maximal distance 3.5 mm away from the end point of the tube. Images with quality scores greater than 25 were included. The maximal bleb wall thickness was calculated by measuring in micrometres the maximal distance between the first reflective signal from the conjunctiva to the top of the sub-Tenon fluid space. The maximal reflectivity of the bleb wall was measured by exporting the scanned images as jpg files and then importing them into the ImageJ software program (Wayne Rasband, National Institutes of Health, Bethesda, MD, USA). Reflectivity was measured in the ellipses that the operator had marked on the bleb wall. The internal morphology of the blebs in both groups was evaluated using the anterior segment optical coherence tomography (AS-OCT) for consequent changes in bleb wall thickness, bleb wall reflectivity, and bleb shape throughout the 6 months of follow-up period.

In addition, optic disc examination using Volk + 90 lens and slit lamp examination, including bleb examination for its shape and vascularity, were performed throughout the 6 months of follow-up period.

3.2. Statistical Analysis. Results were statistically analysed by SPSS version 22 (SPSS Inc., Chicago, IL, USA). Nonpaired *t*-test was used for parametric data. Mann-Whitney and

Friedman tests were used for nonparametric data. Chi-squared (χ^2) and Fisher's exact tests were used for qualitative variables. Spearman test was used for detecting the strength and the direction of association between variables. A *p* value < 0.05 was considered significant.

4. Results

The age of the patients ranged from 42 to 55 years, and there were 17 males and 13 females. In spite of the maximally tolerated medication after previous trabeculectomy surgery, the patients had a high intraocular pressure (IOP), with an IOP in the range of 30 – 36 mmHg (group I) and 30 – 37 mmHg (group II). These patients were diagnosed with three main types of refractory glaucoma; aphakic glaucoma (11 patients), pseudophakic glaucoma (15 patients), and pseudoexfoliation glaucoma (4 patients) (Table 1). This study showed a significant reduction in IOP in both groups throughout the follow-up period, with a greater reduction in group I, where the mean IOP decreased from 32.7 ± 2.1 mmHg in the preoperative period to 13.3 ± 1.6 mmHg after 6 months, whereas in group II, the mean IOP decreased from 33.2 ± 2.2 mmHg in the preoperative period to 14.3 ± 1.4 mmHg after 6 months (*p* value < 0.05). The difference in IOP reduction between the 2 groups was insignificant except at 1 and 3 months, where there was a significant increase in the mean IOP in group II. The mean postoperative IOP in group II at 1 month and 3 months was 20.1 ± 6.4 mmHg and 17.0 ± 1.8 mmHg, respectively, while in group I, the mean postoperative IOP at 1 and 3 months was 14.9 ± 3.1 mmHg and 15.8 ± 3.4 mmHg, respectively (*p* = 0.016 at 1 month and 0.01 at 3 months) (Table 2). There were more patients with the hypertensive phase in group II (6 cases, 40%) when compared with group I (2 cases, 13.3%) (Table 3). The bleb analysis revealed that there was a significant reduction in the maximal bleb wall thickness in both groups at 1 and 3 months, which was mostly associated with the hypertensive phase. In group I, the bleb wall thickness was $754.67 \pm 53.93 \mu\text{m}$ on the first postoperative day and decreased to $684 \pm 81.66 \mu\text{m}$ and $671.6 \pm 69.48 \mu\text{m}$ at 1 and 3 months, respectively, while in group II, the bleb wall thickness was $707.13 \pm 31.7 \mu\text{m}$ on the first postoperative day and decreased to $499.53 \pm 99.1 \mu\text{m}$ and $506 \pm 76.91 \mu\text{m}$ at 1 and 3 months, respectively (Table 4). AS-OCT was also beneficial in describing the changes in maximal bleb wall reflectivity, which increased at 1 and 3 months and decreased again at 6 months, although the difference between both the groups with regard to the bleb reflectivity was insignificant throughout the follow-up period (Table 5). Maximal bleb wall thickness and maximal bleb wall reflectivity were analysed in those patients. There was a more significant reduction in the maximal bleb wall thickness at 1 and 3 months in group II. Maximal bleb wall thickness at 1 month was $540 \pm 14.14 \mu\text{m}$ in group I and was $387.83 \pm 11.67 \mu\text{m}$ in group II (*p* value < 0.05). At 3 months, a mild increase occurred, where maximal bleb wall thickness was $567.5 \pm 31.82 \mu\text{m}$ in group I and $423.67 \pm 9.31 \mu\text{m}$ in group II (*p* value < 0.05) (Table 6). There was a negative correlation between IOP and maximal bleb wall thickness in

TABLE 1: Demographic data and baseline clinical data.

	Group 1 No = 15		Group 2 No = 15		p value
	NO	%	NO	%	
Age (years)	46.33 ± 1.47		47.14 ± 3.33		0.399
Gender					
Male	8	53.3	9	60.0	0.713
Female	7	46.7	6	40.0	
Preoperative baseline IOP (mean ± SD)	32.73 ± 2.12		33.2 ± 2.21		0.560
Type of glaucoma					
Aphakic glaucoma	5	33.4	6	40.0	0.924
Pseudophakic glaucoma	8	53.3	7	46.7	
Pseudoexfoliation glaucoma	2	13.3	2	13.3	
Preoperative medications					
Topical(beta-blocker + CAI + prostaglandin analogue)	13	86.7	12	80.0	0.624
Topical (beta-blocker + CAI + brimonidine)	2	13.3	3	20.0	

IOP = intraocular pressure; SD = standard deviation; CAI = carbonic anhydrase inhibitor.

TABLE 2: IOP of the studied groups.

IOP (mmHg)	Group 1 No = 15	Group 2 No = 15	p value
Preoperative			
Mean ± SD	32.73 ± 2.12	33.2 ± 2.21	0.560
Postoperative 1 day			
Mean ± SD	11.4 ± 2.29	12.33 ± 3.68	0.202
Postoperative 1 week			
Mean ± SD	12.07 ± 1.53	13.27 ± 3.03	0.098
Postoperative 1 month			
Mean ± SD	14.87 ± 3.11	20.13 ± 6.39	0.016*
Postoperative 3 months			
Mean ± SD	15.8 ± 3.41	17 ± 1.81	0.01*
Postoperative 6 months			
Mean ± SD	13.33 ± 1.59	14.27 ± 1.44	0.103
Fried man test (p value)	77.69 (<0.001*)	80.04 (<0.001*)	
Post hoc test	^{1,2,3,4,5,7,8,10,11} <0.05	^{1,2,3,4,5,7,8,10,11,14,15} <0.05	
	^{6,9,12,13,14,15} >0.05	^{6,9,12,13} >0.05	

¹Preoperative-1 day later; ²preoperative-1 week later; ³preoperative-1 month later; ⁴preoperative-3 months later; ⁵preoperative-6 months later; ⁶1 day later-1 week later; ⁷1 day later-1 month later; ⁸1 day later-3 months later; ⁹1 day later-6 months later; ¹⁰1 week later-1 month later; ¹¹1 week-3 months later; ¹²1 week-6 months later; ¹³1 month later-3 months later; ¹⁴1 month-6 months later; ¹⁵3 months-6 months later. *Significant.

the eyes that presented with significant elevated IOP (Hypertensive phase) at 1 and 3 months in both groups. They also presented with a significant decrease in the maximal bleb wall thickness (Table 7). These measures increased again at 6 months and can be represented as a U-shaped pattern (Figure 1). The maximal bleb wall reflectivity increased at 1 and 3 months in both the groups. This increase was greater in group II, where the maximal bleb wall reflectivity was 127.66 ± 32.11 and 121.62 ± 18.23 at 1 and 3 months, respectively, while it was 113.48 ± 38.22 and 106.31 ± 19.56 in group I at 1 and 3 months, respectively. However, this difference between both the groups was insignificant (Table 5). This increase in the maximal bleb wall reflectivity subsided again at 6 months and can be represented as an inverted U-shaped pattern (Figure 2). A significant correlation was reported between the decrease in maximal bleb wall thickness and the increase in maximal bleb wall reflectivity at 1 and 3 months (Hypertensive phase) (Table 8). Postoperative slit lamp biomicroscopy for

the studied groups clarified that externally, the blebs in group I were thinner and less vascular compared to those in group II. However, bleb morphology by AS-OCT provided more details, since the internal morphology of the blebs could be analysed (Figures 3(a) and 3(b)). All the blebs in group I were characterised by diffuse, fluid-filled, large multicystic cavities, numerous intraconjunctival cysts, and hyporeflexive diffuse areas of conjunctival hydration that were seen in all the cases, except the 2 cases in the hypertensive phase. They were characterised by less fluid-filled multicystic cavities, intraconjunctival cysts, and conjunctival hydration (Figure 4) with a greater reduction in the maximal bleb wall thickness and an increase in the maximal bleb wall reflectivity (Table 6). Bleb shape in group II was different; here there was a uniform, fluid-filled cystic cavity without encapsulation in 9 cases (60%) that presented without the hypertensive phase, while 6 cases (40%) with the hypertensive phase were classified as a uniform cystic, fluid-filled cavity with encapsulation occurring in 5

TABLE 3: Postoperative complications of the studied groups.

Postoperative complications	Group I No = 15		Group II No = 15		p value
	NO	%	NO	%	
Hypotony					
No	14	93.3	12	80.0	0.598
Yes	1	6.7	3	20.0	
Shallow AC					
No	14	93.3	12	80.0	0.598
Yes	1	6.7	3	20.0	
Increased IOP					
Negative	13	86.7	9	60.0	0.215
Positive	2	13.3	6	40.0	
Tube exposure					
Negative	14	93.3	13	86.7	0.483
Positive	1	6.7	2	13.3	
Choroidal detachment					
Negative	15	100.0	14	93.3	0.734
Positive	0	0.0	1	6.7	
Hyphema					
Negative	14	93.3	13	86.7	0.974
Positive	1	6.7	2	13.3	
Continuity of antiglaucoma medications					
Two medications	1	6.7	3	20.0	0.513
Three medications	0	0.0	1	6.7	
No medications	14	93.3	11	73.3	

*Significant.

TABLE 4: Maximal bleb wall thickness of the studied groups.

Postoperative maximal bleb wall thickness (μm)	Group 1 No = 15	Group 2 No = 15	p value
1 day			
Mean \pm SD	754.67 \pm 53.93	707.13 \pm 31.7	0.004*
Median	780	719	
Min-max	650–800	640–740	
1 week			
Mean \pm SD	712.33 \pm 66.99	599.93 \pm 41.82	<0.001*
Median	750	590	
Min-max	610–780	550–690	
1 month			
Mean \pm SD	684 \pm 81.66	499.53 \pm 99.1	<0.001*
Median	730	535	
Min-max	530–760	370–625	
3 months			
Mean \pm SD	671.6 \pm 69.48	506 \pm 76.91	<0.001*
Median	710	515	
Min-max	545–745	412–615	
6 months			
Mean \pm SD	718.2 \pm 72.4	620.86 \pm 82.29	0.002*
Median	760	630	
Min-max	560–785	515–725	
Fried man test (p value)	45.329 (<0.001*) 2,3,6,9,10 <0.05	54.247 (<0.001*) 1,2,3,4,5,6,9,10 <0.05	
Post hoc test	1,4,5,7,8 >0.05	7,8 >0.05	

¹1 day later-1 week later; ²1 day later-1 month later; ³1 day later-3 months later; ⁴1 day later-6 months later; ⁵1 week-1 month later; ⁶1 week later-3 months later; ⁷1 week-6 months later; ⁸1 month later-3 months later; ⁹1 month later-6 months later; ¹⁰3 months later-6 months later. *Significant.

cases (33.3) and a less diffuse multicystic bleb with dense fibrosis inside the bleb cavity in 1 case (6.7%) (Figure 5). Intraconjunctival cysts were very limited with less

conjunctival hydration, which might be due to the onset of greater fibrous proliferation compared to group I. AS-OCT was useful to determine the position of the AGV tube in the

TABLE 5: Maximal bleb wall reflectivity of the studied groups.

Postoperative bleb wall reflectivity	Normotensive patients			Hypertensive phase		
	Group I No = 13	Group II No = 9	<i>p</i> value	Group I No = 2	Group II No = 6	<i>p</i> value
	Mean ± SD	Mean ± SD		Mean ± SD	Mean ± SD	
1 day	79.46 ± 45.13	83.44 ± 42.11	0.834	81.18 ± 33.11	84.33 ± 22.65	0.921
Week 1	90.28 ± 17.38	94.28 ± 15.67	0.581	99.44 ± 15.33	105.45 ± 18.33	0.694
1 month	98.76 ± 13.11	111.55 ± 11.24	0.029*	113.48 ± 38.22	127.66 ± 32.11	0.719
3 months	100.43 ± 44.22	115.36 ± 22.16	0.311	106.31 ± 19.56	121.62 ± 18.23	0.508
6 months	97.23 ± 36.63	102.11 ± 20.11	0.693	99.83 ± 19.48	103.65 ± 13.22	0.839

*Significant.

TABLE 6: Maximal bleb wall thickness in patients with hypertensive phase.

Postoperative maximal bleb wall thickness (μm)	Hypertensive phase		<i>p</i> value
	Group I No = 2	Group II No = 6	
Postoperative 1 day			
Mean ± SD	770 ± 28.28	718.67 ± 9.16	
Median	770	718.5	0.044*
Min-max	750–790	710–735	
Postoperative 1 week			
Mean ± SD	645 ± 49.49	584.17 ± 7.36	
Median	645	582.5	0.044*
Min-max	610–680	575–595	
Postoperative 1 month			
Mean ± SD	540 ± 14.14	387.83 ± 11.67	
Median	540	388.5	0.042*
Min-max	530–550	370–400	
Postoperative 3 months			
Mean ± SD	567.5 ± 31.82	423.67 ± 9.31	
Median	567.5	425	0.042*
Min-max	545–590	412–435	
Postoperative 6 months			
Mean ± SD	590 ± 42.43	529.83 ± 13.12	
Median	590	527	0.044*
Min-max	560–620	515–550	

*Significant.

TABLE 7: Correlation between maximal bleb wall thickness and intraocular pressure in studied groups.

Postoperative	Group I		Group II		Total sample	
	<i>r</i>	<i>p</i>	<i>r</i>	<i>p</i>	<i>r</i>	<i>p</i>
1 day	-0.274	0.323	-0.016	0.954	-0.190	0.314
1 week	-0.463	0.082	0.202	0.470	-0.295	0.113
1 month	-0.227	0.416	-0.853	<0.001*	-0.702	<0.001*
3 months	-0.275	0.322	-0.491	0.063	-0.611	<0.001*
6 months	-0.228	0.414	-0.689	0.004*	-0.512	<0.001*

*Significant.

AC in addition to the patency of the AC angle (Figure 6). Regarding the postoperative complications, the hypertensive phase occurred more frequently in group II, where it occurred in 6 cases (40%) with a mean IOP of 25 mmHg (range, 21–29 mmHg), whereas it occurred in 2 cases at 1 month, with one case having an encapsulated bleb visible by AS-OCT; the 2 cases at 1 month were controlled 2 months later with two antiglaucomatous eye drops (Carbonic Anhydrase Inhibitor + Beta-blocker), while 4 cases with encapsulation (26.7%) needed to continue the

antiglaucomatous eye drops till the 6-month follow-up. Three cases (20%) needed two antiglaucomatous eye drops (Carbonic Anhydrase Inhibitor + Beta-blocker) and 1 case (6.7%) received three antiglaucomatous eye drops (Carbonic Anhydrase Inhibitor + Beta-blocker + Prostaglandin Analogue). Only 2 cases (13.3%) in group I showed this hypertensive phase at 3 months, of which only 1 case (6.7%) with an IOP of 26 mmHg needed to continue with two antiglaucomatous eye drops (Carbonic Anhydrase Inhibitor + Beta-blocker). IOP was lowered to 15 mmHg while

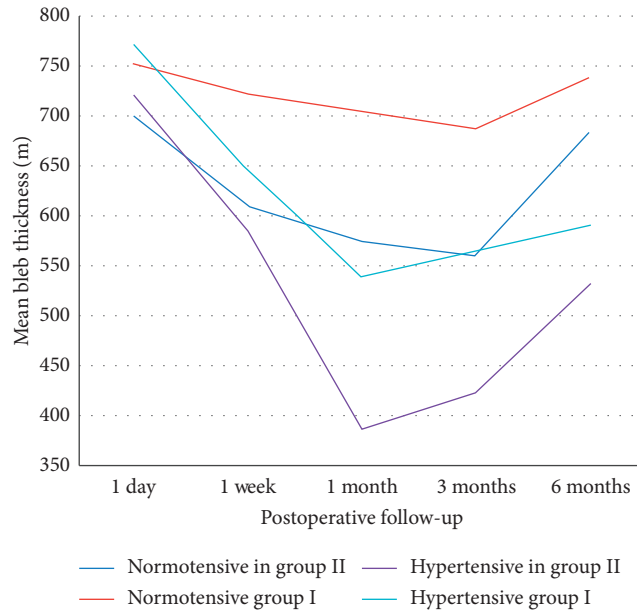


FIGURE 1: U-shaped pattern of the mean maximal bleb wall thickness.

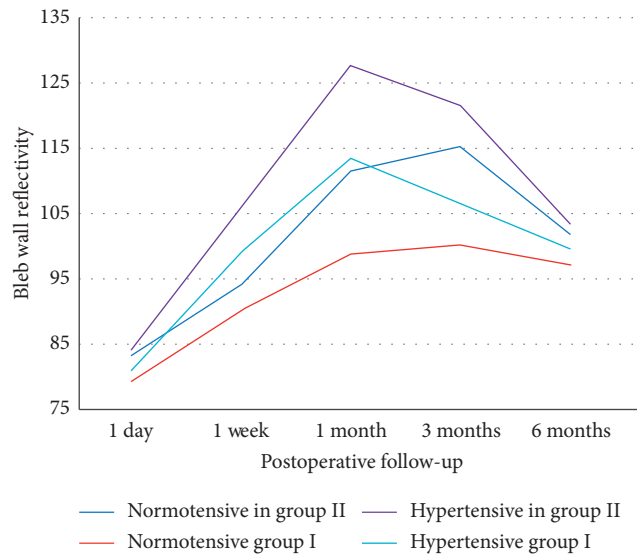


FIGURE 2: Inverted U-shaped pattern of the mean maximal bleb wall reflectivity.

TABLE 8: Correlation between maximal bleb wall thickness and maximal bleb wall reflectivity in studied groups.

Postoperative follow-up period	Group I		Group II		Total sample	
	<i>r</i>	<i>p</i>	<i>r</i>	<i>p</i>	<i>r</i>	<i>p</i>
1 day	-0.197	0.323	-0.113	0.209	-0.168	0.239
1 week	-0.385	0.082	-0.109	0.145	-0.295	0.096
1 month	-0.486	0.032*	-0.327	0.019*	-0.409	0.022*
3 months	-0.609	0.002*	-0.491	0.005*	-0.589	0.003*
6 months	-0.535	0.008*	-0.432	0.009*	-0.495	0.007*

*Significant.

the other case presented with an IOP at 25 mmHg, which was lowered with two antiglaucomatous eye drops (Carbonic Anhydrase Inhibitor + Beta-blocker) after 2 weeks. This treatment was stopped 2 weeks later when the IOP was

lowered to 8 mmHg; the IOP later increased back to 15 mmHg without any further treatment. More postoperative complications were reported in group II such as hypotony, shallow anterior chamber (AC), choroidal

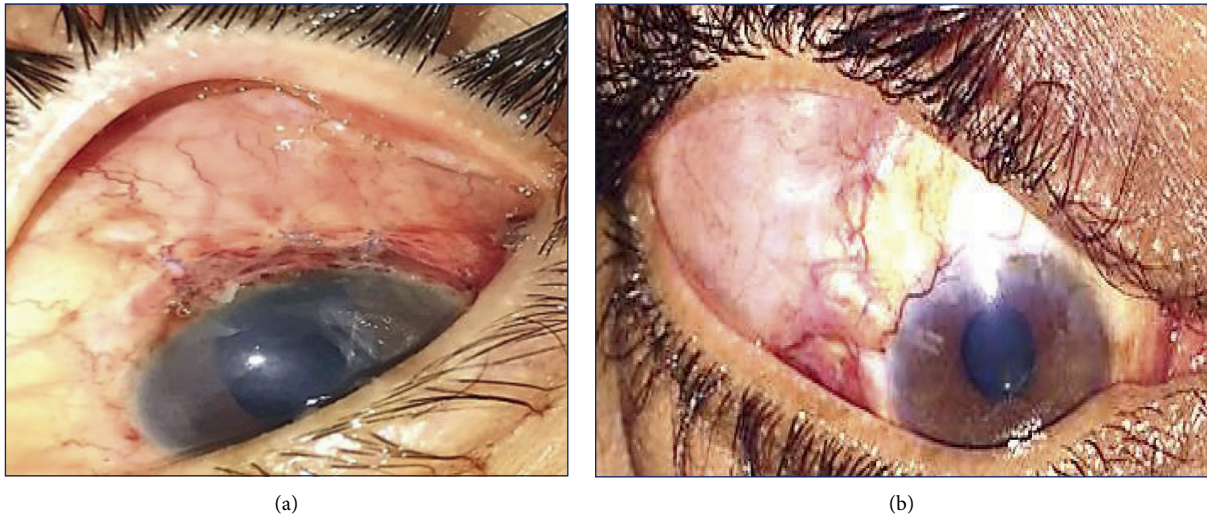


FIGURE 3: (a) A slit lamp biomicroscopy photo of a male patient in group I with IOP at 15 mmHg revealed a thin bleb with minimal vascularisation (3 months after surgery). (b). A slit lamp biomicroscopy photo of a female patient in group II with IOP 28 mmHg revealed a vascularised encysted bleb (1 month after surgery).



FIGURE 4: AS-OCT bleb imaging of a female patient in group I during the hypertensive phase at 3 months; IOP was 26 mmHg. AS-OCT revealed the presence of diffuse multicystic bleb cavity, diffuse hyporeflective conjunctiva with hydration, and intraconjunctival cysts. Maximal bleb wall thickness was $580\ \mu\text{m}$, and bleb wall reflectivity was 103.

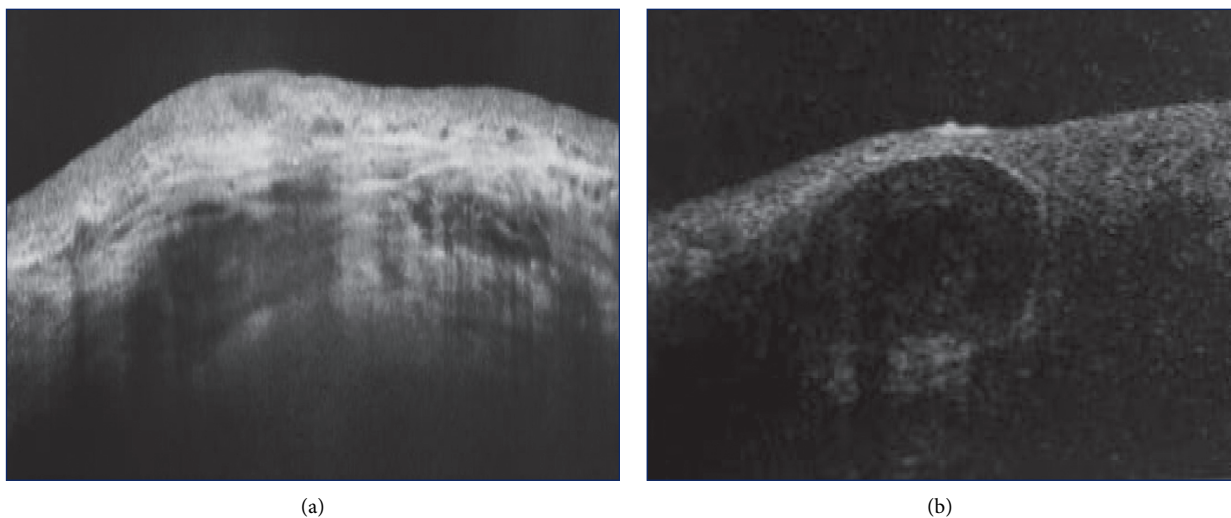


FIGURE 5: (a) AS-OCT bleb imaging of a female patient in group II at 1 month (hypertensive phase); IOP was 29 mmHg. AS-OCT revealed the presence of encapsulated bleb with dense hyperreflective bleb wall with monocystic fluid-filled bleb cavity; maximal bleb wall thickness was $375\ \mu\text{m}$, and bleb wall reflectivity was 132. (b) AS-OCT bleb imaging of a male patient in group II at 3 months (hypertensive phase); IOP was 27 mmHg. AS-OCT revealed the presence of a few number of intraconjunctival cysts and minimal conjunctival hydration with dense hyperreflective areas within the bleb cavity (mostly due to fibrosis); the maximal bleb wall thickness was $389\ \mu\text{m}$, and bleb wall reflectivity was 127.

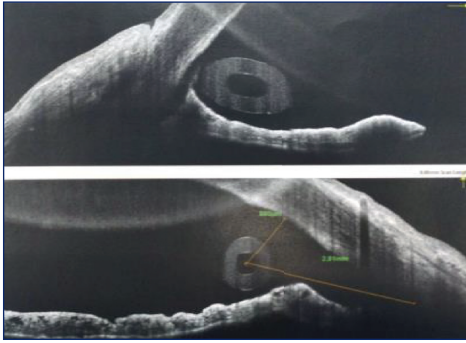


FIGURE 6: AS-OCT imaging 4 months after surgery of a male patient in group I IOP was 14 mmHg with representation of the tube opening in the AC, angle patency, and depth.

detachment, hyphaemia, and tube exposure (Table 3). The preoperative BCVA ranged between 2/60 (two meters) to 0.6 (by Snellen E-chart) in both the groups. With regard to the final postoperative BCVA in group I ($n = 15$), all cases remained stable (100%). For group II ($n = 15$), 4 had worsened (26.7%) and 11 remained stable (73.3%). In group II, 3 cases were associated with the hypertensive phase and showed a decline of 2 lines of the Snellen E-chart. The fourth case was complicated with choroidal detachment and showed a decline of 3 lines of the Snellen E-chart. In group I, the final postoperative visual field dropped from stage 3 to stage 4 in one case, while in group II, it dropped from stage 2 to stage 3 in 3 cases and from stage 3 to stage 4 in one case (Figure 7).

5. Discussion

Although bleb morphology can be evaluated using slit lamp biomicroscopy, it depicts only the external aspect of the bleb without assessing its internal structures [15–17]. AS-OCT is helpful to obtain cross-sectional images of the internal structures of the bleb. In addition, AS-OCT has been shown to be useful in diagnosing Ahmed tube tip position and patency, even in patients with opaque corneas [18, 19].

This study has shown that there were more diffuse functioning multicystic blebs and less thinning of the bleb wall thickness during the hypertensive phase after resection of the Tenon capsule. This might be related to a lesser incidence of fibrosis and a reduced vascularity as well as a better hydration of the tissue around the surgical site (Figure 4). There was no encapsulation that might correlate to the resection of the Tenon, which could have reduced the fibrosis around the valve plate and might have explained the increase in the maximal bleb wall thickness as well as the reduction in the maximal bleb wall reflectivity observed in group I as compared to group II at 1 and 3 months. This could also explain the low incidence of cases with the hypertensive phase in this group.

Some studies reported that the maximum bleb wall thickness was significantly thinner after a successful Ahmed valve implantation. They speculated that a thinner bleb allows better aqueous permeability, resulting in better IOP control. However, these authors noted that the wall

thickness can change over time. Other studies showed that unlike trabeculectomy, surgeons do not concern with bleb wall properties during tube surgery due to manipulation difficulty, relative homogeneity, and high reflectivity related to fibrous changes in the bleb wall preventing AS-OCT bleb analysis. However, bleb properties during tube surgery are also important for postoperative IOP control [20, 21]. These results were in agreement with another cross-sectional observational study that investigated the role of AS-OCT in the imaging of blebs after AGV surgery in 76 patients. The maximum bleb wall thickness was significantly correlated with the postoperative IOP ($r = 0.402$, $p < 0.001$; $r = 0.280$, $p = 0.014$). AS-OCT clarified that the maximum bleb wall thickness was significantly thinner in successful surgeries when compared to unsuccessful surgeries. No significant differences regarding the bleb wall reflectivity were reported [13].

Resection of the Tenon capsule in AGV surgery was a point of interest in a recent study where 30 patients with refractory glaucoma were randomly divided into 2 groups: group I: AGV surgery with resection of the Tenon capsule and grafting was performed in 15 eyes; group II: AGV surgery with autologous scleral graft was performed in 15 eyes. Better surgical outcomes were observed in group I in terms of the IOP-lowering effect and low number of postoperative antiglaucomatous medications (6.7%), in addition to a low incidence of complications such as one case of hypotony (6.7%) and only one case (6.7%) presenting with the hypertensive phase, which has been explained in this study as a consequence of the low incidence of fibrosis that might occur after resection of the Tenon capsule [7].

Other studies showed the significance of changes in bleb wall morphology, as one study enrolled 52 patients who underwent AGV implantation. Postoperative IOP was decreased at each time point during the postoperative follow-up (p value < 0.001 , all), with a peak in the first month. Mean bleb wall thickness was the thinnest 1 month after the surgery. A hypertensive phase was reported in 44 patients (84.6%). This study was different regarding the bleb wall reflectivity, where there was a significant difference between the hypertensive group and the nonhypertensive group at 1 month postoperatively (130.67 ± 27.00 versus 106.57 ± 10.35 ; $p = 0.044$) [22].

A study that compared the conventional AGV surgery method and the Biodegradable Collagen Matrix–Augmented Ahmed Glaucoma Valve method included 43 refractory glaucoma eyes that were followed up for 6 months. The conventional method was performed in 21 eyes, and the Biodegradable Collagen Matrix–Augmented Ahmed Glaucoma Valve method was performed in 22 eyes. Maximal bleb thickness was measured using AS-OCT images, and postoperative blebs were imaged using a Spectralis OCT (Heidelberg Engineering GmbH, Heidelberg, Germany) on postoperative days 1, 30, and 180. The results revealed that the Biodegradable Collagen Matrix–Augmented Ahmed Glaucoma Valve method provided better surgical outcomes and a more maximal bleb wall thickness at 1 and 3 months and, therefore, a less hypertensive phase compared to the conventional AGV surgery method. [23].

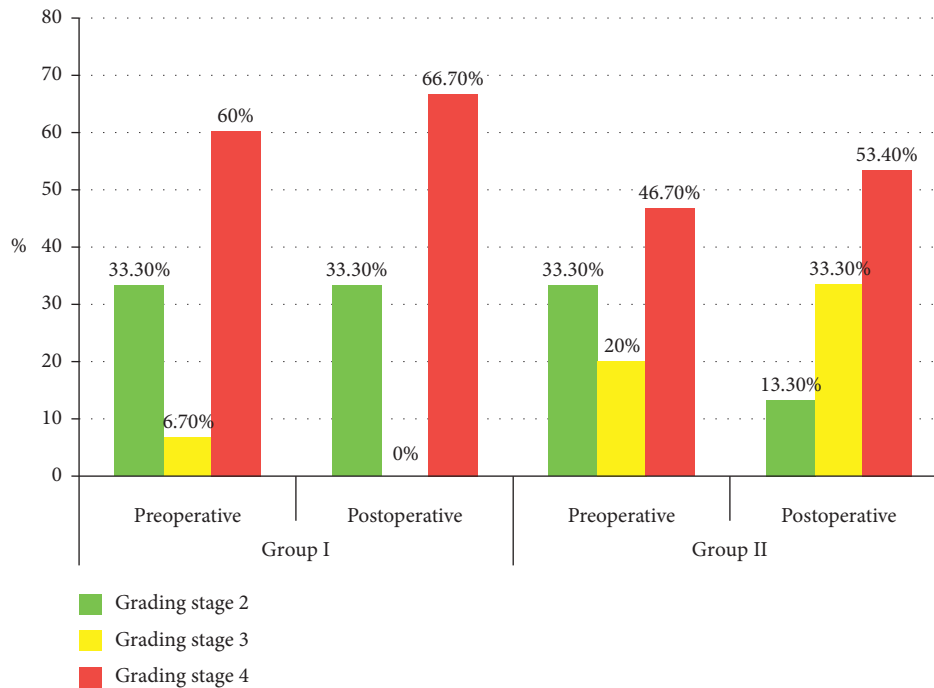


FIGURE 7: Comparison between the two groups with respect to the postoperative visual field.

5.1. Strengths and Limitations. The limitations of this study were a relatively small number of patients and a short-term follow-up. In addition, bleb imaging using AS-OCT required expertise to analyse the measures, and sometimes it was difficult to obtain good results, especially with uncooperative patients. In the near future, we plan to work on a large sample with a long-term follow-up to detect the degree of effectiveness of this surgical technique and to evaluate the long-term changes in the bleb. Strengths of this study were the effectiveness of the AGV surgery with Tenon resection, low cost, minimal time consumption, and an easy dissection in the absence of cicatrising tissues from previous surgeries. AS-OCT was added as a point of interest in this study and may provide important diagnostic data to the previous study that we published, wherein we had clarified the role of Tenon resection in reducing postoperative fibrosis, and therefore the hypertensive phase. AS-OCT was useful to evaluate the changes in bleb morphology during the early postoperative period, when the hypertensive phase may occur at 1–3 months. AS-OCT was also useful to perform a correlation between the bleb morphological changes and the bleb function and, therefore, helped to evaluate the success of the surgery.

6. Conclusions

AS-OCT can be used as a good diagnostic tool for analysing the bleb shape, wall thickness, and wall reflectivity, as well as a prognostic tool that determines the incidence of the hypertensive phase. There was a significant increase in bleb wall thickness in AGV surgery with resection of the Tenon capsule at 1 and 3 months compared to the conventional AGV surgery, which may be the cause for the lower

hypertensive phases that occurred in the AGV surgery with resection of the Tenon capsule.

Data Availability

The data used to support the findings of this study are included within the article.

Ethical Approval

All the procedures performed in studies involving human participants were in accordance with the ethical standards of the institutional committee and with the 1964 Helsinki declaration and its later amendments or comparable ethical standards.

Consent

Informed consent was obtained from all the individual participants included in the study.

Conflicts of Interest

The author has no conflicts of interest in any concept or product described in this article.

References

- [1] S. J. Gedde, J. C. Schiffman, W. J. Feuer, L. W. Herndon, J. D. Brandt, and D. L. Budenz, "Treatment outcomes in the tube versus trabeculectomy (TVT) study after five years of follow-up," *American Journal of Ophthalmology*, vol. 153, no. 5, pp. 789–803, 2012.
- [2] H. J. Jeong, H.-Y. L. Park, and C. K. Park, "Effects of early postoperative intraocular pressure after Ahmed glaucoma

- valve implantation on long-term surgical outcomes,” *Korean Journal of Ophthalmology*, vol. 32, no. 5, pp. 391–399, 2018.
- [3] D. L. Budenz, K. Barton, W. J. Feuer et al., “Treatment outcomes in the Ahmed Baerveldt comparison study after 1 year of follow-up,” *Ophthalmology*, vol. 118, pp. 443–452, 2011.
- [4] I. Riva, G. Roberti, A. Katsanos, F. Oddone, and L. Quaranta, “A review of the Ahmed glaucoma valve implant and comparison with other surgical operations,” *Advances in Therapy*, vol. 34, p. 834, 2017.
- [5] C. H. Hong, A. Arosemena, D. Zurakowski, and R. S. Ayyala, “Glaucoma drainage devices: a systematic literature review and current controversies,” *Survey of Ophthalmology*, vol. 50, no. 1, pp. 48–60, 2005.
- [6] R. Susanna, “Partial Tenon’s capsule resection with adjunctive mitomycin C in Ahmed glaucoma valve implant surgery,” *British Journal of Ophthalmology*, vol. 87, no. 8, pp. 994–998, 2003.
- [7] F. M. Wagdy, “Tenon capsule grafting versus autologous scleral graft in Ahmed glaucoma valve surgery,” *Journal of Ophthalmology*, vol. 2020, Article ID 1248023, 9 pages, 2020.
- [8] C. K. S. Leung, H. Li, R. N. Weinreb et al., “Anterior chamber angle measurement with anterior segment optical coherence tomography: a comparison between slit lamp OCT and Visante OCT,” *Investigative Ophthalmology and Visual Science*, vol. 49, no. 8, pp. 3469–3474, 2008.
- [9] L. M. Sakata, T. L. Wong, H. T. Wong et al., “Comparison of Visante and slit-lamp anterior segment optical coherence tomography in imaging the anterior chamber angle,” *Eye*, vol. 24, no. 4, pp. 578–587, 2010.
- [10] R. Mastropasqua, V. Fasanella, L. Agnifili, C. Curcio, M. Ciancaglini, and L. Mastropasqua, “Anterior segment optical coherence tomography imaging of conjunctival filtering blebs after glaucoma surgery,” *BioMed Research International*, vol. 2014, Article ID 610623, 11 pages, 2014.
- [11] G. Savini, M. Zanini, and P. Barboni, “Filtering blebs imaging by optical coherence tomography,” *Clinical & Experimental Ophthalmology*, vol. 33, no. 5, pp. 483–489, 2005.
- [12] R. Sharma, A. Sharma, T. Arora et al., “Application of anterior segment optical coherence tomography in glaucoma,” *Survey of Ophthalmology*, vol. 59, no. 3, pp. 311–327, 2014.
- [13] K. I. Jung, S. A. Lim, H. L. Park, and C. K. Park, “Visualization of blebs using anterior-segment optical coherence tomography after glaucoma drainage implant surgery,” *Ophthalmology*, vol. 120, no. 5, pp. 978–983, 2013.
- [14] R. Susanna and R. M. Vessani, “Staging glaucoma patient: why and how?” *Open Ophthalmology Journal*, vol. 3, pp. 59–64, 2009.
- [15] M. Singh, J. L. See, M. C. Aquino, L. S. Thean, and P. T. Chew, “High-definition imaging of trabeculectomy blebs using spectral domain optical coherence tomography adapted for the anterior segment,” *Clinical & Experimental Ophthalmology*, vol. 37, pp. 345–351, 2009.
- [16] S. Dorairaj, J. Maslin, and Y. Barkana, “Anterior segment imaging in glaucoma: an updated review,” *Indian Journal of Ophthalmology*, vol. 63, no. 8, pp. 630–640, 2015.
- [17] R. M. Feldman, S. M. El-Harazi, and G. Villaneuva, “Valve membrane adhesion as a cause of Ahmed glaucoma valve failure,” *Journal of Glaucoma*, vol. 6, pp. 10–12, 1997.
- [18] W. Kiddee and G. E. Trope, “Glaucoma tube imaging using anterior segment optical coherence tomography in patients with opaque cornea,” *Journal of Glaucoma*, vol. 22, pp. 773–775, 2013.
- [19] H.-Y. Lopilly Park, K. I. Jung, and C. K. Park, “Serial intracamer visualization of the Ahmed glaucoma valve tube by anterior segment optical coherence tomography,” *Eye*, vol. 26, pp. 1256–1262, 2012.
- [20] M. Singh, P. T. K. Chew, D. S. Friedman et al., “Imaging of trabeculectomy blebs using anterior segment optical coherence tomography,” *Ophthalmology*, vol. 114, pp. 47–53, 2007.
- [21] T. Hamanaka, T. Omata, S. Sekimoto, T. Sugiyama, and Y. Fujikoshi, “Bleb analysis by using anterior segment optical coherence tomography in two different methods of trabeculectomy,” *Investigative Ophthalmology & Visual Science*, vol. 54, pp. 6536–6541, 2013.
- [22] K. In Jung, H. Park, Y. Jung, and C. K. Park, “Serial changes in the bleb wall after glaucoma drainage implant surgery: characteristics during the hypertensive phase,” *Acta Ophthalmologica*, vol. 93, no. 4, pp. e248–53, 2015.
- [23] S. Rho, Y. Sung, K. T. Ma, S. H. Rho, and C. Y. Kim, “Bleb analysis and short-term results of biodegradable collagen matrix-augmented ahmed glaucoma valve implantation: 6-month follow-up,” *Investigative Ophthalmology & Visual Science*, vol. 56, pp. 5896–5903, 2015.

Research Article

Assessment of Scleral and Conjunctival Thickness of the Eye after Ultrasound Ciliary Plasty

Bartłomiej Bolek , Adam Wylęgała, and Edward Wylęgała

Chair and Clinical Department of Ophthalmology, School of Medicine in Zabrze, Medical University of Silesia in Katowice, District Railway Hospital, Katowice, Poland

Correspondence should be addressed to Bartłomiej Bolek; bolek.bartlomiej@gmail.com

Received 24 June 2020; Revised 18 August 2020; Accepted 27 August 2020; Published 24 September 2020

Academic Editor: Karim Mohamed Noriega

Copyright © 2020 Bartłomiej Bolek et al. This is an open access article distributed under the Creative Commons Attribution License, which permits unrestricted use, distribution, and reproduction in any medium, provided the original work is properly cited.

Purpose. This study aims to assess scleral and conjunctival thickness using optical coherence tomography after ultrasound ciliary plasty (UCP) procedure with reference to scleral marks appearing in the area where the ultrasound energy was applied. **Materials and Methods.** Seventy-eight patients with primary and secondary refractory glaucoma participated in this study. Complete ophthalmic examinations including measurements of scleral and conjunctival thickness were performed preoperatively and at 1 week, and 1, 3, 6, 12, 18, and 24 months postoperatively. The parameters were determined using the Swept Source OCT with anterior attachment. Thirty-eight patients (58 scleral marks—23 superior and 35 inferior) fulfilled the inclusion criteria and completed the follow-up period of 24 months. **Results.** The mean \pm SD scleral and conjunctival thickness in superior scleral mark before the procedure and at 1 week, and 1, 3, 6, 12, 18, and 24 months after the procedure was $684.57 \pm 83.58 \mu\text{m}$, $771.78 \pm 112.03 \mu\text{m}$ ($p < 0.001$), $771.74 \pm 100.12 \mu\text{m}$ ($p < 0.001$), $731.38 \pm 83.92 \mu\text{m}$ ($p = 0.012$), $719.52 \pm 73.20 \mu\text{m}$ ($p = 0.037$), $702.91 \pm 66.50 \mu\text{m}$ ($p = 0.247$), $694.13 \pm 72.22 \mu\text{m}$ ($p = 0.482$), and $699.35 \pm 70.68 \mu\text{m}$ ($p = 0.200$), respectively. The mean \pm SD scleral and conjunctival thickness in inferior scleral mark before the procedure and at 1 week, and 1, 3, 6, 12, 18, and 24 months after the procedure was $816.86 \pm 79.30 \mu\text{m}$, $936.37 \pm 107.33 \mu\text{m}$ ($p < 0.001$), $946.00 \pm 130.40 \mu\text{m}$ ($p < 0.001$), $896.63 \pm 123.40 \mu\text{m}$ ($p < 0.001$), $877.69 \pm 114.38 \mu\text{m}$ ($p = 0.003$), $843.03 \pm 71.55 \mu\text{m}$ ($p = 0.021$), $811.86 \pm 68.91 \mu\text{m}$ ($p = 0.731$), and $805.03 \pm 69.52 \mu\text{m}$ ($p = 0.248$), respectively. The transient thickening of the sclera was observed after the procedure; however, after 12 months postoperatively, the parameters returned to the initial value and no significant difference was noted. **Conclusion.** The sclera thickness increases after UCP. However, with time the thickness reduces to its initial value with no significant difference. Clinical implication of the scleral changes lasts shorter than the measured significant difference in scleral thickness.

1. Introduction

Cyclodestruction methods are used to treat mild and severe forms of glaucoma. These methods reduce intraocular pressure (IOP) by decreasing the production of aqueous humor by partially damaging the nonpigmented epithelium of the ciliary body. Ultrasound ciliary plasty (UCP), compared to commonly used diode laser cyclodestruction, allows precise energy concentration through opaque structures, without uncontrolled absorption, at a desired depth and area [1]. As a result, it reduces the damage to adjacent tissues. However, ultrasound energy may affect sclera, leading to an alteration in morphology and morphometry. In the area where the ultrasound energy was applied, a scleral mark

occurs, which macroscopically appears like scleral thinning. Few studies have reported the occurrence of scleral marks but without further examination [2–5]. A study conducted by Mastropasqua et al. showed anatomical modifications of sclera and conjunctiva in one month after UCP [6]. The authors assessed cyst occurrence in the area of ultrasound energy application intending to prove alternative outflow of aqueous humor through the uveoscleral pathway. There is no study examining scleral mark in terms of scleral thinning after UCP. The present study aims to assess scleral and conjunctival thickness using optical coherence tomography (OCT) after UCP with reference to scleral marks appearing in the area of ultrasound energy application in the long-term period.

2. Materials and Methods

This retrospective clinical study was approved by the institutional review board of the Medical University of Silesia (KNW/0022/KB1/78/18). Considering that the study involved a retrospective review of existing data, specific written informed consent was obtained from all patients. However, informed consent regarding the UCP was obtained from the patients who received the procedure.

Seventy-eight patients with primary and secondary refractory glaucoma were enrolled to undergo UCP. The inclusion criteria for the study were: adult patients (≥ 18 years), uncontrolled glaucoma (IOP > 21 mmHg, despite the maximum tolerated doses of antiglaucoma medications), and intolerance to glaucoma medications despite well-controlled IOP. The exclusion criteria were as follows: patients aged < 18 years, IOP > 30 mmHg, neovascular glaucoma, scleral mark not visible after the procedure, poor-quality OCT scan, and previous glaucoma surgeries involving perlimbal interference in the sclera. Thirty-eight patients (58 scleral marks—23 superior and 35 inferior) fulfilled the abovementioned criteria and completed the 24-month follow-up period.

Complete ophthalmic examinations with measurements of sclera and conjunctiva thickness (μm) were performed preoperatively and at 1 week, and 1, 3, 6, 12, 18, and 24 months after the procedure. The parameters were determined using Swept Source OCT with anterior attachment (DRI OCT Triton, Topcon Inc., Tokyo, Japan). Scleral and conjunctival thickness was measured manually, by two operators (BB, AW), using the built-in measuring tool in the OCT device. The mean of both measurements was taken as a result of the analysis. The scleral OCT scans were obtained in a projection perpendicular to the limbus of the cornea in the superior and inferior quadrants of the eye. The thickness was measured in the center of the area where the scleral mark occurred (Figures 1 and 2). Preoperative thickness was measured equidistant from limbus to scleral mark, and the accuracy of the measurement was determined from the control scans obtained after the procedure where scleral marks were visible (Figure 3). The first high reflective tissue signal was considered to be the outer limit of the sclera and conjunctival thickness, and the interface between the sclera (highly reflective) and choroid (less reflective) was considered the inner limit (Figures 1 and 3). Eyes without scleral mark after the procedure were excluded from the study as the exact area of ultrasound energy application could not be determined.

Additionally, IOP (determined using Goldmann applanation tonometer) and the number of antiglaucoma medications were included in the analysis. An IOP reduction of 20% or > 5 mmHg as compared to the baseline value was considered as an indication of successful treatment. Complete success was defined as the cessation of antiglaucoma medications.

The UCP procedure was performed using the EyeOP1 device (Eye Tech Care, Rillieux-la-Pape, France) under intravenous or peribulbar anesthesia. We used a second-generation ring-shaped probe containing six piezoelectric components (transducers) with a high frequency of 21 MHz

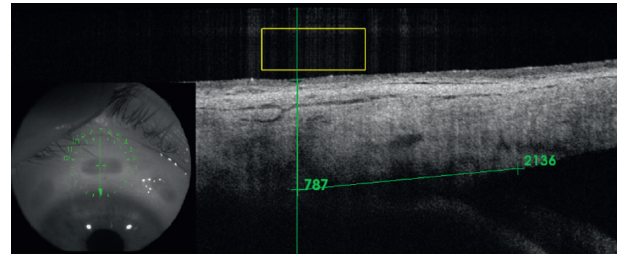


FIGURE 1: OCT scan of a patient three months after UCP—distance from limbus to scleral mark was measured ($2136 \mu\text{m}$) to determine preoperative thickness.

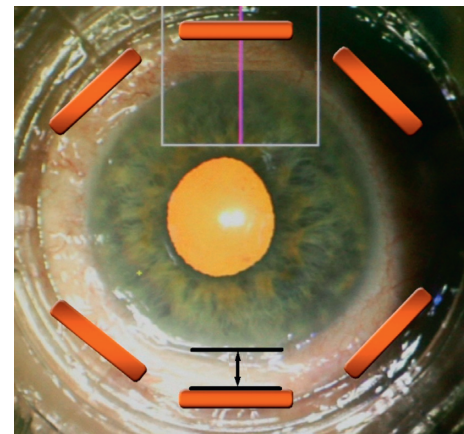


FIGURE 2: Scheme of the scleral and conjunctival measurements after UCP. OCT scans were taken in a projection perpendicular to the limbus of the cornea in the superior and inferior quadrants of the eye (purple continuous line). Thickness values were measured equidistant from the limbus (black continuous line) where the scleral mark occurred (orange rectangle).

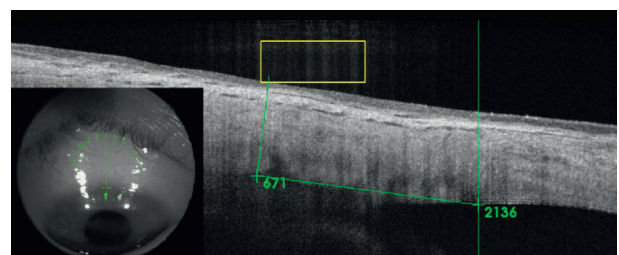


FIGURE 3: OCT scan of a patient before UCP—distance from limbus to the point where sclera and conjunctiva thickness measurements should be taken ($2136 \mu\text{m}$) was derived from the scan obtained after the procedure (Figure 1).

(high-intensity focused ultrasound—HIFU technology). The probe size was determined based on the axial length and white-to-white parameters measured before surgery using IOL Master 700 (Carl Zeiss, Meditec AG, Jena, Germany). The procedure involved precise adjustment of positioning cone at the center of the eye under a surgical microscope, stabilized by a mild vacuum system. The probe was then inserted into the cone and transducers were sequentially activated by footswitch. Each of the six transducers had an

operation time of 8 s with a 20 s interval between the subsequent exposures which made it an approximately 3 min procedure in total (second-generation probe). The preoperative antiglaucoma medications were either continued as before or modified according to the postoperative IOP. Postoperatively, patients were treated topically with ofloxacin (five times a day for two weeks), dexamethasone (five times a day for two weeks, followed by three times a day for two weeks), and atropine (three times a day for two weeks).

Statistical analysis was performed using Statistica Version 13 (TIBCO Software Inc., Palo Alto, CA). Groups of data sets for a given parameter were compared using the Wilcoxon signed-rank test or *t*-test depending on the data distribution. Spearman's correlation analysis was used to investigate the relations between scleral and conjunctival thickness and IOP. A *p* value of 0.05 or less was considered to represent statistical significance.

3. Results

The results are presented for 38 patients (58 scleral marks-23 superior and 35 inferior) during a 2-year follow-up. The patient characteristics are described in Table 1.

The mean \pm SD scleral and conjunctival thickness in superior scleral mark before the procedure and at 1 week, and 1, 3, 6, 12, 18, and 24 months after the procedure was $684.57 \pm 83.58 \mu\text{m}$, $771.78 \pm 112.03 \mu\text{m}$ ($p < 0.001$), $771.74 \pm 100.12 \mu\text{m}$ ($p < 0.001$), $731.38 \pm 83.92 \mu\text{m}$ ($p = 0.012$), $719.52 \pm 73.20 \mu\text{m}$ ($p = 0.037$), $702.91 \pm 66.50 \mu\text{m}$ ($p = 0.247$), $694.13 \pm 72.22 \mu\text{m}$ ($p = 0.482$), and $699.35 \pm 70.68 \mu\text{m}$ ($p = 0.200$), respectively (Table 2).

The mean \pm SD scleral and conjunctival thickness in inferior scleral mark before the procedure and at 1 week, and 1, 3, 6, 12, 18, and 24 months after the procedure was $816.86 \pm 79.30 \mu\text{m}$, $936.37 \pm 107.33 \mu\text{m}$ ($p < 0.001$), $946.00 \pm 130.40 \mu\text{m}$ ($p < 0.001$), $896.63 \pm 123.40 \mu\text{m}$ ($p < 0.001$), $877.69 \pm 114.38 \mu\text{m}$ ($p = 0.003$), $843.03 \pm 71.55 \mu\text{m}$ ($p = 0.021$), $811.86 \pm 68.91 \mu\text{m}$ ($p = 0.731$), and $805.03 \pm 69.52 \mu\text{m}$ ($p = 0.248$), respectively (Table 2).

The mean \pm SD values of IOP measured preoperatively and at 1 week, and 1, 3, 6, 12, 18 and 24 months postoperatively was $22.2 \pm 4.7 \text{ mmHg}$, $15.8 \pm 4.5 \text{ mmHg}$ ($p < 0.001$), $18.9 \pm 5.0 \text{ mmHg}$ ($p < 0.001$), $17.0 \pm 3.7 \text{ mmHg}$ ($p < 0.001$), $17.3 \pm 2.9 \text{ mmHg}$ ($p < 0.001$), $16.2 \pm 2.5 \text{ mmHg}$ ($p < 0.001$), $16.4 \pm 2.8 \text{ mmHg}$ ($p < 0.001$), and $16.0 \pm 3.6 \text{ mmHg}$ ($p < 0.001$), respectively (Table 3, Figure 4). The mean IOP at the last follow-up was reduced by 28.1% (Table 3). The success rate and the complete success rate were 89.7% and 7.7%, respectively.

The mean \pm SD number of antiglaucoma medications preoperatively and at 1 week, and 1, 3, 6, 12, 18 and 24 months postoperatively was 4.0 ± 0.8 , 0.7 ± 0.9 ($p < 0.001$), 0.9 ± 1.0 ($p < 0.001$), 1.6 ± 1.3 ($p < 0.001$), 2.1 ± 1.3 ($p < 0.001$), 2.5 ± 1.3 ($p < 0.001$), 2.6 ± 1.3 ($p < 0.001$), and 2.8 ± 1.3 ($p < 0.001$), respectively (Table 3, Figure 5).

Correlation analysis revealed no correlation between scleral and conjunctival thickness in superior or inferior scleral mark and IOP. The results are presented in Table 4.

TABLE 1: Demographic characteristics

Demographic characteristics	
Age (years), mean (SD) [range]	67.56 \pm 11.63 [26–81]
Gender (male/female)	24/14
Type of glaucoma	
Primary open-angle glaucoma	32
Secondary open-angle glaucoma	
Postpenetrating keratoplasty glaucoma	4
Exfoliative	2
Previous glaucoma treatments	
Endocyclophotocoagulation	1
SLT	4
Lens status	
Phakic	20
Pseudophakic	17
Aphakic	1

SD: standard deviation.

Choroid detachment was observed in one patient (2.6%), and macular edema was also observed in one patient (2.6%). No other major intraoperative or postoperative complications occurred.

The results revealed a significant difference in the scleral and conjunctival thickness after the UCP procedure. However, after 12 months, the parameters returned to the initial values with no significant difference (Figure 6). The decrease in IOP and the number of antiglaucoma medications used were statistically significant (Table 3). There is no correlation between scleral and conjunctival thickness and IOP.

4. Discussion

Currently, the only effective and proven method to treat glaucoma is to reduce IOP [7, 8]. This can be achieved by limiting the production of aqueous humor and/or improving its outflow with pharmacological and surgical methods. Production of aqueous humor can be reduced by partially damaging the nonpigmented epithelium of the ciliary body using laser photocoagulation, cryotherapy, or ultrasound energy. The most common and effective method used for this is transscleral cyclophotocoagulation (TSCP). TSCP is mainly used in severe cases of refractory glaucoma, when previous pharmacological or surgical (filtration or seton) treatment was not successful [9]. Two main disadvantages of cyclodestruction are the limited selectivity of target tissue often which causes damage to adjacent structures (e.g., laser energy is primarily absorbed by pigmented tissues, damaging the iris or choroid) and difficult prediction of the effect in relation to the dose used. TSCP also carries a risk of complications. The most common consequences are pain during and after surgery, conjunctival burn, sclera thinning, and uveitis [10–15]. Rare, but more serious, complications are hypotension, choroidal detachment, choroiditis, retinal detachment, or extremely rare-phthisis bulbi [16]. Endoscopic cyclodestruction (ECP) is better in

TABLE 2: Scleral and conjunctival thickness in superior and inferior scleral mark after UCP—24-month follow-up.

Mean values \pm SD (<i>p</i> value)	Preop	1 week	<i>p</i> value	1 month	<i>p</i> value	3 months	<i>p</i> value	6 months	<i>p</i> value	12 months	<i>p</i> value	18 months	<i>p</i> value	24 months	<i>p</i> value
Superior scleral and conjunctival thickness (μm)	684.57 \pm 83.58	771.78 \pm 112.03	<0.001	771.74 \pm 100.12	<0.001	731.48 \pm 83.92	0.012	719.52 \pm 73.20	0.037	702.91 \pm 66.50	0.247	694.13 \pm 72.22	0.482	699.35 \pm 70.68	0.200
Inferior scleral and conjunctival thickness (μm)	816.86 \pm 79.30	936.37 \pm 107.33	<0.001	946.00 \pm 130.40	<0.001	896.63 \pm 123.40	<0.001	877.69 \pm 114.38	0.003	843.03 \pm 71.55	0.021	811.86 \pm 68.91	0.731	805.03 \pm 69.52	0.248

SD: standard deviation.

TABLE 3: Intraocular pressure and number of hypotensive medications after UCP—24-month follow-up

	Mean IOP ± SD	<i>p</i> value	Number of hypotensive medications SD	<i>p</i> value	% IOP reduction
Preop	22.2 ± 4.7		4.0 ± 0.8		—
1 week	15.8 ± 4.5	<i>p</i> < 0.001	0.7 ± 0.9	<i>p</i> < 0.001	28.8
1 month	18.9 ± 5.0	<i>p</i> < 0.001	0.9 ± 1.0	<i>p</i> < 0.001	14.8
3 months	17.0 ± 3.7	<i>p</i> < 0.001	1.6 ± 1.3	<i>p</i> < 0.001	23.3
6 months	17.3 ± 2.9	<i>p</i> < 0.001	2.1 ± 1.3	<i>p</i> < 0.001	22.3
12 months	16.2 ± 2.5	<i>p</i> < 0.001	2.5 ± 1.3	<i>p</i> < 0.001	27.0
18 months	16.4 ± 2.8	<i>p</i> < 0.001	2.6 ± 1.3	<i>p</i> < 0.001	26.0
24 months	16.0 ± 3.6	<i>p</i> < 0.001	2.8 ± 1.3	<i>p</i> < 0.001	28.1

UCP: ultrasound ciliary plasty; IOP: intraocular pressure; SD: standard deviation.

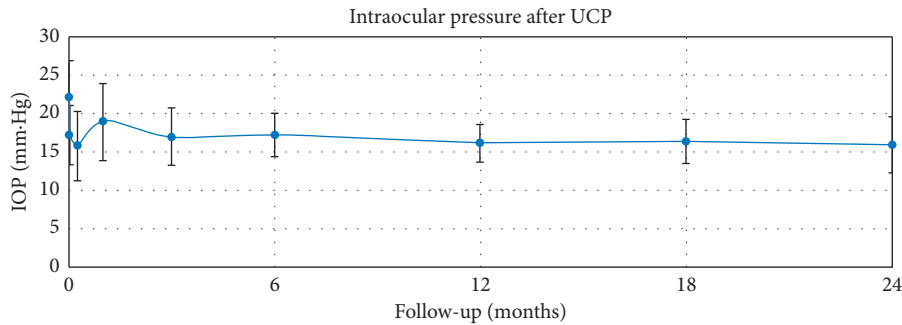


FIGURE 4: Intraocular pressure after UCP—24-month follow-up.

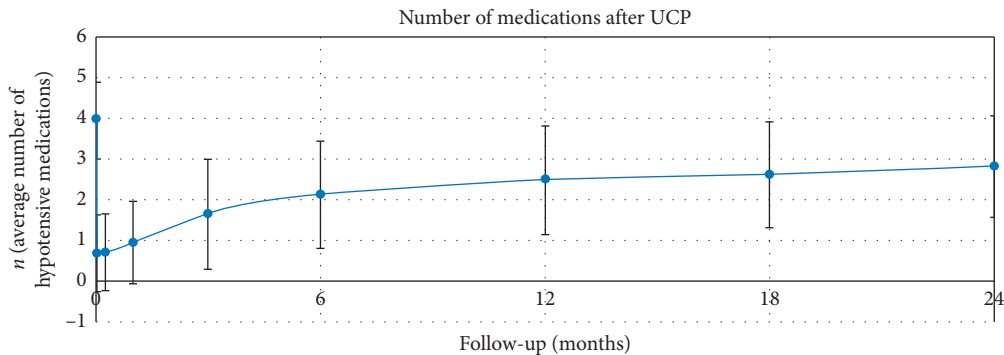


FIGURE 5: The number of antiglaucoma medications after UCP—24-month follow-up.

TABLE 4: Correlation between scleral and conjunctival thickness in superior/inferior scleral mark and IOP after UCP.

SCT versus IOP	Preop		1 week		1 month		3 months		6 months		12 months		18 months		24 months	
	<i>r</i>	<i>P</i> value	<i>r</i>	<i>P</i> value	<i>r</i>	<i>P</i> value	<i>r</i>	<i>P</i> value								
Superior SCT vs. IOP	0.186	0.395	0.343	0.109	0.153	0.487	0.032	0.883	-0.082	0.710	0.143	0.516	0.149	0.497	0.092	0.677
Inferior SCT vs. IOP	0.061	0.727	0.044	0.804	-0.099	0.570	0.003	0.985	0.119	0.497	0.225	0.195	0.300	0.080	0.120	0.491

SCT: scleral and conjunctival thickness; IOP: intraocular pressure.

terms of safety and selectivity compared to TSCP [17, 18]. However, it is an invasive procedure and is recommended only for mild or moderate glaucoma patients undergoing cataract surgery [19, 20]. This procedure also has side effects, and the most common ones are IOP spikes, increased inflammation (compared to phacoemulsification without ECP), and dislocation of the intraocular lens [21, 22].

Compared to the commonly used diode laser cyclo-destruction, the main advantage of the HIFU technology, used in UCP and through a specially designed probe is the possibility of achieving precise energy concentration through opaque structures, without uncontrolled absorption, at a desired depth and area of the ciliary body [1]. As a result, it reduces the damage to adjacent tissues because the

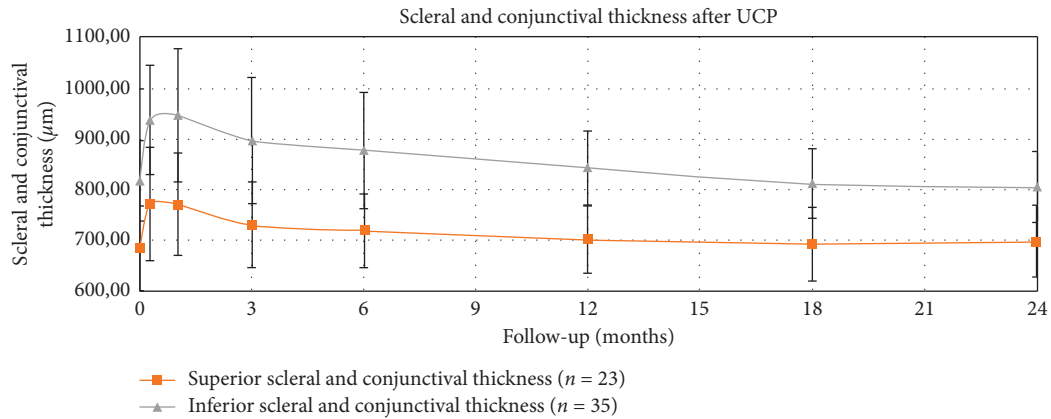


FIGURE 6: Scleral and conjunctival thickness in superior and inferior scleral mark after UCP—24-month follow-up.

amount of heat delivered to the tissue does not depend on its properties, for example, pigmentation, which in the case of the ciliary body may vary from person to person [23–25]. In spite of these advantages, the exact influence of ultrasound energy on the conjunctival and scleral tissues, and indirectly on the cornea, is still unknown.

Although a few studies have reported the appearance of scleral marks after UCP, their authors did not specify those changes consistently. Denis et al. reported scleral thinning without any sign of inflammation, induced corneal astigmatism, or scleral protrusion [3]. Deb-Joardar et al. described these findings as probable focal shrinkage of scleral tissue [2]. On the contrary, a meta-analysis of the UCP procedure reported no scleral thinning observed on OCT; however, it is not supported by any research [4]. The abovementioned studies focused mainly on the efficiency of the procedure without any further examination of the occurrence of scleral marks. These were later analyzed by two studies. The first one conducted by Mastropasqua et al. was designed to assess the alternative outflow of aqueous humor through the uveoscleral pathway using anterior segment OCT (AS-OCT) and confocal microscopy [6]. The authors reported the occurrence of a sclera cyst in the area where the ultrasound energy was applied and attributed it to heat-induced scleral fiber delamination. They did not find any scleral thinning in AS-OCT but could not rule out that occurrence. The second study was conducted on pigs' eyes and histologically reported scleral marks as rearrangement of the tissue. It was observed that collagen presented different elasticity, resistance, permeability, and opacity properties resulting in a more compact and denser structure. Its refractive power differed from that of a healthy area which may explain the translucent and grayish appearance found macroscopically [26].

Not all patients present scleral marks after the UCP procedure. Only two papers reported the exact appearance of scleral marks in treated patients—Deb-Joardar et al. in six out of 28 patients (21%) [2] and De Gregorio et al., in 10 out of 40 of patients (25%). [27] In both reports, a second-generation probe with 8 s exposure time was used. Two more papers reported scleral thinning in one out of 30 patients [28] and two out of 28 patients [29], respectively, and

although the findings were not described as scleral marks, we can assume it as the same phenomenon. However, here, the first-generation probe with 6 s exposure time was used. All of the above studies did not explain how the findings were examined. A meta-analysis of the UCP procedure [4] reported that scleral marks were more common in Indian eyes than in Caucasian eyes, which can be attributed to the more pigmented sclera. It also indicated that there was variation in the pattern of scleral mark development: in some cases, the marks faded over time, whereas in others, the reverse occurred. In our study group (78 patients), the rate of occurrence of visible scleral marks was 77.4%. Undoubtedly, the exposure time of ultrasound energy has an influence on the frequent appearance of scleral marks. However, there is a difference between our results and that of the first two studies, which used the same generation probe, with a predominance of scleral mark occurrence in our study. It is hard to explain the difference since the amount of energy delivered by the same generation probe is always constant. Scleral marks differ in intensity. We examined our patients very thoroughly, looking for scleral marks. Even slightly visible scleral mark was reported. The two cited studies focused mainly on UCP efficacy. The authors reported the scleral mark as a complication and did not explain how the occurrence was examined. Only well visible scleral marks were possibly taken to analysis which could have caused the discrepancies.

Macroscopically, in a slit-lamp examination, scleral marks look like scleral thinning which was the reason for conducting this study. However, after measuring the sclera and conjunctiva, we did not observe thinning in any of our patients. On the contrary, there was a transient thickening (Figures 7 and 8). The measured parameters returned to initial values 18 months after the UCP procedure (with no significant difference). The OCT scans showed more indistinct hyporeflexive scleral tissue in the area where the ultrasound energy was applied. The conjunctiva was intact and changes were visible only in the sclera. However, we did not observe delineated intrascleral hyporeflexive spaces as reported by Mastropasqua et al. [6] or scleral protrusion.

Postoperatively, the patients were treated topically with dexamethasone for one month. The application of this anti-

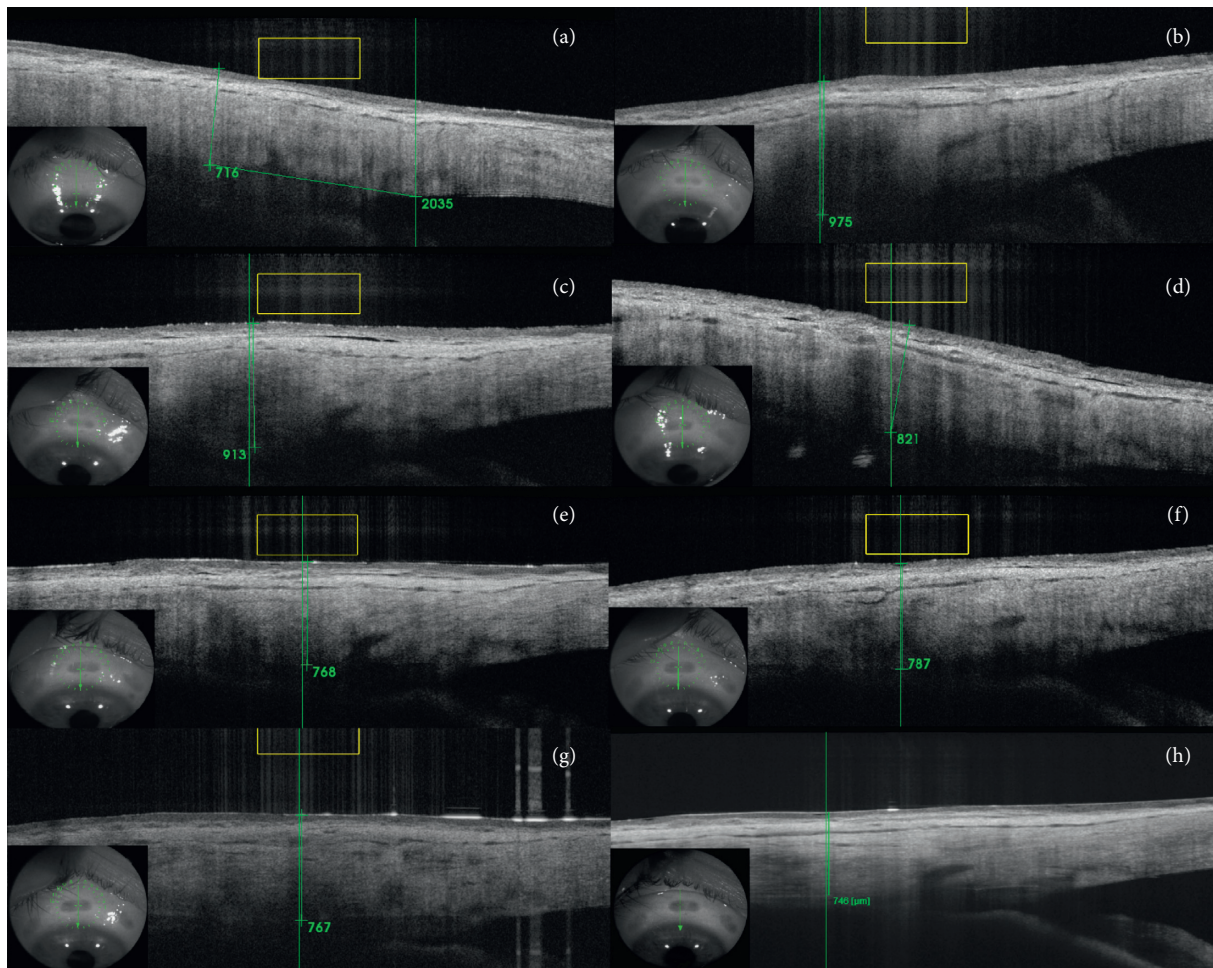


FIGURE 7: Superior-quadrant OCT scans of the sclera and conjunctiva of a patient before the procedure (a), at 1 week (b), and 1 (c), 3 (d), 6 (e), 12 (f), 18 (g), and 24 (h) months after UCP—24-month follow-up period.

inflammatory therapy after UCP can have an influence in terms of conjunctival inflammation or scleral edema. However, dexamethasone was given only during the first month, yet the follow-up period of the study was 2 years. As it is a standard postoperative treatment after any cyclo-destruction procedure, skipping it would lead to negative consequences.

IOP >30 mmHg and neovascular glaucoma were exclusion criteria of our study. Studies on UCP revealed that efficacy in these cases might be unsatisfactory after one treatment [5, 27]. The manufacturer of the UCP device also does not recommend using this type of procedure and six-sector protocol for treating neovascular glaucoma in patients with IOP >30 mmHg. Instead, in such patients, the manufacturer recommends using eight-sector protocol—two additional sectors of the ciliary body are treated. At the beginning of the study, a UCP Flex probe (Eye Tech Care, Rillieux-la-Pape, France) with eight-sector protocol was not yet available.

Previous glaucoma surgeries, like trabeculectomy or TSCP, directly or indirectly involving perilimbal interference in the sclera, were another exclusion criterion of our study. In the scanned area, the sclera needs to be intact to reliably analyze and measure its thickness.

The decrease in IOP and the number of antiglaucoma medications was statistically significant at each follow-up time point. The mean IOP at the last follow-up was reduced by 28.1%, which is similar to other studies [2, 3, 28, 30]. Correlation analysis revealed no correlation between scleral and conjunctival thickness and IOP.

Choroid detachment was observed in one patient (2.6%) in one week after the procedure. This complication resolves in one month after discontinuation of antiglaucoma medications. Macular edema occurred in one patient (2.6%) one month after the procedure, and this patient had coexistence of the epiretinal membrane. Edema resolves in two months after pharmacotherapy—with topical nonsteroidal anti-inflammatory drug and oral carbonic anhydrase inhibitor. No other major intraoperative or postoperative complications, such as cataract, retinal detachment, or phthisis bulbi, were observed.

The present study has some limitations. First, it is not possible to use OCT to precisely distinguish the boundary of sclera and conjunctiva. This was the reason we measured the thickness of both sclera and conjunctiva in the area of energy application. The OCT scans showed the conjunctiva to be intact and changes in tissues after UCP were visible only in

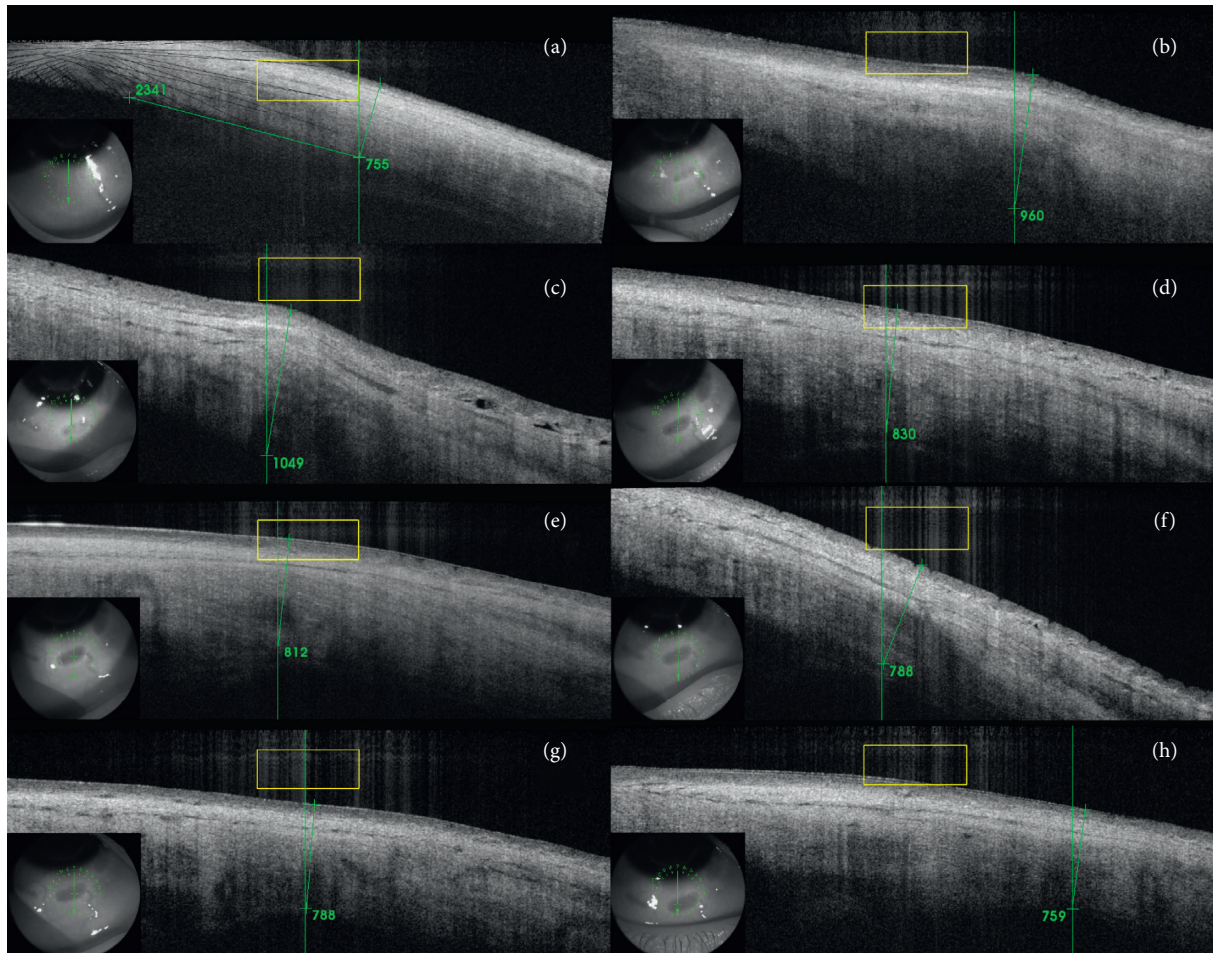


FIGURE 8: Inferior-quadrant OCT scans of the sclera and conjunctiva of a patient before the procedure (a), at 1 week (b), and 1 (c), 3 (d), 6 (e), 12 (f), 18 (g), and 24 (h) months after UCP—24-month follow-up period.

the sclera. Second, OCT scans have limitations in the case of scleral tissue penetration. Not in every scan we can see a clear boundary between the sclera and the choroid. For analysis, we selected those OCT scans in which we could precisely distinguish the scleral boundaries. We did not investigate the choroid because we could not image this site easily using OCT. In our experience, AS-OCT (Casia 2 Swept Source OCT, Tomey, Tokyo, Japan) has lower scleral penetration than Swept Source OCT dedicated to the posterior segment with an anterior segment adapter, despite the best possible manual scan settings. Therefore, a second type of equipment was used. Despite these imperfections, AS-OCT provides more accurate delineation of the anterior segment structures with higher scanning resolution than ultrasound biomicroscopy [31, 32]. Third, the measurement of OCT thickness may present a level of subjectivity. All measurements were performed manually by two operators using the built-in measuring tool in the OCT device. Fourth, in our study, we analyzed the most upper and lower scleral marks. We did not analyze the other four scleral marks (in upper/lower nasal/temporal quadrant). To obtain the OCT scan of

these areas, the patient should look in the opposite direction to the scleral mark. We noticed that in this case, patient's cooperation is worse than looking straight up or down. This resulted in poor-quality OCT scans which were difficult to measure. However, we found no apparent differences in the sclera of those areas compared to the analyzed one.

Despite the assumptions in reducing the energy applied to neighboring tissues in the UCP procedure, the literature and our study show that this cyclodestruction method affects the sclera. However, the effect was transient, and we did not observe scleral thinning or protrusion. On the contrary, there was a temporary thickening. Also, we did not observe any correlation between changes in scleral thickness and IOP. Clinically, changes in the sclera may lead to the appearance of astigmatism after the UCP procedure. In another study conducted by our clinic, we proved that UCP affects corneal topography immediately after the procedure (mostly anterior astigmatism). However, during the course of time (after three months), the corneal parameters return to initial values [33]. Therefore, clinical implication of changes lasts shorter than a significant difference in scleral

thickness. This information shows that there are no contraindications in the profile of patients suitable for this type of surgery in terms of scleral abnormalities. It will also allow safe treatment of refractory glaucoma—the advanced stage of the disease, where pharmacological treatments have already been taken, and this type of surgery is the only way to stop the process of vision loss.

5. Conclusion

Scleral thickness changes after the UCP procedure. However, with time, the parameter returns to its initial value. Clinical implication of sclera changes lasts shorter than the significant measured difference in scleral thickness.

Abbreviations

UCP:	Ultrasound ciliary plasty
SS-OCT:	Swept source optical coherence tomography
TSCP:	Transscleral cyclophotocoagulation
SIA:	Surgical induced astigmatism
IOP:	Intraocular pressure
AXL:	Axial length
WTW:	White to white
HIFU:	High-intensity focused ultrasound.

Data Availability

The numerical data used to support the findings of this study may be released upon application to the Chair and Clinical Department of Ophthalmology, School of Medicine in Zabrze, the Medical University of Silesia in Katowice, District Railway Hospital, Katowice, Poland, who can be contacted at District Railway Hospital, Panewnicka 65, 40-760 Katowice, Poland; e-mail: bartlomiej.bolek@med.sum.edu.pl;

Conflicts of Interest

The authors declare that they have no conflicts of interest.

References

- [1] F. Aptel, T. Charrel, C. Lafon et al., “Miniaturized high-intensity focused ultrasound device in patients with glaucoma: a clinical pilot study,” *Investigative Ophthalmology & Visual Science*, vol. 52, no. 12, pp. 8747–8753, 2011.
- [2] N. Deb-Joardar and K. Reddy, “Application of high intensity focused ultrasound for treatment of open-angle glaucoma in Indian patients,” *Indian Journal of Ophthalmology*, vol. 66, no. 4, pp. 517–523, 2018.
- [3] P. Denis, F. Aptel, J. F. Rouland et al., “Cyclocoagulation of the ciliary bodies by high-intensity focused ultrasound: A 12-month multicenter study,” *Investigative Ophthalmology & Visual Science*, vol. 56, pp. 1089–1096, 2015.
- [4] P. Denis, “Clinical research of ultrasound ciliary plasty and implications for clinical practice,” *European Ophthalmic Review*, vol. 10, no. 2, p. 108, 2016.
- [5] M. A. Torky, Y. A. Al Zafiri, S. M. Hagrass et al., “Safety and efficacy of ultrasound ciliary plasty as a primary intervention in glaucoma patients,” *International Journal of Ophthalmology and Clinical Research*, vol. 11, 2019.
- [6] R. Mastropasqua, L. Agnifili, V. Fasanella et al., “Uveo-scleral outflow pathways after ultrasonic cyclocoagulation in refractory glaucoma: an anterior segment optical coherence tomography and in vivo confocal study,” *British Journal of Ophthalmology*, vol. 100, no. 12, pp. 1668–1675, 2016.
- [7] A. Heijl, M. C. Leske, B. Bengtsson et al., “Reduction of intraocular pressure and glaucoma progression,” *Archives of Ophthalmology*, vol. 120, no. 10, pp. 1268–1279, 2002.
- [8] M. A. Kass, D. K. Heuer, E. J. Higginbotham et al., “The ocular hypertension treatment study,” *Archives of Ophthalmology*, vol. 120, no. 6, pp. 701–713, 2002.
- [9] J. Jankowska-Szmul, D. Dobrowolski, and E. Wylegala, “CO₂ laser-assisted sclerectomy surgery compared with trabeculectomy in primary open-angle glaucoma and exfoliative glaucoma,” *Acta Ophthalmologica*, vol. 96, no. 5, pp. e582–e591, 2018.
- [10] S. A. Vernon, J. M. Koppens, G. J. Menon, and A. K. Negi, “Diode laser cycloablation in adult glaucoma: long-term results of a standard protocol and review of current literature,” *Clinical and Experimental Ophthalmology*, vol. 34, no. 5, pp. 411–420, 2006.
- [11] B. J. Jennings and D. E. Mathews, “Complications of neodymium:YAG cyclophotocoagulation in the treatment of open-angle glaucoma,” *Optometry and Vision Science*, vol. 76, no. 10, pp. 686–691, 1999.
- [12] J. F. Kirwan, P. Shah, and P. T. Khaw, “Diode laser cyclophotocoagulation,” *Ophthalmology*, vol. 109, no. 2, pp. 316–323, 2002.
- [13] M. J. Walland, “Diode laser cyclophotocoagulation: longer term follow up of a standardized treatment protocol,” *Clinical and Experimental Ophthalmology*, vol. 28, no. 4, pp. 263–267, 2000.
- [14] P. Frezzotti, V. Mittica, G. Martone et al., “Longterm follow-up of diode laser transscleral cyclophotocoagulation in the treatment of refractory glaucoma,” *Acta Ophthalmologica*, vol. 88, no. 1, pp. 150–155, 2010.
- [15] V. Pucci, F. Tappainer, S. Borin, and R. Bellucci, “Long-term follow-up after transscleral diode laser photocoagulation in refractory glaucoma,” *Ophthalmologica*, vol. 217, no. 4, pp. 279–283, 2003.
- [16] A. M. Tan, M. Chockalingam, M. C. Aquino, Z. I. L. Lim, J. L. S. See, and P. T. Chew, “Micropulse transscleral diode laser cyclophotocoagulation in the treatment of refractory glaucoma,” *Clinical & Experimental Ophthalmology*, vol. 38, no. 3, pp. 266–272, 2010.
- [17] M. B. Pantcheva, M. Y. Kahook, J. S. Schuman, and R. J. Noecker, “Comparison of acute structural and histopathological changes in human autopsy eyes after endoscopic cyclophotocoagulation and trans-scleral cyclophotocoagulation,” *British Journal of Ophthalmology*, vol. 91, no. 2, pp. 248–252, 2007.
- [18] S. C. Lin, M. J. Chen, M. S. Lin et al., “Vascular effects on ciliary tissue from endoscopic versus trans-scleral cyclophotocoagulation,” *British Journal of Ophthalmology*, vol. 90, no. 4, pp. 496–500, 2006.
- [19] S. Berke, A. Cohen, R. Sturm, R. Caronia, and D. Nelson, “Endoscopic cyclophotocoagulation (Ecp) and phacoemulsification in the treatment of medically controlled primary open-angle glaucoma,” *Journal of Glaucoma*, vol. 9, no. 1, p. 129, 2000.
- [20] M. J. Siegel, W. S. Boling, O. S. Faridi et al., “Combined endoscopic cyclophotocoagulation and phacoemulsification

- versus, phacoemulsification alone in the treatment of mild to moderate glaucoma,” *Clinical & Experimental Ophthalmology*, vol. 43, no. 6, pp. 531–539, 2015.
- [21] R. J. Noecker, M. Y. Kahook, S. J. Berke et al., “Uncontrolled intraocular pressure after endoscopic cyclophotocoagulation,” *Journal of Glaucoma*, vol. 17, no. 3, pp. 250–251, 2008.
- [22] R. J. Noecker and E. C. S. Group, *Complications of Endoscopic Cyclophotocoagulation*, the ASCRS Symp. Cataract. IOL Refract. Surgery, San Diego CA, USA, 2007.
- [23] F. Aptel, T. Charrel, X. Palazzi, J.-Y. Chapelon, P. Denis, and C. Lafon, “Histologic effects of a new device for High-Intensity focused Ultrasound Cyclocoagulation,” *Investigative Ophthalmology & Visual Science*, vol. 51, no. 10, pp. 5092–5098, 2010.
- [24] T. Charrel, F. Aptel, A. Birer et al., “Development of a miniaturized HIFU device for glaucoma treatment with conformal coagulation of the ciliary bodies,” *Ultrasound in Medicine & Biology*, vol. 37, no. 5, pp. 742–754, 2011.
- [25] F. Aptel and C. Lafon, “Therapeutic applications of ultrasound in ophthalmology,” *International Journal of Hyperthermia*, vol. 28, no. 4, pp. 405–418, 2012.
- [26] K. S. Lim, “Ultrasound cycloplasty in glaucoma-mechanisms of action and their possible impact on intraocular pressure,” *European Ophthalmic Review*, vol. 11, no. 1, p. 35, 2017.
- [27] A. De Gregorio, E. Pedrotti, G. Stevan, M. Montali, and S. Morselli, “Safety and efficacy of multiple cyclocoagulation of ciliary bodies by high-intensity focused ultrasound in patients with glaucoma,” *Graefe’s Archive for Clinical and Experimental Ophthalmology*, vol. 255, no. 12, pp. 2429–2435, 2017.
- [28] F. Aptel, P. Denis, J. F. Rouland et al., “High-intensity focused ultrasound treatment for open angle glaucoma,” *Acta Ophthalmologica*, vol. 94, pp. e268–e277, 2016.
- [29] F. Aptel, C. Dupuy, and J. F. Rouland, “Treatment of refractory open-angle glaucoma using ultrasonic circular cyclocoagulation: a prospective case series,” *Current Medical Research and Opinion*, vol. 30, no. 8, pp. 1599–1605, 2014.
- [30] G. Giannaccare, A. Vagge, S. Sebastiani et al., “Ultrasound cyclo-plasty in patients with glaucoma: 1-year results from a multicentre prospective study,” *Ophthalmic Research*, vol. 61, no. 3, pp. 137–142, 2019.
- [31] C. Oliveira, C. Tello, J. Liebmann et al., “Central corneal thickness is not related to anterior scleral thickness or axial length,” *Journal of Glaucoma*, vol. 15, 2006.
- [32] C. Yoo, Y. S. Eom, Y.-W. Suh et al., “Central corneal thickness and anterior scleral thickness in Korean patients with open-angle glaucoma,” *Journal of Glaucoma*, vol. 20, 2011.
- [33] B. Bolek, A. Wylęgała, and W. Edward, “The influence of ultrasound ciliary plasty on corneal parameters,” *Journal of Glaucoma*, 2020.

Research Article

Intraoperative Optical Coherence Tomography Imaging in Corneal Surgery: A Literature Review and Proposal of Novel Applications

Hiroshi Eguchi ¹, Fumika Hotta,¹ Shunji Kusaka,¹ and Yoshikazu Shimomura²

¹Department of Ophthalmology, Kindai University, Faculty of Medicine, 377-2 Ohnohigashi, Osakasayama, Osaka 589-8511, Japan

²Department of Ophthalmology, Fuchu Eye Center, 1-10-17 Hiko-cho, Izumi, Osaka 594-0076, Japan

Correspondence should be addressed to Hiroshi Eguchi; hiroegu0113@gmail.com

Received 26 June 2020; Revised 12 August 2020; Accepted 21 August 2020; Published 11 September 2020

Academic Editor: Sang Beom Han

Copyright © 2020 Hiroshi Eguchi et al. This is an open access article distributed under the Creative Commons Attribution License, which permits unrestricted use, distribution, and reproduction in any medium, provided the original work is properly cited.

Intraoperative optical coherence tomography (*i*OCT) is widely used in ophthalmic surgeries for cross-sectional imaging of ocular tissues. The greatest advantage of *i*OCT is its adjunct diagnostic efficacy, which facilitates to decision-making during surgery. Since the development of microscopic-integrated *i*OCT (MIOCT), it has been widely used mainly for vitreoretinal and anterior segment surgeries. In corneal transplantation, MIOCT allows surgeons to visualise structure underneath the turbid and distorted cornea, which are impossible to visualise with a usual microscope. Real-time visualisation of hard-to-see area reduces the operation time and leads to favorable surgical outcomes. The use of MIOCT is advantageous for a variety of corneal surgical procedures. Here, we have reviewed articles focusing on the utility of *i*OCT and MIOCT in penetrating keratoplasty, deep anterior lamellar keratoplasty, Descemet stripping automated endothelial keratoplasty, and Descemet membrane endothelial keratoplasty. The applications of MIOCT to corneal surgery in terms of surgical education for trainees, emergency surgery, and novel surgery are also discussed, with our cases performed using RESCAN[®] 700.

1. Introduction

Intraoperative optical coherence tomography (*i*OCT) is an imaging modality capable of showing real-time OCT images of the ocular tissue. This system confers advantages for both surgeon and the medical staff in the operating theatre during surgery. Although *i*OCT is now widely adopted to many ophthalmic surgeries for intraoperative cross-sectional imaging of the ocular tissues, there were some hurdles which conventional OCT modality must overcome before it is applied in the operating theatre [1]. The first OCT machines were desktop, stationary, and expensive, since they were initially designed for seated patients in outpatient clinic. Thus, relocating them to the operation theatre for intraoperative use was not practical. Thereafter, lightweight handheld OCTs were introduced, making it possible to bring the OCT machine into the operation theatre for patients in

supine position [2–4]. However, handheld OCTs have limited use in the operation theatre since surgeons need to discontinue surgical manoeuvres when they obtain OCT images or require another medical staff for obtaining the image using this device, which translates to the OCT images not being truly “real time.” Although no article has reported the occurrence of intraoperative infections caused by handheld OCT, its use may increase the risk of intraoperative infection since it entails bringing nonsterile machine from outside of the operation theatre. Involuntary hand movement while using the handheld device also causes artifacts, which leads to lower quality of the acquired images [1]. Subsequently, Ray et al. [5] created their own mount for attaching a handheld OCT to the microscope, which allowed the surgeon or assistant to move the device above the patient’s eye using the microscope foot pedal to ensure maintenance of sterility, improve image quality and

reproducibility, and reduce image capture time. Similarly, Ehlers et al. [6, 7] fastened a handheld probe to the surgical microscope to provide increased stability of the probe and successfully obtained high quality *i*OCT images during vitreoretinal surgery.

Ehlers et al. were the first to demonstrate a microscope-integrated *i*OCT research system, which utilised a spectral domain OCT device attached in the space between the surgeon's eyepiece and microscope objective in a commercial surgical microscope [7, 8]. In recent years, OCT probes have been integrated into the microscope as commercially available products to enable true "real time" imaging of ocular tissues during the surgery, which was termed microscopic-integrated *i*OCT (MIOCT) [9]. The greatest advantage of *i*OCT is its adjunct diagnostic efficacy, which facilitates decision-making during surgery [6, 9, 10]. Its utility has been further enhanced with the advent of MIOCT, which allows the capture of cross-sectional images both on the microscope barrel and head-up monitor [10] without the need to discontinue surgical manoeuvre.

*i*OCT was initially developed for anterior segment surgery [11]. Thereafter, it has been applied to vitreoretinal surgeries, with numerous articles on such applications being published. These include its use for macular hole [5, 12, 13], epiretinal membrane [5, 14–16], retinal detachment [6, 17–19], and vitreomacular traction [15, 20, 21], among others [22–27]. Subsequently, its application has been expanded to include glaucoma surgery [28–31] and corneal transplantation [7, 9, 32–55]. To our knowledge, three systems are currently commercially available in worldwide: Rescan[®] 700 (Carl Zeiss Meditec, Germany), OPMedT (OPMedT, Germany), and Biotigen/Leica EnFocus (Leica, Germany). In this review, we will focus on the utility of *i*OCT or MIOCT for corneal surgeries, specifically penetrating keratoplasty (PK), deep anterior lamellar keratoplasty (DALK), Descemet stripping automated endothelial keratoplasty (DSAEK), and Descemet membrane endothelial keratoplasty (DMEK). New applications of MIOCT to both corneal surgery and in surgical education by introducing treated cases using Rescan[®] 700 will be discussed. A report on the application of MIOCT to the latest corneal surgery will also be introduced.

2. Penetrating Keratoplasty (PK)

In PK, structures on the underside of the cornea, which are distorted at the host-graft interface, are hard to identify. If the structure in the anterior chamber underneath a severe peripheral corneal scar has changed during surgery, it is also difficult to detect the alteration using a typical microscope. During corneal suturing, after trephination of the host cornea, iris incarceration and iridocorneal adhesion can occur at anytime because eyeball is opened. MIOCT is useful in all the aforementioned situations, since it enables the visualisation of the endothelium layer, which runs beneath the host-graft interface [39]. The host-graft interface can be continually assessed during surgery by *i*OCT or MIOCT, which can help to prevent overriding/underriding of the graft and ensure proper apposition at the host-graft interface [40].

For the same reason as mentioned above, there could be value in the use of MIOCT in PK for educational purpose, especially for the verification of needle depth during suturing. Ideally, when suturing the graft to the host cornea, these structures' representative Descemet membranes (DMs) should be at the same height. If they were sutured at the different height, the grafted cornea may dissociate when the stitches are removed in the future. Therefore, the needle should be passed through a relatively deep corneal stroma, keeping the DMs of both host and graft cornea in mind. However, if the cornea is cloudy, it is not possible to determine the depth at where the needle is located using a typical microscope. If the host and graft were lifted with forceps so that these cross-sections could be visualised, the depth of the needle penetration into the cornea can be determined. However, such manoeuvre is impossible and undesirable in many cases. Therefore, the depth of the passed needle is usually estimated using the surgeon's hand.

Two studies have reported visualisation of the penetration depth of the syringe needle by *i*OCT in human [33] and porcine cornea [41], but no reports of *i*OCT confirmation of suture needle depth in the human corneal suturing in PK has yet been published. In the PK case presented in this study, confirmation of the position of the needle passing through the cornea was possible through the use of MIOCT. If the needle depth was found to be shallow, determining whether the thread should be rethreaded was made by the use of MIOCT and determining if the needle has unintentionally penetrated through the host or graft cornea (Figure 1(a)). The needle is then rethreaded accordingly, and the host and the graft are adjusted to the appropriate DM height (Figure 1(b)). Even for a skilled corneal surgeon, passing the suture needle into the cornea at the appropriate depth each time is not easy. Therefore, MIOCT would be useful in training of novice doctors for corneal suturing, especially in terms of verifying needle depth during the procedure. This verification may also be useful in emergency corneal suturing in cases of corneal rupture and corneal perforation.

3. Deep Anterior Lamellar Keratoplasty (DALK)

In DALK, surgeons always need to assess the thickness of residual corneal stroma carefully during stromal excision. Even though it may appear that a significant amount of cornea has been removed when viewed from above under a typical microscope, MIOCT often reveals that more cornea remains than expected when the cross section is examined by MIOCT. Ehlers et al. reported in two articles that *i*OCT facilitated changes in dissection depth in 38–56% of cases [7, 9]. The use of air or ophthalmic viscoelastic bubbles during stromal excision [56] has led to the cornea becoming cloudy and the area underneath becoming completely invisible by a typical microscope. The surgeon therefore recognises DM detachment by observing big bubble formed in the corneal stroma which pushes the injected air in the anterior chamber. Although easy for a skilled surgeon, determining this using a typical microscope may be difficult for a novice DALK surgeon. Even in such circumstances,

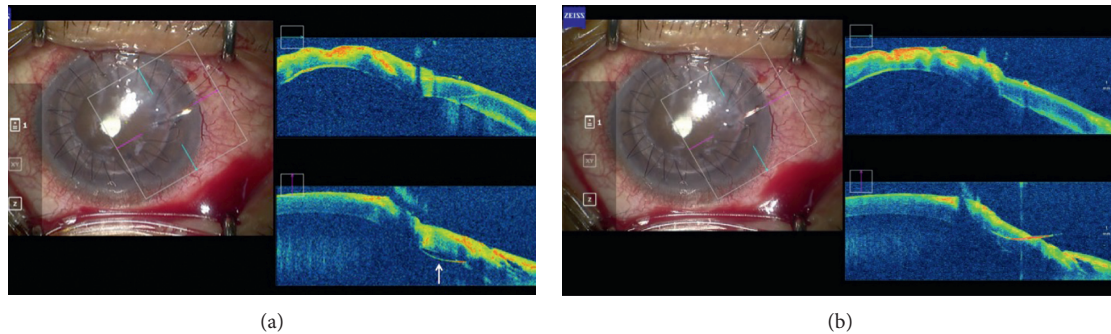


FIGURE 1: MIOCT images of the graft suture. (a) Needle penetration. When the 10-0 nylon needle was threaded through the graft, needle penetration was suspected based on the surgeon's judgment using his/her hand. MIOCT clearly showed that the needle penetrated and was located under the corneal endothelium (arrow). (b) MIOCT image after the corneal resuture. Once the needle is removed and the graft is restitched, the needle is threaded deep into the cornea appropriately.

MIOCT can provide clear cross-sectional images of the stromal lamella, the bubbles in the stroma, and the movement of the DM (Figure 2(a)). When the DM has completely detached and the corneal stroma remaining over it is excised with scissors, full awareness of the depth of the DM should be kept in mind. If scissors were carelessly inserted into the deep stroma, the DM would rupture. In such situation, MIOCT can pinpoint a location between the DM and scissors (Figure 2(b)). MIOCT has also been reported as useful for assessing the location of the DM, for facilitating manual stromal excision, for assisting with the visualisation of the injected syringe needle into the stroma, and the assessing bare DMs [34, 35]. Furthermore, the measurement of the dissection depth of the corneal stroma by MIOCT has been reported to be an important factor of DALK success rate without conversion to PK [36]. These articles also substantiate the view that MIOCT is useful for education for novice DALK surgeons.

The utility of MIOCT for the visualisation of the misdirected air into the posterior chamber at the end of the DALK has been reported [39]. When microperforation of DM occurred during stromal excision, air injection into the anterior chamber should be performed. If the case had narrow angle, the air can be misdirected into the posterior chamber. In such case, MIOCT can detect the iris protrusion caused by air in the posterior chamber easily, which results in the prevention from high intraocular pressure in the early postoperative stage by injection fluid to let the air under the iris float immediately. It is often evident upon viewing the behaviour of the iris and air using a typical microscope, but the observation with MIOCT is more reliable for distorted cornea. MIOCT is useful for corneal surgeons in all proficiency levels in every surgical step of DALK.

4. Descemet Striping-Automated Endothelial Keratoplasty (DSAEK)

The advantage of MIOCT in DSAEK is its ability to visualise the relationship between the graft and the host cornea by viewing their cross-sections intraoperatively. This is true for both cases where the host cornea is relatively transparent and also in cases in which it is not. A study that used a

handheld OCT noted that donor adherence can occur despite the residual interface space between the host cornea and the DSAEK graft at the end of the surgery, with the need for further research reported [42]. At this time, the space between the host cornea and the DSAEK graft might remain at the end of the surgery in many cases even if the surgeon had assumed that the graft had successfully adhered to the host cornea by air injection into the anterior chamber. The *iCOT* has been suggested to be beneficial in elucidating the pathogenesis of phenomenon affecting surgical outcomes in DSAEK. Subsequently, another study which used a portable spectral domain OCT system with a customised microscope mount pointed out the association between the transient interface fluid, which can be observed intraoperatively on MICOT, and the texture interface opacity, which appears postoperatively, suggesting that intraoperative MIOCT findings are associated with postoperative outcomes [43].

After insertion of the DSAEK graft, the residual interface space between the graft and the host cornea is massaged on the host cornea to facilitate complete adhesion of the host and graft. However, the space widens after the massage in some cases, with the speculated cause being the inability of the curvature of the graft to match perfectly to that of the host cornea (Figures 3(a) and 3(b)). This is due to the cornea being not completely spherical and the DSAEK graft not always being punched in the centre of the grafted cornea each time. If the residual space between the host and the graft is widened after the massage, it would have been possible to attach the graft in all case by rotating the graft and performing an air injection only once, without the need for a repeat air or gas injection. Although further prospective studies are needed to warrant this procedure, this method was conceived only from the observations made by MIOCT.

Shazly et al. [49] and Pasricha et al. [50] reported that MIOCT is a valuable tool in performing DSAEK for severe opaque cornea cases in terms of viewing graft adherence to the host cornea. Similarly, the utility of MIOCT for determining the relationship between the DSAEK graft and the iris or vitreous in complicated case after multiple surgeries is also proposed. Patients who have undergone multiple internal ocular surgeries often have abnormal anatomical structures in their anterior chamber and corneal opacities.

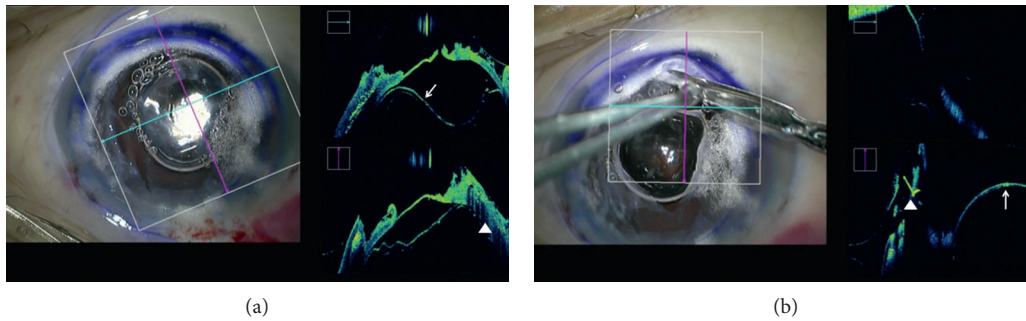


FIGURE 2: MIOCT images of DALK case. (a) Descemet membrane detachment. MIOCT shows cross-sectional images of both the Descemet membrane (arrow) detachment and the lamella dissected by air (arrow head). (b) Removal of the residual corneal stroma with scissors. The location between the Descemet membrane (arrow) and the scissors (arrow head) is roughly displayed by MIOCT, which contributes to the prevention of Descemet membrane rupture by preventing unintentional contact of the tip of scissors with the membrane.

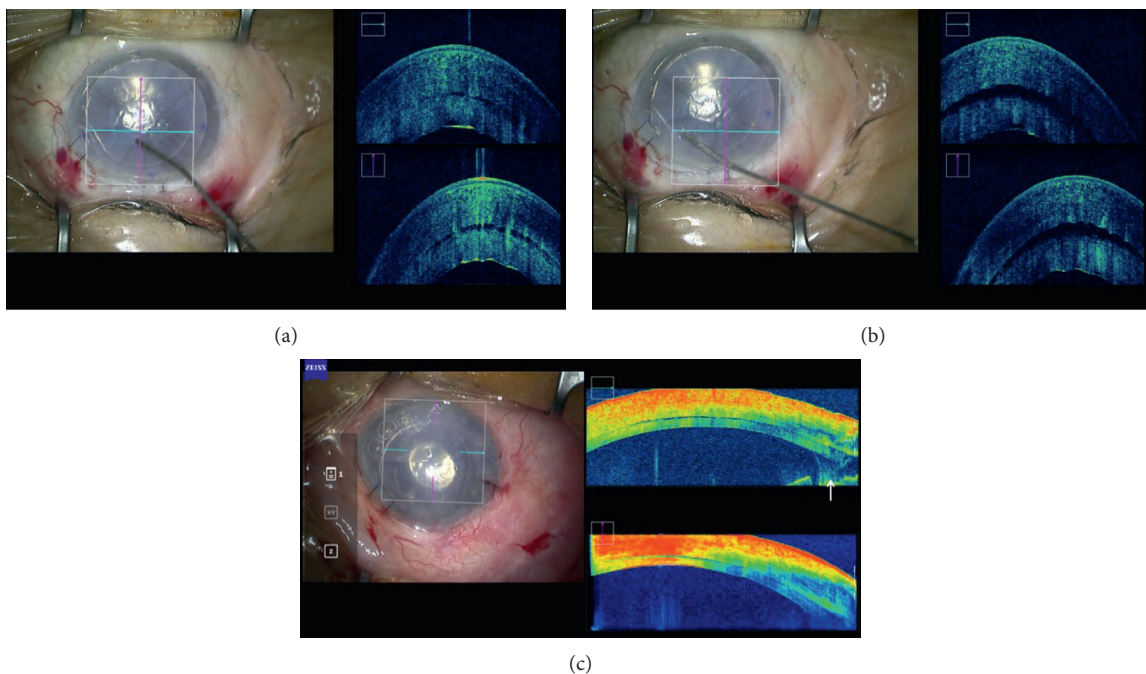


FIGURE 3: Residual interface space between the DSAEK graft and the host cornea. (a) Before corneal massage, a slight interface space between the DSAEK graft and the host cornea was observed. (b) Immediately after the corneal massage, the residual interface space widened. (c) DSAEK for advanced bullous keratopathy after multiple surgeries. Severe opacities in the cornea disturbed visualisation in the anterior chamber. MIOCT displayed a wide peripheral anterior synechia and a vitreous strand (arrow) touching the DSAEK graft.

Severe opacities in the peripheral cornea interfere with the determination of the relationship between the edge of the DSAEK graft and the iris. In our patient with DSAEK who had advanced bullous keratopathy after multiple surgeries for cataract, retinal detachment, and glaucoma, MIOCT visualised the peripheral anterior synechia (PAS). Indeed, the finding can be observed upon preoperative examination in an outpatient clinic by usual OCT. However, after certain surgical manoeuvres, the structures in the anterior chamber would change. In this case, in the middle of the surgery, the PAS was found to be wider than expected, and a vitreous strand incarcerating into the surgical wound was observed to be disturbing the DSAEK graft attach in the centre of the

host cornea (Figure 3(c)). After goniosynechialysis and anterior vitrectomy, the graft was attached satisfactorily. This case substantiates the view that MIOCT can facilitate central placement of the DSAEK graft and decrease the risk of postoperative rejection and secondary glaucoma following DSAEK by allowing detection of abnormal structures in the anterior chamber during surgery.

5. Descemet Membrane Endothelial Keratoplasty (DMEK)

MICOT plays a major role in the success of DMEK. In every step in DMEK, MIOCT imaging facilitates decision-making,

resulting in a high surgical success rate. Its most valuable utility is visualisation of DMEK graft orientation after its insertion into the anterior chamber. If stromal oedema was mild, the orientation of the DMEK graft could be ascertained with a microscope-integrated slit-scan system (Figure 4(a)). However, images captured by MICOT (Figure 4(b)) are superior. If the patient had a severe stromal oedema, MIOCT would be essential. If the initial surgery is unsuccessful and the DMEK graft is floating in the anterior chamber, the entire cornea would be marked oedema since the host endothelial cells have already been removed along with the DM. In the second surgery for graft correction in such cases, the orientation of the graft moving freely within the anterior chamber intraoperatively cannot be ascertained without MIOCT. Even if the DMEK graft was opened as its front and reversed successfully with air, its peripheral part may be folded down. If a scalpel is used to puncture the host corneal epithelium to correct the folded area, it is necessary to determine whether the endothelial cell side of the graft was folded in contact with the host cornea or to the anterior chamber. Making this decision would not be possible without MIOCT (Figures 4(c) and 4(d)).

Another application of MIOCT to DMEK would be its ability to aid in the decision to discontinue DMEK in the case where strong anterior chamber inflammation occurred during surgery. This study reports a case wherein a DMEK graft curled up, became fixed, and could not be opened with any subsequent manoeuvre. Preoperatively, the patient denied having any underlying disease, which may have cause intraocular inflammation. However, during surgery, the anterior chamber began to become rapidly cloudy after the iris was touched. Although there was no obvious fibrin aggregation, MICOT showed cloudiness inside the curled DMEK graft (Figure 4(e)). The rapid increase in anterior chamber inflammatory was concluded to have been due to blood-aqueous barrier break-down, causing the aqueous humor to become viscous and the curled DMEK graft to become impossible to open, as if it had been glued on. Eventually, DMEK was abandoned, but DSAEK was performed for correction later on. MIOCT greatly aids DMEK in all its stages after the graft insertion.

6. Emergency Surgery for Corneal Trauma

In this study, two cases of patients who underwent emergency surgeries for corneal trauma using MIOCT are reported. The first case made use of MIOCT for determining the depth of the foreign body in the cornea. A sharp and pointed plant thorn deeply pierced in the cornea and was removed in emergency surgery at the operation theatre. Preoperative examination by OCT showed the DM near the plant thorn protruded (Figure 5(a)). Removal at the outpatient clinic was deemed risky because the manoeuvre itself could penetrate the cornea. Otherwise, the cornea would have already perforated by plant thorn, and the anterior chamber would have collapsed after removal. A small amount of aqueous humor leaked after the removal as

expected. MIOCT found no opacity in the wound (Figure 5(b)), which indicated that no foreign body was left in the corneal wound and the DM protrusion to have disappeared. Without MIOCT, corneal scraping would consider because the deep side of the wound cannot be found using a typical microscope. Performing scraping may cause both enlargement of the wound and more aqueous humor leakage, which results in the corneal scar.

The second case was a partial alkali burn of the cornea. In the case of a corneal alkali burn, the depth of the corneal opacity may have changed between the time of OCT imaging at the outpatient clinic and during the actual operation at the operation theatre, since alkali can melt protein. MIOCT can estimate the depth of corneal opacities in emergency surgery (Figure 5(c)). These two cases substantiate the view that MIOCT aids in decision-making during emergency surgery for corneal trauma.

7. Other Applications

Siebelmann et al. [57] reported the use of MIOCT for drainage of acute corneal hydrops in keratoconus. They performed the surgery using a combination of suturing and gas-aided reattachment of the DM, which may be facilitated by MIOCT. Tong et al. [58] reported the use of MIOCT in Bowman layer transplantation, which is a new type of corneal transplantation. MIOCT facilitates visualisation of the air-endothelial reflex dissection plane even under blood, oedema, or scarring. Schmidt et al. [59] reported the use of MIOCT in a corneal biopsy of a stromal opacity caused by immune deposits. They concluded that MIOCT assisted in identifying the corneal pathology for biopsy, which is in agreement with the findings in the aforementioned corneal trauma cases. Mazzotta and Caragiuli [60] reported the use of *i*OCT during corneal cross-linking and recommended intraoperative optical pachymetry evaluation before starting UV-A irradiation. Ghaffari et al. [61] and Pahuja et al. [62] also reported the use of *i*OCT or MIOCT during corneal cross-linking to evaluate the corneal pachymetry during the surgery. Kobayashi et al. [63] used MIOCT not for surgery but for evaluation of donor cornea tissues through the viewing chamber. They concluded that intact PK donors and prestripped DMEK donors are distinguishable by MIOCT, which may be beneficial for their institute where many corneal surgeons perform multiple corneal transplantations on the same day.

8. Current Limitations and Future Prospects

In cases of low-intensity corneal opacity, the structures in the anterior chamber can be ascertained. However, in cases of high-intensity corneal opacity, observation of the anterior chamber in detail is difficult (Figure 6(a)). The structures to be observed during anterior segment surgery are much thicker than the retina. Therefore, when observing the deep side of the anterior chamber, such as the iris or the angle, the cornea appears as an inverted ghost image superimposed on the structure to be observed (Figure 6(b)) [64]. This is a

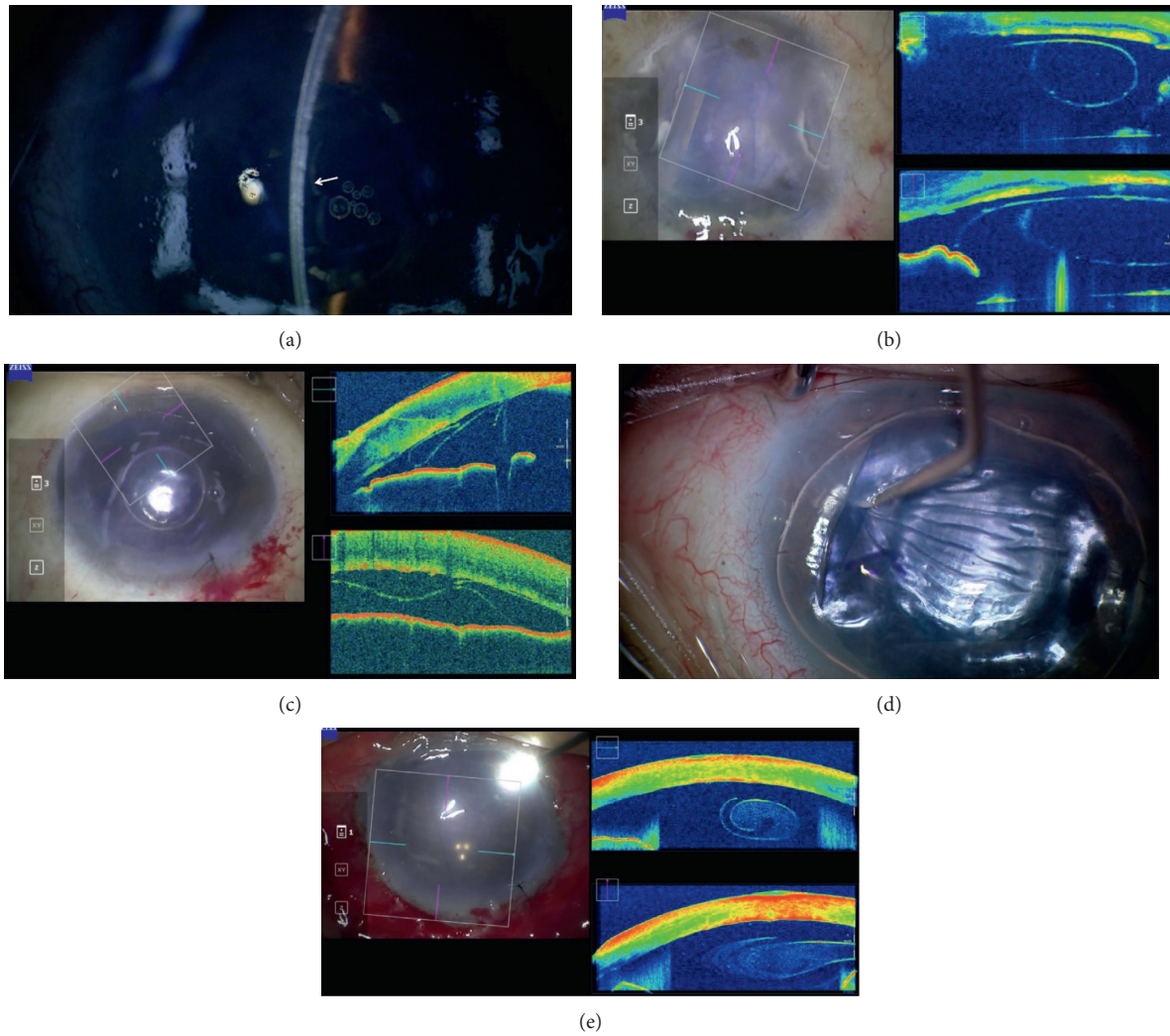


FIGURE 4: MIOCT images of DMEK cases. (a) Images of DMEK graft after insertion into the anterior chamber using a microscope-integrated slit-scan system. In the case of mild stromal oedema, the orientation of the DMEK graft can be ascertained (white arrow). (b) MIOCT images of the DMEK graft insertion into the anterior chamber. The graft orientation is clearly displayed as reverse even in the case of severe stromal oedema caused by Axenfeld–Rieger syndrome. In terms of images for decision-making, MIOCT images are much better than those of slit-scan systems. (c) Images after air injection for sticking the DMEK graft to the host cornea. The most peripheral part of the inserted DMEK graft in the anterior chamber is folded down. The MIOCT can display whether the graft folded toward the host or the anterior chamber. (d) Images of addressing the folded area by a scalpel. MIOCT image facilitates the manoeuvre of using the scalpel from the epithelial side. (e) MIOCT images of a DMEK graft, which never opened using any manoeuvre. The graft was curled strongly. MIOCT showed cloudiness inside the curled DMEK grafts, suggestive of viscous liquid which “glued” the graft on.

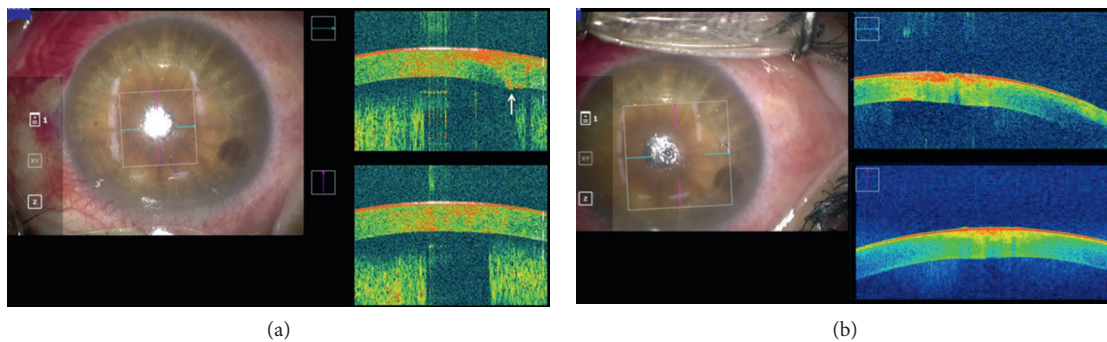


FIGURE 5: Continued.

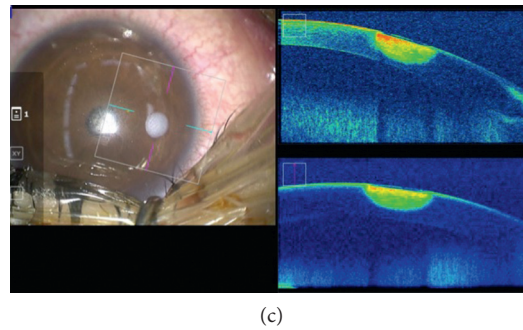


FIGURE 5: MIOCT images in cases of corneal trauma. (a) MIOCT image of a plant thorn piercing the deep cornea. Preoperative examination revealed that the DM near the plant thorn protruded (arrow), which was suggestive of corneal perforation. (b) MIOCT image immediately after removal of the plant thorn. No high-intensity shadow suggestive of residual foreign bodies in the cornea was found. (c) MIOCT image of a partial alkali burn in the cornea. The opacity was found to spread approximately to three-quarters of the corneal depth. If there is a delay between outpatient clinic examination and emergency surgery, the depth of the cornea opacity can be checked again to determine if the effect of alkali has progressed since the initial examination.

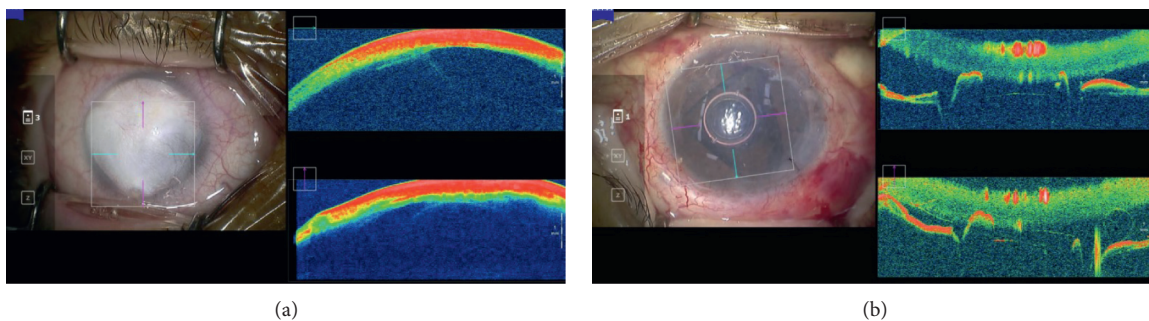


FIGURE 6: Limitations of MIOCT for corneal surgery. (a) MIOCT image of high-intensity congenital corneal opacity at the beginning of the surgery. Although the iris adhesions to the endothelial side of the cornea can be discerned, further detailed observation is not possible. (b) MIOCT image of DMEK case. An inverted ghost image of the cornea obscures the edge of the DMEK graft.

limitation of OCT that has not overcome since spectral-domain OCT for outpatient clinic use was made available. A small *i*OCT probe that is inserted into the eye has been developed, and its usefulness has been confirmed in animal experiments [65, 66]. It is hoped that in the future, this device will be able to be used like an intraocular endoscopes, helping to overcome the aforementioned limitations. In recent years, heads-up surgery has begun to gain popularity. A large MIOCT image displayed on a monitor while operating during heads-up surgery would amplify the benefits of MIOCT [67].

9. Conclusions

In conclusion, despite the aforementioned limitations, MIOCT aids the corneal surgeon in accurate and rapid intraoperative decision-making for all kinds of keratoplasty, thereby reducing operation times and improving postoperative outcomes for each procedure. MIOCT also has educational utility by allowing novice surgeons to be taught corneal suturing techniques and allows them to complete lamellar surgeries successfully. Novel applications of MIOCT have been reported, with more surgeons likely to use it in the future.

Data Availability

Data sharing is not applicable to this article as no datasets were generated or analysed in the current study.

Conflicts of Interest

The authors declare that there are no conflicts of interest regarding the publication of this paper.

References

- [1] J. P. Ehlers, "Intraoperative optical coherence tomography: past, present, and future," *Eye*, vol. 30, no. 2, pp. 193–201, 2016.
- [2] A. W. Scott, S. Farsiu, L. B. Enyedi, D. K. Wallace, and C. A. Toth, "Imaging the infant retina with a hand-held spectral-domain optical coherence tomography device," *American Journal of Ophthalmology*, vol. 147, no. 2, pp. 364–373, 2009.
- [3] P. N. Dayani, R. Maldonado, S. Farsiu, and C. A. Toth, "Intraoperative use of handheld spectral domain optical coherence tomography imaging in macular surgery," *Retina*, vol. 29, no. 10, pp. 1457–1468, 2009.
- [4] M. Ecsedy, A. Szamosi, C. Karko' et al., "A comparison of macular structure imaged by optical coherence tomography in

- preterm and full-term children,” *Investigative Ophthalmology & Visual Science*, vol. 48, no. 11, pp. 5207–5211, 2007.
- [5] R. Ray, D. E. Barañano, J. A. Fortun et al., “Intraoperative microscope-mounted spectral domain optical coherence tomography for evaluation of retinal anatomy during macular surgery,” *Ophthalmology*, vol. 118, no. 11, pp. 2212–2217, 2011.
- [6] J. P. Ehlers, M. P. Ohr, P. K. Kaiser, and S. K. Srivastava, “Novel microarchitectural dynamics in rhegmatogenous retinal detachments identified with intraoperative optical coherence tomography,” *Retina*, vol. 33, no. 7, pp. 1428–1434, 2013.
- [7] J. P. Ehlers, W. J. Dupps, P. K. Kaiser et al., “The prospective intraoperative and perioperative ophthalmic imaging with optical coherence tomography (pioneer) study: 2-year results,” *American Journal of Ophthalmology*, vol. 158, no. 5, pp. 999–1007, 2014.
- [8] Y. K. Tao, J. P. Ehlers, C. A. Toth, and J. A. Izatt, “Intraoperative spectral domain optical coherence tomography for vitreoretinal surgery,” *Optics Letters*, vol. 35, no. 20, pp. 3315–3317, 2010.
- [9] J. P. Ehlers, J. Goshe, W. J. Dupps et al., “Determination of feasibility and utility of microscope-integrated optical coherence tomography during ophthalmic surgery,” *JAMA Ophthalmology*, vol. 133, no. 10, pp. 1124–1132, 2015.
- [10] M. Khan and J. P. Ehlers, “Clinical utility of intraoperative optical coherence tomography,” *Current Opinion in Ophthalmology*, vol. 27, no. 3, pp. 201–209, 2016.
- [11] G. Geerling, M. Müller, C. Winter, H. Hoerauf, S. Oelckers, and H. Laqua, “Intraoperative 2-dimensional optical coherence tomography as a new tool for anterior segment surgery,” *Archives of Ophthalmology*, vol. 123, no. 2, pp. 253–257, 2005.
- [12] J. P. Ehlers, D. Xu, P. K. Kaiser, R. P. Singh, and S. K. Srivastava, “Intrasurgical dynamics of macular hole surgery,” *Retina*, vol. 34, no. 2, pp. 213–221, 2014.
- [13] P. Yee, D. D. Sevgi, J. Abraham, S. K. Srivastava, T. Le, and A. Uchida, “iOCT-assisted macular hole surgery: outcomes and utility from the DISCOVER study,” *British Journal of Ophthalmology*, pp. 1–7, 2020.
- [14] E. Bruyère, E. Philippakis, B. Dupas, P. Nguyen-Kim, R. Tadayoni, and A. Couturier, “Benefit of intraoperative optical coherence tomography for vitreomacular surgery in highly myopic eyes,” *Retina*, vol. 38, no. 10, pp. 2035–2044, 2018.
- [15] C. I. Falkner-Radler, C. Glittenberg, M. Gabriel, and S. Binder, “Intrasurgical microscope-integrated spectral domain optical coherence tomography-assisted membrane peeling,” *Retina*, vol. 35, no. 10, pp. 2100–2106, 2015.
- [16] J. P. Ehlers, M. Khan, D. Petkovsek et al., “Outcomes of intraoperative OCT-assisted epiretinal membrane surgery from the PIONEER study,” *Ophthalmology Retina*, vol. 2, no. 4, pp. 263–267, 2018.
- [17] L. M. Lytvynchuk, C. G. Glittenberg, S. Ansari-Shahrezaei, and S. Binder, “Intraoperative optical coherence tomography assisted analysis of pars plana vitrectomy for retinal detachment in morning glory syndrome: a case report,” *BMC Ophthalmology*, vol. 17, no. 1, p. 134, 2017.
- [18] J. R. Abraham, S. K. Srivastava, J. L. Reese, and J. P. Ehlers, “Intraoperative OCT features and postoperative ellipsoid mapping in primary macula-involving retinal detachments from the PIONEER study,” *Ophthalmology Retina*, vol. 3, no. 3, pp. 252–257, 2019.
- [19] J. R. Abraham, S. K. Srivastava, T. K. Le et al., “Intraoperative OCT-assisted retinal detachment repair in the DISCOVER study: impact and outcomes,” *Ophthalmology Retina*, vol. 4, no. 4, pp. 378–383, 2020.
- [20] J. P. Ehlers, T. Tam, P. K. Kaiser, D. F. Martin, G. M. Smith, and S. K. Srivastava, “Utility of intraoperative optical coherence tomography during vitrectomy surgery for vitreomacular traction syndrome,” *Retina*, vol. 34, no. 7, pp. 1341–1346, 2014.
- [21] A. Kumar, R. Ravani, A. Mehta, S. Simakurthy, and C. Dhull, “Outcomes of microscope-integrated intraoperative optical coherence tomography-guided center-sparing internal limiting membrane peeling for myopic traction maculopathy: a novel technique,” *International Ophthalmology*, vol. 38, no. 4, pp. 1689–1696, 2015.
- [22] J. P. Ehlers, K. Kernstine, S. Farsiu, N. Sarin, R. Maldonado, and C. A. Toth, “Analysis of pars plana vitrectomy for optic pit-related maculopathy with intraoperative optical coherence tomography,” *Archives of Ophthalmology*, vol. 129, no. 11, pp. 1483–1486, 2011.
- [23] S. H. Chavala, S. Farsiu, R. Maldonado, D. K. Wallace, S. F. Freedman, and C. A. Toth, “Insights into advanced retinopathy of pre-maturity using handheld spectral domain optical coherence tomography imaging,” *Ophthalmology*, vol. 116, no. 12, pp. 2448–2456, 2005.
- [24] J. P. Ehlers, J. F. Griffith, and S. K. Srivastava, “Intraoperative optical coherence tomography during vitreoretinal surgery for dense vitreous hemorrhage in the pioneer study,” *Retina*, vol. 35, no. 12, pp. 2537–2542, 2015.
- [25] A. Pujari, P. Sharma, S. Phuljhele et al., “Intraoperative optical coherence tomography-guided scleral suture passage while performing surgery on extraocular muscles,” *Indian Journal of Ophthalmology*, vol. 66, no. 11, pp. 1654–1655, 2018.
- [26] J. Tao, H. Wu, Y. Chen et al., “Use of iOCT in vitreoretinal surgery for dense vitreous hemorrhage in a Chinese population,” *Current Eye Research*, vol. 44, no. 2, pp. 219–224, 2019.
- [27] S. Yaginuma, M. Inoue, Y. Itoh, H. Takahashi, and A. Hirakata, “Utility of intraoperative optical coherence tomography in acute endophthalmitis,” *Retinal Cases & Brief Reports*, vol. 14, no. 1, pp. 27–30, 2020.
- [28] L. M. Heindl, S. Siebelmann, T. Dietlein et al., “Future prospects: assessment of intraoperative optical coherence tomography in Ab Interno Glaucoma surgery,” *Current Eye Research*, vol. 40, no. 12, pp. 1288–1291, 2015.
- [29] S. Siebelmann, C. Cursiefen, A. Lappas, and T. Dietlein, “Intraoperative optical coherence tomography enables non-contact imaging during canaloplasty,” *Journal of Glaucoma*, vol. 25, no. 2, pp. 236–238, 2016.
- [30] B. Junker, J. Jordan, C. Framme, and A. Pielen, “Intraoperative optical coherence tomography and ab interno trabecular meshwork surgery with the Trabectome,” *Clinical Ophthalmology*, vol. 11, pp. 1755–1760, 2017.
- [31] R. S. Kumar, M. U. Jariwala, J. P. Venugopal, N. K. Puttaiah, and R. Balu, “A pilot study on feasibility and effectiveness of intraoperative spectral-domain optical coherence tomography in glaucoma surgery,” *Transactional Vision Science and Technology*, vol. 4, no. 2, p. 2, 2014.
- [32] N. Sharma, N. Aron, P. Kakkar, and J. S. Titiyal, “Continuous intraoperative OCT guided management of post-deep anterior lamellar keratoplasty descemet’s membrane detachment,” *Saudi Journal of Ophthalmology*, vol. 30, no. 2, pp. 133–136, 2016.
- [33] P. Bhullar, O. M. Carrasco-Zevallos, A. Dandridge et al., “Intraocular pressure and big bubble diameter in deep anterior lamella keratoplasty: an ex-vivo microscope-integrated

- OCT with heads-up display," *Asia-Pacific Journal of Ophthalmology (Philadelphia, Pa.)*, vol. 6, no. 5, pp. 412–417, 2017.
- [34] L. De Benito-Llopis, J. S. Mehta, R. I. Angunawela, M. Ang, and D. T. Tan, "Intraoperative anterior segment optical coherence tomography: a novel assessment tool during deep anterior lamellar keratoplasty," *American Journal of Ophthalmology*, vol. 157, no. 2, pp. 334–341, 2017.
- [35] P. Steven, C. Le Blanc, E. Lankenau et al., "Optimising deep anterior lamellar keratoplasty (DALK) using intraoperative online optical coherence tomography (iOCT)," *British Journal of Ophthalmology*, vol. 98, no. 7, pp. 900–904, 2017.
- [36] V. Scorcio, M. Busin, A. Lucisano, J. Beltz, A. Carta, and G. Scorcio, "Anterior segment optical coherence tomography-guided big-bubble technique," *Ophthalmology*, vol. 120, no. 3, pp. 471–476, 2013.
- [37] J. Au, J. Goshe, W. J. Dupps, S. K. Srivastava, and J. P. Ehlers, "Intraoperative optical coherence tomography for enhanced depth visualization in deep anterior lamellar keratoplasty from the PIONEER study," *Cornea*, vol. 34, no. 9, pp. 1039–1043, 2015.
- [38] M. H. Chaniyara, R. Bafna, J. Urkude, and N. Sharma, "Rescuing the host Descemet's membrane in full-thickness traumatic wound dehiscence in deep anterior lamellar keratoplasty: intraoperative optical coherence tomography (iOCT)-guided technique," *BMJ Case Reports*, vol. 2017, pp. 1–3, 2017.
- [39] H. Eguchi, S. Kusaka, E. Arimura-Koike et al., "Intraoperative optical coherence tomography (RESCAN 700) for detecting iris incarceration and iridocorneal adhesion during keratoplasty," *International Ophthalmology*, vol. 37, no. 3, pp. 761–765, 2017.
- [40] J. Titiyal, M. Kaur, and R. Falera, "Intraoperative optical coherence tomography in anterior segment surgeries," *Indian Journal of Ophthalmology*, vol. 65, no. 2, pp. 116–121, 2017.
- [41] J. P. Ehlers, S. K. Srivastava, D. Feiler, A. I. Noonan, A. M. Rollins, and Y. K. Tao, "Integrative advances for OCT-guided ophthalmic surgery and intraoperative OCT: microscope integration, surgical instrumentation, and heads-up display surgeon feedback," *PLoS One*, vol. 20, no. 9, Article ID e105224, 2014.
- [42] P. B. Knecht, C. Kaufmann, M. N. Menke, S. L. Watson, and M. M. Bosch, "Use of intraoperative fourier-domain anterior segment optical coherence tomography during Descemet stripping endothelial keratoplasty," *American Journal of Ophthalmology*, vol. 150, no. 3, pp. 360–365, 2010.
- [43] V. V. Juthani, J. M. Goshe, S. K. Srivastava, and J. P. Ehlers, "Association between transient interface fluid on intraoperative OCT and textural interface opacity after DSAEK surgery in the PIONEER study," *Cornea*, vol. 33, no. 9, pp. 887–892, 2014.
- [44] E. Wylegala, A. K. Nowinska, E. Wroblewska-Czajka, and D. Janiszewska, "Donor disc attachment assessment with intraoperative spectral optical coherence tomography during descemet stripping automated endothelial keratoplasty," *Indian Journal of Ophthalmology*, vol. 61, no. 9, pp. 511–513, 2013.
- [45] A. Miyakoshi, O. Hironori, M. Otsuka, and A. Hayashi, "Efficacy of intraoperative anterior segment optical coherence tomography during Descemet's stripping automated endothelial keratoplasty," *ISRN Ophthalmology*, vol. 2014, Article ID 562062, 2014.
- [46] K. Hallahan, B. Cost, J. M. Goshe, W. J. Dupps, S. K. Srivastava, and J. P. Ehlers, "Intraoperative interface fluid dynamics and clinical outcomes for intraoperative optical coherence tomography-assisted Descemet stripping automated endothelial keratoplasty from the PIONEER study," *American Journal of Ophthalmology*, vol. 173, no. 1, pp. 16–22, 2014.
- [47] J. G. Steverink and R. P. L. Wisse, "Intraoperative optical coherence tomography in descemet stripping automated endothelial keratoplasty: pilot experiences," *International Ophthalmology*, vol. 37, no. 4, pp. 939–944, 2017.
- [48] T. Ide, J. Wang, A. Tao et al., "Intraoperative use of three-dimensional spectral-domain optical coherence tomography," *Ophthalmic Surgery, Lasers, and Imaging*, vol. 41, no. 2, pp. 250–254, 2010.
- [49] T. A. Shazly, L. K. To, I. P. Conner, and L. Espandar, "Intraoperative optical coherence tomography-assisted descemet stripping automated endothelial keratoplasty for anterior chamber fibrous ingrowth," *Cornea*, vol. 36, no. 6, pp. 757–759, 2017.
- [50] N. D. Pasricha, C. Shieh, O. M. Carrasco-Zevallos et al., "Real-time microscope-integrated OCT to improve visualization in DSAEK for advanced bullous keratopathy," *Cornea*, vol. 34, no. 12, pp. 1606–1610, 2015.
- [51] S. J. Lang, S. Heinzelmann, D. Böhringer, T. Reinhard, and P. Maier, "Indications for intraoperative anterior segment optical coherence tomography in corneal surgery," *International Ophthalmology*, 2020.
- [52] A. Saad, E. Guilbert, A. Grise-Dulac, P. Sabatier, and D. Gatinel, "Intraoperative OCT-assisted DMEK," *Cornea*, vol. 34, no. 7, pp. 802–807, 2015.
- [53] B. Cost, J. M. Goshe, S. Srivastava, and J. P. Ehlers, "Intraoperative optical coherence tomography-assisted descemet membrane endothelial keratoplasty in the DISCOVER study," *American Journal of Ophthalmology*, vol. 160, no. 3, pp. 430–437, 2015.
- [54] A. S. Patel, J. M. Goshe, S. K. Srivastava, and J. P. Ehlers, "Intraoperative optical coherence tomography-assisted descemet membrane endothelial keratoplasty in the DISCOVER study: first 100 cases," *American Journal of Ophthalmology*, vol. 210, pp. 167–173, 2020.
- [55] P. Steven, C. Le Blanc, K. Velten et al., "Optimizing descemet membrane endothelial keratoplasty using intraoperative optical coherence tomography," *JAMA Ophthalmology*, vol. 131, no. 9, pp. 1135–1142, 2013.
- [56] O. Muftuoglu, P. Toro, R. N. Hogan et al., "Sarnicola air-visco bubble technique in deep anterior lamellar keratoplasty," *Cornea*, vol. 32, no. 4, pp. 527–532, 2013.
- [57] S. Siebelmann, A. Händel, M. Matthaei, B. Bachmann, and C. Cursiefen, "Microscope-integrated optical coherence tomography-guided drainage of acute corneal hydrops in keratoconus combined with suturing and gas-aided reattachment of descemet membrane," *Cornea*, vol. 38, no. 8, pp. 1058–1061, 2019.
- [58] C. M. Tong, J. S. Parker, P. W. Dockery, R. S. Birbal, and G. R. J. Melles, "Use of intraoperative anterior segment optical coherence tomography for Bowman layer transplantation," *Acta Ophthalmology*, vol. 97, no. 7, pp. e1031–e1032, 2019.
- [59] E. M. Schmidt, H. C. Stiefel, D. C. Houghton, and W. D. Chamberlain, "Intraoperative optical coherence tomography to guide corneal biopsy," *Cornea*, vol. 38, no. 5, pp. 639–641, 2019.
- [60] C. Mazzotta and S. Caragiuli, "Intraoperative corneal thickness measurement by optical coherence tomography in keratoconic patients undergoing corneal collagen cross-linking," *American Journal of Ophthalmology*, vol. 157, no. 6, pp. 1156–1162, 2014.

- [61] R. Ghaffari, M. Mortazavi, P Anvari et al., "Intraoperative optical coherence tomography to evaluate the effect of the eyelid speculum on corneal pachymetry during accelerated corneal cross-linking (9mW/cm²)," *Eye (London)*, vol. 32, no. 2, pp. 579–585, 2018.
- [62] N. Pahuja, R. Shetty, C. Jayadev, R. Nuijts, B. Hedge, and V. Arora, "Intraoperative optical coherence tomography using the RESCAN 700: preliminary results in collagen cross-linking," *Biomed Research International*, vol. 2015, Article ID 572698, 2015.
- [63] A. Kobayashi, H. Yokogawa, N. Mori, and K. Sugiyama, "Visualization of pre-cut DSAEK and pre-stripped DMEK donor corneas by intraoperative optical coherence tomography using the RESCAN 700," *BMC Ophthalmology*, vol. 16, p. 135, 2016.
- [64] M. M. Farouk, T. Naito, K Shinomiya et al., "Optical coherence tomography reveals new insight into the accommodation mechanism," *Journal of Ophthalmology*, vol. 2015, Article ID 510459, 2015.
- [65] K. M. Joos and J.-H. Shen, "Miniature real-time intraoperative forward-imaging optical coherence tomography probe," *Biomedical Optics Express*, vol. 4, no. 8, pp. 1342–1350, 2013.
- [66] S. Yang, M. Balicki, T. S Wells et al., "Improvement of optical coherence tomography using active handheld micromanipulator in vitreoretinal surgery," *Conference Proceedings: Annual International Conference of the IEEE Engineering in Medicine and Biology Society. IEEE Engineering in Medicine and Biology Society. Annual Conference*, vol. 2013, pp. 5674–5677, 2013.
- [67] Y. K. Tao, S. K. Srivastava, and J. P. Ehlers, "Microscope-integrated intraoperative OCT with electrically tunable focus and heads-up display for imaging of ophthalmic surgical maneuvers," *Biomedical Optics Express*, vol. 5, no. 6, pp. 1877–1885, 2014.

Research Article

Intraoperative Optical Coherence Tomography Analysis of Clear Corneal Incision: Effect of the Lateral Stromal Hydration

Jiri Cendelin,^{1,2} Stepan Rusnak ,^{1,3} and Lenka Hecova^{1,3}

¹Center of Eye Microsurgery Ofta, Pilsen, Czech Republic

²Department of Ophthalmology, 2nd Faculty of Medicine, Charles University in Prague and Motol University Hospital, Prague, Czech Republic

³Department of Ophthalmology, Faculty of Medicine in Pilsen, Charles University in Prague and University Hospital in Pilsen, Prague, Czech Republic

Correspondence should be addressed to Stepan Rusnak; rusnak@fnplzen.cz

Received 1 June 2020; Revised 25 July 2020; Accepted 26 August 2020; Published 8 September 2020

Academic Editor: Karim Mohamed Noriega

Copyright © 2020 Jiri Cendelin et al. This is an open access article distributed under the Creative Commons Attribution License, which permits unrestricted use, distribution, and reproduction in any medium, provided the original work is properly cited.

Aim of the Study. The aim of this prospective study was to analyse the effect of lateral stromal hydration on the morphology of clear corneal incision architecture using the microscope integrated anterior segment OCT. **Methods.** The cohort included 65 clear corneal incisions of 49 patients who underwent cataract surgery. Corneal incisions were recorded using a Leica Proveo 8 microscope with an intraoperative OCT EnFocus™ device continuously during the surgery. Corneal incision morphology before and after lateral stromal hydration was analysed. **Results.** Good adaptation of the corneal incision before hydration was present in 39 cases (60%), in 16 cases (24.6%), the prominence of posterior lip was present, and, in 10 cases (15.4%), the posterior lip tongue was inverted/retracted into the incision. In 38 cases (58.5%), hydration had no effect on the incision architecture; most often, it was primarily a well-adapted corneal incision (46.2%), less often an incision with posterior lip prominence (10.8%), or tongue inversion into the incision (1.6%) prior to hydration. Hydration worsened the incision architecture in 14 cases (21.5%); most often, it induced/worsened posterior lip prominence (15.4%), less often posterior lip retraction (1.6%), tongue inversion into the incision (1.6%), gap development in the peripheral part of the corneal incision (1.6%), or incomplete opening of the corneal incision (1.6%). In 13 cases (20%), hydration improved the incision architecture, especially in cases with inverted or retracted posterior lip tongue (12.3%), less often in cases with posterior lip prominence (7.7%). **Conclusion.** Lateral stromal hydration seldom affects the condition of the corneal incision. Still, it can cause both deterioration and improvement of the corneal incision architecture. Intraoperative OCT provides real-time monitoring of corneal incision morphology during hydration procedure.

1. Introduction

Cataract surgery is the most common surgical procedure worldwide, with about 10 million patients undergoing surgery annually [1]. Clear corneal incision (CCI) is currently the most common technique for the construction of an incision in cataract surgery. Stromal hydration of the corneal incision significantly increases incision tightness and reduces postoperative suction of fluid from the eye surface into the anterior chamber [2]. Various techniques of corneal incision closure by hydration have been described [3–6]. Lateral hydration has been performed since the early 1990s [7] and is the most commonly used technique of corneal

incision hydration. The technique of lateral stromal hydration consists of gentle irrigation of the balanced salt solution (BSS) into the lateral walls of the incision with visible whitening of the corneal stroma.

For checking the corneal incision tightness after its hydration, the surgeons normally rely on visual examination using an operating microscope and palpation. However, they have no control over whether the stromal hydration has caused distortion of the corneal incision. The visualization of the central orifice of the incision may also be insufficient [8].

Corneal incisions can be easily visualized using anterior segment optical coherence tomography (AS-OCT), used mainly in postoperative period to observe hydration

decrease, incision tightness, and presence of complications (e.g., Descemet's membrane detachment, central orifice gaping, and tufted tongue of posterior lip). An intraoperative AS-OCT monitoring of corneal incision during cataract surgery is used rarely; some authors appreciate the possibility of evaluating the morphological features of the corneal incision, such as the length, width, and angle of the incision, respectively, the presence of epithelial disruption, wound gaping, endothelial condition, and Descemet's membrane condition [9–12].

The aim of this prospective study was to assess the effect of lateral stromal hydration on the incision architecture with the help of microscope integrated intraoperative AS-OCT.

2. Methods

The group included 65 clear corneal incisions of consecutive cataract surgeries of 49 patients (Table 1). The group consisted of 34 women (69.4%) and 15 men (30.6%); the mean age of the patients was 71.2 years (median 73.0 years). No other ocular diseases were diagnosed in the cohort.

At the beginning of the procedure, under the topical local anesthesia, 2.6 mm or 2.5 mm perlimbal clear corneal incisions were performed just in front of the capillary line. Corneal incisions were performed with a disposable bevel-up knife (BVI Beaver Xstar Safety Slit Bevel-Up Knife, 2.6 mm or 2.5 mm) with a depth indicator with the reference line 2 mm from the tip. After immersion of the 2 mm knife-tip into the cornea, the knife pointed into the anterior chamber (Figure 1). For the purpose of this study short, long or irregular incisions were excluded.

Patients from the cohort underwent uncomplicated standard cataract surgery (PROVEO Leica Microsystems microscope, Stellaris® ELITE™ Bausch & Lomb microsurgical system); all operations were performed by one surgeon. Preoperatively, all patients signed standard informed consent for cataract surgery. The study was performed in accordance with the Declaration of Helsinki for Human Research.

Corneal incisions were closed by the method of lateral stromal hydration with a curved cannula with BSS. When checking the wound tightness, the wound area was dried and the intraocular pressure was temporarily increased (by irrigating of BSS into the anterior chamber); in cases of ambiguity, a Seidel test was performed with a sterile fluorescein strip. Corneal incisions were recorded using a Leica Proveo 8 microscope with an intraoperative OCT EnFocus™ device (Biotigen Inc., Leica Microsystems Company, NC) continuously during the surgery. For the purpose of this study, an Ultra-Deep OCT unit was used with a display of up to 11 mm in depth and a resolution degree of ≤ 9 micrometres. Corneal incisions were continuously monitored with AS-OCT during the surgery. Images covering the entire area of the incision just before and after hydration were selected from the records and evaluated. Longitudinal scans were evaluated before and after hydration at the site of the worst adaptation of the incision.

As well-adapted incision, the cases with the attached ceiling and floor in the entire extent of the incision were considered (Figure 2(a)). The cases with eversion or

TABLE 1: Patients group characteristics.

Group of patients	49 patients	65 corneal incisions
Gender	Women 34 (69.4%)	Men 15 (30.6%)
Age	Mean 71.2 years	Median 73.0 years

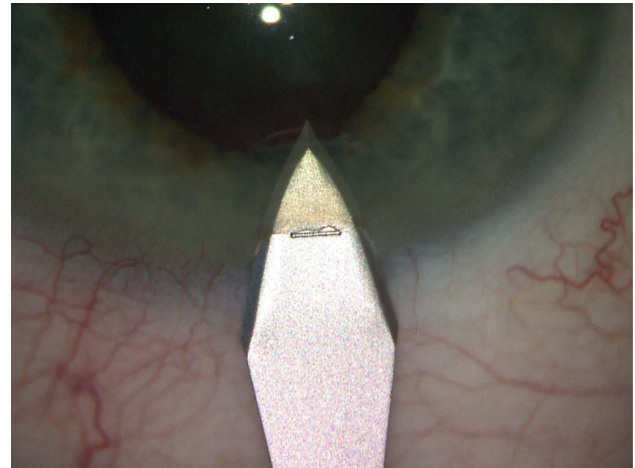


FIGURE 1: Bevel-up knife with a depth indicator with the reference line 2 mm from the tip.

detachment of the central part of the lower lobe towards the anterior chamber were described as an incision with prominence of the posterior lip (Figure 3(a)). Incisions with tongue inversion (Figure 3(c)) were cases with inversion of the central part of the posterior lip towards the wound. Finally, tongue retraction (Figure 4) was described in cases where there was an apparent shortening of the lower lobe with exposure of the central part of the incision ceiling towards the anterior chamber.

The study dealt only with the possibility of the actual influence of lateral stromal hydration on corneal incision morphology. In cases of the incision deformation or leakage after hydration, the incision shape was adjusted or additional hydration was performed.

3. Results

The results are summarized in Table 2.

3.1. Condition of Corneal Incision before Hydration. Good adaptation of the corneal incision (i.e., well-adapted posterior lip without signs of retraction or prominence, good tightness of the incision) was observed in 39 cases (60%), in 16 cases (24.6%), different prominence of the posterior lip was observed, and, in 10 cases (15.4%), tongue inversion into the incision or tongue retraction was observed.

3.2. Influence of Lateral Hydration on Architecture of Corneal Incision. In 38 cases (58.5%), lateral stromal hydration had no effect on the corneal incision architecture; 30 of them

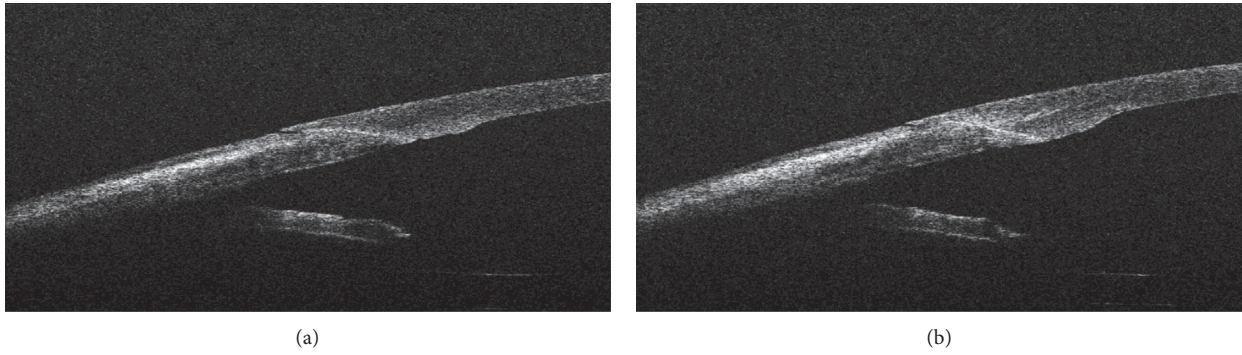


FIGURE 2: Well-adapted corneal incision before hydration (a); lateral stromal hydration had no effect on corneal incision architecture (b).

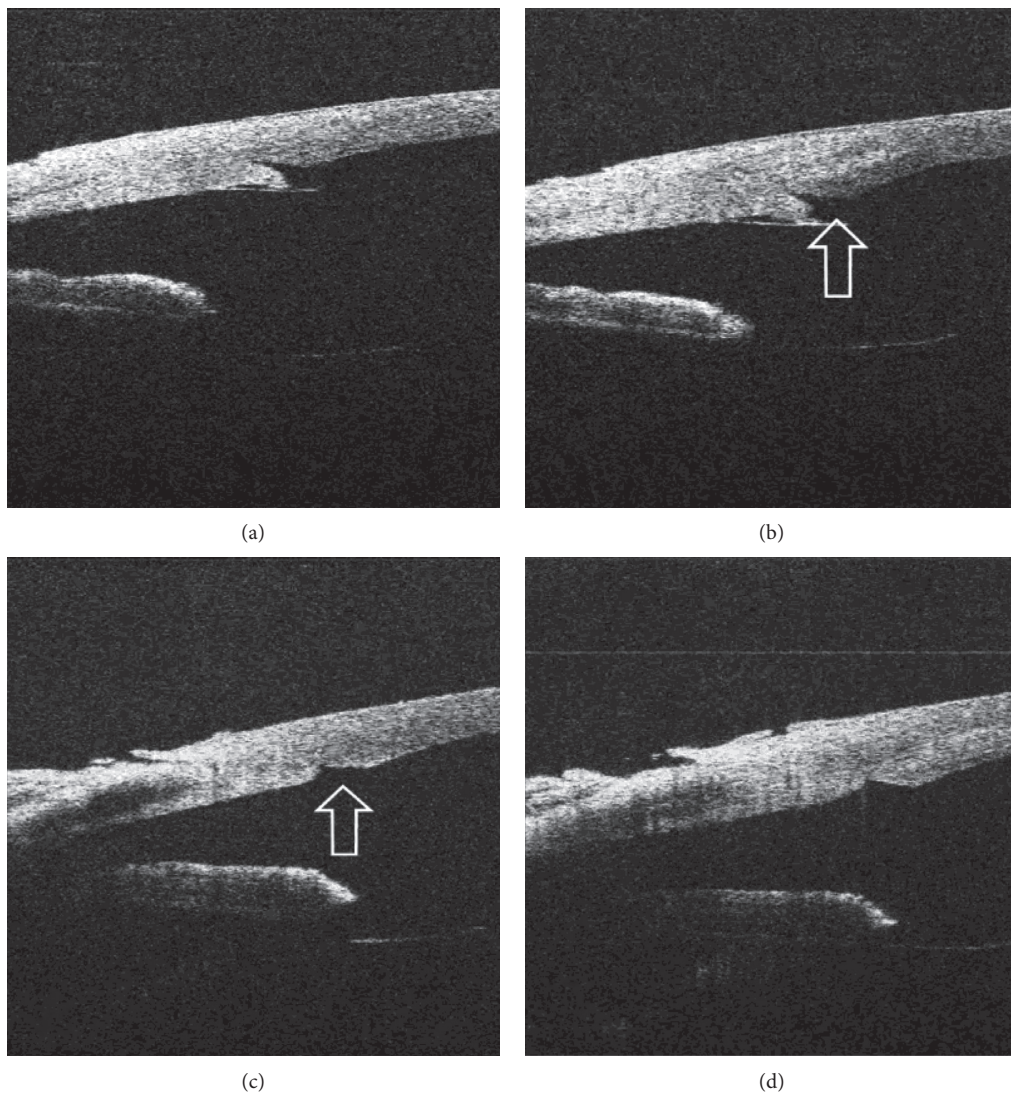


FIGURE 3: Prominence of posterior lip of the corneal incision before (a) and after (b) hydration, tongue inversion into the incision before (c) and after (d) hydration. In both cases, lateral stromal hydration had no significant effect on corneal incision architecture. The arrow shows the exposed central part of the incision ceiling; this may explain the gap of the incision orifice visible with a operating microscope (see Figure 3(b) corresponds with 5(a), respectively, and 3(c) with 5(b)).

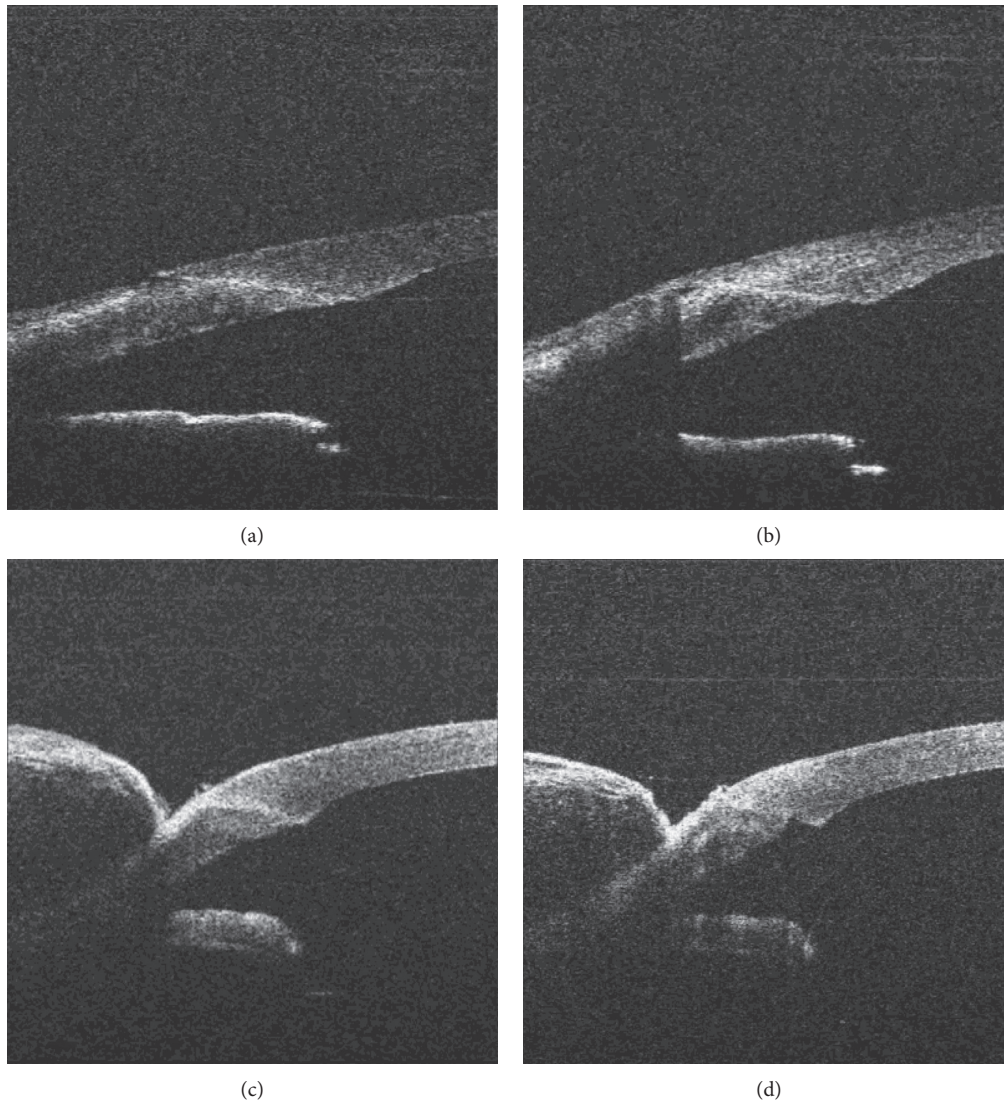


FIGURE 4: Worsening of corneal incision morphology after its hydration. Well-adapted corneal incision before hydration (a), anterior lip prominence centrally from the inner orifice developed after lateral stromal hydration (b). Tongue inversion into the incision before (c) and after (d) lateral stromal hydration.

TABLE 2: Condition of corneal incision before and after hydration.

	Before hydration	>	Well-adapted	Posterior lip prominence	After hydration			
					Tongue inversion/retraction	Anterior lip prominence	Gap development	Incision opening
Well-adapted	39 (60%)	>	30 (46.2%)	6 cases (9.6%)	1 (1.6%)	0	1 (1.6%)	1 (1.6%)
Posterior lip prominence	16 (24.6%)	>	5 (8%)	10 (16%)	0	1 (1.6%)	0	0
Tongue inversion/retraction	10 (15.4%)	>	8 (12.8%)	0	2 (3, 2%)	0	0	0

(46.2%) were primarily well-adapted corneal incisions (Figure 2); in 7 cases (10.8%), prominence of posterior (internal) lip and, in one case, (1.6%) tongue inversion into the incision prior to hydration had been presented (Figures 3 and 5).

In 14 cases (21.5%), lateral stromal hydration worsened the condition of the corneal incision. In 10 cases (15.4%), it was the development of posterior lip prominence (of which 4 were slightly present before the incision hydration but lateral hydration worsened the condition of the posterior lip)

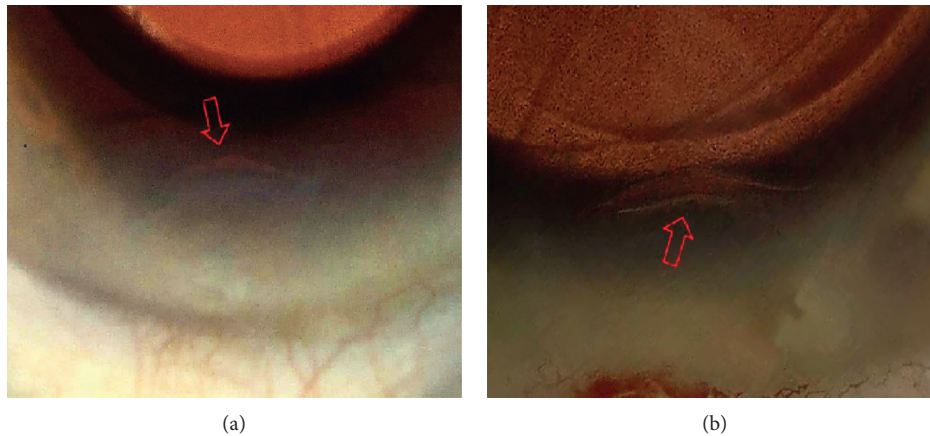


FIGURE 5: Photos of corneal incisions: the gap of the incision orifice (exposed central part of the incision ceiling) seen in photo from standard intraoperative video with different OCT findings (see Figure 3).

(Figure 6), in one case (1.6%), hydration led to anterior lip prominence centrally from the inner orifice, in one case (1.6%), hydration worsened the tongue inversion in the incision (Figure 4), in one case (1.6%), a gap developed in the periphery of the corneal incision, and, in one case (1.6%), more than two-thirds of the incision opened longitudinally (Figure 7).

In 13 cases (20%), lateral stromal hydration improved the corneal incision architecture. In 8 cases (12.3%), after hydration, the inverted or retracted tongue of the corneal incision was strengthened and adapted or was slightly protruding; in 5 cases (7.7%), the prominence of the posterior lip decreased after hydration (Figure 8).

Wound leakage after hydration occurred in two cases; in one case of tongue inversion (Figure 4(d)), the leakage stopped after the posterior lip was adjusted manually; in the second case (Figure 7(d)), the leakage was eliminated by increasing of the intraocular pressure for 30 seconds).

4. Discussion

Sutureless clear corneal incision (CCI) is the most common method for incision wound constructing in cataract surgery [1]. However, this type of incision is associated with an increased risk of postoperative endophthalmitis development [13–15]. According to Taban et al. [14], the risk of postoperative endophthalmitis in corneal incision is 0.189%, compared to 0.074% in scleral incision, respectively, 0.062% in limbal incision. Microorganisms have two main ways of how to get into the eye and cause infection, either during the surgery itself or in the early postoperative period before epithelialization of the sutureless corneal incision. Stromal hydration of the corneal incision reduces the risk of postoperative endophthalmitis development, increases incision tightness, and reduces intraocular fluid leakage through the incision to the eye surface, while reducing postoperative suction of fluid from the eye surface into the anterior chamber. Vasavada et al. [2] applied 0.0125% trypan blue to the eye surface with and without hydration of the corneal incision and detected a statistically significantly lower

($p < 0.001$) concentration of trypan blue in the anterior chamber of the hydrated incision group.

There are two main techniques for corneal incision closure by hydration. Conventional lateral stromal hydration consists of gentle irrigation of the balanced salt solution (BSS) into the lateral walls of the incision, followed with a visible whitening of the corneal stroma [7]. Other possibility is the hydration into the supraincisional pocket (the so-called Wong incision), i.e., an additional incision performed in the anterior lip in front of the original corneal incision with a corneal knife to a depth of approximately 160 μm [5]. According to Mifflin et al. [3], hydration in the supraincisional pocket is significantly better than conventional lateral stromal hydration in preventing wound leakage due to direct pressure on the posterior lip of the corneal incision. However, this method may carry an additional risk of epithelial damage development and increased astigmatism [3].

The tightness of a corneal incision after its hydration is normally assessed visually (visible fluid leakage from the wound, corneal stroma whitening after hydration, presence of flaccid posterior lip, etc.) and with palpation eventually with a modified Seidel test [4]. The visualization of the central orifice of the incision can be also insufficient [8]. Calladine and Packard [16] and Behrens et al. [17], respectively, draw attention to the risk of corneal incision leakage after hydration has ceased. The persistence of hydration of the corneal incision is a subject of further discussion [9–11].

Corneal incisions can be easily visualized by AS-OCT; it is especially used in the postoperative period to monitor the loss of hydration [9, 11], tightness of the incision, and the presence of complications. Calladine and Tanner [10] investigated the effect of stromal hydration on corneal incision architecture using an AS-CT; if measured 1 hour after stromal hydration, it significantly increases the length of the corneal incision and it is associated with an increased incidence of local Descemet's membrane detachment compared to incision without hydration. Bang et al. [11] performed corneal incision analysis using OCT 2 hours, 1 day, 1 week, 1 month, and 3 months after surgery and

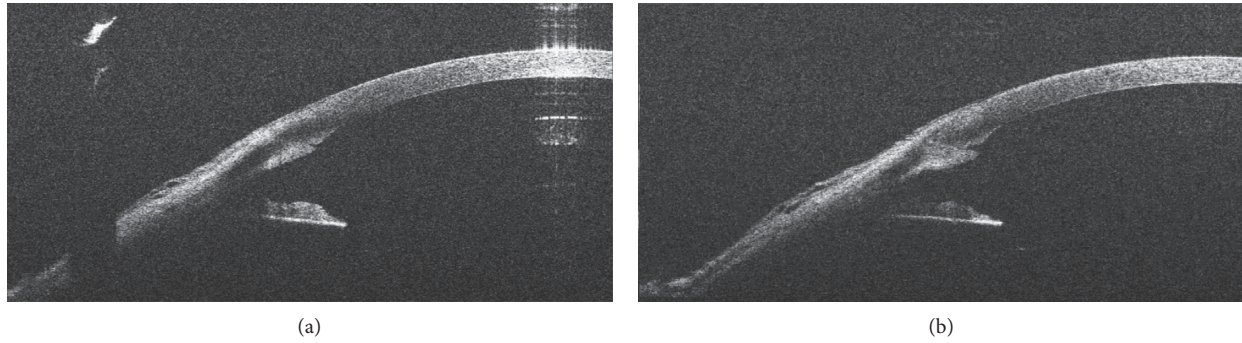


FIGURE 6: Worsening of corneal incision morphology after its hydration. Posterior lip prominence presented before hydration (a) worsened after lateral stromal hydration (b).

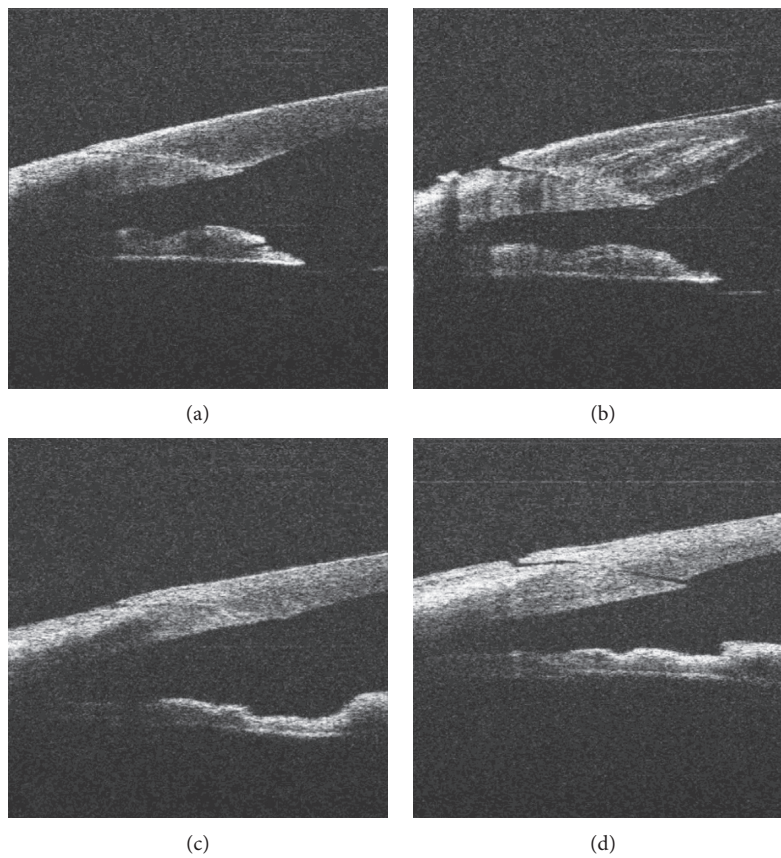


FIGURE 7: Worsening of corneal incision morphology after its hydration. Well-adapted corneal incision before hydration (a); gap development in the corneal incision periphery after lateral stromal hydration (b). Well-adapted corneal incision before hydration (c); corneal incision almost opened longitudinally after lateral stromal hydration (d).

compared the effect of lateral stromal hydration on the incision architecture. In addition to corneal thickness, incision length (2.2 mm and 2.8 mm, resp.), and angle, he observed the presence of epithelial or endothelial wound gaping and local Descemet's membrane detachment. According to the results of this study, smaller corneal incisions (2.2 mm) are more vulnerable to external influences (e.g., stromal hydration) and less stable than larger incisions.

Several authors are interested in the use of intraoperative anterior segmental OCT in anterior segment surgery. In

2018, Ehlers et al. [18] published the 3-year results of the DISCOVER study, which focuses on the feasibility and benefits of microscope integrated OCT during various ophthalmological surgeries. Intraoperative OCT appears to be a useful aid for anterior segment surgery, especially in positioning of DSAK, DMEK, and intracorneal inlays. In 43.4% of anterior segment operations, the surgeons concluded that the current information that they had continually acquired during surgery had an impact on their surgical decisions and altered the surgical procedure. Tital

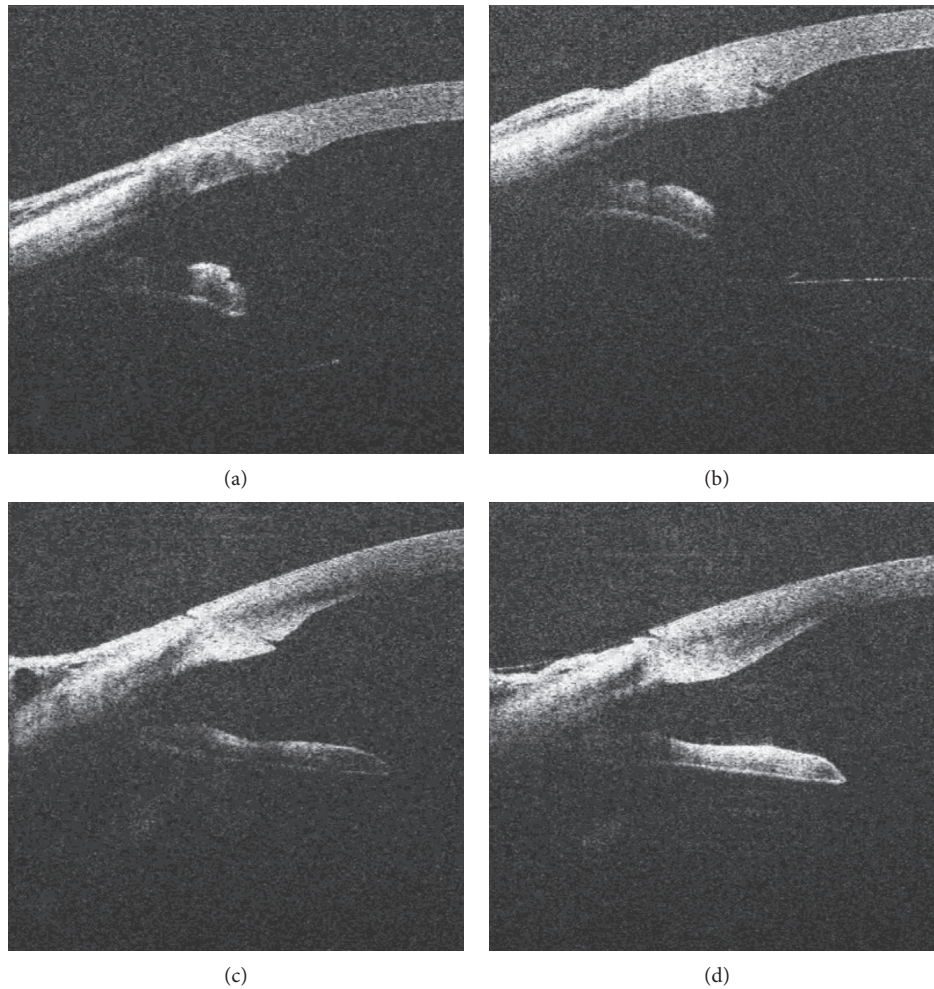


FIGURE 8: Improvement of corneal incision morphology after its hydration. Inverted tongue of the corneal incision before hydration (a) and after lateral stromal hydration inverted tongue strengthened up and slight prominence of posterior lip appeared (b). Prominence of the posterior lip (c); decrease after lateral stromal hydration (d).

et al. [19] studied morphology of the inner orifice of the corneal incision using an intraoperative AS-OCT and conducted an irregular incision to be a predisposition for local Descemet's membrane detachment. The highest incidence of local Descemet's membrane detachment was observed during final stromal hydration of the incision. Almutlak et al. [20] presented the use of microscope integrated AS-OCT; the authors were able to follow the corneal wound architecture, its development during the procedure, and the condition of the Descemet's membrane. Das et al. [21] used intraoperative AS-OCT in both microincision and femtosecond laser assisted cataract surgery. Using AS-OCT, the surgeon could actually evaluate the morphological features of the corneal incision, such as the length, width, and angle of the incision, respectively, the presence of epithelial disruption, wound gaping, endothelial condition, and Descemet's membrane condition. The authors also marginally mention the possibility of the intraoperative monitoring (using AS-OCT) of stromal hydration efficacy and adequacy. However, they do not deal with the effect of hydration on the corneal wound morphology in detail.

In our cohort, corneal incisions were continuously monitored using intraoperative AS-OCT. The aim of our work was to evaluate the morphology of the incision before and after hydration. According to the results of our study, lateral hydration least affects primarily well-adapted corneal incisions. Even in the cases of primarily well-adapted incisions, the effect of the lateral hydration may not be ideal and hydration may lead to posterior lip prominence, less often to anterior lip prominence centrally from the inner orifice, tongue inversion into the incision, gap development in the corneal incision periphery, or even to its incomplete opening. In cases of tongue inversion into the corneal wound, lateral stromal hydration may cause worsening of the inversion. In cases of prominence of the posterior lip, lateral hydration does not alter, worsen, or normalize the wound morphology approximately equally.

The primary condition of the incision before the hydration seems to be the most important factor. Distortion of the incision can be caused by different straining, deformations, and self-hydration during the surgery. With an

unarmed microscope without AS-OCT, the surgeon may have limited the possibility of assessing the actual condition of the incision.

Lateral hydration may improve or worsen the corneal incision morphology at the end of the surgery, which may be the cause of clinically apparent failure, i.e., persistence or new leakage of the corneal incision after its hydration.

Our study demonstrates the value of microscope integrated intraoperative OCT in perioperative evaluation of corneal incisions. The possibility of detecting tongue inversion into the incision, which may not be noticeable due to the clouding after corneal incision hydration and may lead to incision incompetence, seems to be the most useful [8]. Intraoperative OCT provides an excellent opportunity to monitor the corneal incision morphology in real time and allows the surgical procedure in the hydration phase to be modified dynamically and purposefully to achieve the best tightness and architecture of the corneal wound.

Data Availability

The data used to support the findings of this study are included within the article.

Conflicts of Interest

The authors declare no conflicts of interest.

References

- [1] A. Foster, "Vision 2020: the cataract challenge," *Community Eye Health*, vol. 13, no. 32, pp. 17–19, 2000.
- [2] A. R. Vasavada, M. R. Praveen, D. Pandita et al., "Effect of stromal hydration of clear corneal incisions: quantifying ingress of trypan blue into the anterior chamber after phacoemulsification," *Journal of Cataract & Refractive Surgery*, vol. 33, no. 4, pp. 623–627, 2007.
- [3] M. D. Mifflin, K. Kinard, and M. C. Neuffer, "Comparison of stromal hydration techniques for clear corneal cataract incisions: conventional hydration versus anterior stromal pocket hydration," *Journal of Cataract & Refractive Surgery*, vol. 38, no. 6, pp. 933–937, 2012.
- [4] C. Matossian, S. Makari, and R. Potvin, "Cataract surgery and methods of wound closure: a review," *Clinical Ophthalmology (Auckland, N.Z.)*, vol. 9, pp. 921–928, 2015.
- [5] M. Wong, "Securing clear corneal incisions," *Cataract & Refractive Surgery Today*, vol. 3, pp. 25–27, 2003.
- [6] G. Nithyanandarajah, Y. Athanasiadis, P. Scollo, B. Sharma, A. Dorgham, and A. Sharma, "Hydration of the anterior stroma in phacoemulsification cataract surgery," *Journal of Cataract & Refractive Surgery*, vol. 40, no. 5, pp. 702–704, 2014.
- [7] I. H. Fine, "Corneal tunnel incision with a temporal approach," "Corneal tunnel incision with a temporal approach," in *Clear-corneal Cataract Surgery and Topical Anesthesia*, I. H. Fine, R. A. Fichman, and H. B. Grabow, Eds., p. 25, Slack, Thorofare, NJ, USA, 1993.
- [8] D. Y. Tam, M. R. Vagefi, and A. Naseri, "The clear corneal tongue: a mechanism for wound incompetence after phacoemulsification," *American Journal of Ophthalmology*, vol. 143, no. 3, pp. 526–528, 2007.
- [9] S. Fukuda, K. Kawana, Y. Yasuno, and T. Oshika, "Wound architecture of clear corneal incision with or without stromal hydration observed with 3-dimensional optical coherence tomography," *American Journal of Ophthalmology*, vol. 151, no. 3, pp. 413–419, 2011.
- [10] D. Calladine and V. Tanner, "Optical coherence tomography of the effects of stromal hydration on clear corneal incision architecture," *Journal of Cataract & Refractive Surgery*, vol. 35, no. 8, pp. 1367–1371, 2009.
- [11] J.-W. Bang, J.-H. Lee, J.-H. Kim, and D.-H. Lee, "Structural analysis of different incision sizes and stromal hydration in cataract surgery using anterior segment optical coherence tomography," *Korean Journal of Ophthalmology*, vol. 29, no. 1, pp. 23–30, 2015.
- [12] H. I. Fine, R. S. Hoffman, and M. Packer, "Profile of clear corneal cataract incisions demonstrated by ocular coherence tomography," *Journal of Cataract & Refractive Surgery*, vol. 33, no. 1, pp. 94–97, 2007.
- [13] H. Cao, L. Zhang, L. Li, and S. Lo, "Risk factors for acute endophthalmitis following cataract surgery: a systematic review and meta-analysis," *PLoS One*, vol. 8, no. 8, Article ID e71731, 2013.
- [14] M. Taban, A. Behrens, R. L. Newcomb et al., "Acute endophthalmitis following cataract surgery: a systematic review of the literature," *Archives of Ophthalmology*, vol. 123, no. 5, pp. 613–620, 2005.
- [15] G. Wejde, B. Samolov, S. Seregard, G. Koranyi, and P. G. Montan, "Risk factors for endophthalmitis following cataract surgery: a retrospective case-control study," *Journal of Hospital Infection*, vol. 61, no. 3, pp. 251–256, 2005.
- [16] D. Calladine and R. Packard, "Clear corneal incision architecture in the immediate postoperative period evaluated using optical coherence tomography," *Journal of Cataract & Refractive Surgery*, vol. 33, no. 8, pp. 1429–1435, 2007.
- [17] A. Behrens, W. J. Stark, K. A. Pratzler, and P. J. McDonnell, "Dynamics of small-incision clear cornea wounds after phacoemulsification surgery using optical coherence tomography in the early postoperative period," *Journal of Refractive Surgery*, vol. 24, no. 1, pp. 46–49, 2008.
- [18] J. P. Ehlers, Y. S. Modi, P. E. Pecun et al., "The discover study 3-year results: feasibility and usefulness of microscope-integrated intraoperative OCT during ophthalmic surgery," *Ophthalmology*, vol. 125, no. 7, pp. 1014–1027, 2018.
- [19] J. Titiyal, M. Kaur, and R. Falera, "Intraoperative optical coherence tomography in anterior segment surgeries," *Indian Journal of Ophthalmology*, vol. 65, no. 2, pp. 116–121, 2017.
- [20] M. Almutlak, T. Aloniazan, and W. May, "Real-time optical coherence tomography incorporated in the operating microscope during cataract surgery," *Middle East African Journal of Ophthalmology*, vol. 24, no. 3, pp. 156–158, 2017.
- [21] S. Das, M. K. Kummelil, V. Kharbanda et al., "Microscope integrated intraoperative spectral domain optical coherence tomography for cataract surgery: uses and applications," *Current Eye Research*, vol. 41, no. 5, pp. 643–652, 2016.

Research Article

Function and Morphology of the Meibomian Glands Using a LipiView Interferometer in Rotating Shift Medical Staff

Jing Zhang ¹, Zhengzheng Wu,² Liangnan Sun,¹ and Xin-hua Liu ¹

¹Shenzhen Eye Hospital, Shenzhen Key Laboratory of Ophthalmology, Affiliated Shenzhen Eye Hospital of Jinan University, Shenzhen. No. 18, Zetian Road, Futian District, Shenzhen 518040, Guangdong, China

²Department of Ophthalmology, Sichuan Academy of Medical Sciences & Sichuan Provincial People's Hospital, Chengdu 610072, China

Correspondence should be addressed to Xin-hua Liu; xhualiu@sohu.com

Received 28 March 2020; Revised 4 July 2020; Accepted 25 July 2020; Published 17 August 2020

Guest Editor: Yu-Chi Liu

Copyright © 2020 Jing Zhang et al. This is an open access article distributed under the Creative Commons Attribution License, which permits unrestricted use, distribution, and reproduction in any medium, provided the original work is properly cited.

Purpose. To investigate the function and morphology of meibomian glands (MG) in night shift medical staff (MS). **Methods.** Sixty-two eyes of 31 patients in the MS group and 59 eyes of 31 patients in the control group were consecutively enrolled. All participants completed Ocular Surface Disease Index (OSDI) and Standard Patient Dry Eye Evaluation (SPEED) questionnaires for dry eye severity, as well as Schirmer I and tear break-up time (TBUT) tests. LipiView® II Ocular Surface Interferometer was used for lipid layer thickness (LLT), MG dropout, and partial blink (PB) rate tests. MG expression was measured with an MG evaluator. **Results.** The OSDI score in the MS group was 22.39 ± 13.42 , which was significantly higher than that in the control group (9.87 ± 6.64 , $Z = -3.997$, $P = 0.001$). The SPEED score in the MS group was 7.94 ± 3.81 , which was significantly higher than in the control group (3.65 ± 2.11 , $Z = -4.766$, $P = 0.001$). There was no significant difference in Schirmer I test between the MS group and control group ($Z = -1.346$, $P = 0.178$). TBUT in MS group was significantly shorter than that in the control group ($Z = -5.201$, $P = 0.001$). The mean LLT of the MS group was 55.02 ± 21.17 nm significantly thinner than that of the control group 72.76 ± 21.62 nm ($Z = -4.482$, $P = 0.001$). MG loss occurred in 45.16% of affected eyes in the MS group and 16.13% of affected eyes in the control group, and the difference was statistically significant ($\chi^2 = 14.352$, $P = 0.001$). MG yielding liquid secretion and MG yielding secretion score were significantly lower in the MS group than in the control group ($Z = -3.641$, $P = 0.001$; $Z = -3.146$, $P = 0.001$, resp.). There was a negative correlation between mean LLT and SPEED score (Spearman $r = -0.363$, $P = 0.045$). **Conclusions.** Night shift MS had a higher incidence of MGD compared to day workers.

1. Introduction

Dry eye disease (DED) is one of the most common ocular surface diseases [1]. Previous studies have found the prevalence of dry eye to be 6.8% in American adults, 17.9% in Korean elderly, 31.40% in China, and 32% in northern India [2–5]. DED is a multifactorial disease, of which meibomian gland dysfunction (MGD) is one of the main causes [6]. There are several overlapping risk factors between DED and MGD, including female gender, topical medications, contact lens wear, refractive surgery, and demodicosis [7]. Environmental and occupational factors are strongly associated with DED [8]. Occupational conditions of exposure to

conditioning/heating, dust, and cooking fumes) account for more than half of dry eye patients in the hospital's underlying population [8].

Shift work is very common in modern society. About 20% of the working population in industrialized countries needs to rotate night work [9]. In particular, rotating night shifts is a requirement for the majority of medical staff (MS). Previous studies have shown that shift work leads to circadian rhythm disturbances and several cardiovascular risk diseases, such as hypertension, high triglyceride levels, and metabolic syndrome [10].

A major problem faced by shift workers is sleep disturbance, including lack of sleep, difficulty falling asleep, and not feeling refreshed after sleeping [11]. Sleep deprivation

(SD) is considered as one of the risk factors for DED [5]. Sleep duration of ≥ 9 h/d has been found to be a protective factor for dry eye symptoms [12]. Patients with obstructive sleep apnea syndrome (OSAS) have a tendency to develop dry eye [13]. In addition, the prevalence of sleep and mood disorders was higher in patients with DED than in patients with other ocular surface diseases, and the severity of sleep quality was correlated with the grade of DED [14, 15]. Improvement in sleep quality has been shown to be beneficial in DED patients [16]. The purpose of this study was to investigate the ocular surface health of MS who regularly work night shifts and evaluate their dry eye tendency.

2. Subjects and Methods

2.1. Study Design and Patients. Participants were recruited through public advertisements in Sichuan Academy of Medical Sciences and Sichuan Provincial People's Hospital between January 2018 and July 2018. The inclusion criteria for MS group were as follows: the occupation being physicians or nurses, age from 18 to 40 years, with more than half year of night shift work experience (working at nights 12 h for at least three times per month). Inclusion criteria for the control group were as follows: age from 18 to 40 years, daytime workers with regular routines, without night shift rotation, and without sleep disorders. Participants in both groups were excluded for the following reasons: history of ocular trauma; history of ocular surgery; history of regular contact lens wear; active eye diseases (e.g., blepharitis and conjunctivitis); systemic diseases that may affect the ocular surface (e.g., autoimmune diseases, diabetes and thyroid disease, and hyperlipidemia); use of ocular medications within a week, including creams, ointments, or artificial tears; and pregnant or lactating women. All the study procedures were performed in accordance with the principles of the World Medical Association Declaration of Helsinki. Ethical approval was obtained from the Ethics Committee of Sichuan Academy of Medical Sciences and Sichuan Provincial People's Hospital (ethical approval number: 2018210).

2.2. Ocular Surface Parameters Assessments. The Ocular Surface Disease Index (OSDI) and the Standard Patient Dry Eye Evaluation (SPEED) questionnaire were used to evaluate eye discomfort symptoms [17–20]. The OSDI assesses the frequency of ocular discomfort symptoms, changes in vision-related quality of life, and environmental triggers during the week prior to the assessment [18]. OSDI scores are graded from 0 to 12 (no symptoms), 13 to 32 (mild and moderate symptoms), and 33 to 100 (severe symptoms) [18]. The SPEED questionnaire was designed to explore the frequency and severity of ocular symptoms and the timing of their appearance [19]. SPEED scores are graded from 0 to 5 (no symptoms), 6 to 14 (mild and moderate symptoms), and 15 to 28 (severe symptoms) [19, 20].

Tear break-up time (TBUT) was measured using fluorescein sodium test strips (Tianjin Jingming New Technology Development Co., Ltd., China). Subjects were asked

to look upwards and a drop of a saline-moistened fluorescent strip was placed on the lower palpebral conjunctiva and measured after several blinks. The time interval between the last blink and the first black spot (tear film defect) that appeared after the fluorescein was evenly distributed over the cornea was recorded as TBUT (seconds). Record the average of the 3 measured TBUT. BUT less than 10 seconds indicates tear film instability. Schirmer I test was used to measure the secretory function of the main lacrimal gland. In the absence of topical anesthesia, a standard 5 mm \times 35 mm Schirmer strip was placed in the medial and lateral third of the lower fornix with the eye blinking naturally for 5 min. Wet zone length less than 5 mm was considered as inadequate tear secretion.

Lipid layer thickness (LLT), partial blink (PB), and MG morphology were assessed using a LipiView® II Ocular Surface Interferometer (TearScience, Inc. Morrisville, NC, USA). After adjustment to the appropriate sitting position, patients were instructed to fixate on a flashing light source with natural blinking and to acquire the LLT and PB within 20 seconds. Following eversion of the eyelids, lower lid gland imaging was acquired using a LipiView® II. ImageJ software was used to measure total MG area and MG dropout area. The MG loss rate = MG dropout area/total MG area. MG dropout degree was graded according to the following scale (Figure 1): grade 0 (without loss of MG), grade 1 (loss of <33% of the total MG area), grade 2 (loss of MG area between 33% and 67%), and grade 3 (loss of >67% of the entire MG area).

An MG evaluator (TearScience, Inc.) was applied to observe MG liquid secretions. This was performed with a stable pressure of 3 psi for 10 to 15 seconds at 1–2 mm below the lower eyelid margin. A total of 15 glands were observed in three locations (nasal, middle, and temporal) of the lower eyelid, with five glands in each location [21]. The MG secretion quality of each gland was scored from 0 to 3 (3: clear liquid secretion, 2: colored liquid secretion, 1: concentrated, similar to toothpaste). MG yielding liquid secretion (MGYLS), MG yielding clear liquid secretion (MGYCS), and MG yielding secretion score (MGYSS) were recorded from all 15 glands of the lower eyelid. $MGYLS \leq 6$ or $MGYSS \leq 18$ represents a clear oil secretion dysfunction in MG.

Subjects completed the tests in the following order: first, each participant signed informed consent, completed the OSDI and SPEED questionnaires, and provided general information. Second, a LipiView® II Ocular Surface Interferometer measurement was performed to obtain both PB rate and LLT. Third, TBUT and Schirmer I test were performed, and then MG secretion was measured by MG evaluators. Finally, MG morphology images of the lower eyelid were obtained using a LipiView® II Ocular Surface Interferometer. At least 10 min should elapse between each examination. Patients should rest with eyes closed during the examination interval.

2.3. Statistical Analyses. Data analysis was performed using IBM SPSS statistics version 19 statistical software (SPSS Inc., Chicago, IL, USA). BMI was compared between the two

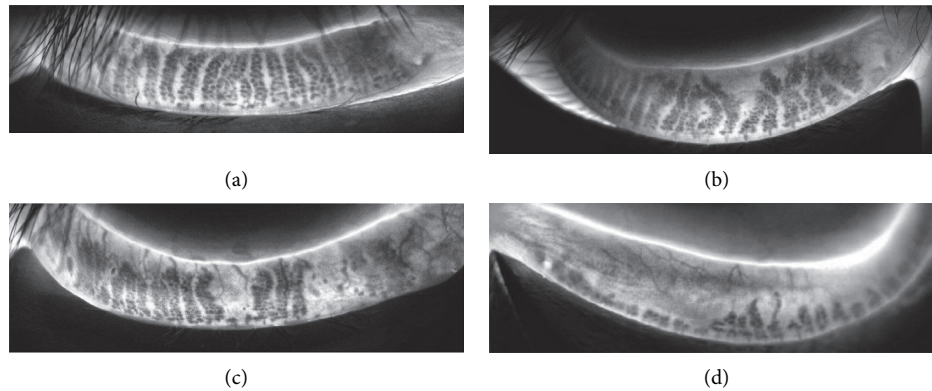


FIGURE 1: LipiView® II images of penetrating infrared light source for different MG dropout degrees. (a) Grade 0 (without loss of MG). (b) Grade 1 (loss of <33% of the total MG area). (c) Grade 2 (loss of MG area between 33% and 67%). (d) Grade 3 (loss of >67% of the entire MG area).

groups using the independent-sample *t*-test. The comparison of age, TBUT, Schirmer I, LLT, PB rate, MGYLS, MGYCS, MGYSS, OSDI score, and SPEED score between the two groups was performed using the Wilcoxon signed-rank test. Comparison of gender and MG dropout between the two groups were performed using the Chi-square test. The correlation among the cumulative days of night work, SPEED score, OSDI score, TBUT, Schirmer I value, mean LLT, and MG loss in MS group was analyzed using the Spearman test. All tests were two-tailed, and *P* values less than 0.05 were considered statistically significant.

3. Results

3.1. Subject Characteristics Comparison. Sixty-two eyes of 31 participants (including 25 physicians and 6 nurses) in the MS group and 59 eyes of 31 participants in the control group were included in this study. The comparison of subject characteristics and various ocular parameters between MS group and the control group is shown in Table 1. Body mass index (BMI) was calculated as weight (kg) divided by height squared (m). There were no significant differences in BMI between MS group and the control group ($t = -0.517$, $P = 0.205$). However, the gender difference between the two groups was statistically significant (Chi-square test, $\chi^2 = 6.458$, $P = 0.011$). The mean age of the MS group was 26.55 ± 3.15 years (range 20 to 36 years), which was slightly higher than 21.91 ± 4.33 years (range 18 to 33 years) of the control group ($Z = -4.106$, $P = 0.001$).

3.2. Dry Eye Parameters comparison. The OSDI questionnaire scores for asymptomatic, mild-to-moderate, and severe symptoms in the MS group and the control group were 16.1% versus 54.8%; 54.8% versus 45.2%; and 25.8% versus 0%, respectively. The OSDI score in the MS group was 22.39 ± 13.42 , which was significantly higher than 9.87 ± 6.64 in the control group ($Z = -3.997$, $P = 0.001$). The SPEED questionnaire scores for asymptomatic (35.5% vs. 83.9%), mild-to-moderate (58.1% vs. 16.1%), and severe (6.5% vs. 0%) symptoms were compared in the MS group and the

TABLE 1: Comparison between medical staff (MS) group and control group.

	MS group	Control group	<i>P</i> value
N/eyes	31/62	31/59	
M:F	10:21	20:11	0.011 ^{&}
Age (y)	26.55 ± 3.15	21.91 ± 4.33	0.001*
BMI	20.92 ± 2.00	21.19 ± 2.72	0.607 [#]
<i>DE parameters</i>			
TBUT(s)	4.63 ± 3.58	7.83 ± 3.33	0.001*
Schirmer I (mm)	19.97 ± 10.17	17.77 ± 6.58	0.178*
SPEED (score)	7.94 ± 3.81	3.65 ± 2.11	0.000*
OSDI (score)	22.39 ± 13.42	9.87 ± 6.64	0.001*
<i>MGD parameters</i>			
Max ICU (nm)	76.03 ± 18.73	90.06 ± 13.91	0.001*
Mean ICU (nm)	55.02 ± 21.17	72.76 ± 21.62	0.001*
Min ICU (nm)	44.58 ± 18.42	58.23 ± 19.28	0.001*
PB rate (%)	63.72 ± 35.81	68.18 ± 35.29	0.534*
MGYLS (score)	5.43 ± 3.98	8.33 ± 4.50	0.001*
MGYCS (score)	4.68 ± 4.09	6.00 ± 4.74	0.112*
MGYSS (score)	15.48 ± 11.78	22.50 ± 13.01	0.002*

MS: medical staff; N: number; M: male; F: female; BMI: body mass index; TBUT: tear film break-up time; SPEED: standard patient evaluation of eye dryness; OSDI: Ocular Surface Disease Index; ICU: interferometry color units; PB: partial blink; MGD: meibomian gland dysfunction; MGYLS: meibomian gland yielding liquid secretion; MGYCS: meibomian gland yielding clear liquid secretion; and MGYSS: meibomian gland yielding secretion score. [&]Chi-square test; *Wilcoxon signed-rank test; [#]Independent-sample *t*-test.

control group. The SPEED score in the MS group was 7.94 ± 3.81 , which was significantly higher than 3.65 ± 2.11 in the control group ($Z = -4.766$, $P = 0.001$). TBUT in the MS group was significantly shorter than that in the control group ($Z = -5.201$, $P = 0.001$). However, there was no significant difference in Schirmer I test between the two groups ($Z = -1.346$, $P = 0.178$).

3.3. MGD Parameters comparison. LLT was quantified using mean interference color units (ICU) (1 ICU = 1 nm). Max ICU, mean ICU, and min ICU were significantly thinner in the MS group than in the control group ($Z = -4.356$, $P = 0.001$; $Z = -4.482$, $P = 0.001$; $Z = -4.414$, $P = 0.001$,

resp.). Mean LLT ≤ 60 nm accounted for 69.35% of the eyes in the MS group and 33.87% of the eyes in the control group. MG dropout had occurred in 45.16% of the affected eyes in the MS group and in 16.13% of the affected eyes in the control group. The MG dropout grading for both groups is presented in Figure 2(a). There was significant difference between the two groups for MG dropout (Chi-square test, $\chi^2 = 14.352$, $P = 0.001$). There was no statistically significant difference in PB rate between MS group and control group ($Z = -0.622$, $P = 0.534$). Both MGYLS and MGYSS were significantly lower in the MS group than in the control group ($Z = -3.641$, $P = 0.001$; $Z = -3.146$, $P = 0.002$, resp.). However, there was no significant difference in MGYCS between the two groups ($Z = -1.587$, $P = 0.112$). MGYLS ≤ 6 and MGYSS ≤ 18 for both groups are shown in Figure 2(b).

3.4. Correlation of Ocular Surface Parameters. The right eyes of the MS were selected to study the correlations of the ocular surface parameters. The cumulative days of night shift work in the MS group were 142.26 ± 112.07 (36,480) days, which were not correlated with SPEED score, OSDI score, TBUT, Schirmer I value, mean LLT, and MG loss (Spearman $r = 0.141, 0.274, 0.195, -0.241, 0.042, 0.192$, all $P > 0.05$). The mean LLT was negatively correlated with SPEED score (Spearman $r = -0.363$, $P > 0.045$) but not significantly correlated with Schirmer I, TBUT, or OSDI score and MG loss (Spearman $r = 0.142, -0.044, -0.346, 0.042$, $P = 0.447, 0.815, 0.057, 0.823$, all $P > 0.05$).

4. Discussion

MGD is the main cause of evaporative DED [22]. Aging is one of the risk factors for MGD [23]. The prevalence of MGD in the Asian population was approximately 33% in patients aged < 30 years and 72% in patients aged ≥ 60 years [4]. In our study, although MS working night shifts were slightly older than day workers, the participants were all young adults aged 18–36 years. We further investigated the association of age with ocular surface parameters and showed no association of age with mean LLT and MG loss. Therefore, we believe that risk factors associated with shift work may exacerbate MGD.

As expected, in this study we found that MS who regularly worked night shifts had more severe and frequent dry eye symptoms than those daytime workers. Although tear secretion function was normal, 90.32% of the affected eyes had shortened TBUTs, 69.35% of the affected eyes had LLT ≤ 60 nm, and 45% of the affected eyes had MG dropout. LLT measurement was used as a diagnostic tool for MGD [24]. A previous study found LLT ≤ 60 nm in 74% of patients with severe dry eye symptoms [25]. MS with frequent night shifts causes tear film instability but does not affect tear secretion. Therefore, dry eye in MS is not water deficit but excessive evaporation. Shift work primarily results in sleep disturbances, with acute symptoms including difficulty falling asleep, reduced sleep duration, and somnolence in the following days [11]. Previous studies have reported that sleep disorders and DED interact with each other [13–16]. Poor

sleep quality has been reported in 45% of young and middle-aged DED office workers [26]. Fifty patients diagnosed with OSAS were reported to have significantly higher OSDI scores, shorter TBUT, and lower Schirmer values compared to control subjects [13]. SD throughout the day in healthy men caused tear hyperosmolarity, shortened TBUT, and decreased tear secretion, while all SD-induced changes in ocular surface parameters returned to normal levels after one day [12]. Decreased tear secretion and lacrimal gland hypertrophy induced by SD 10-days mice can also be restored to relatively normal levels at 2 weeks [27]. The researches indicate that short-term effects of SD can be compensated. Another study found that dry eye symptoms, tear film instability, and conjunctival hyperemia were aggravated after night shifts in 50 hospital staffs, but the basal Schirmer test increased [28]. They concluded that increased Schirmer test values may be a compensation for stress caused by SD [28]. In our study, the examination of the MS group was not performed on the day of the end of the night shift work, but on other normal working days to avoid temporary effects of SD. Since the tear secretion function of the MS group was not affected in our study, we believe that the secretion function of their lacrimal glands may be compensated or even unaffected.

Previous studies have found an increased incidence of metabolic syndrome such as elevated blood pressure, elevated triglyceride and glucose levels, low HDL cholesterol, and abdominal overweight in shift workers compared to day workers [29, 30]. Shift work was also associated with breast cancer, cardiovascular disease, and pregnancy complications [31–33]. Night shift work disturbs the circadian system, alters sleep activity patterns, and inhibits melatonin production, and these changes can promote inflammation and tumorigenesis and have immunosuppressive effects [31–33]. Inadequate sleep has been shown to be associated with feeling tired and stressed and pessimism [27]. Shift work MS has a high incidence of psychosocial problems such as depression, stress, anxiety, and sleep disorders [34]. Psychosocial problems have been reported to be involved in the neuropathic mechanisms of DED [34].

In our study, the cumulative days of night shift work were not associated with DED parameters and MGD parameters. The SPEED score of night shift MS was negatively correlated with mean LLT, and the more severe and frequent the dry eye condition, the thinner the lipid layer, which was consistent with the previous studies [25]. Different intensity and frequency of night shift work and mental stress of MS in different departments may affect the changes of ocular surface parameters. Dry eye is an inflammatory condition [35]. Cortisol is an important anti-inflammatory hormone in human physiology [36]. Shift work disrupts cortisol production, a marker of HPA axis activation under stress conditions, and may be an important cause of dry eye [37]. Poor sleep quality has been reported to be associated with lower testosterone levels, affecting the development of dry eye [38]. Whether MS with night shift affects different hormone expressions that influence the formation of dry eye still needs further study.

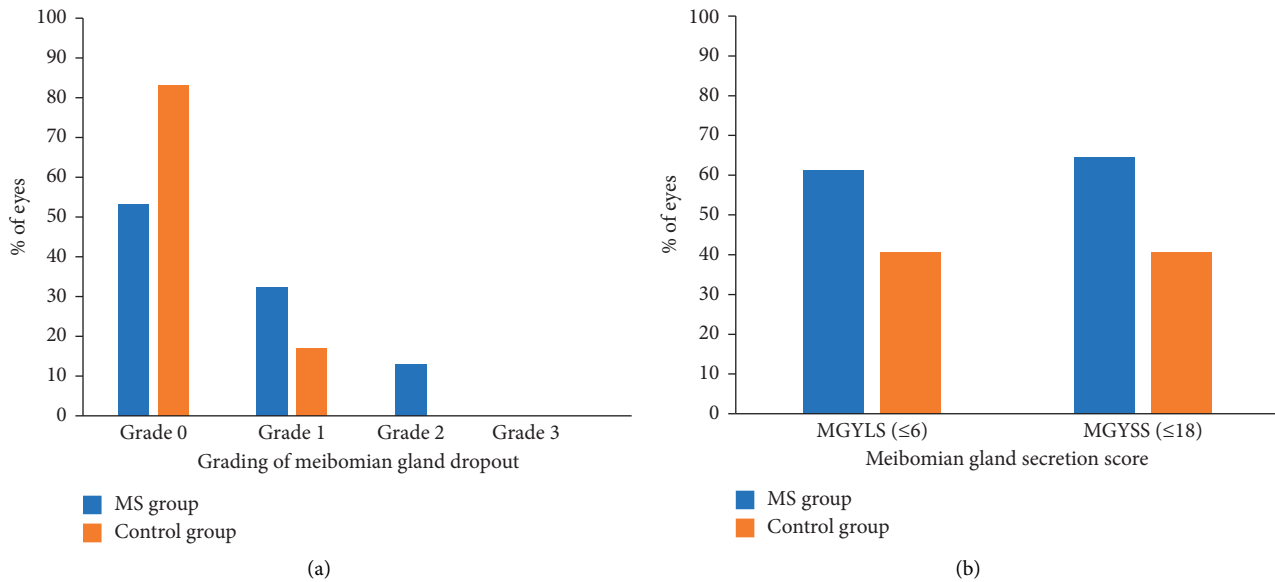


FIGURE 2: Comparison of meibomian gland dropout grading (a) and meibomian gland secretion score (b) between medical staff (MS) group and control group.

This study has several limitations. First, only single-center MS members were included in this study, which may have selection bias. Second, night shift working hours and assessment of sleep quality were not accurately recorded. Third, most front-line middle-aged MS need to work night shifts, so MS who do not work night shifts were not used as controls in this study. Fourth, the effect of different night shift working modes on the ocular surface needs further analysis.

In conclusion, we should pay much attention to the ocular surface health of rotating shift medical workers. Early treatment of the asymptomatic phase of MGD may delay progression to the symptomatic phase and reverse its pathological progression.

Data Availability

All data used to support the findings of this study are available from the corresponding author upon request.

Conflicts of Interest

No potential conflicts of interest were reported by the authors.

Acknowledgments

This work was supported by the Sanming Project of Medicine in Shenzhen under Grant no. SZSM201812091.

References

- [1] J. Shimazaki, Y. Nomura, S. Numa et al., "Prospective, multicenter, cross-sectional survey on dry eye disease in Japan," *Advances in Therapy*, vol. 37, no. 1, pp. 316–328, 2020.
- [2] K. F. Farrand, M. Fridman, I. Ö. Stillman, and D. A. Schaumberg, "Prevalence of diagnosed dry eye disease in the United States among adults aged 18 years and older," *American Journal of Ophthalmology*, vol. 182, pp. 90–98, 2017.
- [3] K. I. Kim, Y. S. Park, R. H. Kim, and J. H. Kim, "Factors associated with dry eye symptoms in elderly Koreans: The fifth Korea national health and nutrition examination survey 2010–2012," *Korean Journal of Family Medicine*, vol. 40, no. 1, pp. 22–30, 2019.
- [4] P. Song, W. Xia, M. Wang et al., "Variations of dry eye disease prevalence by age, sex and geographic characteristics in China: A systematic review and meta-analysis," *Journal of Global Health*, vol. 8, no. 2, Article ID 020503, 2018.
- [5] J. S. Titiyal, R. C. Falera, M. Kaur, V. Sharma, and N. Sharma, "Prevalence and risk factors of dry eye disease in North India: Ocular surface disease index-based cross-sectional hospital study," *Indian Journal of Ophthalmology*, vol. 66, no. 2, pp. 207–211, 2018.
- [6] J. P. Craig, K. K. Nichols, E. K. Akpek et al., "TFOS DEWS II definition and classification report," *The Ocular Surface*, vol. 15, no. 3, pp. 276–283, 2017.
- [7] T. Caffery, S. Chow, K. Wan, and H. Yuen, "Update on the association between dry eye disease and meibomian gland dysfunction," *Hong Kong Medical*, vol. 25, no. 1, pp. 38–47, 2019.
- [8] J. Li, K. Zheng, Z. Deng et al., "Prevalence and risk factors of dry eye disease among a hospital-based population in southeast China," *Eye & Contact Lens: Science & Clinical Practice*, vol. 41, no. 1, pp. 44–50, 2015.
- [9] K. Zheng, R. Baan, Y. Grosse et al., "Carcinogenicity of shift-work, painting, and fire-fighting," *The Lancet Oncology*, vol. 8, no. 12, pp. 1065–1066, 2007.
- [10] Y. Secretan, B. Perret, J. B. Ruidavets et al., "Shift work and cardiovascular risk factors: New knowledge from the past decade," *Archives of Cardiovascular Diseases*, vol. 104, no. 12, pp. 636–668, 2011.
- [11] T. Åkerstedt, "Shift work and disturbed sleep/wakefulness," *Sleep Medicine Reviews*, vol. 2, no. 2, pp. 117–128, 1998.
- [12] Y. B. Lee, J. W. Koh, J. Y. Hyon, W. R. Wee, J. J. Kim, and Y. J. Shin, "Sleep deprivation reduces tear secretion and impairs the tear film," *Investigative Ophthalmology & Visual Science*, vol. 55, no. 6, pp. 3525–3531, 2014.

- [13] E. E. Karaca, H. T. Akçam, F. Uzun, Ş. Özdek, and T. Ulukavak Çiftçi, "Evaluation of ocular surface health in patients with obstructive sleep apnea syndrome," *Türk Oftalmoloji Dergisi*, vol. 46, no. 3, pp. 104–108, 2016.
- [14] M. Ayaki, M. Kawashima, K. Negishi, and K. Tsubota, "High prevalence of sleep and mood disorders in dry eye patients: Survey of 1,000 eye clinic visitors," *Neuropsychiatric Disease and Treatment*, vol. 11, pp. 889–894, 2015.
- [15] M. Ayaki, M. Kawashima, K. Negishi, T. Kishimoto, M. Mimura, and K. Tsubota, "Sleep and mood disorders in dry eye disease and allied irritating ocular diseases," *Scientific Reports*, vol. 6, no. 1, Article ID 22480, 2016.
- [16] M. Ayaki, I. Toda, N. Tachi, K. Negishi, and K. Tsubota, "Preliminary report of improved sleep quality in patients with dry eye disease after initiation of topical therapy," *Neuropsychiatric Disease and Treatment*, vol. 12, pp. 329–337, 2016.
- [17] C. McAlinden, R. Gao, Q. Wang et al., "Rasch analysis of three dry eye questionnaires and correlates with objective clinical tests," *The Ocular Surface*, vol. 15, no. 2, pp. 202–210, 2017.
- [18] K. Zhu, S. Kyei, S. N. Mensah, S. Ocansey, L. S. Abu, and E. A. Kyere, "Ocular surface disease index (OSDI) versus the standard patient evaluation of eye dryness (SPEED)," *Cornea*, vol. 35, no. 2, pp. 175–180, 2016.
- [19] W. Ngo, P. Situ, N. Keir, D. Korb, C. Blackie, and T. Simpson, "Psychometric properties and validation of the standard patient evaluation of eye dryness questionnaire," *Cornea*, vol. 32, no. 9, pp. 1204–1210, 2013.
- [20] K. Asiedu, "Rasch analysis of the standard patient evaluation of eye dryness questionnaire," *Eye & Contact Lens: Science & Clinical Practice*, vol. 43, no. 6, pp. 394–398, 2017.
- [21] D. A. Sullivan, B. D. Sullivan, J. E. Evans et al., "Androgen deficiency, Meibomian gland dysfunction, and evaporative dry eye," *Annals of the New York Academy of Sciences*, vol. 966, no. 1, pp. 211–222, 2002.
- [22] D. A. Schirra, J. J. Nichols, E. B. Papas, L. Tong, M. Uchino, and K. K. Nichols, "The international workshop on meibomian gland dysfunction: report of the subcommittee on the epidemiology of, and associated risk factors for, MGD," *Investigative Ophthalmology & Visual Science*, vol. 52, no. 4, pp. 1994–2005, 2011.
- [23] A. J. Bron and J. M. Tiffany, "The contribution of meibomian disease to dry eye," *The Ocular Surface*, vol. 2, no. 2, pp. 149–164, 2004.
- [24] D. Finis, N. Pischel, S. Schrader, and G. Geerling, "Evaluation of lipid layer thickness measurement of the tear film as a diagnostic tool for Meibomian gland dysfunction," *Cornea*, vol. 32, no. 12, pp. 1549–1553, 2013.
- [25] Y.-B. Chou, N.-W. Fan, and P.-Y. Lin, "Value of lipid layer thickness and blinking pattern in approaching patients with dry eye symptoms," *Canadian Journal of Ophthalmology*, vol. 54, no. 6, pp. 735–740, 2019.
- [26] M. Kawashima, M. Uchino, N. Yokoi et al., "The association of sleep quality with dry eye disease: The Osaka study," *Clinical Ophthalmology*, vol. 10, pp. 1015–1021, 2016.
- [27] S. Uchino, K. Ning, J. Zhou et al., "Sleep deprivation disrupts the lacrimal system and induces dry eye disease," *Experimental & Molecular Medicine*, vol. 50, no. 3, p. e451, 2018.
- [28] A. Guo and H. Torabifard, "Dry eye signs and symptoms in night-time workers," *Journal of Current Ophthalmology*, vol. 29, no. 4, pp. 270–273, 2017.
- [29] M. A. Roomi and M. Mohammadnezhad, "Prevalence of metabolic syndrome among apparently healthy workforce," *Journal of Ayub Medical College, Abbottabad:JAMC*, vol. 31, no. 2, pp. 252–254, 2019.
- [30] D. De Bacquer, M. Van Risseghem, E. Clays, F. Kittel, G. De Backer, and L. Braeckman, "Rotating shift work and the metabolic syndrome: A prospective study," *International Journal of Epidemiology*, vol. 38, no. 3, pp. 848–854, 2009.
- [31] E. L. Haus and M. H. Smolensky, "Shift work and cancer risk: potential mechanistic roles of circadian disruption, light at night, and sleep deprivation," *Sleep Medicine Reviews*, vol. 17, no. 4, pp. 273–284, 2013.
- [32] R. J. Reiter, D.-X. Tan, A. Korkmaz, and S. Ma, "Obesity and metabolic syndrome: Association with chronodisruption, sleep deprivation, and melatonin suppression," *Annals of Medicine*, vol. 44, no. 6, pp. 564–577, 2012.
- [33] S. Puttonen, M. Härmä, and C. Hublin, "Shift work and cardiovascular disease - pathways from circadian stress to morbidity," *Scandinavian Journal of Work, Environment & Health*, vol. 36, no. 2, pp. 96–108, 2010.
- [34] C. W. Mcmonnies, "The potential role of neuropathic mechanisms in dry eye syndromes," *Journal of Optometry*, vol. 10, no. 1, pp. 5–13, 2017.
- [35] T. Yamaguchi, "Inflammatory response in dry eye," *Investigative Ophthalmology & Visual Science*, vol. 59, no. 14, pp. 192–199, 2018.
- [36] M. W. Whitehouse, "Anti-inflammatory glucocorticoid drugs: Reflections after 60 years," *Inflammopharmacology*, vol. 19, no. 1, pp. 1–19, 2011.
- [37] E. W. M. Hung, K. J. Aronson, M. Leung, A. Day, and J. Tranmer, "Shift work parameters and disruption of diurnal cortisol production in female hospital employees," *Chronobiology International*, vol. 33, no. 8, pp. 1045–1055, 2016.
- [38] C. Lord, Z. Sekerovic, and J. Carrier, "Sleep regulation and sex hormones exposure in men and women across adulthood," *Pathologie Biologie*, vol. 62, no. 5, pp. 302–310, 2014.

Clinical Study

Comparison of Different Types of Corneal Foreign Bodies Using Anterior Segment Optical Coherence Tomography: A Prospective Observational Study

Tao Wang,¹ Lei Zhong,¹ Shiyi Yin,¹ Tiancheng Bao,¹ Jiezheng Yang,¹ Ting Wang,² and Shiqi Ling ¹

¹Department of Ophthalmology, Third Affiliated Hospital of Sun Yat-Sen University, Guangzhou, Guangdong, China

²State Key Laboratory of Ophthalmology, Zhongshan Ophthalmic Center, Sun Yat-sen University, Guangzhou, Guangdong, China

Correspondence should be addressed to Shiqi Ling; lingshiqi123@163.com

Received 26 March 2020; Revised 15 June 2020; Accepted 15 July 2020; Published 11 August 2020

Guest Editor: Karim Mohamed-Noriega

Copyright © 2020 Tao Wang et al. This is an open access article distributed under the Creative Commons Attribution License, which permits unrestricted use, distribution, and reproduction in any medium, provided the original work is properly cited.

Purpose. The present study highlighted the value of anterior segment optical coherence tomography (AS-OCT) for different types of corneal foreign bodies in humans. **Methods.** This study was a prospective observational study. The patients included were divided into two groups. If the patients were directly diagnosed based on eye injury history and slit-lamp examination, then they were assigned to Group A. Otherwise, the patients were assigned to Group B. We compared and described the characteristics of the corneal foreign body in both groups using AS-OCT. **Results.** From October 2017 to January 2020, 36 eyes of 36 patients (9 females and 27 males) with a mean age of 37.8 ± 11.7 years were included in the study. Patients in Group A were the majority and accounted for 72.2% (26/36). High signals on AS-OCT images were the main constituent and accounted for 92.3% (24/26) in Group A and 70.0% (7/10) in Group B. Most of the patients in Group A, 96.2% (25/26), had clear boundaries. A blurred boundary was observed in 70.0% (7/10) of the patients in Group B. The foreign bodies on AS-OCT images had key characteristics of a high signal followed by a central zone shadowing effect and a low signal followed by a marginal zone shadowing effect. Further, all of the lesions could be directly located in Group B, and 92.3% (24/26) of the patients in Group A did not have directly located lesions. Six representative cases are described in detail. **Conclusions.** AS-OCT is a valuable tool in the diagnosis and management of corneal foreign bodies, especially for unusual corneal foreign body.

1. Introduction

Corneal foreign bodies (FBs) are one of most common ophthalmological emergency cases. Patients with corneal foreign body (FB) have multiple ocular symptoms, including red eye, foreign body sensation, irritation, tearing, pain, and blurred vision. The timely and appropriate removal of a corneal FB is necessary [1–3]. Although the diagnosis and management of corneal FB is generally easily made based on the history and slit-lamp examination, there are some unusual cases of FB that create difficulties in the diagnosis and choosing most appropriate removal method due to the variety of FB [4–6].

Recently, optical coherence tomography (OCT), as a noninvasive examination technology, greatly improved the ophthalmologists' understanding and perception of diseases. The introduction of spectral-domain (SD) OCT technology and Fourier-domain (FD) OCT system led to a significant increase in acquisition speed and imaging resolution of the anterior segment [7, 8]. Anterior segment OCT (AS-OCT) generates detailed images and digital information on the anterior segment, and it was widely used to assess the phenotypes of the anterior segment of the eye such as corneal thickness and anterior chamber [9–11]. There were several case reports of corneal FBs using AS-OCT [12, 13] and observations of different corneal FB in vitro using AS-

OCT [14]. However, no article indicates the diagnosis basis of cornea FB using AS-OCT.

The aim of the present study is to highlight the value of AS-OCT for the diagnosis of corneal FB and provide references for its management. In this study, we described the clinical findings and AS-OCT characteristics of different types of corneal FBs, compared the difference of two types of corneal foreign bodies, and pointed out a preliminary method for diagnosis of corneal foreign body using AS-OCT.

2. Materials and Methods

The present perspective observational study screened patients from October 2017 to January 2020 in our clinic with a diagnosed or suspected diagnosed corneal FB. All patients who were included this study met the following conditions:

- (1) Participated voluntarily in this study
- (2) Diagnosed or had a suspected diagnosis of cornea FB
- (3) Were able to complete the anterior segment examinations with clear anterior segment color photography and AS-OCT scanning
- (4) Had lesions with a depth that did not exceed 2/3 of the corneal thickness
- (5) Had no apparent corneal infection signs

Patients who did not meet any of the above criteria were not included in the study. This study adhered to tenets of the Declaration of Helsinki and was approved by the institutional review board and ethics committee from the Third Affiliated Hospital of Sun Yat-San University.

When the patient presented to our clinic, emergency treatment, such as topical anesthesia and flushing the conjunctival sac, was administered if necessary. Each patient underwent a careful, comprehensive eye examination. After slit-lamp examination, anterior segment color photography was taken, and the AS-OCT (3D OCT-2000, Topcon, Tokyo, Japan) scanner focused on lesions using the radial anterior segment protocol. The scan diameter was 6.0 mm, and a radial 12 hour scan was performed. One section of the clear images was used for used for evaluation and measurement.

In general, the patients with corneal FBs have clinical characteristics, such as a clear history of ocular trauma and ocular symptoms of red eye, foreign body sensation, irritation, tearing, pain, and blurred vision [3]. According to the clinical findings, we divided the patients into two groups (Group A and Group B). Three authors participated in the evaluation. Patients who could be diagnosed as corneal FB based on the medical history and anterior segment color photography were classified into Group A. If any of the three evaluators had doubts about the patient's diagnosis based on the medical history and the anterior segment color photography, the patient was classified into Group B.

We used the signal of the normal corneal tissue surrounding the lesions as a reference. If the signal of the lesions was stronger than the surrounding tissue signal, it was a hyperreflective signal (high signal). When the signal of the lesions was weaker than the surrounding tissue, it was a

hyporefective signal (low signal). The signal deep in the FB was weaker or even disappeared, which was regarded as signal attenuation and was called a shadowing effect [5, 7, 14].

Statistical data are described as frequencies and percentages for categorical data and means \pm SD for numerical data using SPSS version 24 (SPSS Inc., Chicago, IL, USA).

3. Results

Thirty-six eyes of 36 patients (9 females and 27 males) with a mean age of 37.8 ± 11.7 years were included in the study.

Group A included 72.2% (26/36) patients, and Group B included 27.8% (10/36) patients. Metallic corneal FB was the most common observation and was observed in 65.7% (23/35) of all patients. In Group A, metallic corneal FB was observed in 88.5% (23/26) of patients, and only nonmetallic corneal FB were observed in Group B, 90.0% (9/10). One patient in Group B had a clear history of eye trauma and was eventually excluded from the diagnosis of corneal FB because of poor corneal epithelial healing.

Corneal FBs have some characteristics in AS-OCT images. A shadowing effect in the central zone behind the high signal and the marginal zone following the low signal was observed in both groups. FBs with high reflection signals were the most common in Group A (92.3%, 24/26) and Group B (70.0%, 7/10). Notably, the high and low signals of the FB corresponded to the central zone shadowing effect and marginal zone shadowing effect, respectively.

The location of corneal FBs is an important reference for selecting the removal ways of FBs. Increasing the depth and area of treatment will influence the time required to heal and may cause more visible corneal scars [3]. The selection of appropriate FB removal method, such as wiping, picking out, or scraping, is helpful to reduce corneal tissue damage and scar formation. The depth of the FB was generally indirectly located (92.3%, 24/26). However, whether there was a high or low signal in Group B, the location could be directly accomplished.

All descriptive characteristics of the study participants are summarized in Table 1.

To further demonstrate the value of AS-OCT in the diagnosis and management of different corneal FBs, six representative cases, including two cases in Group A and four cases in Group B, are reported in detail. The clinical details of each patient are presented in Table 2.

3.1. Case 1. A 31-year-old man presented to our clinic with redness in his left eye, photophobia, and foreign body sensation. He used an electric saw to cut iron two days prior. Slit-lamp examination revealed an iron FB surrounded by a slight haze (Figure 1(a), arrowhead). Corneal FB was easily diagnosed. The FB was removed via picking and scraping.

AS-OCT scanning showed a single high signal with clear boundary (Figure 1(b), arrowhead) following by central zone shadowing effect (Figure 1(b), star). The depth of the FB could not be directly located.

TABLE 1: Clinical characteristics of all patients.

	Group A	Group B
Gender (F/M)	6/20	3/7
Age (years)	38.4 ± 11.5	36.1 ± 12.0
Metallic FB	23	0
Nonmetallic FB	2	9
Mixed FB	1	0
H signal	24	7
L signal	2	3
Clear boundary	25	3
Blurred boundary	1	7
Central shadowing	24	6
Marginal shadowing	2	3
Direct location	2	10
Indirect location	24	0

TABLE 2: Clinical details and AS-OCT characteristics of cases.

Case no.	1	2	3	4	5	6
Group	A	A	B	B	B	B
Sex/age	M/31	M/69	F/30	M/39	M/62	M/28
Numbers of FB	Single	Multiple	Single	Multiple	Single	None
Nature of FB	Metallic	Mixed	Nonmetallic	Nonmetallic	Nonmetallic	*
Reflective signal	High	High	Low	High	High	High
Border of lesions	Clear	Unclear	Clear	Unclear	Unclear	Unclear
Shadowing effect	Central	Central	Marginal	Central	Central	Negative
Location depth	Indirect	Direct	Direct	Direct	Direct	Direct

*The case eventually proved to be free of FBs.

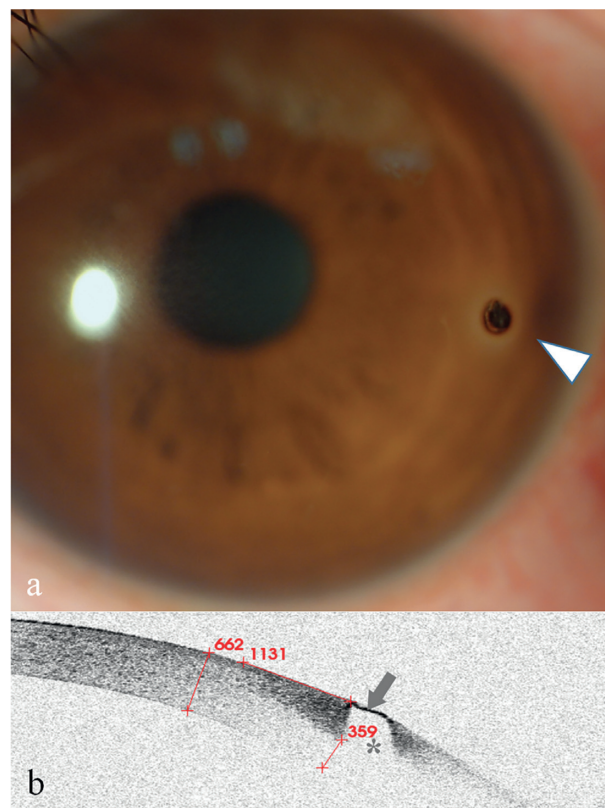


FIGURE 1: Anterior segment and AS-OCT image for Case 1. (a) Anterior segment photograph showed a corneal FB and inflammatory infiltration around the FB at an approximately 3:00 o'clock location approaching the limbus (arrowhead). (b) AS-OCT image showed that the FB showed a single high signal with clear boundary (arrow) following a central zone shadowing effect (star). The depth of the FB was estimated indirectly by subtracting the thickness of the underside of the high-reflected signal surrounding a FB (359 m) from the thickness of the cornea (662 m), which was less than 303 μm .

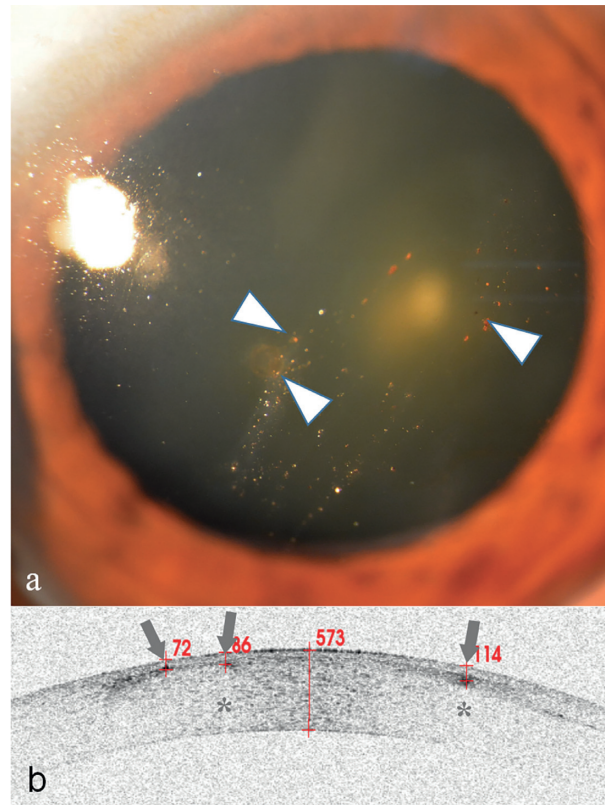


FIGURE 2: Anterior segment and AS-OCT image for Case 2. (a) Anterior segment photograph showing multiple small granular corneal lesions in the shallow cornea (arrowheads). (b) AS-OCT showed that there were three high signals with blurred boundary (arrows). Two of the signals had a central zone shadowing effect (stars). They were directly located and were 72, 86, and 114 μm beneath the corneal surface.

3.2. Case 2. A 69-year-old man presented with itching eyes for several weeks. Slit-lamp examination revealed multiple granular corneal opacities (Figure 2(a), arrowheads) in his left cornea. Corneal fluorescein staining was negative. The patient remembered that his left eye was injured by a tire explosion one decade ago. An old multiple corneal FB diagnosis was concluded. Because of the long harmless history, these FBs were not further treated.

AS-OCT scanning showed some high signals with blurred boundary (Figure 2(b), arrows) followed by a central zone shadowing effect (Figure 2(b), stars) in the deep part of the epithelium and the superficial portion of the stroma. The depth of the FB was directly located (Figure 2(b)).

3.3. Case 3. A 30-year-old woman presented with redness in her right eye that lasted for two weeks. She experienced no other discomfort. Examination revealed a light brown mass on the temporal limbus of her right cornea (Figure 3(a), arrowhead), and vascularization was observed in the center of the lesion. Corneal fluorescein staining was negative on the mass surface. On further questioning, her history revealed that a FB may have been blown into her eye one month ago, but she reported no discomfort, and no treatment was administered. Her diagnosis was a suspected corneal FB, and corneal neoplasm could not be excluded.

AS-OCT scanning showed a single low signal with clear boundary (Figure 3(b), arrow) followed by a marginal zone

shadowing effect (Figure 3(b), stars). The depth of the FB was directly located. The FB was picked out using a needle and was confirmed as a translucent shell-like FB.

3.4. Case 4. A 39-year-old man presented to the emergency room because glass glue was splashed into his right eye 30 minutes prior. After emergency treatment, he was further examined. Slit-lamp examination revealed cream-like particulates (Figure 4(a), arrowhead) and microfolds on the cornea (Figure 4(a), star). His diagnosis was not clear because his corneal degeneration may be due to chemical injuries, FB of residual glue, or both.

AS-OCT examinations revealed multiple high signals with blurred boundary (Figure 4(b), arrows) followed by a central zone shadowing effect (Figure 4(b), stars). The lesions were located on the corneal surface. The corneal thickness was in the normal range of 546 μm , and the corneal stromal signal was intact. The diagnosis was corneal chemical injury (corneal epithelial degeneration) and corneal FB (glass glue). Because the lesions were located in a shallow and wide range on the cornea, wiping the FB with wet swabs was used for treatment. No other damage to the cornea was found during the follow-up days.

3.5. Case 5. A 62-year-old man with blurred vision in his right eye for six months was diagnosed with viral keratitis at his local hospital and continuously received antiviral

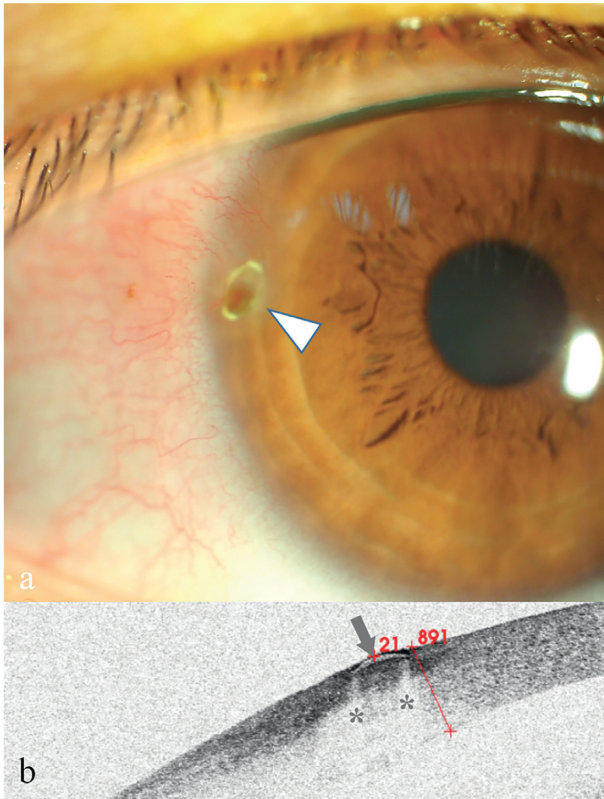


FIGURE 3: Anterior segment and AS-OCT image for Case 3. (a) Anterior segment photograph: at 9:00 o'clock inside the limbus (arrowhead), a light brown mass was observed without surface fluorescence staining, and fluorescein gathered around the edges. Neovascularization was also seen. (b) AS-OCT image showing that a crescent-shaped low reflective signal (arrowhead) with bilateral marginal zone shadowing (stars) was found 21 μm below the epithelium surface.

therapy. He denied a history of eye injuries. Slit-lamp showed a white lump on the cornea in the pupil region (Figure 5(a), arrowhead). His diagnosis was drug-induced keratitis with a suspected corneal FB.

AS-OCT revealed a high signal with blurred boundary (Figure 5(b), arrowhead) in the epithelial layer, under which was a partially continuous epithelium. It was followed by a central zone shadowing effect (Figure 5(b), star). The lesions were scraped with a needle. On the following day, his cornea was restored to nearly transparent, and his visual acuity went from 20/100 back to 20/25.

3.6. Case 6. A 28-year-old man complained of a constant foreign body sensation in his right eye. His right eye was cut by his broken glasses approximately 2 weeks prior. Careful inspection with the slit-lamp revealed a slight bulge in the peripheral cornea (Figure 6(a), white arrowhead). Corneal fluorescein staining was negative (Figure 6(a), green arrowhead). His diagnosis was a suspected corneal FB.

AS-OCT scanning showed a high signal with blurred boundary (Figure 6(b), arrow), but there was no shadowing

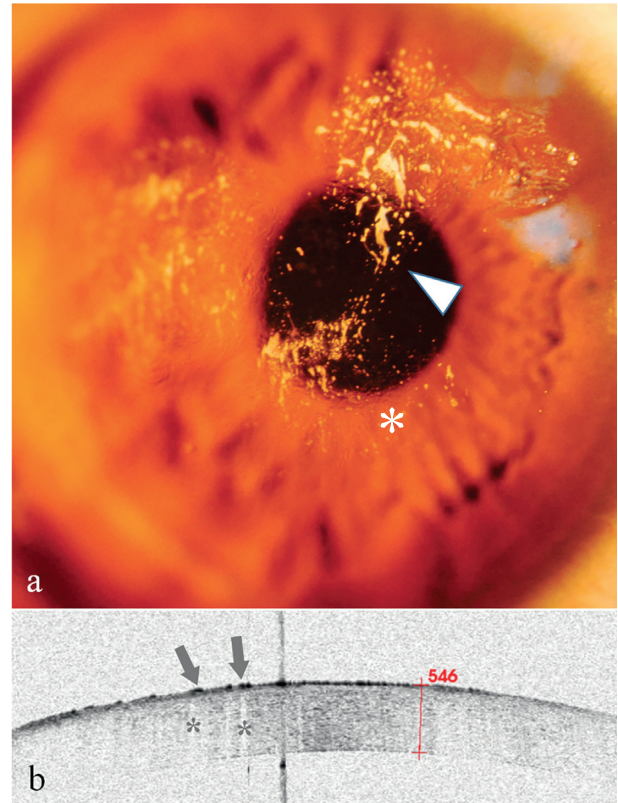


FIGURE 4: Anterior segment and AS-OCT image for Case 4. (a) Anterior segment photograph showing multiple cream-like corneal opacities (arrowheads) surrounding a wrinkled transparent cornea. (b) AS-OCT image showed multiple spines (high signals) with blurred boundary (arrows) on the superficial epithelium followed by a central zone shadowing effect (stars). The corneal thickness was 546 μm , within the normal range.

effect beneath the lesion. It was directly located and was 136 μm in the cornea. Because of the poor epithelial healing in the lesion area that caused the foreign body sensation, scraping the epithelium of the lesion area was chosen. There was no FB to be further confirmed.

4. Discussion

From this study, we can obtain a method of using AS-OCT to diagnose corneal foreign body. In addition, through the localization of corneal foreign body, a more appropriate means of removing corneal foreign body is selected. To the best of our knowledge, this study is the first article that indicates the diagnosis basis of cornea FB using AS-OCT.

AS-OCT clearly showed the fine structure of the cornea [15–17]. The presence of a FB damages the consistency of the corneal structure, which provides the basis for the diagnosis of a FB. FBs show high or low signals on AS-OCT images. High signals followed by a shadowing effect were reported in previous literature [5, 14, 18]. However, these studies ignored the phenomenon that the low signals could also be followed by a shadowing effect, which we named a marginal zone shadowing effect. We hypothesized that this effect may

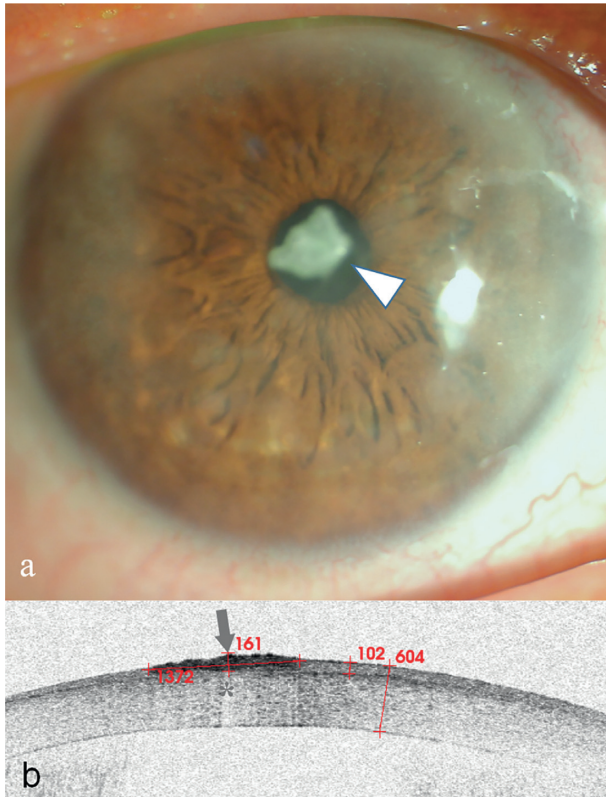


FIGURE 5: Anterior segment and AS-OCT image for Case 5. (a) Anterior segment photograph showing a patchy cloud-like haze over the cornea and a cloudy milky lump in front of the pupil (arrowhead). (b) AS-OCT scanning showed there was a lesion of high signal with blurred boundary (arrow) followed by a central zone shadowing effect (star). The lesion had a diameter of $1372\ \mu\text{m}$. The corneal thickness was $604\ \mu\text{m}$, and the epithelial thickness was $102\ \mu\text{m}$. A layer of continuous epithelium tissue was seen on the bottom of the lesion.

be a total reflection phenomenon resulting from the rupture of the corneal tissue around the FB.

Comparing the AS-OCT characteristics of two groups, we could develop the diagnostic criteria for corneal FB using AS-OCT as follows:

- (1) Eye injury history
- (2) The consistency of the corneal layers being broken
- (3) High or low signals with clear boundaries
- (4) High or low signals with blurred boundaries
- (5) Lesions associated with central or marginal zone shadowing effect

If conditions (1) + (2) + (3) + (5) were met, then a corneal FB was diagnosed.

If conditions (1) + (2) + (4) + (5) were met, then a corneal FB was highly suspected.

When conditions (1) and (2) are met, and there is a high signal with blurred boundary but a lack of condition (5), the diagnosis of corneal FB using AS-OCT should be fairly cautious. The local inflammation, corneal scarring, or corneal neoplasm should be investigated [19–24].

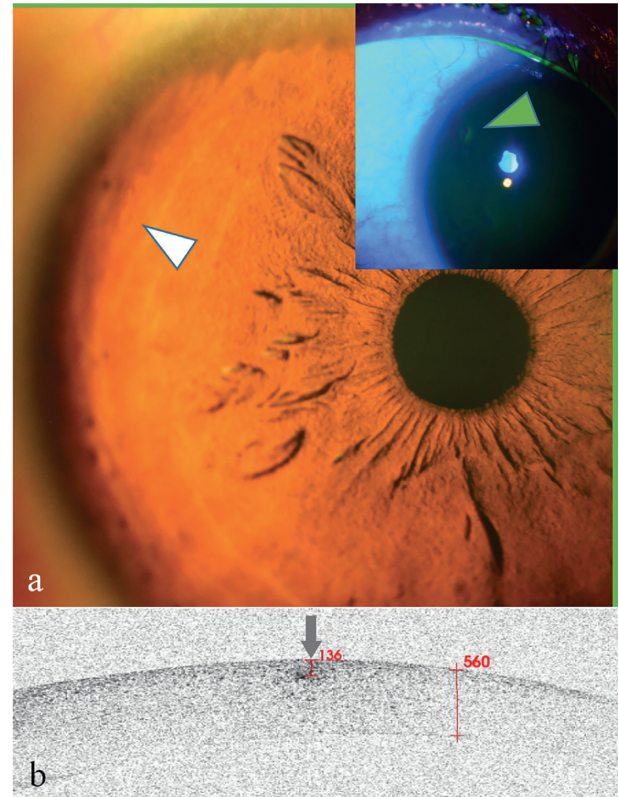


FIGURE 6: Anterior segment and AS-OCT image for Case 6. (a) Anterior segment photograph showed a slight bulge at 10:00 o'clock in the peripheral cornea (white arrowhead). Corneal fluorescein staining was negative (arrowhead). (b) AS-OCT scanning showed there was a lesion of high signal with blurred boundary (arrow) without a shadowing effect. The lesion was directly located and was $136\ \mu\text{m}$ beneath the corneal surface.

AS-OCT scanning may also help optimize the removal of FB. The choice of a suitable corneal FB removal method helps reduce the corneal damage and the formation of corneal scars. According to the location of the corneal FB on the AS-OCT, especially in Group B, we selected different methods to minimize the damage to the cornea and reduce the risk of visual impairment. For example, if the FB was located in the epithelial layer and mobile, and Bowman's layer was untouched, wiping methods were preferred to avoid the forming of a corneal scar. With the application of AS-OCT technology, the frequency of patients' visits may be reduced.

The present study has some limitations. First, the number of subjects we studied was relatively small compared to the various types of corneal FB. Second, there were not enough negative controls, such as corneal infection or degeneration, to further validate the criteria. Therefore, the diagnostic method we summarized need more cases to continue improvements. Third, we used 3D OCT-2000 for AS-OCT scanning in this study, which is a spectral-domain optical coherence tomography developed for the ocular fundus. Although AS-OCT with the cornea anterior module was functional, the AS-OCT observation of corneal FB was hampered by a number of limitations.

In summary, the results of the present study suggest that AS-OCT is a very valuable tool for the diagnosis of corneal FB, especially for some unusual cases. AS-OCT scanning could provide a reference for the selection of FB management through direct or indirect FB localization. The value of AS-OCT application in the corneal FB should be further strengthened.

Data Availability

The data used to support the findings of this study are available from the corresponding author upon request.

Disclosure

None of the authors has a financial or personal relationship with other people or organizations that could inappropriately influence or bias the results.

Conflicts of Interest

The authors declare that they have no conflicts of interest.

Authors' Contributions

Dr. Tao Wang, Lei Zhong, and Shiyi Yin contributed equally to this work.

References

- [1] G. McGwin Jr., A. Xie, and C. Owsley, "Rate of eye injury in the United States," *Archives of Ophthalmology*, vol. 123, no. 7, pp. 970–976, 2005.
- [2] G. McGwin Jr. and C. Owsley, "Incidence of emergency department-treated eye injury in the United States," *Archives of Ophthalmology*, vol. 123, no. 5, pp. 662–666, 2005.
- [3] C. P. Guier and T. J. Stokkermans, "Cornea foreign body removal," in *StatPearls*, Treasure Island (FL): StatPearls Publishing, Treasure Island, FL, USA, 2020.
- [4] R. Girgis and S. Verma, "Unusual corneal foreign body," *Eye*, vol. 23, no. 7, p. 1609, 2009.
- [5] H. A. Al-Ghadeer and A. Al-Assiri, "Identification and localization of multiple intrastromal foreign bodies with anterior segment optical coherence tomography and ocular pentacam," *International Ophthalmology*, vol. 34, no. 2, pp. 355–358, 2014.
- [6] A. Portero, E. Carreño, D. Galarreta, and J. M. Herreras, "Corneal inflammation from pine processionary caterpillar hairs," *Cornea*, vol. 32, no. 2, pp. 161–164, 2013.
- [7] P. E. Napoli, M. Nioi, L. Mangoni et al., "Fourier-domain OCT imaging of the ocular surface and tear film dynamics: a review of the state of the art and an integrative model of the tear behavior during the inter-blink period and visual fixation," *Journal of Clinical Medicine*, vol. 9, no. 3, p. 668, 2020.
- [8] M. Ang, M. Baskaran, R. M. Werkmeister et al., "Anterior segment optical coherence tomography," *Progress in Retinal and Eye Research*, vol. 66, pp. 132–156, 2018.
- [9] A. Ishibazawa, S. Igarashi, K. Hanada et al., "Central corneal thickness measurements with fourier-domain optical coherence tomography versus ultrasonic pachymetry and rotating Scheimpflug camera," *Cornea*, vol. 30, no. 6, pp. 615–619, 2011.
- [10] A. Domínguez-Vicent, C. Trussardi, U. Wogatai, R. Montés-Micó, and R. Brautaset, "Precision of high-resolution OCT for anterior chamber measurement: agreement with Scheimpflug imaging," *Journal of Refractive Surgery*, vol. 32, no. 11, pp. 766–772, 2016.
- [11] G. Czajkowski, B. J. Kaluzny, A. Laudenska, G. Malukiewicz, and J. J. Kaluzny, "Tear meniscus measurement by spectral optical coherence tomography," *Optometry and Vision Science*, vol. 89, no. 3, pp. 336–342, 2012.
- [12] A. R. Celebi, A. E. Kilavuzoglu, U. E. Altiparmak, C. B. Cosar, and A. Ozkiris, "The role of anterior segment optical coherence tomography in the management of an intra-corneal foreign body," *Springerplus*, vol. 5, no. 1, p. 1559, 2016.
- [13] J.-L. Bacquet, A. Fel, R. Belazzougui, and B. Bodaghi, "Deep intracorneal foreign body: anterior segment OCT," *Journal Français d'Ophthalmologie*, vol. 38, no. 10, pp. 1012–1013, 2015.
- [14] S. Armarnik, M. Mimouni, D. Goldenberg et al., "Characterization of deeply embedded corneal foreign bodies with anterior segment optical coherence tomography," *Graefes' Archive for Clinical and Experimental Ophthalmology*, vol. 257, no. 6, pp. 1247–1252, 2019.
- [15] J. P. Ehlers, "Intraoperative optical coherence tomography: past, present, and future," *Eye*, vol. 30, no. 2, pp. 193–201, 2016.
- [16] W. W. Binotti, B. Bayraktutar, M. C. Ozmen, S. M. Cox, and P. Hamrah, "A review of imaging biomarkers of the ocular surface," *Eye & Contact Lens: Science & Clinical Practice*, vol. 46, no. 2, pp. S84–S105, 2020.
- [17] R. M. Werkmeister, S. Sapeta, D. Schmidl et al., "Ultra-high-resolution OCT imaging of the human cornea," *Biomedical Optics Express*, vol. 8, no. 2, pp. 1221–1239, 2017.
- [18] H. Jiao, L. J. Hill, L. E. Downie, and H. R. Chinnery, "Anterior segment optical coherence tomography: its application in clinical practice and experimental models of disease," *Clinical and Experimental Optometry*, vol. 102, no. 3, pp. 208–217, 2019.
- [19] C. Shipton, J. Hind, J. Biagi, and D. Lyall, "Anterior segment optical coherence tomographic characterisation of keratic precipitates," *Contact Lens and Anterior Eye*, vol. 20, pp. 30003–30005, 2020.
- [20] W. Soliman, M. A. Nassr, K. Abdelazeem, and A. K. Al-Hussaini, "Appearance of herpes simplex keratitis on anterior segment optical coherence tomography," *International Ophthalmology*, vol. 39, no. 12, pp. 2923–2928, 2019.
- [21] M. A. Oliveira, A. Rosa, M. Soares et al., "Anterior segment optical coherence tomography in the early management of microbial keratitis: a cross-sectional study," *Acta Médica Portuguesa*, vol. 33, no. 5, pp. 318–325, 2019.
- [22] M. Das, S. A. Menda, A. K. Panigrahi et al., "Repeatability and reproducibility of slit lamp, optical coherence tomography, and scheimpflug measurements of corneal scars," *Ophthalmic Epidemiology*, vol. 26, no. 4, pp. 251–256, 2019.
- [23] N. Morishige, K. Magome, A. Ueno, T.-A. Matsui, and T. Nishida, "Relations among corneal curvature, thickness, and volume in keratoconus as evaluated by anterior segment-optical coherence tomography," *Investigative Ophthalmology & Visual Science*, vol. 60, no. 12, pp. 3794–3802, 2019.
- [24] Y. S. Shen, J. L. Hu, and C. C. Hu, "Anterior high-resolution OCT in the diagnosis and management of corneal squamous hyperplasia mimicking a malignancy: a case report," *BMC Ophthalmology*, vol. 19, no. 1, p. 235, 2019.

Review Article

Objective Imaging Diagnostics for Dry Eye Disease

Sang Beom Han ¹, Yu-Chi Liu ^{2,3,4}, Karim Mohamed-Noriega ⁵, Louis Tong ^{2,3,4},
and Jodhbir S. Mehta ^{2,3,4}

¹Department of Ophthalmology, Kangwon National University School of Medicine, Kangwon National University Hospital, Chuncheon, Republic of Korea

²Singapore National Eye Centre, Singapore

³Singapore Eye Research Institute, Singapore

⁴Department of Ophthalmology, Yong Loo Lin School of Medicine, National University of Singapore, Singapore

⁵Department of Ophthalmology, University Hospital, Faculty of Medicine, Autonomous University of Nuevo Leon, Monterrey, Mexico

Correspondence should be addressed to Jodhbir S. Mehta; jodmehta@gmail.com

Received 16 April 2020; Accepted 3 July 2020; Published 22 July 2020

Academic Editor: Antonio Queiros

Copyright © 2020 Sang Beom Han et al. This is an open access article distributed under the Creative Commons Attribution License, which permits unrestricted use, distribution, and reproduction in any medium, provided the original work is properly cited.

Traditional diagnostic tests for dry eye disease (DED), such as fluorescein tear film break-up time and the Schirmer test, are often associated with poor reproducibility and reliability, which make the diagnosis, follow-up, and management of the disease challenging. Advances in ocular imaging technology enables objective and reproducible measurement of changes in the ocular surface, tear film, and optical quality associated with DED. In this review, the authors will discuss the application of various imaging techniques, such as, noninvasive tear break-up time, anterior segment optical coherence tomography, in vivo confocal microscopy, meibography, interferometry, aberrometry, thermometry, and tear film imager in DED. Many studies have shown these devices to correlate with clinical symptoms and signs of DED, suggesting the potential of these imaging modalities as alternative tests for diagnosis and monitoring of the condition.

1. Introduction

Dry eye disease (DED) is a multifactorial disease characterized by a loss of homeostasis of the tear film [1]. It is a highly prevalent disease that can affect up to one-third of the people worldwide [2, 3]. The disease is associated with symptoms such as ocular discomfort, dryness, pain, foreign body sensation, and visual disturbance [4, 5], which significantly interfere with daily activities including reading, driving, watching TV, and using mobile devices or computer [2, 3]. In clinical practice, the diagnosis and management of DED is often difficult because of its multifactorial nature, as well as discrepancy between dry eye signs and symptoms [2, 6–8]. Moreover, conventional diagnostic tests for DED, such as the fluorescein tear film break-up time (TBUT) and the Schirmer test, often show unsatisfactory reliability and reproducibility, which also renders the diagnosis and monitoring of the condition challenging [9].

Advances in technology led to the development of various imaging devices that have enabled visualization and evaluation of the tear film and ocular surface, such as noninvasive tear break-up time measurements, anterior segment optical coherence tomography, confocal microscopy, meibography, interferometry, aberrometry, thermography, and tear film imager [10].

In this review, we aim to provide an overview of imaging devices for DED and discuss the application of the modalities for clinical practice and research for DED.

2. Noninvasive Tear Break-Up Time (NITBUT)

The TBUT reflects the stability and quality of the tear film, which is crucial for maintenance of ocular surface integrity and clear vision [1, 11]. Measurement of the TBUT has

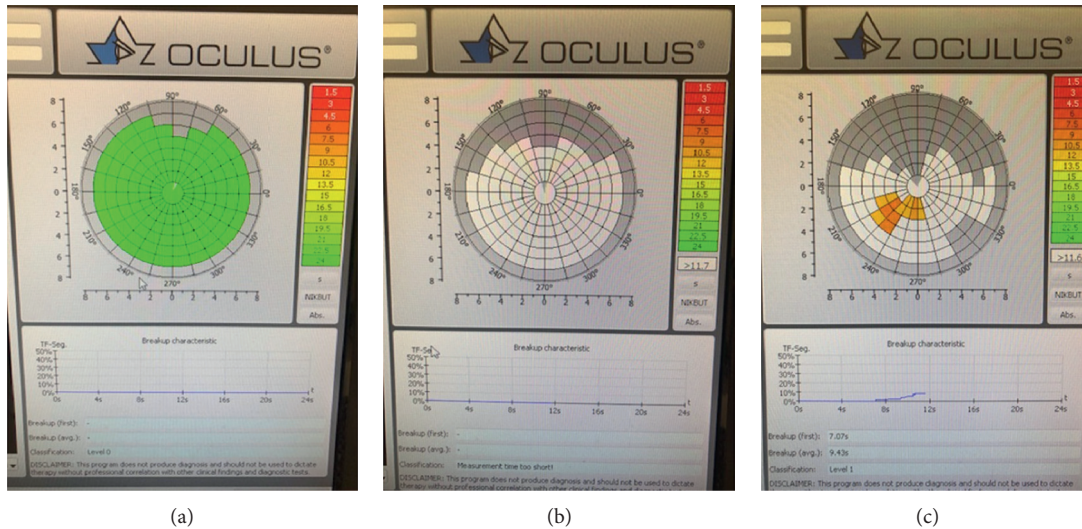


FIGURE 1: Noninvasive tear film break-up time (NIBUT) using the Oculus Keratograph 5 M (Oculus Optikgeräte GmbH, Wetzlar, Germany) presented as a tear film break-up color-code map. (a) No tear film break-up by 22–23 sec. (b) Immediately after tear film break-up. (c) At 7 sec after blinking.

generally been performed after fluorescein dye instillation [10]. However, the variability of the concentration and amount of the dye leads to reduced reliability and reproducibility [12]. Reflex tearing induced by fluorescein instillation can also lead to decreased accuracy [12]. Moreover, the fluorescein TBUT is unable to simultaneously evaluate the tear break-up across the entire corneal surface [10].

The noninvasive TBUT (NIBUT) was developed to overcome these limitations [10, 11]. Instead of using fluorescein dye instillation, the NIBUT measurement involves application of topographic systems to evaluate changes in a regularly patterned image projected onto the tear film that reflects compromised tear film integrity [11, 13]. Changes in reflected videokeratographic mires or grids from an illuminated placido disc are observed to detect tear film disruption (Figure 1) [13].

The NIBUT was shown to have a correlation with the dry eye symptom score and a good diagnostic value for DED [14, 15]. Dry Eye Workshop II (DEWS II) suggested the NIBUT with a cutoff value of ≤ 10 seconds as an indicator for diagnosis of DED with 82% to 84% sensitivity and 76% to 94% specificity [16]. The NIBUT was also revealed to be useful for monitoring of treatment response in DED [15].

Bandlitz et al. [17] recently reported that objective measurement of the NIBUT using the Keratograph 5 M (Oculus Optikgeräte GmbH, Wetzlar, Germany) showed good repeatability and reasonable agreement with subjective NIBUT measurement using the Tearscope Plus (Keeler, Windsor, UK), Polaris (bon Optic, Lübeck, Germany), and EasyTear Viewplus (Easytear, Rovereto, Italy), which also support viability of the NIBUT in the diagnosis and treatment of DED [15].

However, measurement of the NIBUT using two different topography platforms, the Keratograph 5 M and RT-7000 Auto Refractor-Keratometer (Tomey, Nagoya, Japan), showed poor agreement [18], suggesting that measured

values using different topographers with different algorithms should not be assessed interchangeably [10].

Although the NIBUT has a correlation with the fluorescein TBUT, its results should be carefully interpreted as it actually evaluates the thinning of the tear film, not the break-up of the full-thickness of the tear film [19].

3. Anterior Segment Optical Coherence Tomography

Anterior segment optical coherence tomography (AS-OCT) produces cross-sectional images of anterior segment structures by low-coherence interferometry [10, 20]. The technique enables measurement of tear meniscus parameters important for the diagnosis and monitoring of DED [16, 21–26], such as the tear meniscus height (TMH) and tear meniscus area (TMA) [10, 20, 27], without reflex tearing due to its noncontact nature and rapid image acquisition [11, 27].

Ibrahim et al. [22] showed that the TMH measured by time-domain (TD) OCT was correlated with strip meniscometry, corneal staining scores, and the Schirmer score. Spectral-domain (SD) OCT enabled higher resolution and faster image acquisition compared to TD-OCT, resulting in improved image quality with minimal artifact, as well as enhanced repeatability [27–29]. SD-OCT allowed improved sensitivity and specificity for the TMH and TMA as diagnostic biomarkers for DED compared to TD-OCT [11, 22]. SD-OCT findings also showed a close correlation with dry eye symptoms and the Schirmer score [24]. Qiu et al. [30] reported that diagnostic accuracy of SD-OCT was the highest for Sjögren's syndrome, moderately acceptable for non-Sjögren's aqueous-deficient DED, and the lowest for evaporative DED, suggesting the SD-OCT can be a viable option in the diagnosis of aqueous-deficient DED [30]. AS-OCT was also shown to be able to accurately measure the thickness of the overall tear film [31, 32]. Sher et al. [33]

demonstrated that AS-OCT may also be helpful for the quantitative evaluation of corneal epithelial erosion.

AS-OCT is also useful for monitoring of treatment responses in DED [34–36]. Measurement of the TMH using TD-OCT might be effective in monitoring tear meniscus changes after punctal occlusion [35]. SD-OCT was useful for quantifying the sequential changes of tear meniscus parameters after artificial tear instillation [37]. Nagahara et al. [38] showed that the TMH decreased with CL wear and increased after the instillation of diquafosol sodium. Although the TMH and TMA measured using AS-OCT may be valuable biomarkers for DED [11], factors including the time-from-blink, palpebral aperture, presence of conjunctivochalasis, and lid length should be considered in the interpretation of these tear meniscus measurements [39].

Swept source OCT (SS-OCT) enables acquisition of three-dimensional images, as well as an enhanced scanning speed and greater imaging depth compared to TD and SD-OCT [40], which allows the measurement of the tear meniscus volume (TMV) in addition to the TMH and TMA [41]. The TMH, TMV, and TMA measured using SS-OCT showed a correlation with the corneal staining score, BUT, and Schirmer score [25]. All three parameters showed the strongest correlation with the Schirmer score, suggesting that the tear meniscus parameters mostly reflect the quantity of tear fluid [25]. SS-OCT was also useful for evaluation of increased tear meniscus parameters after installation of eye drops, such as sodium hyaluronate, diquafosol, and rebamipide [34].

En-face OCT may be useful for observation of changes in the ocular surface, particularly due to its noncontact nature and large scan width [42]. Ghouali et al. [43] evaluated the palisade of Vogt using this device to determine the changes in the limbal anatomy in DED patients and showed that the visibility score of the palisades was lower in DED patients with a decreased score in accordance with the severity of DED [43].

AS-OCT is expected to be useful for the diagnosis of meibomian gland dysfunction (MGD), one of the most common causes of DED [44]. Hwang et al. [45] introduced a method of developing 3D images of meibomian glands (MGs) by reconstructing a series of tomograms of MGs captured by high-speed SD-OCT. SS-OCT can provide 3D high-resolution images of MG acini and ducts that cannot be observed by infrared meibography [46]. OCT meibography showed a decreased MG length and width in obstructive MGD, which correlated with ocular surface symptoms and signs [47]. However, so far, there are only preliminary data; thus, further studies are needed for clinical application of MG imaging using OCT [48].

4. In Vivo Confocal Microscopy

In vivo confocal microscopy (IVCM) a noninvasive method that provides real-time imaging of the ocular surface at the histologic level, which enables the evaluation of changes in cells reflecting ocular surface damage and inflammation, such as corneal epithelial cells, keratocytes, and dendritic

cells [1, 10, 49, 50]. IVCM also allows for observation of changes in the corneal nerve associated with DED [49].

In 2003, Tuominen et al. [51] reported that IVCM demonstrated reduced central corneal thickness, patchy alterations or irregularities in corneal epithelial cells, activated keratocytes reflected by abnormal hyper-reflectivity, and abnormal morphology of sub-basal nerve fiber bundles resembling nerve sprouting, suggesting active neural regeneration in Sjögren's syndrome [51]. Villani et al. [52] showed that IVCM revealed reduced density of the superficial epithelial cells, as well as decreased central corneal thickness in Sjögren's syndrome [52]. Other studies also showed decreased cell densities in the superficial corneal epithelial layer in both Sjögren's syndrome and non-Sjögren's DED [53–55].

Several studies showed decreased sub-basal nerve density, as well as increased number of beadings and nerve tortuosity in both Sjögren's syndrome and non-Sjögren's DED [50, 52, 54–57]. These changes in corneal nerves had correlation with corneal sensitivity, dry eye symptoms, and the Schirmer score [55–57]. By contrast, Zhang et al. [58] reported that IVCM showed increased corneal nerve density in Sjögren's syndrome. However, they also reported increased tortuosity in corneal nerves in Sjögren's syndrome [58]. Morphologic changes including beading and tortuosity may reflect an attempted regeneration of the corneal nerve [51, 52, 55] and suggested to be indices of metabolic activity of the sub-basal nerve plexus [57].

Dendritic cells are antigen-presenting cells that play an important role in ocular surface immunology [59]. In DED, desiccation stress causes proinflammatory stimulation on the ocular surface, which conceivably promotes migration and maturation of dendritic cells (Figure 2) [59]. Lin et al. [60] demonstrated increased dendritic cells in the central cornea in both Sjögren's syndrome and non-Sjögren's DED [60]. They also revealed an increased number of "activated" dendritic cells characterized by the increased dendrites [60]. Kheirkhah et al. [61] demonstrated marked increase in dendritic cell density at the sub-basal epithelial region in aqueous-deficient immunologic DED, such as Sjögren's syndrome and graft versus host disease (GVHD), compared with the aqueous-deficient nonimmunologic DED, evaporative DED, and controls [61].

IVCM was shown to be useful for the monitoring of treatment responses in DED [59]. Using an in vivo laser-scanning confocal microscope (Heidelberg Retina Tomograph, Rostock Corneal Module (HRT-RCM); Heidelberg Engineering GmG, Heidelberg, Germany), Villani et al. [62] demonstrated that the density of sub-basal dendritic cells and activated keratocytes significantly decreased after 4 weeks of treatment with topical steroid. Iaccheri et al. [63] reported increased cell density of the corneal intermediate epithelium, decreased activated keratocytes, and reduced tortuosity of corneal nerve fibers after 6 months of treatment with 0.05% topical cyclosporine in DED [63]. Levy et al. [64] also reported an increase in corneal sub-basal nerves and a decrease in dendritic cell density after 6 months of treatment with topical 0.05% cyclosporine in Sjögren's syndrome. IVCM also demonstrated decreased corneal basal epithelial

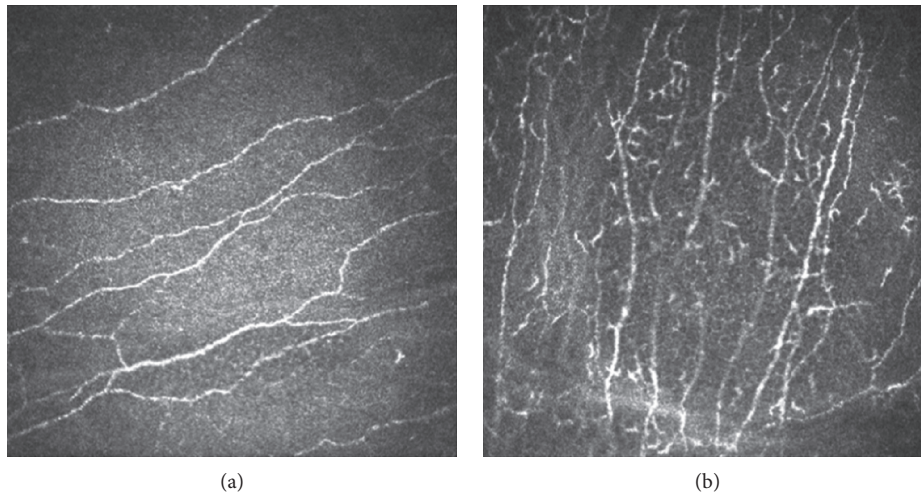


FIGURE 2: In vivo confocal microscopy. (a) Normal sub-basal nerve plexus. (b) Increased dendritic cells in dry eye disease.

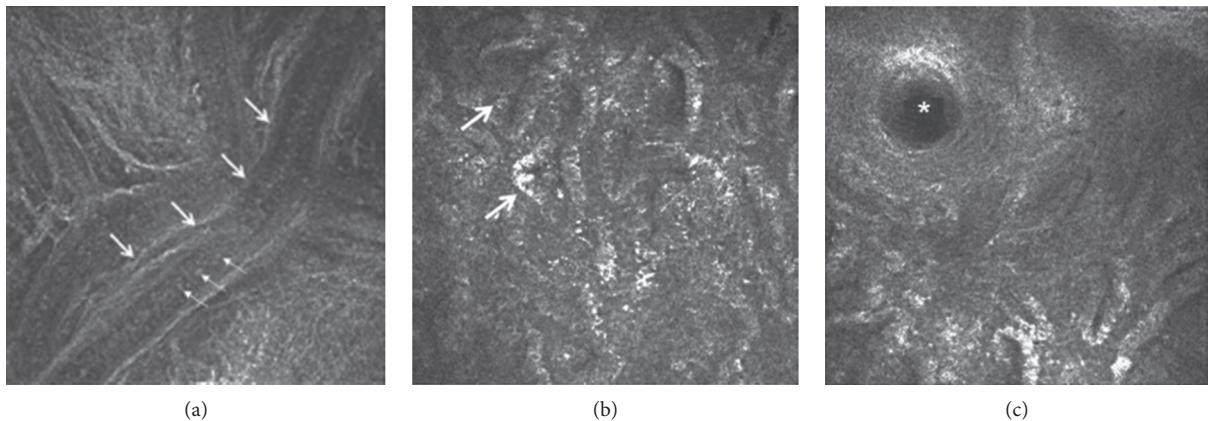


FIGURE 3: (a) In vivo confocal microscopy showing the meibomian gland duct of one of the meibomian glands of the upper eyelid. Large arrows show the wall of the terminal duct and small arrows show the meibum within. (b) The multiple irregular globular structures (arrows) indicate the acini of meibomian glands. (c) The orifice of a single meibomian gland is shown by the asterisk.

cell density and reduced numbers of nerve beadings after treatment with autologous serum eye drops [65, 66].

IVCM can also provide high-resolution imaging of the MGs; thus, it can be useful for the evaluation of the MG morphology at a cellular level, which is important for the diagnosis of MGD (Figure 3) [10, 67]. IVCM enabled determination of novel MG parameters, e.g., meibomian gland acinar unit density (MGAUD), shortest diameter (MGASD) and longest diameter (MGALD), and inflammatory cell density [67, 68]. These parameters have a significant correlation with tear film parameters, ocular surface signs, and MG expressibility [67, 68].

IVCM with HRT-RCM demonstrated morphologic alterations in MGD, such as enlargement of glandular acinar units, extensive periglandular inflammatory cell infiltration, and hyperkeratinization of the ductal epithelium [67–69]. In severe MGD, atrophy in MGs with extensive periglandular fibrosis was observed [70].

Ibrahim et al. [68] revealed that MGD was associated with lower MGAUD, larger MGASD and MGALD, and

higher inflammatory cell density. Matsumoto et al. [70] also reported similar findings and showed the acinar unit density and diameters had association with the severity of MG dropout and expressibility. They also showed a significant reduction in the inflammatory cell density of MGs after treatment with lid hygiene, topical 0.5% levofloxacin and 0.1% fluorometholone, and oral 100 mg minocycline [70]. Ban et al. [71] demonstrated that patients with DED/GVHD had significantly lower MGAUD, shorter MGASD and MGALD, and a higher fibrosis grade compared to those with non-DED/non-GVHD. Villani et al. [72] revealed that patients with Sjögren's syndrome had greater acinar density, shorter diameters, higher density of periglandular inflammatory cells, and lower secretion reflectivity compared with those with MGD.

However, IVCM has a limitation that it is not capable of cellular and tissue phenotyping, and analysis is only based on morphology and reflectivity [48]. The small field of view (<0.25 mm [2]) is also a major limitation of the device [48].

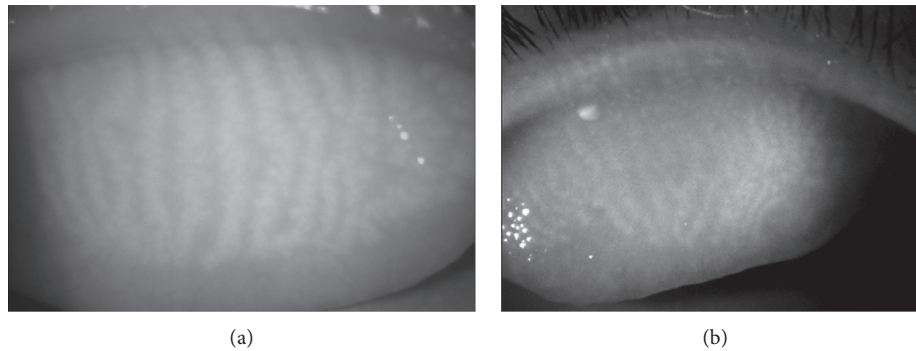


FIGURE 4: (a) Infrared meibography showing relatively normal meibomian glands in the upper eyelid. Brighter areas indicate glandular areas, whereas darker areas indicate intergland tissue. (b) Meibography showing slight atrophy of the meibomian glands in the proximal margin of the tarsal plate. The abnormal area is greyish without typical whitish tracks that represent the glands.

5. Infrared Meibography

Noncontact infrared meibography based on combined transillumination with infrared photography provides two-dimensional silhouette of MGs [10, 73]. The technique has been widely used for the evaluation of MG dropout since its introduction in 2008, as it can provide improved image quality with a short acquisition time and minimal patient discomfort (Figure 4) [74]. In meibography, healthy meibum is visualized as a light area due to its autofluorescence [11, 73]. Dark areas in the MG conceivably indicate loss of acinar tissue or an altered meibum condition, which is determined as MG dropout [73, 75].

Among various grading scales proposed for MG dropout [76], the Gestalt grading scale and meiboscale were recommended by the MGD Workshop [74, 75]. In the Gestalt grading scale, grading of each lid is performed on a scale from 1 to 4, based on the ratio of partial glands as follows [11]: grade 1 = no partial glands; grade 2 = less than 25% partial glands; grade 3 = 25% to 75% partial glands; and grade 4 = greater than 75% partial glands [11]. In the meiboscale, each lid is graded based on the ratio of MG dropout: grade 0 = no loss of MGs; grade 1 = area loss $\leq 25\%$; grade 2 = area loss $\leq 50\%$; grade 3 = area loss $\leq 75\%$; and grade 4: area loss $\leq 100\%$ [77].

Recently, continuous grading scales using semi-automated software that automatically calculates the ratio of the area of MG loss to the total area of the eyelid have been developed [11, 78]. As the ratio of MG dropout is expressed as numeric values ranging from 0 to 100, the continuous scales may be advantageous for evaluating subtle changes that may not be detected using categorical grading scales and can facilitate the determination of efficacy of treatment, such as intraductal probing and eyelid warming [11, 79, 80].

The area of MG dropout showed a positive correlation with the meibum grade [81, 82]. Both the severity of MGD and the percentage of MG dropout had a correlation with the TBUT, dry eye symptom score, and corneal stain score [83]. The ductal length and acini area measured by meibography were correlated with the tear film, corneal stain score, and meibum level [84]. Arita et al. [85] demonstrated the correlation between MG dropout and Schirmer's score in MGD, suggesting that tear fluid production may increase to

compensate for tear film instability due to MGD. MG dropout measured using infrared meibography has proven to be useful for differential diagnosis of MGD and aqueous deficiency DED [86].

However, infrared meibography has a limitation that it cannot provide three-dimensional images of the deeper structures [10]. Hence, the MG dropout evaluated by infrared meibography should be carefully interpreted [10]. Additional information using AS-OCT or IVCM might be helpful for the diagnosis and monitoring of MGD.

6. Interferometry

Tear interferometry is a noninvasive method for the investigation of the tear lipid layer by visualization of the reflection of light at the lipid-aqueous interface of the tear film [10, 87, 88]. Interferometry allows objective evaluation of tear film properties, such as lipid layer thickness, break-up characteristics and changes in thickness of the tear film, its distribution, and wetting patterns with sequential blinking [81, 89, 90].

Yokoi et al. [91] showed that grading of the lipid layer interference pattern had a significant correlation with the corneal staining score and TBUT. Goto et al. [92] developed a tear interference color chart for the DR-1 α interferometer (Kowa, Nagoya, Japan), which can be useful for converting tear interference color information to the lipid layer thickness (LLT) [92]. Subsequently, Arita et al. [93] showed that the DR-1 α interferometer could measure the TMH as reliably as SS-OCT and showed that the interferometric TMH had correlation with Schirmer's score. Arita et al. [88] also described a difference in interferometric patterns among aqueous-deficient DED, MGD, and normal control on the DR-1 α interferometry, suggesting that the device can be helpful for differential diagnosis of subtypes of DED.

The DR-1 α interferometer is also capable of kinetic analysis of spread and stability of the lipid layer [94]. MGD was associated with significantly increased lipid spread time [94]. The kinetic analysis can also be helpful for evaluation of the improvement of the lipid layer after treatment, e.g., low-dose lipid application on the lid margin or punctal occlusion [95, 96].

The LipiView II (LVII) ocular surface interferometer (TearScience, Johnson and Johnson Vision, Jacksonville, FL, USA) is capable of providing quantitative information of the LLT, as well as images of MGs using a patented Lid Everter and infrared diodes for eversion and illumination of the eyelid [10, 97]. Ji et al. [81] showed that LLT measured using the LVII had a significant correlation with the TBUT, MGD grade, and MG dropout, suggesting that it can be an alternative to traditional dry eye tests. Eom et al. [98] also revealed that LLT measured with LVII was negatively correlated to MG loss and obstructive MGD was associated with lower LLT [98]. LLT may reflect the changes in meibum secretion and be helpful for differential diagnosis of MGD [10]; LLT would be increased in hypersecretory MGD and decreased in obstructive MGD [99]. However, the LLT should be carefully interpreted as it can be affected by factors, such as age, sex, and ocular surgical history [100].

7. Wavefront and Double-Pass Aberrometry

DED is often associated with complaints including blurred vision, glare, and fluctuating vision with blinking, which is difficult to measure by conventional visual acuity testing [19, 101]. As the air-tear film interface forms the first refractive component of the eye, irregularity of the tear film in DED may cause decreased optical quality [10].

Tear film instability increases higher-order aberrations (HOAs) and ocular forward light scattering, resulting in “fluctuating vision with blinking” and “glare,” respectively [101]. Damage in the central cornea, i.e., the overlying optical zone, is associated with increased HOAs and corneal backward light scattering, leading to “blurred vision” [101].

Quantification of HOA using wavefront sensors, such as the Shack–Hartmann aberrometer, allows evaluation of optical aberrations associated with DED [102–104]. Wavefront sensing has shown that break-up of the tear film was associated with increased HOAs both in photopic and scotopic conditions [102]. Sequential measurement of HOAs demonstrated that superficial punctate keratopathy may aggravate both baseline HOAs and sequential postblink changes in HOAs in patients with DED [105]. Sequential wavefront measurements in eyes with a short TBUT have shown that a prolonged blink interval leads to increased HOAs with a marked upward curve after blinking, suggesting that suppressed blinking, such as while working with a video display terminal, can result in reduced optical quality [106]. Denoyer et al. [107] also reported a progressive increase in postblink HOAs in patients with DED and the correlation of the changes in HOAs with the OSDI score and TBUT [107].

Evaluation of the objective scatter index (OSI) obtained using the double-pass image of a point source projected on the retina enables the quantification of the ocular light scattering that cannot be measured using conventional wavefront sensors [104, 108, 109]. Using the double-pass aberrometer, Tan et al. [110] showed an increase in the OSI in patients with DED and the correlation between the OSI change and severity of DED. The rate of change in the OSI was correlated to the corneal staining score [111]. Koh et al.

[112] revealed that DED was associated with greater ocular forward light scattering and corneal backward light scattering. Superficial punctate keratopathy overlying the optical zone was related to increased corneal backward light scattering [112].

An improvement in HOA and light scattering was reported after instilling artificial tear drops in patients with DED [113]. Serial examinations showed increased HOAs and forward light scattering immediately after the instillation of a highly viscous 0.3% sodium hyaluronate solution and the instillation of 2% rebamipide suspension, respectively, accounting for a temporal reduction in optical quality after instillation of eye drops with high viscosity or suspensibility [114].

8. Thermography

Infrared thermography is used to measure the amount of infrared radiation emitted from the ocular surface using an infrared thermal camera; thus, it allows a noninvasive evaluation of the changes in the ocular surface temperature (OST) caused by tear fluid evaporation [10, 115]. Decrease in the OST had a correlation with the TBUT and NIBUT [116, 117], conceivably, because tear film instability facilitates tear fluid evaporation and heat loss [116]. Su et al. [115] demonstrated that the OST difference 3 seconds after blinking was correlated with the TMH and Schirmer score.

Using a thermographic device (Ocular Surface Thermographer; OST, Tomey, Nagoya, Japan), Kamao et al. [117] reported that DED was associated with a greater decrease in the OST at 10 seconds after eye opening and suggested that changes in the OST could be an indicator for DED. Tan et al. [118] also showed that the temperature of the extreme nasal conjunctiva at 5 and 10 seconds after eye opening was a good detector for DED. Arita et al. [119] revealed that obstructive MGD was associated with lower surface temperature of the tarsal conjunctiva, which might increase the viscosity of the meibum and result in obstruction of the glands [119].

9. Tear Film Imager

The tear film imager (TFI) is a new technology that provides real-time images of the mucoaqueous and lipid tear layers [120]. Using spectral interference technology, this instrument enables noninvasive measurement of parameters including the thickness of mucoaqueous and lipid layers, thickness change rate, and the break-up time with a large field of view and nanometer axial resolution [120, 121].

Segev et al. [121] recently revealed that the device can reproducibly measure the mucoaqueous thickness which correlates with the Schirmer score. Lipid break-up time measurement with the TFI had a correlation with the TBUT [121]. DED was associated with lower mucoaqueous thickness and shorter lipid break-up time [121]. Cohen et al. [122] demonstrated that the TFI was capable of creating detailed maps of the lipid layer thickness and quantifying the lipid map uniformity due to its nanometer thickness resolution, which could be helpful for the diagnosis and treatment of DED.

10. Conclusions

Advances in ocular imaging technology have enabled objective and reproducible evaluation of ocular surface change, tear film parameters, and optical quality associated with DED; thus, they can be useful for diagnosis and management of the disease, as well as elucidation of its pathogenesis [123].

Studies have indicated the efficacy of various imaging modalities, i.e., the NIBUT for evaluation of the TBUT, AS-OCT for quantification of tear meniscus parameters, IVCN for high-resolution visualization of the ocular surface, infrared meibography for evaluation of MG dropout, interferometry for the measurement of the tear lipid layer, wavefront aberrometry and the OSI for the quantification of optical quality, thermography for the detection of changes in the OST, and the TFI for the evaluation of mucoaqueous and lipid layers [10].

With technological developments, these imaging devices are expected to provide more precise and accurate information on structural and functional changes associated with DED. Further studies are, therefore, warranted for clinical application of these devices and establishment of guidelines for the use of the modalities for diagnosis and management of DED.

Conflicts of Interest

The authors declare no conflicts of interest.

Acknowledgments

This study was conducted with the support of a research grant of Kangwon Institute for Unification Studies, Kangwon National University, in 2019, and the Basic Science Research Program through the National Research Foundation of Korea (NRF) funded by the Ministry of Education (Grant no. NRF-2017R1D1A1B03029983).

References

- [1] J. P. Craig, K. K. Nichols, E. K. Akpek et al., "TFOS DEWS II definition and classification report," *The Ocular Surface*, vol. 15, no. 3, pp. 276–283, 2017.
- [2] S. B. Han, J. Y. Hyon, S. J. Woo et al., "Prevalence of dry eye disease in an elderly Korean population," *Archives of Ophthalmology*, vol. 129, no. 5, pp. 633–638, 2011.
- [3] P.-Y. Lin, S.-Y. Tsai, C.-Y. Cheng, J.-H. Liu, P. Chou, and W.-M. Hsu, "Prevalence of dry eye among an elderly Chinese population in Taiwan: the Shihpai eye study," *Ophthalmology*, vol. 110, no. 6, pp. 1096–1101, 2003.
- [4] B. Miljanovic, K. A. Trivedi, M. R. Dana et al., "Relation between dietary $n-3$ and $n-6$ fatty acids and clinically diagnosed dry eye syndrome in women," *The American Journal of Clinical Nutrition*, vol. 82, no. 4, pp. 887–893, 2005.
- [5] M. Uchino, D. A. Schaumberg, M. Dogru et al., "Prevalence of dry eye disease among Japanese visual display terminal users," *Ophthalmology*, vol. 115, no. 11, pp. 1982–1988, 2008.
- [6] C. Baudouin, M. Irkec, E. M. Messmer et al., "Clinical impact of inflammation in dry eye disease: proceedings of the ODISSEY group meeting," *Acta Ophthalmologica*, vol. 96, no. 2, pp. 111–109, 2017.
- [7] S. B. Han, H. K. Yang, J. Y. Hyon, and W. R. Wee, "Association of dry eye disease with psychiatric or neurological disorders in elderly patients," *Clinical Interventions in Aging*, vol. 12, pp. 785–792, 2017.
- [8] J. Vehof, D. Kozareva, P. G. Hysi, and C. J. Hammond, "Prevalence and risk factors of dry eye disease in a British female cohort," *British Journal of Ophthalmology*, vol. 98, no. 12, pp. 1712–1717, 2014.
- [9] K. K. Nichols, G. L. Mitchell, and K. Zadnik, "The repeatability of clinical measurements of dry eye," *Cornea*, vol. 23, no. 3, pp. 272–285, 2004.
- [10] T. C. Y. Chan, K. H. Wan, K. C. Shih, and V. Jhanji, "Advances in dry eye imaging: the present and beyond," *British Journal of Ophthalmology*, vol. 102, no. 3, pp. 295–301, 2018.
- [11] W. W. Binotti, B. Bayraktutar, M. C. Ozmen, S. M. Cox, and P. Hamrah, "A review of imaging biomarkers of the ocular surface," *Eye Contact Lens*, vol. 46, no. 2, pp. 84–105, 2019.
- [12] M. E. Johnson and P. J. Murphy, "The Effect of instilled fluorescein solution volume on the values and repeatability of TBUT measurements," *Cornea*, vol. 24, no. 7, pp. 811–817, 2005.
- [13] T. Goto, X. Zheng, S. Okamoto, and Y. Ohashi, "Tear film stability analysis system: introducing a new application for videokeratography," *Cornea*, vol. 23, no. 8, pp. S65–S70, 2004.
- [14] D. G. Fuller, K. Potts, and J. Kim, "Noninvasive tear breakup times and ocular surface disease," *Optometry and Vision Science*, vol. 90, no. 10, pp. 1086–1091, 2013.
- [15] P. Prabhasawat, N. Tesavibul, and W. Mahawong, "A randomized double-masked study of 0.05% cyclosporine ophthalmic emulsion in the treatment of meibomian gland dysfunction," *Cornea*, vol. 31, no. 12, pp. 1386–1393, 2012.
- [16] J. S. Wolffsohn, R. Arita, R. Chalmers et al., "TFOS DEWS II diagnostic methodology report," *The Ocular Surface*, vol. 15, no. 3, pp. 539–574, 2017.
- [17] S. Bandlitz, B. Peter, T. Pflugi et al., "Agreement and repeatability of four different devices to measure non-invasive tear breakup time (NIBUT)," *Contact Lens and Anterior Eye*, vol. 42, no. 6, p. e3, 2020.
- [18] R. Lee, S. Yeo, H. T. Aung, and L. Tong, "Agreement of noninvasive tear break-up time measurement between Tomey RT-7000 Auto refractor-keratometer and Oculus Keratograph 5M," *Clinical Ophthalmology*, vol. 10, pp. 1785–1790, 2016.
- [19] T. Kojima, M. Dogru, M. Kawashima, S. Nakamura, and K. Tsubota, "Advances in the diagnosis and treatment of dry eye," *Progress in Retinal and Eye Research*, p. 100842, 2020, In press.
- [20] D. Huang, E. Swanson, C. Lin et al., "Optical coherence tomography," *Science*, vol. 254, no. 5035, pp. 1178–1181, 1991.
- [21] J. C. Mainstone, A. S. Bruce, and T. R. Golding, "Tear meniscus measurement in the diagnosis of dry eye," *Current Eye Research*, vol. 15, no. 6, pp. 653–661, 1996.
- [22] O. M. A. Ibrahim, M. Dogru, Y. Takano et al., "Application of visante optical coherence tomography tear meniscus height measurement in the diagnosis of dry eye disease," *Ophthalmology*, vol. 117, no. 10, pp. 1923–1929, 2010.
- [23] S. Zhou, Y. Li, A. T.-H. Lu et al., "Reproducibility of tear meniscus measurement by Fourier-domain optical coherence tomography: a pilot study," *Ophthalmic Surgery, Lasers, and Imaging*, vol. 40, no. 5, pp. 442–447, 2009.
- [24] P. Nguyen, D. Huang, Y. Li et al., "Correlation between optical coherence tomography-derived assessments of lower

- tear meniscus parameters and clinical features of dry eye disease," *Cornea*, vol. 31, no. 6, pp. 680–685, 2012.
- [25] R. Akiyama, T. Usui, and S. Yamagami, "Diagnosis of dry eye by tear meniscus measurements using anterior segment swept source optical coherence tomography," *Cornea*, vol. 34, no. 11, pp. S115–S120, 2015.
- [26] X. Qiu, L. Gong, X. Sun, and H. Jin, "Age-related variations of human tear meniscus and diagnosis of dry eye with Fourier-domain anterior segment optical coherence tomography," *Cornea*, vol. 30, no. 5, pp. 543–549, 2011.
- [27] J. L. B. Ramos, Y. Li, and D. Huang, "Clinical and research applications of anterior segment optical coherence tomography - a review," *Clinical & Experimental Ophthalmology*, vol. 37, no. 1, pp. 81–89, 2009.
- [28] H. H. Chan, Y. Zhao, T. A. Tun, and L. Tong, "Repeatability of tear meniscus evaluation using spectral-domain Cirrus HD-OCT and time-domain Visante OCT," *Contact Lens and Anterior Eye*, vol. 38, no. 5, pp. 368–372, 2015.
- [29] H. Canan, R. Altan-Yaycioglu, B. Ulas, S. Sizmaz, and M. Coban-Karatas, "Interexaminer reproducibility of optical coherence tomography for measuring the tear film meniscus," *Current Eye Research*, vol. 39, no. 12, pp. 1145–1150, 2014.
- [30] X. Qiu, L. Gong, Y. Lu, H. Jin, and M. Robitaille, "The diagnostic significance of Fourier-domain optical coherence tomography in Sjögren syndrome, aqueous tear deficiency and lipid tear deficiency patients," *Acta Ophthalmologica*, vol. 90, no. 5, pp. e359–e366, 2012.
- [31] Y. Bai, W. Ngo, B. Gu, Y. Zhang, and J. J. Nichols, "An imaging system integrating optical coherence tomography and interferometry for in vivo measurement of the thickness and dynamics of the tear film," *BioMedical Engineering OnLine*, vol. 17, no. 1, p. 164, 2018.
- [32] S. Szegedi, U. Scheschy, D. Schmidl et al., "Effect of single instillation of two hyaluronic acid-based topical lubricants on tear film thickness in patients with dry eye syndrome," *Journal of Ocular Pharmacology and Therapeutics*, vol. 34, no. 9, pp. 605–611, 2018.
- [33] I. Sher, A. Tzameret, A. M. Szalapak et al., "Multimodal assessment of corneal erosions using optical coherence tomography and automated grading of fluorescein staining in a rabbit dry eye model," *Translational Vision Science & Technology*, vol. 8, no. 1, p. 27, 2019.
- [34] R. Akiyama-Fukuda, T. Usui, T. Yoshida, and S. Yamagami, "Evaluation of tear meniscus dynamics using anterior segment swept-source optical coherence tomography after topical solution instillation for dry eye," *Cornea*, vol. 35, no. 5, pp. 654–658, 2016.
- [35] O. M. A. Ibrahim, M. Dogru, T. Kojima et al., "OCT assessment of tear meniscus after punctal occlusion in dry eye disease," *Optometry and Vision Science*, vol. 89, no. 5, pp. E770–E776, 2012.
- [36] P. E. Napoli, G. M. Satta, F. Coronella, and M. Fossarello, "Spectral-domain optical coherence tomography study on dynamic changes of human tears after instillation of artificial tears," *Investigative Ophthalmology & Visual Science*, vol. 55, no. 7, pp. 4533–4540, 2014.
- [37] M. C. Bujak, S. Yiu, X. Zhang, Y. Li, and D. Huang, "Serial measurement of tear meniscus by FD-OCT after instillation of artificial tears in patients with dry eyes," *Ophthalmic Surgery, Lasers, and Imaging*, vol. 42, no. 4, pp. 308–313, 2011.
- [38] Y. Nagahara, S. Koh, N. Maeda, K. Nishida, and H. Watanabe, "Prominent decrease of tear meniscus height with contact lens wear and efficacy of eye drop instillation," *Eye & Contact Lens: Science & Clinical Practice*, vol. 41, no. 5, pp. 318–322, 2015.
- [39] T. C. Chan, C. Ye, P. K. Ng, E. Y. M. Li, H. K. L. Yuen, and V. Jhanji, "Change in tear film lipid layer thickness, corneal thickness, volume and topography after superficial cauterization for conjunctivochalasis," *Scientific Reports*, vol. 5, no. 1, p. 12239, 2015.
- [40] M. T. Leite, H. L. Rao, L. M. Zangwill, R. N. Weinreb, and F. A. Medeiros, "Comparison of the diagnostic accuracies of the spectralis, cirrus, and RTVue optical coherence tomography devices in glaucoma," *Ophthalmology*, vol. 118, no. 7, pp. 1334–1339, 2011.
- [41] R. Fukuda, T. Usui, T. Miyai, S. Yamagami, and S. Amano, "Tear meniscus evaluation by anterior segment swept-source optical coherence tomography," *American Journal of Ophthalmology*, vol. 155, no. 4, pp. 620–624, 2013.
- [42] R. Tahiri Joutei Hassani, H. Liang, M. El Sanharawi et al., "En-face optical coherence tomography as a novel tool for exploring the ocular surface: a pilot comparative study to conventional B-scans and in vivo confocal microscopy," *The Ocular Surface*, vol. 12, no. 4, pp. 285–306, 2014.
- [43] W. Ghoulali, R. Tahiri Joutei Hassani, Z. Djerada et al., "In vivo imaging of palisades of Vogt in dry eye versus normal subjects using en-face spectral-domain optical coherence tomography," *PLoS One*, vol. 12, no. 11, Article ID e0187864, 2017.
- [44] C. Baudouin, E. M. Messmer, P. Aragona et al., "Revisiting the vicious circle of dry eye disease: a focus on the pathophysiology of meibomian gland dysfunction," *British Journal of Ophthalmology*, vol. 100, no. 3, pp. 300–306, 2016.
- [45] H. S. Hwang, J. G. Shin, B. H. Lee et al., "In Vivo 3D meibography of the human eyelid using real time imaging fourier-domain OCT," *PLoS One*, vol. 8, no. 6, Article ID e67143, 2013.
- [46] Y.-S. Yoo, K.-S. Na, D. Y. Kim, S.-W. Yang, and C.-K. Joo, "Morphological evaluation for diagnosis of dry eye related to meibomian gland dysfunction," *Experimental Eye Research*, vol. 163, pp. 72–77, 2017.
- [47] Q. Liang, Z. Pan, M. Zhou et al., "Evaluation of optical coherence tomography meibography in patients with obstructive meibomian gland dysfunction," *Cornea*, vol. 34, no. 10, pp. 1193–1199, 2015.
- [48] E. Villani and R. Arita, "Imaging of meibomian glands: from bench to bedside and back," *Eye*, vol. 33, no. 5, pp. 695–697, 2019.
- [49] E. Villani, F. Bonsignore, E. Cantalamessa, M. Serafino, and P. Nucci, "Imaging biomarkers for dry eye disease," *Eye & Contact Lens: Science & Clinical Practice*, vol. 46, pp. 141–145, 2019.
- [50] A. Alhatem, B. Cavalcanti, and P. Hamrah, "In vivo confocal microscopy in dry eye disease and related conditions," *Seminars in Ophthalmology*, vol. 27, no. 5-6, pp. 138–148, 2012.
- [51] I. S. J. Tuominen, Y. T. Konttinen, M. H. Vesaluoma, J. A. O. Moilanen, M. Helinto, and T. M. T. Tervo, "Corneal innervation and morphology in primary Sjögren's syndrome," *Investigative Ophthalmology & Visual Science*, vol. 44, no. 6, pp. 2545–2549, 2003.
- [52] E. Villani, D. Galimberti, F. Viola, C. Mapelli, and R. Ratiglia, "The cornea in Sjögren's syndrome: an in vivo confocal study," *Investigative Ophthalmology & Visual Science*, vol. 48, no. 5, pp. 2017–2022, 2007.

- [53] X. Zhang, Q. Chen, W. Chen, L. Cui, H. Ma, and F. Lu, "Tear dynamics and corneal confocal microscopy of subjects with mild self-reported office dry eye," *Ophthalmology*, vol. 118, no. 5, pp. 902–907, 2011.
- [54] B. Erdélyi, R. Kraak, A. Zhivov, R. Guthoff, and J. Németh, "In vivo confocal laser scanning microscopy of the cornea in dry eye," *Graefe's archive for clinical and experimental ophthalmology*, vol. 245, no. 1, pp. 39–44, 2007.
- [55] J. M. B. T. del Castillo, M. A. S. Wasfy, C. Fernandez, and J. Garcia-Sanchez, "An in vivo confocal masked study on corneal epithelium and subbasal nerves in patients with dry eye," *Investigative Ophthalmology & Visual Science*, vol. 45, no. 9, pp. 3030–3035, 2004.
- [56] E. Villani, F. Magnani, F. Viola et al., "In vivo confocal evaluation of the ocular surface morpho-functional unit in dry eye," *Optometry and Vision Science*, vol. 90, no. 6, pp. 576–586, 2013.
- [57] J. M. Benitez-Del-Castillo, M. C. Acosta, M. A. Wassfi et al., "Relation between corneal innervation with confocal microscopy and corneal sensitivity with noncontact esthesiometry in patients with dry eye," *Investigative Ophthalmology & Visual Science*, vol. 48, no. 1, pp. 173–181, 2007.
- [58] M. Zhang, J. Chen, L. Luo, Q. Xiao, M. Sun, and Z. Liu, "Altered corneal nerves in aqueous tear deficiency viewed by in vivo confocal microscopy," *Cornea*, vol. 24, no. 7, pp. 818–824, 2005.
- [59] Y. Matsumoto and O. M. A. Ibrahim, "Application of in vivo confocal microscopy in dry eye disease," *Investigative Ophthalmology & Visual Science*, vol. 59, no. 14, p. 41, 2018.
- [60] H. Lin, W. Li, N. Dong et al., "Changes in corneal epithelial layer inflammatory cells in aqueous tear-deficient dry eye," *Investigative Ophthalmology & Visual Science*, vol. 51, no. 1, pp. 122–128, 2010.
- [61] A. Kheirkhah, R. Rahimi Darabad, A. Cruzat et al., "Corneal epithelial immune dendritic cell alterations in subtypes of dry eye disease: a pilot in vivo confocal microscopic study," *Investigative Ophthalmology & Visual Science*, vol. 56, no. 12, pp. 7179–7185, 2015.
- [62] E. Villani, E. Garoli, V. Termine, F. Pichi, R. Ratiglia, and P. Nucci, "Corneal confocal microscopy in dry eye treated with corticosteroids," *Optometry and Vision Science*, vol. 92, no. 9, pp. e290–e295, 2015.
- [63] B. Iaccheri, G. Torroni, C. Cagini et al., "Corneal confocal scanning laser microscopy in patients with dry eye disease treated with topical cyclosporine," *Eye*, vol. 31, no. 5, pp. 788–794, 2017.
- [64] O. Levy, A. Labbé, V. Borderie et al., "Increased corneal sub-basal nerve density in patients with Sjögren syndrome treated with topical cyclosporine A," *Clinical & Experimental Ophthalmology*, vol. 45, no. 5, pp. 455–463, 2017.
- [65] G. Mahelkova, K. Jirsova, P. Seidler Stangova et al., "Using corneal confocal microscopy to track changes in the corneal layers of dry eye patients after autologous serum treatment," *Clinical and Experimental Optometry*, vol. 100, no. 3, pp. 243–249, 2017.
- [66] F. Semeraro, E. Forbice, G. Nascimbeni et al., "Effect of autologous serum eye drops in patients with Sjögren syndrome-related dry eye: clinical and in vivo confocal microscopy evaluation of the ocular surface," *In Vivo*, vol. 30, no. 6, pp. 931–938, 2016.
- [67] Y. Matsumoto, E. A. Sato, O. M. Ibrahim, M. Dogru, and K. Tsubota, "The application of in vivo laser confocal microscopy to the diagnosis and evaluation of meibomian gland dysfunction," *Molecular Vision*, vol. 14, pp. 1263–1271, 2008.
- [68] O. M. A. Ibrahim, Y. Matsumoto, M. Dogru et al., "The efficacy, sensitivity, and specificity of in vivo laser confocal microscopy in the diagnosis of meibomian gland dysfunction," *Ophthalmology*, vol. 117, no. 4, pp. 665–672, 2010.
- [69] E. Villani, G. Ceresara, S. Beretta, F. Magnani, F. Viola, and R. Ratiglia, "In vivo confocal microscopy of meibomian glands in contact lens wearers," *Investigative Ophthalmology & Visual Science*, vol. 52, no. 8, pp. 5215–5219, 2011.
- [70] Y. Matsumoto, Y. Shigeno, E. A. Sato et al., "The evaluation of the treatment response in obstructive meibomian gland disease by in vivo laser confocal microscopy," *Graefe's Archive for Clinical and Experimental Ophthalmology*, vol. 247, no. 6, pp. 821–829, 2009.
- [71] Y. Ban, Y. Ogawa, O. M. Ibrahim et al., "Morphologic evaluation of meibomian glands in chronic graft-versus-host disease using in vivo laser confocal microscopy," *Molecular Vision*, vol. 17, pp. 2533–2543, 2011.
- [72] E. Villani, S. Beretta, M. De Capitani, D. Galimberti, F. Viola, and R. Ratiglia, "In vivo confocal microscopy of meibomian glands in Sjögren's syndrome," *Investigative Ophthalmology & Visual Science*, vol. 52, no. 2, pp. 933–939, 2011.
- [73] R. Arita, "Meibography: a Japanese perspective," *Investigative Ophthalmology & Visual Science*, vol. 59, no. 14, pp. DES48–DES55, 2018.
- [74] R. Arita, K. Itoh, K. Inoue, and S. Amano, "Noncontact infrared meibography to document age-related changes of the meibomian glands in a normal population," *Ophthalmology*, vol. 115, no. 5, pp. 911–915, 2008.
- [75] G. Geerling, J. Tauber, C. Baudouin et al., "The international workshop on meibomian gland dysfunction: report of the subcommittee on management and treatment of meibomian gland dysfunction," *Investigative Ophthalmology & Visual Science*, vol. 52, no. 4, pp. 2050–2064, 2011.
- [76] J. J. Nichols, D. A. Berntsen, G. L. Mitchell, and K. K. Nichols, "An assessment of grading scales for meibography images," *Cornea*, vol. 24, no. 4, pp. 382–388, 2005.
- [77] H. Pult and B. Riede-Pult, "Comparison of subjective grading and objective assessment in meibography," *Contact Lens and Anterior Eye*, vol. 36, no. 1, pp. 22–27, 2013.
- [78] A. Tomlinson, A. J. Bron, D. R. Korb et al., "The international workshop on meibomian gland dysfunction: report of the diagnosis subcommittee," *Investigative Ophthalmology & Visual Science*, vol. 52, no. 4, pp. 2006–2049, 2011.
- [79] S. L. Maskin, "Intraductal meibomian gland probing relieves symptoms of obstructive meibomian gland dysfunction," *Cornea*, vol. 29, no. 10, pp. 1145–1152, 2010.
- [80] R. Arita, N. Morishige, R. Shirakawa, Y. Sato, and S. Amano, "Effects of eyelid warming devices on tear film parameters in normal subjects and patients with meibomian gland dysfunction," *The Ocular Surface*, vol. 13, no. 4, pp. 321–330, 2015.
- [81] Y. W. Ji, J. Lee, H. Lee, K. Y. Seo, E. K. Kim, and T.-I. Kim, "Automated measurement of tear film dynamics and lipid layer thickness for assessment of non-Sjögren dry eye syndrome with meibomian gland dysfunction," *Cornea*, vol. 36, no. 2, pp. 176–182, 2017.
- [82] H. M. Kim, Y. Eom, and J. S. Song, "The relationship between morphology and function of the meibomian glands," *Eye & Contact Lens: Science & Clinical Practice*, vol. 44, no. 1, pp. 1–5, 2018.
- [83] D. Gulmez Sevim, K. Gumus, and M. Unlu, "Reliable, noncontact imaging tool for the evaluation of meibomian gland function: sirius meibography," *Eye & Contact Lens: Science & Clinical Practice*, vol. 46, pp. 135–140, 2020.

- [84] Y. Ban, S. Shimazaki-Den, K. Tsubota, and J. Shimazaki, "Morphological evaluation of meibomian glands using noncontact infrared meibography," *The Ocular Surface*, vol. 11, no. 1, pp. 47–53, 2013.
- [85] R. Arita, N. Morishige, S. Koh et al., "Increased tear fluid production as a compensatory response to meibomian gland loss: a multicenter cross-sectional Study," *Ophthalmology*, vol. 122, no. 5, pp. 925–933, 2015.
- [86] R. Arita, K. Itoh, S. Maeda, K. Maeda, A. Tomidokoro, and S. Amano, "Efficacy of diagnostic criteria for the differential diagnosis between obstructive meibomian gland dysfunction and aqueous deficiency dry eye," *Japanese Journal of Ophthalmology*, vol. 54, no. 5, pp. 387–391, 2010.
- [87] J. E. McDonald, "Surface phenomena of tear films," *Transactions of the American Ophthalmological Society*, vol. 66, pp. 905–939, 1968.
- [88] R. Arita, N. Morishige, T. Fujii et al., "Tear interferometric patterns reflect clinical tear dynamics in dry eye patients," *Investigative Ophthalmology & Visual Science*, vol. 57, no. 8, pp. 3928–3934, 2016.
- [89] D. Finis, N. Pischel, S. Schrader, and G. Geerling, "Evaluation of lipid layer thickness measurement of the tear film as a diagnostic tool for Meibomian gland dysfunction," *Cornea*, vol. 32, no. 12, pp. 1549–1553, 2013.
- [90] M. G. Doane, "An instrument for in vivo tear film interferometry," *Optometry and Vision Science*, vol. 66, no. 6, pp. 383–388, 1989.
- [91] N. Yokoi, Y. Takehisa, and S. Kinoshita, "Correlation of tear lipid layer interference patterns with the diagnosis and severity of dry eye," *American Journal of Ophthalmology*, vol. 122, no. 6, pp. 818–824, 1996.
- [92] E. Goto, M. Dogru, T. Kojima, and K. Tsubota, "Computer-synthesis of an interference color chart of human tear lipid layer, by a colorimetric approach," *Investigative Ophthalmology & Visual Science*, vol. 44, no. 11, pp. 4693–4697, 2003.
- [93] R. Arita, K. Yabusaki, T. Hirono et al., "Automated measurement of tear meniscus height with the kowa DR-1 α tear interferometer in both healthy subjects and dry eye patients," *Investigative Ophthalmology & Visual Science*, vol. 60, no. 6, pp. 2092–2101, 2019.
- [94] E. Goto and S. C. Tseng, "Differentiation of lipid tear deficiency dry eye by kinetic analysis of tear interference images," *Archives of Ophthalmology*, vol. 121, no. 2, pp. 173–180, 2003.
- [95] E. Goto, M. Dogru, K. Fukagawa et al., "Successful tear lipid layer treatment for refractory dry eye in office workers by low-dose lipid application on the full-length eyelid margin," *American Journal of Ophthalmology*, vol. 142, no. 2, pp. 264–270, 2006.
- [96] E. Goto and S. C. G. Tseng, "Kinetic analysis of tear interference images in aqueous tear deficiency dry eye before and after punctal occlusion," *Investigative Ophthalmology & Visual Science*, vol. 44, no. 5, pp. 1897–1905, 2003.
- [97] S. Wong, S. Srinivasan, P. J. Murphy, and L. Jones, "Comparison of meibomian gland dropout using two infrared imaging devices," *Contact Lens and Anterior Eye*, vol. 42, no. 3, pp. 311–317, 2019.
- [98] Y. Eom, J.-S. Lee, S.-Y. Kang, H. M. Kim, and J.-S. Song, "Correlation between quantitative measurements of tear film lipid layer thickness and meibomian gland loss in patients with obstructive meibomian gland dysfunction and normal controls," *American Journal of Ophthalmology*, vol. 155, no. 6, pp. 1104–1110, 2013.
- [99] E. Knop, N. Knop, T. Millar, H. Obata, and D. A. Sullivan, "The international workshop on meibomian gland dysfunction: report of the subcommittee on anatomy, physiology, and pathophysiology of the meibomian gland," *Investigative Ophthalmology & Visual Science*, vol. 52, no. 4, pp. 1938–1978, 2011.
- [100] J. W. Jung, S. Y. Park, J. S. Kim, E. K. Kim, K. Y. Seo, and T.-I. Kim, "Analysis of factors associated with the tear film lipid layer thickness in normal eyes and patients with dry eye syndrome," *Investigative Ophthalmology & Visual Science*, vol. 57, no. 10, pp. 4076–4083, 2016.
- [101] S. Koh, "Mechanisms of visual disturbance in dry eye," *Cornea*, vol. 35, no. 1, pp. S83–S88, 2016.
- [102] S. Koh, N. Maeda, T. Kuroda et al., "Effect of tear film break-up on higher-order aberrations measured with wavefront sensor," *American Journal of Ophthalmology*, vol. 134, no. 1, pp. 115–117, 2002.
- [103] N. Maeda, T. Fujikado, T. Kuroda et al., "Wavefront aberrations measured with Hartmann-Shack sensor in patients with keratoconus," *Ophthalmology*, vol. 109, no. 11, pp. 1996–2003, 2002.
- [104] A. M. Elhusseiny, A. A. Khalil, R. H. El Sheikh et al., "New approaches for diagnosis of dry eye disease," *International Journal of Ophthalmology*, vol. 12, no. 10, pp. 1618–1628, 2019.
- [105] S. Koh, N. Maeda, Y. Hirohara et al., "Serial measurements of higher-order aberrations after blinking in patients with dry eye," *Investigative Ophthalmology & Visual Science*, vol. 49, no. 1, pp. 133–138, 2008.
- [106] S. Koh, N. Maeda, Y. Hori et al., "Effects of suppression of blinking on quality of vision in borderline cases of evaporative dry eye," *Cornea*, vol. 27, no. 3, pp. 275–278, 2008.
- [107] A. Denoyer, G. Rabut, and C. Baudouin, "Tear film aberration dynamics and vision-related quality of life in patients with dry eye disease," *Ophthalmology*, vol. 119, no. 9, pp. 1811–1818, 2012.
- [108] J. L. Güell, J. Pujol, M. Arjona, F. Diaz-Douton, and P. Artal, "Optical quality analysis system; instrument for objective clinical evaluation of ocular optical quality," *Journal of Cataract & Refractive Surgery*, vol. 30, no. 7, pp. 1598–1599, 2004.
- [109] P. Artal, A. Benito, G. M. Perez et al., "An objective scatter index based on double-pass retinal images of a point source to classify cataracts," *PLoS One*, vol. 6, no. 2, Article ID e16823, 2011.
- [110] C.-H. Tan, A. Labbé, Q. Liang et al., "Dynamic change of optical quality in patients with dry eye disease," *Investigative Ophthalmology & Visual Science*, vol. 56, no. 5, pp. 2848–2854, 2015.
- [111] A. Benito, G. M. Pérez, S. Mirabet et al., "Objective optical assessment of tear-film quality dynamics in normal and mildly symptomatic dry eyes," *Journal of Cataract & Refractive Surgery*, vol. 37, no. 8, pp. 1481–1487, 2011.
- [112] S. Koh, N. Maeda, C. Ikeda et al., "Ocular forward light scattering and corneal backward light scattering in patients with dry eye," *Investigative Ophthalmology & Visual Science*, vol. 55, no. 10, pp. 6601–6606, 2014.
- [113] D. Diaz-Valle, P. Arriola-Villalobos, S. E. García-Vidal et al., "Effect of lubricating eyedrops on ocular light scattering as a measure of vision quality in patients with dry eye," *Journal of Cataract & Refractive Surgery*, vol. 38, no. 7, pp. 1192–1197, 2012.
- [114] S. Koh, N. Maeda, C. Ikeda et al., "Effect of instillation of eyedrops for dry eye on optical quality," *Investigative*

- Ophthalmology & Visual Science*, vol. 54, no. 7, pp. 4927–4933, 2013.
- [115] T. Y. Su, W. T. Ho, C. Y. Lu, S. W. Chang, and H. K. Chiang, “Correlations among ocular surface temperature difference value, the tear meniscus height, Schirmer’s test and fluorescein tear film break up time,” *British Journal of Ophthalmology*, vol. 99, no. 4, pp. 482–487, 2015.
- [116] C. Purslow and J. Wolffsohn, “The relation between physical properties of the anterior eye and ocular surface temperature,” *Optometry and Vision Science*, vol. 84, no. 3, pp. 197–201, 2007.
- [117] T. Kamao, M. Yamaguchi, S. Kawasaki, S. Mizoue, A. Shiraishi, and Y. Ohashi, “Screening for dry eye with newly developed ocular surface thermographer,” *American Journal of Ophthalmology*, vol. 151, no. 5, pp. 782–791, 2011.
- [118] L. L. Tan, S. Sanjay, and P. B. Morgan, “Screening for dry eye disease using infrared ocular thermography,” *Contact Lens and Anterior Eye*, vol. 39, no. 6, pp. 442–449, 2016.
- [119] R. Arita, R. Shirakawa, S. Maeda, M. Yamaguchi, Y. Ohashi, and S. Amano, “Decreased surface temperature of tarsal conjunctiva in patients with meibomian gland dysfunction,” *JAMA Ophthalmology*, vol. 131, no. 6, pp. 818–819, 2013.
- [120] Y. Cohen, S. Epshtein, A. Harris, R. Gefen, L. Kagemann, and Y. Arieli, “Tear film imager for dynamic mapping of the human tear film,” *Applied Optics*, vol. 58, no. 29, pp. 7987–7995, 2019.
- [121] F. Segev, N. Geffen, A. Galor et al., “Dynamic assessment of the tear film muco-aqueous and lipid layers using a novel tear film imager (TFI),” *British Journal of Ophthalmology*, vol. 104, no. 1, pp. 136–141, 2020.
- [122] Y. Cohen, S. Trokel, Y. Arieli, S. Epshtien, R. Gefen, and A. Harris, “Mapping the lipid layer of the human tear film,” *Cornea*, vol. 39, no. 1, pp. 132–135, 2020.
- [123] T. C. Y. Chan, S. S. W. Chow, K. H. N. Wan, and H. K. L. Yuen, “Update on the association between dry eye disease and meibomian gland dysfunction,” *Hong Kong Medical Journal*, vol. 25, no. 1, pp. 38–47, 2019.

Research Article

Observation of Gonio Structures during Microhook Ab Interno Trabeculotomy Using a Novel Digital Microscope with Integrated Intraoperative Optical Coherence Tomography

Akiko Ishida, Kazunobu Sugihara, Tomoki Shirakami, Aika Tsutsui, Kaoru Manabe, and Masaki Tanito 

Department of Ophthalmology, Shimane University Faculty of Medicine, Izumo, Japan

Correspondence should be addressed to Masaki Tanito; tanito-oph@umin.ac.jp

Received 7 June 2020; Accepted 29 June 2020; Published 17 July 2020

Guest Editor: Karim Mohamed-Noriega

Copyright © 2020 Akiko Ishida et al. This is an open access article distributed under the Creative Commons Attribution License, which permits unrestricted use, distribution, and reproduction in any medium, provided the original work is properly cited.

Purpose. Observation of ocular structures using microscope-integrated intraoperative optical coherence tomography (iOCT) has been adopted. Using the novel digital ophthalmic microscope, ARTEVO 800 with iOCT, we tested the feasibility of trabecular meshwork (TM) imaging during microhook ab interno trabeculotomy, a minimally invasive glaucoma surgery. **Methods.** The nasal and temporal sides of the TM/inner wall of Schlemm's canal were incised more than 3 clock hours in 14 glaucomatous eyes of 10 patients. To observe the trabeculotomy site, iOCT was performed with the real-time five-line scan mode under observation using a Swan-Jacob gonioscopy lens. The success of the imaging and visibility of the trabeculotomy cleft and its incisional patterns (i.e., anterior, middle, or posterior pattern) were determined by reviewing the iOCT video files. **Results.** OCT images of the region of interest were acquired successfully in 100% of the 28 nasal or temporal sides in 14 eyes, although the trabeculotomy cleft was not visualized in four (14%) sides due to blockage of the OCT signal by a blood clot. Based on the predominant locations of the TM flaps in 24 of the acquired images, the trabeculotomy clefts were classified as anterior incisional patterns in 13 (54%), middle incisional patterns in nine (38%), and posterior incisional patterns in two (8%). **Conclusion.** Intraoperative imaging of the gonio structures including the trabeculotomy cleft was feasible using the ARTEVO 800 with iOCT in combination with a gonioscopy.

1. Introduction

Trabeculotomy is a glaucoma surgery that reduces intraocular pressure (IOP) by eliminating aqueous flow resistance by cleavage of the trabecular meshwork (TM) and inner walls of Schlemm's canal at the point of outflow resistance of the aqueous humor. A new technique, i.e., the ab interno approach, for performing trabeculotomies has been reported recently in which the TM is incised or excised using specialized devices under direct observation of the anterior-chamber angle structure [1, 2]. We initially reported a case of both eyes of one patient with steroid-induced glaucoma who underwent a novel ab interno trabeculotomy, which we referred to as microhook ab interno trabeculotomy (μ LOT) [3]. Because of the substantial IOP decrease in that case, we began to perform the procedure in other cases and reported

the early postoperative results and safety profile of μ LOT [4–7]. The features of μ LOT, which include conjunctival and scleral sparing with the ab interno technique, short surgical time, moderate IOP reduction, and no bleb-related complications, fulfill the conditions of minimally invasive glaucoma surgery (MIGS) [8].

Optical coherence tomography (OCT) is an indispensable diagnostic tool for managing numerous ophthalmic diseases. Observation of the ocular microarchitectural structures using microscope-integrated intraoperative OCT (iOCT) was initially conducted using an external portable OCT system mounted on a microscope [9] and, more recently, using an OCT system integrated into surgical microscopes [10]. iOCT was adopted initially in vitreoretinal surgery to assess macular holes and epiretinal membranes [10], in corneal surgery to visualize the donor cornea during

endothelial keratoplasty [11], and in cataract surgery to evaluate the intraocular lens position [12]. Several studies have used the iOCT device during glaucoma surgeries to image the scleral lake during canaloplasty [13], refine bleb needling [14], assess gonio structures during Trabectome (NeoMedix, Tustin, CA, USA) procedures [15], adjust the tube position during tube-shunt surgery [16], and assess changes in the angle recess in plateau iris syndrome [17].

We previously reported the feasibility results of gonio structure observation during MIGS using a microscope-iOCT device (RESCAN 700, Carl Zeiss Meditec AG, Jena, Germany) [18]. In the current study, we report our initial feasibility assessment using the novel digital ophthalmic microscope (ARTEVO 800 with iOCT, Carl Zeiss Meditec AG) to visualize the incised TM observation during μ LOT.

2. Methods

This retrospective observational study included 14 consecutive glaucomatous eyes of 10 subjects (5 men, 5 women; mean \pm standard deviation age, 66.9 ± 9.5 years, range 47–78 years) who underwent μ LOT with iOCT to reduce IOP in February 2020. The study adhered to the tenets of the Declaration of Helsinki; the institutional review board (IRB) of Shimane University Hospital reviewed and approved the research (No. 20200227-2). Preoperatively, all subjects provided written informed consent for surgery; however, the IRB approval did not require that each patient provide written informed consent for publication; instead, the study protocol was posted at the study institutions to notify participants about the study. The subjects' demographic data included the glaucoma types, i.e., six (43%) eyes with primary open-angle glaucoma, five (36%) with pseudoexfoliation glaucoma, two (14%) with mixed-mechanism glaucoma, and one (7%) with steroid-induced glaucoma. Eleven (79%) eyes were phakic and three (21%) were pseudophakic. No eye had a history of having undergone a previous glaucoma surgery. The procedure included μ LOT alone in six (43%) eyes and μ LOT combined with cataract surgery in eight (57%) eyes.

The μ LOT procedure was performed through two corneal side ports as reported previously [1]. Briefly, a spatula-shaped microhook (M-2215, Inami, Tokyo, Japan) was used, which was designed specifically for use during μ LOT. Viscoelastic material (1% sodium hyaluronate, Healon, AMO Japan, Tokyo, Japan) was injected into the anterior chamber through the clear corneal ports created using a 20-gauge micro-vitreoretinal knife (Mani, Utsunomiya, Japan) at the 2–3 and 9–10 o'clock positions. A microhook was inserted into the anterior chamber through the corneal port using a Swan-Jacob gonioscope lens (Ocular Instruments, Bellevue, WA, USA) to observe the angle opposite to the corneal port. The tip of the microhook then was inserted into Schlemm's canal and moved circumferentially to incise the inner wall of Schlemm's canal and TM over 3 clock hours (Figure 1(a)). Using the same procedure, LOT was performed in the opposite angle using a microhook inserted through the other corneal port. In cases of combined surgery, before μ LOT, phacoemulsification cataract surgery was performed through a 2.2 mm wide clear corneal incision created at the

9–10 o'clock position (i.e., temporal incision for the right eye and nasal incision for the left eye); a one-piece soft acrylic intraocular lens (Vivonex iSert XY1, Hoya, Tokyo, Japan) was inserted through the same clear corneal incision. Then, μ LOT was performed through the 2.2 mm clear corneal incision and a clear corneal port created at the 2–3 o'clock position in both eyes.

iOCT then was performed to assess the gonio structures in the temporal and nasal sides of each eye, i.e., a total of 28 images from the 14 eyes, using the ARTEVO 800 with iOCT that was equipped with spectral domain OCT. Because of poor penetration of the light source, the angle structure was not visualized through the limbal tissue. Alternatively, the gonio structure was visualized under observation with a Swan-Jacob gonioscope lens using the real-time five-line scan mode (scan width, 6.0 mm; scan interval, 0.75 mm; scan depth 2.9 mm) (Figure 1(b), Video 1). The iOCT image was recorded in mp4 format. After iOCT imaging, the viscoelastic material was aspirated through the handpieces and the corneal ports were closed by corneal stromal hydration. Typically, surgical time of combined and solo surgeries were 10 and 4 minutes, respectively; and additional 2 minutes were required to obtain iOCT images in 2 locations (i.e., 1 minute each for nasal or temporal angle).

One author (MT) reviewed the iOCT videos and assessed the success of imaging, visibility of the trabeculotomy cleft, and incisional patterns (i.e., anterior, middle, or posterior pattern) (Figure 2) according to a previous report on the RESCAN 700 [18].

3. Results

At the final follow-up visit at 1.6 ± 0.6 months postoperatively, the baseline IOP of 20.4 ± 3.3 mmHg decreased to 15.0 ± 3.9 mmHg (25% reduction, $P < 0.0001$, Wilcoxon signed-rank test). The baseline number of glaucoma medications of 3.1 ± 1.3 remained unchanged at 2.7 ± 0.6 ($P = 0.1386$). The baseline best-corrected visual acuity of 0.2 ± 0.4 in logarithm of the minimum angle of resolution (logMAR) notation was unchanged at 0.1 ± 0.3 ($P = 0.6108$), and the visual acuity did not decrease in any eye more than 0.2 logMAR. Other than perioperative hyphema in all eyes and a transient IOP elevation of more than 30 mmHg in two (14%) eyes, no surgery-related complications were recorded.

A review of the surgical videos showed that the OCT images successfully captured the areas of interest in all (100%) of the 28 nasal and temporal angles in 14 eyes in which iOCT was performed. Of them, the trabeculotomy cleft was seen in 24 (86%) nasal and temporal sectors of 14 eyes (Figures 3(a)–3(c)) but was not visualized due to blockage of the OCT signal in four (14%) sides in four eyes (Figure 3(d), blue arrow). Of the 24 sides, based on the appearance of the acquired images, the incisional patterns were classified as anterior incisional patterns in 13 (54%) (Figure 3(a), posterior-based flap), middle incisional patterns in nine (38%) (Figure 3(b), posterior- and anterior-based flaps), and posterior incisional patterns in two (8%) (Figure 3(c), anterior-based flap), according to the predominant locations of the TM flaps.

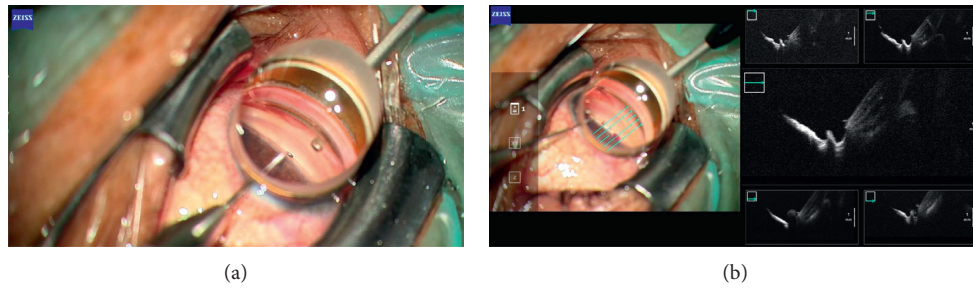


FIGURE 1: Intraoperative integrated optical coherence tomography (iOCT) during microhook ab interno trabeculotomy. (a) Intraoperative findings during microhook ab interno trabeculotomy. Under observation using a Swan-Jacob gonioprism lens, a microhook is inserted into Schlemm's canal. In this left eye, the nasal angle is being incised with the straight microhook that is inserted from the temporal corneal port. (b) Intraoperative observation of the incised trabecular meshwork and inner wall of Schlemm's canal by five-line scans using the ARTEVO 800 with iOCT in combination with a Swan-Jacob gonioprism lens. In this left eye, the nasal angle is visualized with iOCT. The green arrows indicate the scan direction.

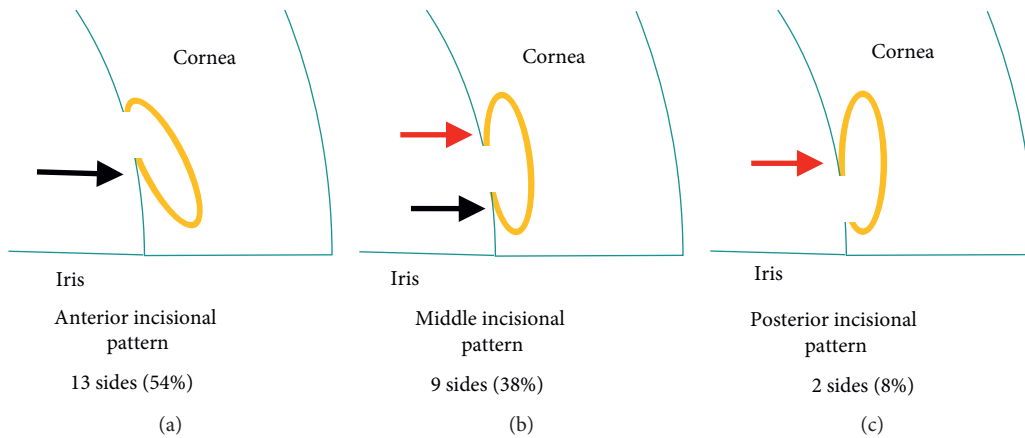


FIGURE 2: Schematic drawings of the three patterns of the trabeculotomy clefts. Based on the flap locations (black and red arrows), the trabeculotomy cleft is classified into an anterior (a), middle (b), or posterior (c) incisional patterns. The black and red arrows indicate posterior- and anterior-based flaps, respectively. The yellow ovals indicate Schlemm's canal. This figure is a modification of our previous publication in the *Journal of Ophthalmology* [18].

4. Discussion

Using the RESCAN 700, Siebelmann et al. reported that good visualization of the gonio structures can be achieved through a deep sclerectomy window during canaloplasty [13]; while Junker et al. [15] and we [18] reported that Schlemm's canal could not be visualized through the full-thickness sclera because of poor penetration of the 840 nm light source. In the current study, we reconfirmed that Schlemm's canal could not be visualized through the full-thickness sclera using the ARTEVO 800. In contrast to direct observation, we successfully observed a trabeculotomy cleft and the lumen of Schlemm's canal using the combination of the ARTEVO 800 and a gonioprism. Previously, using the RESCAN 700 and a gonioprism, OCT images were not obtained in 17% of observations due to the lengthy time required to frame/focus the image [18]. Junker et al. pointed out that one of the biggest problems associated with gonio-structure imaging by iOCT is focusing on the region of interest [15]; thus, iOCT of the gonio structures performed

in combination with a gonioprism requires experience for successful image acquisition. In the current study, OCT images were obtained for 100% of eyes using iOCT. In addition to the improved skills of the operator/surgeons, improvement in hardware/operating software (e.g., ease of focusing) of the ARTEVO 800 compared with the RESCAN 700 might be associated with this increased image acquisition, but this is inconclusive since the detailed specifications of the iOCT device of the ARTEVO 800 have not been released. Real-time iOCT "during" the TM incision, rather than "after" the TM incision, is ideal, although the "during" iOCT is still difficult to perform with current ARTEVO800; thus, further improvement of its usability is desired.

According to our previous study, based on the appearance of the acquired images of the 24 sides, we successfully classified the trabeculotomy cleft into three incisional patterns. In our previous study using the RESCAN 700, the patterns were determined as comprising 60%, 30%, and 10% of the anterior, middle, and posterior incisional patterns, respectively, during μ LOT [18]. Therefore, we

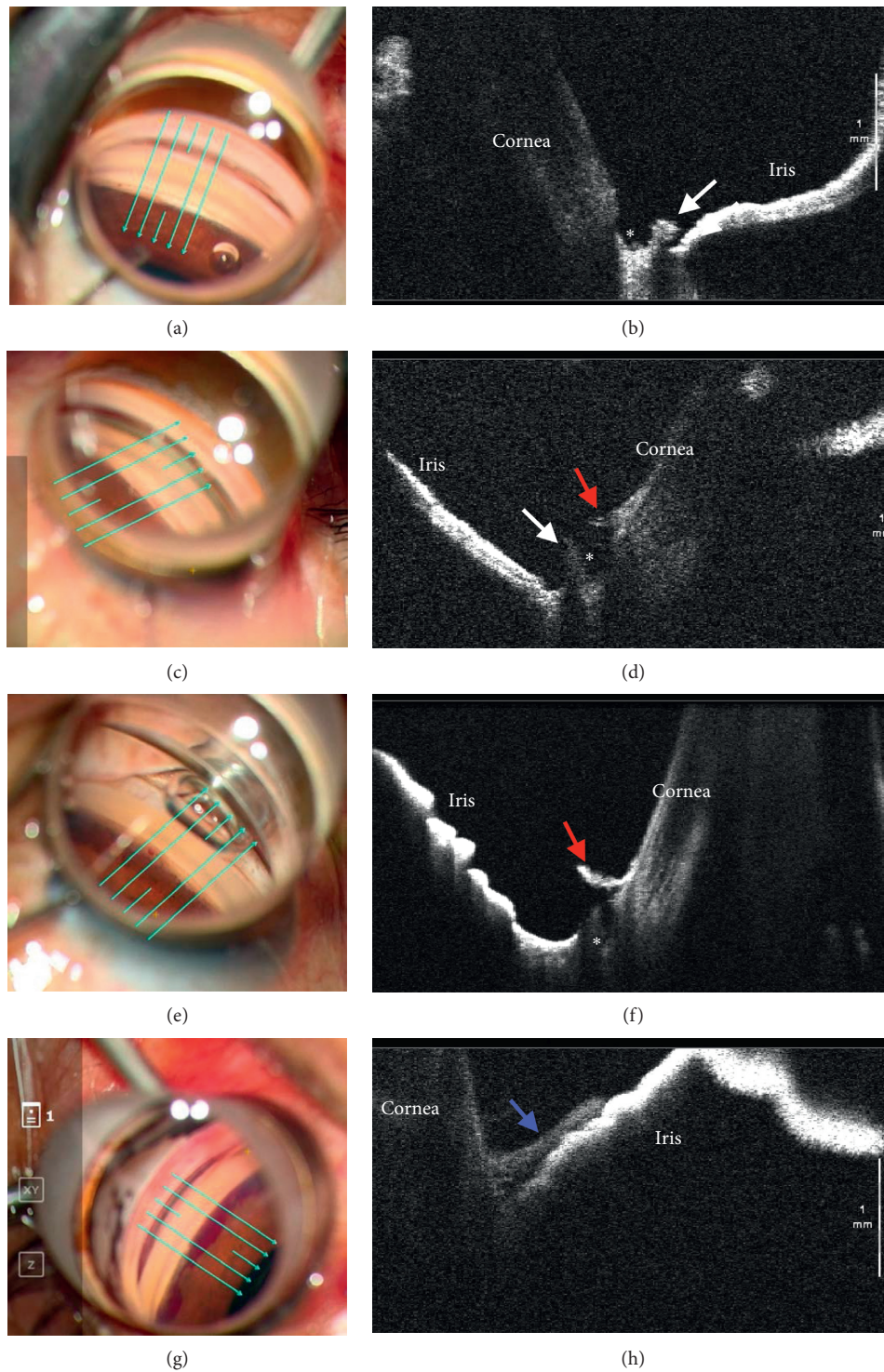


FIGURE 3: Representative microscope-integrated optical coherence tomography (OCT) images of trabeculotomy site. Based on the flap locations (white and red arrows), the trabeculotomy cleft are classified into an anterior incisional pattern (a, b) (seen with posterior-based flaps predominantly), middle incisional pattern (c, d) (seen with posterior- and anterior-based flaps), or posterior incisional pattern (e, f) (seen with anterior-based flap predominantly). (g, h) The trabeculotomy cleft is unclear because the OCT signal is blocked by a blood clot. The white arrows indicate a posterior-based flap; red arrows, an anterior-based flap; blue arrow, a blood clot; green arrows, the direction of the scan; and asterisk, the lumen of Schlemm's canal.

confirmed that the cleft at the anterior edge of the TM was the most frequently observed pattern after the incision using a microhook; this should be associated with significant IOP reductions after μ LOT, although the association between the patterns or extent of TM incision and surgical efficacy needs clarification.

In conclusion, intraoperative imaging of the gonio structures including the trabeculotomy cleft was feasible using the ARTEVO 800 with iOCT in combination with a gonioprism. This technique might be useful to confirm the proper incision of the inner wall of Schlemm's canal during trabeculotomy.

Data Availability

The data used to support the findings of this study are included within the article.

Ethical Approval

All procedures were performed in accordance with the ethical standards of the responsible committee on human experimentation (institutional and national) and with the Helsinki Declaration of 1964, as revised in 2013. The institutional review board of Shimane University Hospital reviewed and approved the research (No. 20200227-2).

Consent

Preoperatively, all subjects provided written informed consent for surgery; however, the IRB approval did not require that each patient provide written informed consent for publication; instead, the protocol was posted at the study institutions to notify participants about the study.

Conflicts of Interest

The microhooks used in this study are codeveloped by Masaki Tanito and Inami & Co., Ltd. (Tokyo, Japan). Dr. Tanito receives royalties from Inami & Co., Ltd.

Supplementary Materials

Video 1: real-time observation of the incised trabecular meshwork using the ARTEVO 800 with microscope-integrated optical coherence tomography in combination with a gonioprism. (*Supplementary Materials*)

References

- [1] M. Tanito, "Microhook ab interno trabeculotomy, a novel minimally invasive glaucoma surgery," *Clinical Ophthalmology*, vol. 12, pp. 43–48, 2018, <https://search.crossref.org/?q=Microhook+ab+interno+trabeculotomy%2C+a+novel+minimally+invasive+glaucoma+surgery.+Clinical+Ophthalmology+%28Auckland%2C+N.Z.%29>.
- [2] M. Tanito and M. Matsuo, "Ab-interno trabeculotomy-related glaucoma surgeries," *Taiwan Journal of Ophthalmology*, vol. 9, no. 2, pp. 67–71, 2019.
- [3] M. Tanito, I. Sano, Y. Ikeda, and E. Fujihara, "Microhook ab interno trabeculotomy, a novel minimally invasive glaucoma surgery, in eyes with open-angle glaucoma with scleral thinning," *Acta Ophthalmologica*, vol. 94, no. 5, pp. e371–e372, 2016.
- [4] M. Tanito, I. Sano, Y. Ikeda, and E. Fujihara, "Short-term results of microhook ab interno trabeculotomy, a novel minimally invasive glaucoma surgery in Japanese eyes: initial case series," *Acta Ophthalmologica*, vol. 95, no. 5, pp. e354–e360, 2017.
- [5] M. Tanito, Y. Ikeda, and E. Fujihara, "Effectiveness and safety of combined cataract surgery and microhook ab interno trabeculotomy in Japanese eyes with glaucoma: report of an initial case series," *Japanese Journal of Ophthalmology*, vol. 61, no. 6, pp. 457–464, 2017.
- [6] M. Tanito, Y. Matsuzaki, Y. Ikeda, and E. Fujihara, "Comparison of surgically induced astigmatism following different glaucoma operations," *Clinical Ophthalmology*, vol. 11, pp. 2113–2120, 2017.
- [7] M. Tanito, K. Manabe, M. Mochiji, Y. Takai, and Y. Matsuoka, "Comparison of anterior chamber flare among different glaucoma surgeries," *Clinical Ophthalmology*, vol. 13, pp. 1609–1612, 2019.
- [8] I. I. K. Ahmed, "MIGS and the FDA: what's in a name?" *Ophthalmology*, vol. 122, no. 9, pp. 1737–1739, 2015.
- [9] J. P. Ehlers, W. J. Dupps, P. K. Kaiser et al., "The Prospective Intraoperative and Perioperative Ophthalmic Imaging With Optical Coherence Tomography (PIONEER) study: 2-year results," *American Journal of Ophthalmology*, vol. 158, no. 5, pp. 999–1007.e1, 2014.
- [10] J. P. Ehlers, Y. S. Modi, P. E. Pecan et al., "The DISCOVER study 3-year results," *Ophthalmology*, vol. 125, no. 7, pp. 1014–1027, 2018.
- [11] A. Kobayashi, H. Yokogawa, N. Mori, and K. Sugiyama, "Visualization of pre-cut DSAEK and pre-stripped DMEK donor corneas by intraoperative optical coherence tomography using the RESCAN 700," *BMC Ophthalmology*, vol. 16, no. 1, p. 135, 2016.
- [12] L. M. Lytvynchuk, C. G. Glittenberg, C. I. Falkner-Radler et al., "Evaluation of intraocular lens position during phacoemulsification using intraoperative spectral-domain optical coherence tomography," *Journal of Cataract & Refractive Surgery*, vol. 42, no. 5, pp. 694–702, 2016.
- [13] S. Siebelmann, C. Cursiefen, A. Lappas, and T. Dietlein, "Intraoperative optical coherence tomography enables non-contact imaging during canaloplasty," *Journal of Glaucoma*, vol. 25, no. 2, pp. 236–238, 2016.
- [14] T. Dada, D. Angmo, N. Midha, and T. Sidhu, "Intraoperative optical coherence tomography guided bleb needling," *Journal of Ophthalmic and Vision Research*, vol. 11, no. 4, pp. 452–454, 2016.
- [15] B. Junker, J. Jordan, C. Framme, and A. Pielen, "Intraoperative optical coherence tomography and ab interno trabecular meshwork surgery with the Trabectome," *Clinical Ophthalmology*, vol. 11, pp. 1755–1760, 2017.
- [16] S. S. Swaminathan and T. C. Chang, "Use of intraoperative optical coherence tomography for tube positioning in glaucoma surgery," *JAMA Ophthalmology*, vol. 135, no. 12, pp. 1438–1439, 2017.
- [17] V. Pathak Ray, V. Puri, H. K. Peguda, and D. P. Rao, "Intraoperative ASOCT determined changes in angle recess in plateau iris syndrome post phaco alone and post phaco-endocycloplasty," *Graefes Archive for Clinical and Experimental Ophthalmology*, vol. 257, no. 3, pp. 663–664, 2019.
- [18] M. Tanito, "Optical coherence tomography observation of gonio structures during microhook ab interno trabeculotomy," *Journal of Ophthalmology*, vol. 2017, p. 4, 2017.

Clinical Study

The Effectiveness of Ultrasound Biomicroscopic and Anterior Segment Optical Coherence Tomography in the Assessment of Anterior Segment Tumors: Long-Term Follow-Up

Joanna Konopińska , Łukasz Lisowski , Ewa Wasiluk, Zofia Mariak ,
and Iwona Obuchowska 

Department of Ophthalmology, Medical University of Białystok, M. Skłodowska-Curie 24A STR, 15-276 Białystok, Poland

Correspondence should be addressed to Joanna Konopińska; joannakonopinska@o2.pl

Received 29 March 2020; Accepted 22 May 2020; Published 17 June 2020

Guest Editor: Sang Beom Han

Copyright © 2020 Joanna Konopińska et al. This is an open access article distributed under the Creative Commons Attribution License, which permits unrestricted use, distribution, and reproduction in any medium, provided the original work is properly cited.

Background. Differential diagnosis and follow-up of small anterior segment tumors constitute a particular challenge because they determine further treatment procedures. The aim of this study was to evaluate the efficacy of the UBM (ultrasound biomicroscopy) and AS-OCT (anterior segment optical coherent tomography) in distinguishing different types of anterior segment lesions. **Methods.** It was a retrospective, noncomparative study of case series of 89 patients with the suspicion of anterior segment tumor referred to the Ophthalmology Clinic, Medical University of Białystok, Poland, between 2016 and 2020. UBM was used to assess tumor morphology including height, location, and internal and external features. In cases in which UBM did not provide enough data, the AS-OCT images were analyzed. The data on demographics, best corrected visual acuity (BCVA), intraocular pressure (IOP), and rate of complications were also collected. Patients were followed up from 1 to 48 months. **Results.** The mean observation period was 26.61 ± 16.13 months. Among the patients, there were 62 women and 27 men at a mean age of 55.59 ± 19.48 (range: from 20 to 89 years.) The types of tumors were cysts (41%), solid iris tumors (37.1%), ciliary body tumors (7.9%), peripheral anterior synechiae (PAS 3.4%), corneal tumors (4.5%), and others (5.6%). Patients with cysts were younger than patients with solid iris tumor ($p = 0.002$). Women had a cyst as well as solid iris tumor more frequently than men, but less often a ciliary body tumor ($p < 0.05$). The horizontal size of tumor was positively correlated with patients' age ($r_s = 0.38$ and $p = 0.003$) and negatively correlated with visual acuity ($r_s = -0.42$ and $p = 0.014$). During the 4 years of diagnosis, only 2.2% of lesions exhibited growth (growth rate of 0.02 mm per year). Among 15 cases in which visualization with UBM was not satisfactory (mostly iris nevi), AS-OCT was helpful in diagnosis of 13 patients. **Conclusions.** Both UBM and AS-OCT are effective methods in detection and diagnosis of tumors of the anterior eye segment, but in some cases, AS-OCT adds additional value to the diagnosis. Many lesions can be managed conservatively because they did not demonstrate growth during 4 years of the follow-up period.

1. Introduction

Detection and monitoring of anterior segment tumors is a major challenge due to their location, which makes direct visualization of these lesions in a basic ophthalmological examination difficult. Consequently, many tumors remain undiagnosed for a long time or are diagnosed too late when they are large enough to produce ocular symptoms. Therefore, the use of additional tests for the early diagnosis of anterior segment tumors is necessary. These examinations

should enable the assessment of tumor parameters such as size, location, infiltration of surrounding structures, and growth rate. This is now possible due to the development of such techniques of imaging the anterior segment of the eye as high-frequency ultrasound biomicroscopy (UBM) and anterior segment optical coherence tomography (AS-OCT).

UBM is recognized as the gold standard in the imaging of anterior segment tumors [1]. This test uses high-frequency ultrasound, from 20 MHz to 100 MHz, which allows a resolution of 20–50 μm , with tissue penetration up to

4–7 mm. With its help, in a noninvasive and detailed way, it is possible to visualize the anatomy of the anterior segment of the eye, especially structures inaccessible to visualization in a standard examination using a slit lamp. These include, for example, the anterior chamber angle, ciliary body, the peripheral part of the lens, haptens of artificial intraocular lens (IOL), or even the outermost parts of the retina. UBM provides also accurate biometric measurements of assessed eyeball structures [1–4].

Modern AS-OCT devices use a light beam with a wavelength of 1310 nm, which allows us to obtain high axial resolution, even up to 5–7 μm with the spectral-domain OCT. However, AS-OCT limitation includes a penetration depth of 3–6 mm at a scan width up to 6–16 mm and poor penetration through the iris pigment epithelium, which in some cases of lesions located behind the iris allows only visualization of their anterior walls. It is a noncontact and quick test, and it is a perfect complement to UBM [4, 5].

Although several studies comparing AS-OCT with UBM in assessment of anterior segment tumors [5–8] have been published, there is very little information on the long-term follow-up of these tumors in the literature.

The purpose of this study is to evaluate the characteristics of anterior segment tumors, which were referred to the Ophthalmology Clinic Medical University of Białystok between 2016 and 2020, with the usage of these two methods of imaging, i.e., UBM and AS-OCT. We tried to determine which techniques provide better visualization and characterization of certain anterior segment tumors. We have also reported our experiences with long-term follow-up of these tumors to detect the growth and the rate of other morphological features related to the higher risk of malignancy.

2. Materials and Methods

This study was approved by the Bioethics Committee of the Medical University of Białystok in accordance with the ethical standards of the 1964 Declaration of Helsinki and its later amendments or comparable ethical standards. All the patients gave written, fully informed consent for the examination and the use of their clinical data for publication.

We conducted a retrospective review of the medical records and electronic images of all patients with suspected anterior segment tumors who were examined at the Department of Ophthalmology, Medical University in Białystok between April 2016 and February 2020. We obtained the following data from medical records: gender, age, BCVA, IOP, anterior segment clinical evaluation, images obtained with UBM (Aviso S, Quantel Medical, Paris, France v 5.0.0), and AS-OCT (Spectralis Tracking Laser Tomography, Heidelberg Engineering).

UBM was performed in all patients, and this test was considered the gold standard in the diagnosis of anterior segment tumors [1]. UBM was performed by two experienced researchers (JK and ŁŁ) according to the method described earlier [8] with a 50 MHz transducer. Images were obtained at the radical meridian through the largest tumor thickness using an eyecup filled with 1% methylcellulose and distilled water.

Ultrasound images were evaluated for the type of lesion, size, location, penetration into the anterior chamber or outside the iris pigment epithelium, echogenicity, external structure (regular/irregular), infiltration of surrounding structures, iris pigmentation, and documented growth. The dimensions of the iris tumors were determined as the largest dimension of the base and the largest dimension of the height, drawn in a line perpendicular to each other, with an accurate determination of the o'clock position. If the lesion was in the cornea, its thickness was not included in the measurement of the size of the lesion (as long as the resolution of the test allowed to distinguish this boundary).

The height of the ciliary body tumors was measured perpendicularly from the internal surface of the sclera to the tumor surface at the thickest portion of the tumor. The growth of a lesion was defined as an increase of its height by at least 20% in comparison with the previous measurement in two separate tests [9]. Imaging parameters were set uniformly during all tests: using a gain of 100 decibels (db), Dyn = 50 db and Tgc = 0 db, and a time-gain control of 5 db/min.

In cases where no change was seen in the UBM image, the patient underwent AS-OCT. This test was performed by an experienced researcher (ŁŁ) using the IR20°ART + OCT 15° (3 mm) protocol, and the anterior chamber evaluation module was always used in the same way. To minimize the risk of distortion, it was ensured that the light beam ran perpendicularly to the iris and the tested lesion, and corneal reflex was clearly visible. The best quality scan was used for the analysis.

Based on ultrasound assessment, the lesions were classified into the following groups: cysts, solid iris lesions, ciliary body tumors, peripheral anterior synechiae (PAS), corneal tumors, and others. More than 3 cysts in the eye were classified as multiple cysts [10]. Follow-up visits were scheduled at six-month intervals. If disturbing symptoms (an increase in IOP; presence of tortuous and dilated vessels going towards the lesion) were observed, the frequency of visits was higher and adapted to the local condition.

2.1. Statistical Analysis. Statistical analysis was performed using R 3.5.1. The studied variables were presented with the use of descriptive statistics. Nominal variables were compared between groups by Fisher's exact test. The normality of the distribution of quantitative variables was assessed using the Shapiro–Wilk test, skewness and kurtosis indicators, and visual assessment of histograms. Group comparisons for quantitative data were performed by the Mann–Whitney *U* test or the Kruskal–Wallis test with the Dunn test, when appropriate. The Bonferroni correction was employed because of multiple comparisons. A comparative analysis of the tumor size with individual tests was performed with the Wilcoxon test for dependent measurements. Correlation of the tumor size with selected quantitative parameters was checked by Spearman's rank correlation coefficient. The significance level $\alpha = 0.05$ was used, and all statistical tests were two-sided.

3. Results

The study involved 89 patients with suspected anterior segment tumor. They were 62 women and 27 men at an average age of 55.59 ± 19.48 years, with a range of 20–89 years.

Tumor-like lesions were revealed in UBM in 74 people (83% of the group). In 13 (14.6%) subsequent cases, the diagnosis was confirmed by AS-OCT. Only in two patients with iris nevi, visible in the slit lamp, it was not possible to visualize the change in either UBM or AS-OCT. Finally, it was found that cysts ($n=37$, 42%) and solid iris lesions ($n=33$, 37%) were the most common anterior segment lesions in the study group. Other less-frequent lesions were ciliary body tumors ($n=7$, 7.9%), corneal tumors ($n=4$, 4.5%), PAS ($n=3$, 3.4%), and other lesions ($n=5$, 5.6%). Other lesions included 2 cases of corneal leukoma, conjunctival nevus, thinning of the sclera with a translucent choroid after childhood esophoria surgery, and IOL decentration causing iris elevation. UBM provided effective visualization in 74 cases (80.1%). However, in 15 cases, UBM did not show tumor mass, and these were 7 solid iris lesions (Figure 1.), 3 PAS cases, 1 IOL displacement, 1 conjunctival nevus, 2 cases of corneal leukoma, and 1 case of scleral thinning after childhood esophoria surgery. The AS-OCT images of these patients were analyzed. In 5 cases, the lesion was revealed, namely, iris nevus (Figure 2). In 2 cases of corneal leukoma, AS-OCT could accurately determine the boundary between the cornea and the growing lesion (Figure 3). In the other 2 cases, the lesion could not be visualized either.

Tumor size measurements were made based on UBM. The average values of the base width and height of all measured tumors are presented in Table 1.

In addition, the mean horizontal and vertical dimensions of the solid iris tumor were significantly smaller than those of the ciliary body tumor $p = 0.018$ and $p < 0.001$, respectively, and the horizontal dimension of the cyst was also significantly smaller from that of the corneal tumor ($p = 0.017$).

A statistically significant difference was found for both horizontal and vertical tumor dimensions depending on the type of lesion (Table 3). The mean horizontal and vertical dimensions of the cyst were significantly different than the ciliary body tumor dimension ($p < 0.001$ and $p = 0.017$, respectively). In addition, the mean horizontal and vertical dimensions of solid iris tumor were significantly different than those of ciliary body tumor ($p = 0.018$ and $p < 0.001$, respectively). The mean horizontal cyst dimension was also significantly different from that of the corneal tumor ($p = 0.017$).

The mean age of the patients was significantly statistically different ($p = 0.006$) between the patients with particular types of tumor (Table 4). A post hoc analysis indicated that patients with cysts were much younger than patients with solid iris tumor ($p = 0.002$). A significant relationship between tumor type and gender was also found. Women had a cyst more frequently than men (45% of women and 33% of men) as well as solid iris tumor (36% vs. 26%, respectively).



FIGURE 1: A patient with iris nevus which was not visualized in UBM.

In turn, men had a ciliary body tumor (15% of men and 5% of women) and other changes (15% vs. 2%, respectively) more frequently than women (Table 5).

Comparison of BCVA and IOP values depending on the type of tumor revealed that patients with cysts had significantly higher BCVA than patients with other lesions (Table 6). However, no correlation was found between the IOP value and tumor type (Table 7).

A tumor horizontal size was positively correlated with patients' age ($r_s = 0.38$, $p = 0.003$) and negatively correlated with visual acuity ($r_s = -0.42$, $p = 0.014$). Both the demonstrated correlations had a moderate strength. The relationship between the horizontal and vertical dimensions of the tumor and the IOP value was not confirmed (Table 8).

The assessment of the anterior segment of the eye in the slit lamp revealed additional symptoms besides the tumor in 5 patients. In 2 cases of ciliary body tumor, the following complications were observed: 1 sectoral cataract and 1 inflammatory reaction in the anterior uvea. Increased IOP values were found in 3 patients with multiple cysts. These patients were treated with the Nd: YAG laser to perforate the cyst walls and drain the internal fluid according to the earlier described technique [11]. After the procedure, normalization of IOP was observed in two of these patients; in one of them, it was necessary to include hypotensive treatment.

Follow-up examinations were routinely performed on all patients every 6 months, with the exception of 10 individuals who already had disturbing symptoms during the first examination that could indicate malignancy. These were as follows: all cases of ciliary body tumors (7 patients), 1 case of iris tumor due to visible additional symptoms: tortuous vessels going from the angle of infiltration to the tumor mass, 1 case of iris tumor and concomitant sectoral cataract, and 1 case of iris tumor with signs of infiltration into the filtration angle. These patients were immediately referred for further diagnostics and possible treatment to a specialist center of intraocular cancer treatment.

In 2 patients, tumor growth by $\geq 20\%$, when compared to the first examination, was confirmed by a follow-up. These patients were immediately referred for further diagnosis, like in the abovementioned cases. Of all the patients referred to another ophthalmology center, 2 returned with confirmation of the malignant process. They underwent brachytherapy and were referred to further observation at the place of residence. In 3 patients, the tumor process was excluded, and further follow-up was recommended. The fate of the

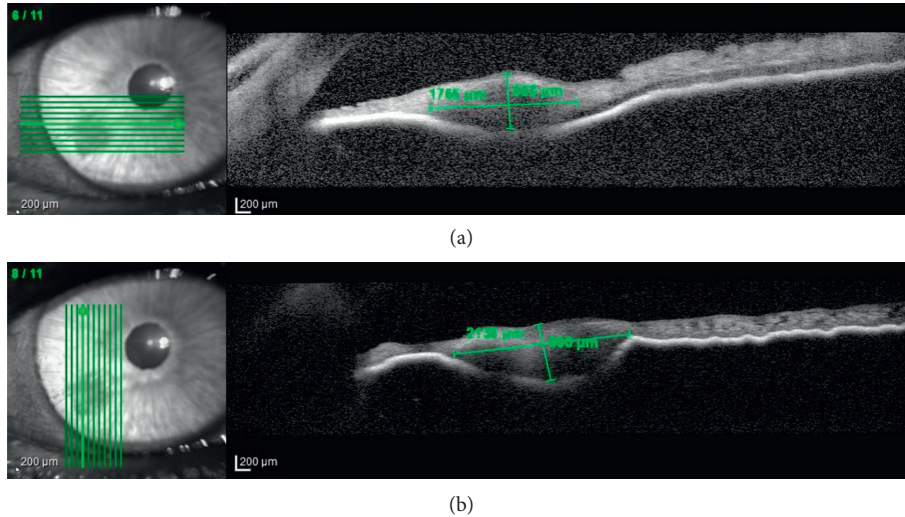


FIGURE 2: Well-visible iris nevus on the AS-OCT image in the same patient.

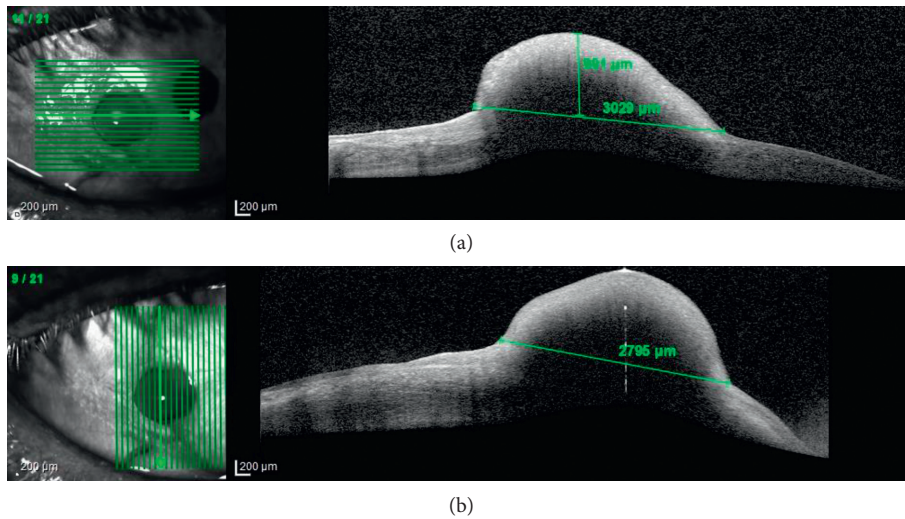


FIGURE 3: A well-visible boundary of corneal leukoma.

TABLE 1: Tumor size mean values, median values, standard deviations, and the range at the first visit.

Tumor size (mm)	<i>n</i>	Mean	SD	Median	Q1–Q3	Range
Base width	74	2.97	2.32	2.36	1.79–2.90	0.96–12.87
Height	74	1.38	0.87	1.10	0.81–1.41	0.48–4.60

Comparison of average tumor sizes does not indicate significant statistical differences between men and women (Table 2).

remaining patients is unknown to us. Ultimately, in the remaining patients, the follow-up ranged from 1 to 48 months. The average follow-up length was 26.61 ± 16.13 months.

4. Discussion

Iris elevation or focal discoloration in the anterior segment of the eye is always an alarming symptom for the ophthalmologist. In our study, it turned out that in 92% of cases, this translated into the presence of a tumor (42% of cysts,

37% of solid iris tumor, 7.9% of ciliary body tumor, or 4.5% of corneal tumor), and only in 8% of cases, the cause may be different (PAS, scleral thinning, IOL decentration, or corneal leukoma).

Documenting objective tumor growth is always a challenge, and without the use of additional imaging tools, it cannot be precise. Taking a photograph of the anterior segment of the eye may be helpful but only allows imaging of the lesion surface. Sequential UBM allows detection of the tumor size change. Therefore, it allows, in some cases, to avoid invasive diagnostics, i.e., fine-needle aspiration or

TABLE 2: Tumor size mean values, median values, standard deviations, and the range by gender.

Gender	<i>n</i>	Base width (mm)			<i>p</i>	<i>n</i>	Height (mm)		<i>p</i> *
		Mean (SD)	Median (range)				Mean (SD)	Median (range)	
Females	53	2.95 ± 2.34	2.29 (0.96; 12.87)		52	1.40 ± 0.90	1.09 (0.48; 4.60)		
Males	21	3.03 ± 2.31	2.41 (1.31; 11.33)	0.512	19	1.33 ± 0.80	1.21 (0.53; 3.93)	0.886	

*Mann-Whitney *U* test.

TABLE 3: Tumor size mean values, median values, standard deviations, and the range by tumor types.

Tumor type	<i>n</i>	Base width (mm)			<i>p</i>	<i>n</i>	Height (mm)		<i>p</i> *
		Mean (SD)	Median (range)				Mean (SD)	Median (range)	
Cyst	37	2.07 ± 0.91	1.87 (1.04; 5.64) ^{a,b}		37	1.20 ± 0.60	1.09 (0.63; 4.04) ^d		
Solid iris tumor	26	2.40 ± 0.70	2.29 (0.96; 3.83) ^c	<0.001	26	0.92 ± 0.37	0.81 (0.48; 2.15) ^{e,f}	<0.001	
Ciliary body tumor	7	5.72 ± 3.02	4.75 (2.41; 11.33) ^{a,c}		7	2.65 ± 1.06	3.18 (1.14; 3.93) ^{d,f}		
Corneal tumor	4	6.34 ± 4.28	6.23 (2.50; 10.38) ^b		4	1.77 ± 0.89	1.72 (0.86; 2.79)		

*Kruskal-Wallis test; a-f: significant differences in the post hoc Dunn test (a: $p < 0.001$, b: $p = 0.017$, c: $p = 0.018$, d: $p = 0.017$, e: $p = 0.010$, and f: $p < 0.001$).

TABLE 4: Age mean values, median values, standard deviations, and the range by a tumor type.

Age, years	<i>n</i>	Mean (SD)	Median (range)	<i>p</i> *
Cyst	37	43.94 ± 20.52	39.00 (20.00; 86.00) ^a	0.006
Solid iris tumor	26	63.80 ± 14.96	65.00 (23.00; 86.00) ^a	
Ciliary body tumor	7	64.60 ± 14.26	62.00 (47.00; 81.00)	
Corneal tumor	4	62.25 ± 16.15	59.00 (48.00; 83.00)	

*Kruskal-Wallis test; a: significant difference in the post hoc Dunn test ($p = 0.002$).

TABLE 5: Tumor type between females and males.

Tumor type	Females	Males	<i>p</i> *
Cyst	28 (45.2)	9 (33.3)	0.038
Solid iris tumor	26 (35.5)	7 (25.9)	
Ciliary body tumor	3 (4.8)	4 (14.8)	
Anterior synechiae	1 (1.6)	2 (7.4)	
Corneal tumor	3 (4.8)	1 (3.7)	
Other	1 (1.6)	4 (14.8)	

*Fisher's exact test; data presented as *n* (% of sex).

TABLE 6: BCVA mean values, median values, standard deviations, and the range by a tumor type.

BCVA	<i>n</i>	Mean (SD)	Median (range)	<i>p</i> *
Cyst	37	0.87 ± 0.25	1.00 (0.20; 1.00) ^a	0.038
Solid iris tumor	33	0.82 ± 0.20	0.85 (0.50; 1.00)	
Others	11	0.58 ± 0.35	0.50 (0.05; 1.00) ^a	

*Kruskal-Wallis test; a: significant difference in the post hoc Dunn test ($p = 0.016$).

iridocyclectomy [4, 11]. In our study, tumor growth was observed only in 2.2% of patients. Other features (i.e., tumor size, presence of abnormal tortuous vessels, sectoral cataract, and inflammation in the anterior chamber) resulted in the referral for further oncological diagnosis of 10 patients (11%). In the study by Shields et al., in 200 cases, 24% were finally qualified as lesions requiring further oncological diagnosis [12].

Cysts (42%) were the most common change in our study group. Cysts in the anterior segment of the eye can be classified as primary or secondary ones. Primary cysts are epithelial, while secondary ones may be the result of

implantation, tumor metastasis, parasitic infections, or chronic use of miotics. Primary cysts rarely cause complications or impair BCVA [4]. They have thin, regular walls and a hypoechogenic interior. Secondary cysts involve the risk of many complications such as corneal edema, uveitis, secondary angle-closure glaucoma, astigmatism, or cataracts due to lens compression. These disorders usually involve significant visual impairment [1, 11]. In our study, in three cases of multiple and binocular cysts, we observed an increase in IOP, but we did not observe cases with reduced BCVA. Implantation cysts originating from the conjunctival epithelium, cornea, or eyelid skin are the results of

TABLE 7: IOP mean values, median values, standard deviations, and the range by a tumor type.

IOP, mmHg	<i>n</i>	Mean (SD)	Median (range)	* <i>p</i>
Cyst	37	15.71 ± 2.78	16.00 (10.00; 20.00)	0.747
Solid iris tumor	33	15.00 ± 2.89	14.00 (12.00; 20.00)	
Others	11	15.86 ± 3.48	17.00 (11.00; 21.00)	

*Kruskal–Wallis test.

TABLE 8: Correlation between tumor size and age, BCVA, and IOP.

Correlation with tumor size	Base width		Height	
	Spearman's rank correlation coefficient r_s	<i>p</i>	Spearman's rank correlation coefficient r_s	<i>p</i>
Age, years	0.38	0.003	−0.11	0.390
BCVA	−0.42	0.014	−0.15	0.420
IOP	−0.31	0.113	−0.02	0.939

penetrating trauma or surgical intervention. They can take the form of compact masses (pearl-like cysts), reservoirs filled with liquid, or they can cause endothelial hyperplasia. They are usually large (about 5 mm in cross section) and have thick walls (about 0.4 mm). They may contain serous, echo-negative fluid content (serous cysts). It is very important to distinguish the cyst from the echo-negative space inside the tumor that corresponds to the focus of necrosis or the lumen of a large blood vessel.

However, UBM does not allow to distinguish serous content, erythrocytes, or inflammatory cells, so histopathology still plays a key role in such cases [1]. Their growth varies; initially, they can grow rapidly and later remain unchanged. By reaching large sizes, they can overgrow the iris, causing its atrophy, as well as they penetrate into the posterior chamber. In our study, there were 5 secondary cysts: 1 caused by trauma in childhood, 2 previous surgeries: phacotrabeculectomy and ECCE, and in 2 cases, the reason was not revealed.

The use of AS-OCT is of limited significance in the case of central cysts, under the iris pigment epithelium. Numerous studies confirm UBM advantage over AS-OCT in detecting these changes [3, 13–15]. The pigment epithelium absorbs light to a large extent, and its cells are linked tightly by means of desmosomes, as a result of which it is impossible to visualize the circumference of the cyst. Peripheral cysts, located in the iridociliary sulcus, are partially covered with colorless epithelium, and the links between its cells are less tight and have gaps, so their visualization with AS-OCT is possible at least partially [1].

There are studies describing the family occurrence of iris cysts with dominant autosomal inheritance [16, 17]. In these cases, multiple cysts often cover more than 180° of the filtration angle. In our study group, we had 1 case of siblings (brother and sister) with multiple binocular cysts. In such cases, it would be worth extending the diagnostics to other family members. Centrally located primary cysts in adults are usually asymptomatic, and even signs of spontaneous regression have been observed, although they may also slowly increase with time [18]. No such cases were observed in our study. Sometimes, cysts can cause an increase in IOP due to the obstruction of filtration angle or clogging of the

openings of trabecular meshwork by mucus released from the secondary cyst [18]. In our study, only 3 patients had an increase in IOP, and these were multiple cysts that covered >180° of the filtration angle. Our study confirmed the conclusions of Shields et al. that primary iris cysts rarely progress and affect BCVA and IOP levels [12]. In Shield's study, they accounted for 21% of cases in the group of patients referred for examination with suspected tumor. Binocular and multiple cysts accounted for 37.8% [10] in another study and 16% (6 cases) in our study.

The second most common diagnosis among our group was solid iris tumors. They occur in the form of localized foci of pigmentation of the iris, which are flat or slightly elevated. Sometimes, these lesions can grow and infiltrate surrounding tissues [19]. The diagnosis of this type of lesions is particularly important, especially when they reveal signs of pupil displacement, ectropion uvea, or cataracts in the adjacent quadrant, due to the possibility of melanoma on their basis.

Typically, the iris tumors look like weak-reflective plaques surrounding the thickened iris stroma. A lesion close to the base of the iris can cause its deflection [10]. Certain characteristics of neoplastic transformation, i.e., location, presence of abnormal vessels, or uneven edge of the lesion, can be assessed during the slit-lamp examination. However, imaging of penetration through the pigment lamina, confirmation of the growth of the lesion, infiltration of structures, or confirmation of uneven echogenicity are not possible without the use of additional devices [19]. In our study, this was confirmed in 4 cases of iris tumors (12%).

In 7 patients with iris tumor, the ultrasound image could not be obtained due to the lack of reflections caused by the resolution of the test. These were mainly the cases of iris nevi. Of these, in 5 patients, AS-OCT showed high-resolution images on the basis of which it could be concluded that the nevus does not penetrate through the iris pigment epithelium, which is an important prognostic feature. AS-OCT may also be a useful alternative in imaging small, non-pigmented iris tumors (with a thickness of not more than 1.3 mm and a base width of not more than 3 mm) [20].

In the study by Hau et al. [13], it was shown that the possibility of accurate imaging of iris nevi with dimensions

≤ 2 mm of the base width and 0.6 mm in height was 87.1% of all cases, and in the study by Razzaq et al., it was as much as 96% [21]. Moreover, greater precision in determining the tumor size that is possible with AS-OCT (no additional echoes as in the case of UBM) allows the calculation of an adequate brachytherapy dose for confirmation of melanoma [21]. However, if the lesion was larger or penetrated into the area behind the iris, it was not possible to visualize its entire volume. In this case, as well as in highly pigmented lesions, ultrasound imaging is more helpful due to better penetration compared to light energy.

All cases of ciliary body tumors were referred for further oncological diagnostics, since there are studies showing that melanomas of this area are more aggressive than melanomas of the iris or choroid due to the rich vascularization of the ciliary body, which increases the risk of distributing cancer cells with blood or large initial tumor size related to its late detection [9]. In addition, at the time of diagnosis, they were large, on average 5.72×4.75 mm. Moreover, in each of these cases, there was a reduced BCVA and uveitis in one case.

There are several weak spots in our study. It was a retrospective study, and tumor growth criteria were retrospectively defined. Moreover, UBM is characterized by intraobserver and interobserver variability depending on the experience of the ultrasound technician [22–24]. Measurement of the greatest thickness in lesions with irregular contours can also be difficult, although it is much easier to determine the exact position of the transducer during the measurement. Despite these drawbacks, a large study group and long observation period can constitute the advantage of the study.

5. Conclusions

In conclusion, in the diagnostics of cysts and small anterior ocular tumors, UBM provides key information about their exact location and anatomical structure, i.e., echogenicity of the inside of the lesion, its structure, shape, contour (regular, irregular), wall thickness, and location relative to the surrounding structures (infiltration) and an increase in the size of the cyst or tumor visible in subsequent tests. These are important diagnostic and prognostic parameters. In some cases, when the lesion cannot be visualized by ultrasound, AS-OCT is helpful in diagnosing them and taking further therapeutic steps due to the possibility of obtaining a high-resolution image. UBM is still the gold standard in the diagnosis of anterior segment tumors, and AS-OCT is a valuable complement. Long-term observation of the lesions shows that most of the lesions are mild and asymptomatic, and they do not cause complications and do not require treatment. However, it should be remembered that histopathology is still of key importance for diagnosis and implementation of appropriate treatment for anterior segment tumors.

Data Availability

The data used to support this study can be obtained from the corresponding author upon request. The names and

personal data of the participants cannot be released due to ethical aspects.

Disclosure

This study was performed as a part of employment of the authors in the Medical University of Białystok, Poland.

Conflicts of Interest

The authors declare that they have no conflicts of interest.

References

- [1] I. Georgalas, P. Petrou, D. Papaconstantinou, D. Brouzas, C. Koutsandrea, and M. Kanakis, "Iris cysts: a comprehensive review on diagnosis and treatment," *Survey of Ophthalmology*, vol. 63, no. 3, pp. 347–364, 2018.
- [2] B. Kuzmanović Elabjer, M. Bušić, D. Miletić, M. Bjeloš, N. Vukojević, and D. Bosnar, "Possible role of standardized echography complementing ultrasound biomicroscopy in tumors of the anterior eye segment: a study in a series of 13 patients," *Journal of Ultrasound*, vol. 21, no. 3, pp. 209–215, 2018.
- [3] K. Janssens, M. Mertens, N. Lauwers, R. J. de Keizer, D. G. Mathysen, and V. De Groot, "To study and determine the role of anterior segment optical coherence tomography and ultrasound biomicroscopy in corneal and conjunctival tumors," *Journal of Ophthalmology*, vol. 2016, Article ID 1048760, 11 pages, 2016.
- [4] H. C. Köse, K. Gündüz, and M. B. Hoşal, "Iris cysts: clinical features, imaging findings, and treatment results," *Turkish Journal of Ophthalmology*, vol. 50, no. 1, pp. 31–36, 2020.
- [5] R. Neupane, R. Gaudana, and S. H. S. Boddu, "Imaging techniques in the diagnosis and management of ocular tumors: prospects and challenges," *The AAPS Journal*, vol. 20, no. 6, p. 97, 2018.
- [6] E. Vizvári, Á. Skribek, N. Polgár, A. Vörös, P. Sziklai, and E. Tóth-Molnár, "Conjunctival melanocytic naevus: diagnostic value of anterior segment optical coherence tomography and ultrasound biomicroscopy," *PLoS One*, vol. 13, no. 2, Article ID e0192908, 2018.
- [7] A. H. Skalet, Y. Li, C. D. Lu et al., "Optical coherence tomography angiography characteristics of Iris melanocytic tumors," *Ophthalmology*, vol. 124, no. 2, pp. 197–204, 2017.
- [8] C. J. Pavlin, K. Harasiewicz, M. D. Sherar, and F. S. Foster, "Clinical use of ultrasound biomicroscopy," *Ophthalmology*, vol. 98, no. 3, pp. 287–295, 1991.
- [9] D. J. Weisbrod, C. J. Pavlin, W. Xu, and E. R. Simpson, "Long-term follow-up of 42 patients with small ciliary body tumors with ultrasound biomicroscopy," *American Journal of Ophthalmology*, vol. 149, no. 4, pp. 616–622, 2010.
- [10] F. A. Marigo, K. Esaki, P. T. Finger et al., "Differential diagnosis of anterior segment cysts by ultrasound biomicroscopy," *Ophthalmology*, vol. 106, no. 11, pp. 2131–2135, 1999.
- [11] S. S. Shanbhag, M. Ramappa, S. Chaurasia, and S. I. Murthy, "Surgical management of acquired implantation iris cysts: indications, surgical challenges and outcomes," *British Journal of Ophthalmology*, vol. 103, no. 8, pp. 1179–1183, 2019.
- [12] J. A. Shields, M. W. Kline, and J. J. Augsburger, "Primary iris cysts: a review of the literature and report of 62 cases," *British Journal of Ophthalmology*, vol. 68, no. 3, pp. 152–166, 1984.
- [13] S. C. Hau, V. Papastefanou, S. Shah, M. S. Sagoo, M. Restori, and V. Cohen, "Evaluation of iris and iridociliary body lesions

- with anterior segment optical coherence tomography versus ultrasound B-scan,” *British Journal of Ophthalmology*, vol. 99, no. 1, pp. 81–86, 2015.
- [14] H. Ishikawa, “Anterior segment imaging for glaucoma: OCT or UBM?” *British Journal of Ophthalmology*, vol. 91, no. 11, pp. 1420–1421, 2007.
- [15] F. Li, K. Gao, X. Li, S. Chen, W. Huang, and X. Zhang, “Anterior but not posterior choroid changed before and during Valsalva manoeuvre in healthy Chinese: a UBM and SS-OCT study,” *British Journal of Ophthalmology*, vol. 101, no. 12, pp. 1714–1719, 2017.
- [16] S. Singh, M. Dogra, D. Katoch, and M. Dogra, “Bilateral iris cysts in an infant with retinopathy of prematurity,” *Indian Journal of Ophthalmology*, vol. 67, no. 12, p. 2062, 2019.
- [17] A. Vela, J. C. Rieser, and D. G. Campbell, “The heredity and treatment of angle-closure glaucoma secondary to iris and ciliary body cysts,” *Ophthalmology*, vol. 91, no. 4, pp. 332–337, 1984.
- [18] G. J. Brent, D. M. Meisler, R. Krishna, and G. Baerveldt, “Spontaneous collapse of primary acquired iris stromal cysts,” *American Journal of Ophthalmology*, vol. 122, no. 6, pp. 886–887, 1996.
- [19] F. A. Marigo and P. T. Finger, “Anterior segment tumors: current concepts and innovations,” *Survey of Ophthalmology*, vol. 48, no. 6, pp. 569–593, 2003.
- [20] H. Krema, R. A. Santiago, J. E. Gonzalez, and C. J. Pavlin, “Spectral-domain optical coherence tomography versus ultrasound biomicroscopy for imaging of nonpigmented iris tumors,” *American Journal of Ophthalmology*, vol. 156, no. 4, pp. 806–812, 2013.
- [21] L. Razzaq, K. E. Der Spek, G. P. M. Luyten, and R. J. W. De Keizer, “Anterior segment imaging for iris melanocytic tumors,” *European Journal of Ophthalmology*, vol. 21, no. 5, pp. 608–614, 2011.
- [22] J. Kosmala, I. Grabska-Liberek, I. Grabska-Liberek, and R. Stanislovas Ašoklis, “Recommendations for ultrasound examination in ophthalmology. Part I: ultrabiomicroscopic examination,” *Journal of Ultrasonography*, vol. 18, no. 75, pp. 344–348, 2018.
- [23] S. F. Urbak, “Ultrasound biomicroscopy. III. Accuracy and agreement of measurements,” *Acta Ophthalmologica Scandinavica*, vol. 77, no. 3, pp. 293–297, 1999.
- [24] S. F. Urbak, J. K. Pedersen, and T. T. Thorsen, “Ultrasound biomicroscopy. II. Intraobserver and interobserver reproducibility of measurements,” *Acta Ophthalmologica Scandinavica*, vol. 76, no. 5, pp. 546–549, 1998.

Research Article

Endothelial Plaques as Sign of Hyphae Infiltration of Descemet's Membrane in Fungal Keratitis

Xiaolin Qi,¹ Ting Liu,² Man Du,¹ and Hua Gao ^{1,2}

¹Eye Hospital of Shandong First Medical University, State Key Laboratory Cultivation Base, Shandong Provincial Key Laboratory of Ophthalmology, Shandong Eye Institute, Shandong First Medical University and Shandong Academy of Medical Sciences, Jinan, China

²State Key Laboratory Cultivation Base, Shandong Provincial Key Laboratory of Ophthalmology, Shandong Eye Institute, Shandong First Medical University and Shandong Academy of Medical Sciences, Qingdao, China

Correspondence should be addressed to Hua Gao; gaohua100@126.com

Received 14 February 2020; Revised 3 April 2020; Accepted 12 May 2020; Published 26 May 2020

Guest Editor: Karim Mohamed-Noriega

Copyright © 2020 Xiaolin Qi et al. This is an open access article distributed under the Creative Commons Attribution License, which permits unrestricted use, distribution, and reproduction in any medium, provided the original work is properly cited.

Background. To evaluate the relationship between corneal endothelial plaques and fungal hyphae infiltration in fungal keratitis. **Methods.** Retrospective cross-sectional study of 60 fungal keratitis patients who underwent keratoplasty between January 2013 and March 2017. The endothelial plaques were graded as follows: grade 1, 1–3 endothelial plaques; grade 2, 4–8 endothelial plaques; and grade 3, more than 8 endothelial plaques or dense, merging endothelial plaques. The fungal pathogen culture and histopathology of diseased Descemet's membrane were evaluated. **Results.** According to endothelial plaque grading, 3 patients were grade 1, 29 patients were grade 2, and 28 patients were grade 3. The PK surgery was performed in 57 patients with endothelial plaques of grade 2 and grade 3 and DALK surgery in 3 patients of grade 1. The predominating fungal pathogens were *Aspergillus* species (63.2%). All 57 patients with grade 2 and grade 3 had fungal hyphae in Descemet's membrane based on calcofluor white staining or PAS staining. In patients with grade 3, more hyphae and inflammatory cells were found in Descemet's membrane. The immunohistochemical staining of endothelial plaques revealed that CD15 and CD68 were positive in most cells. During the follow-up, 2 out of 3 patients who underwent DALK had recurrent fungal keratitis. **Conclusions.** Endothelial plaques are considered as a sign of hyphae infiltrating Descemet's membrane. PK should be performed once plaques are detected in endothelium during the surgery.

1. Introduction

Fungal keratitis (FK) is a severe infectious corneal disease in developing countries [1–3]. In China, more than 50% of infectious keratitis cases are the result of a fungal infection [4]. Clinical manifestations of fungal keratitis include elevated lesions and necrosis, pseudopodia, corneal ring, endothelial plaque, and hypopyon [3, 5]. According to the reported literature, the presence of endothelial plaque was considered as a risk factor for lamellar keratoplasty treatment failure [6–8]. However, due to the lack of histopathological evidence, the formation of endothelial plaques is related to anterior chamber reaction of severe fungal infections, or hyphae infiltration of Descemet's membrane remains unclear. Furthermore, it is often difficult to choose

deep anterior lamellar keratoplasty (DALK) or penetrating keratoplasty (PK) when encountering endothelial plaques during keratoplasty surgery. In this study, we attempted to use histological evidence to show that endothelial plaques are a reliable sign of hyphae infiltration of Descemet's membrane, thus providing surgical guidance in these circumstances.

2. Methods

2.1. Patients. We adhered to the principles outlined in the Declaration of Helsinki, and this study was approved by the ethics committee of Shandong Eye Hospital. A total number of 242 patients with fungal keratitis underwent keratoplasty between January 2013 and March 2017, including DALK for

89 patients, and PK for 153 patients were reviewed retrospectively. The inclusion criteria were as follows: (1) the hyphae were detected by corneal smear examination or laser scanning confocal microscopy (Heidelberg Instruments, GmbH, Heidelberg, Germany); (2) over 4/5 of the corneal thickness was infected or infiltrated as observed by slit-lamp microscopy, laser scanning confocal microscopy, and anterior segment optical coherence tomography (As-OCT); (3) antifungal medication as reported in our previous studies [9, 10] was given for at least 2 weeks but was ineffective. The patients detected with no endothelial plaque and diagnosed with perforation were excluded from this study. Finally, a total of 60 patients (60 eyes) were included (26 men and 34 women). Their mean age was 40.5 years (range 31–68 years).

A comprehensive eye examination was performed with a slit-lamp, including measuring the size of fungal ulcer and the depth of hypopyon. The methods were as follows. Photos of the corneas were obtained with a digital camera at the slit-lamp (Topcon, DC-3), and a picture of a graduated scale under the same magnification ratio was taken. Then, the pictures of the corneas and the graduated scale were opened in Adobe Photoshop software. After dragging the graduated scale to the cornea with the move tool, the size of fungal ulcer and the depth of hypopyon were measured and recorded.

2.2. Endothelial Plaque Evaluation. All the surgeries were planned as DALK preoperatively, and the decision of performing DALK or PK was made according to the evaluation of endothelial plaques after exposure of Descemet's membrane with the big-bubble technique. All surgeries were performed by a single surgeon (H.G.). The detailed surgical procedure was introduced in our previous report [11]. After Descemet's membrane was exposed, the endothelial plaques were assessed under the surgical microscope and graded as follows: grade 1, 1–3 endothelial plaques; grade 2, 4–8 endothelial plaques; and grade 3, more than 8 endothelial plaques or dense, merging endothelial plaques. If only 1–3 endothelial plaques (grade 1) were visible, DALK was performed. If more than 3 endothelial plaques (grade 2–3) were visible, PK was performed instead. After endothelial plaque evaluation, patients with endothelial plaques of grade 1 continued the surgery as DALK, and those with grades 2 and 3 were converted to PK.

After surgery, the diseased Descemet's membrane and the corneal lamellar tissue were sent for fungal pathogen culture and histopathological examination with calcofluor white and periodic acid-Schiff (PAS) staining.

2.3. Calcofluor White Staining of Descemet's Membrane. After PK, Descemet's membranes were stained with calcofluor white staining. Briefly, a drop of 1% calcofluor white (Sigma, St. Louis, USA) was added to Descemet's membranes obtained during PK, which were incubated for 2 min at room temperature and washed three times in normal saline. Fungal hyphae were observed using a fluorescence E800 microscope (Nikon, Tokyo, Japan). With calcofluor white staining, the fungal hyphae were bright blue against a dark background.

2.4. Histopathological Examination and Immunohistochemical Detection. Corneal buttons obtained during DALK or PK surgery were fixed in 4% formalin. These corneal buttons were half-cut along the central line. Serially graded ethanol baths followed by xylene were used to dehydrate the tissues before they were immersed in paraffin wax. The samples were embedded in paraffin molds, and serial slices (4 μ m) were stained with PAS stain (Maxin, Fujian, China). The hyphae were observed by light microscopy (Olympus BX60, Tokyo, Japan). Six microscopic fields (\times 400) were randomly chosen in each cornea, and the number of fungal hyphae and inflammatory cells per field were counted for the statistical analysis.

The expressions of a neutrophil marker (CD15) and a macrophage marker (CD68) were detected with immunohistochemical staining. Briefly, 4 μ m-sections were obtained from the paraffin-embedded corneal buttons. The antigens were recovered by microwaving the sections, and the endogenous peroxidase activity was quenched with a 3% solution of hydrogen peroxide for 10 min. The sections were incubated with primary antibodies (mouse anti-CD15 or CD68; Maxin, Fujian, China) for 60 min at 37°C after which they were incubated with HRP-conjugated goat anti-mouse IgG for 30 min at 37°C. The peroxidase activity was visualized by incubating the sections in a solution of diaminobenzidine (DAB; Maxin, Fujian, China). Negative controls were performed in the absence of primary antibodies. Finally, the samples were mounted and examined under a microscope (Olympus BX60, Tokyo, Japan).

2.5. Statistical Analysis. All data were analyzed with SPSS software (version 17.0, SPSS Inc., Chicago, IL, USA). Student's *t* test was used to compare the hyphae and inflammatory cell counts between patients with grade 2 and grade 3 endothelial plaques. The data are shown as the mean \pm standard deviation, and a *P* value <0.05 was considered statistically significant.

3. Results

3.1. Patient Information. KOH smears and laser scanning confocal microscopy were hyphae positive in all 60 patients. The mean size of fungal ulcer was 6.9 ± 0.6 mm \times 6.2 ± 0.5 mm before surgery. Hypopyon was present in 38 eyes, measuring 1.5 ± 0.9 mm (range: 0.2–4 mm).

3.2. Endothelial Plaque Evaluation and Surgery. All 60 patients had a varying degree of endothelial plaques, including 3 patients in grade 1, 29 patients in grade 2, and 28 patients in grade 3. The 3 patients with grade 1 underwent DALK surgery, whereas 57 patients with grade 2 and grade 3 underwent PK surgery (Figure 1). After the surgery, the mean follow-up time was 4.1 ± 2.6 months (range: 3–6 months).

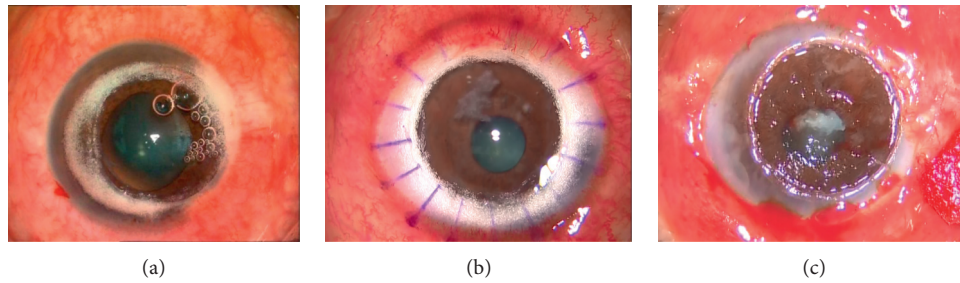


FIGURE 1: Representative pictures of grade 1 (a), grade 2 (b), and grade 3 (c) endothelial plaques after exposing Descemet's membrane during keratoplasty surgery.

3.3. Fungal Pathogen Distribution. In 38 fungal pathogens positively cultured, 24 (63.2%) were identified as *Aspergillus* species, 10 (26.3%) were *Fusarium* species, 2 (5.2%) were *Alternaria* species, and 2 (5.2%) were *Colletotrichum* species. There were also 22 unidentified species.

3.4. Calcofluor White Stain Evaluation. With calcofluor white stain, 29 patients with grade 2 and 28 patients with grade 3 were all hyphae positive in Descemet's membranes. The hyphae had many branches and were bamboo-structured and surrounded with inflammatory cells. The representative hyphae in Descemet's membranes of patients with grade 2 and grade 3 are shown in Figure 2.

3.5. Histopathology and Immunohistochemical Evaluation. PAS staining the corneal stroma and Descemet's membrane was positive for fungal hyphae in all eyes. In patients with grade 3, the destruction of the cornea stroma was severe, and more hyphae and inflammatory cells were found in the deep stroma and Descemet's membrane. In patients with grade 2, the inflammation was moderate, and there were less hyphae in the deep stroma and Descemet's membrane (Figure 3). Both the number of hyphae and inflammatory cells per high-power field were significantly different between the patients with grade 3 and grade 2 ($P < 0.01$) (Figure 4). Immunohistochemical staining of endothelial plaques revealed that most cells were positive for CD15 (neutrophils) or CD68 (macrophages) (Figure 5).

3.6. Fungal Recurrence. Recurrent FK occurred in 2 out of 3 patients who underwent DALK. One eye recurred at 3 days after DALK surgery and at 5 days in another eye. The cultured fungal pathogens were both *Aspergillus* species in the 2 patients. No fungal recurrence was observed after PK surgery.

4. Discussion

The big-bubble-DALK was reported to be effective in the treatment of fungal keratitis. However, during the DALK surgery, if endothelial plaques were present, the doctor often faced a dilemma over whether to continue the DALK procedure or choose the PK procedure. There have been disputes about the possible correlation between hyphae

infiltration and endothelial plaques [12–15]. Some researchers believed that the hyphae may invade the deep corneal stroma to cause an anterior chamber reaction as well as endothelial plaques with the progression of the disease, but no direct pathologic evidence was available [16, 17]. Therefore, it is necessary to study the components of corneal endothelial plaques and their relationship to hyphae penetrating Descemet's membrane, which may help clinical doctors to make an informed choice for surgical procedures.

Corneal endothelial plaques in FK contain a large number of acute inflammatory and immune cells. Our immunohistochemical staining revealed that the corneal endothelial plaques were mainly composed of neutrophils and macrophages surrounding the penetrating hyphae. This structure reflects the body's defense system against invading microorganisms such as the hyphae penetrating into the anterior chamber. Kiryu et al. [18] found that hyphae surrounded by neutrophils showed double or triple cell wall formation and sometimes a hypha-in-hypha structure in dexamethasone-treated corneal lesions. This special structure was regarded as a protective device for the survival of *Fusarium* species to evade the host's immune system.

Calcofluor white stain is an easy and direct staining method for fungi and is more sensitive for detecting fungal hyphae than the traditional PAS stain on paraffin sections. With direct calcofluor white stain, all patients had hyphae distribution in Descemet's membrane. Histological examination further verified that more hyphae and inflammatory cells were found in the grade 3 patients than in the grade 2 patients with PAS stain. Out of 3 patients with grade 1 endothelial plaques who underwent DALK, 2 patients had recurrent FK after DALK, further suggesting the close relationship between endothelial plaques and hyphae infiltration. These results indicate that endothelial plaques are a reliable sign of hyphae infiltration of Descemet's membrane.

The patients with 4/5 of the corneal thickness infected or infiltrated by hyphae and antifungal medication ineffective for 2 weeks are suggested to undergo keratoplasty. The exact procedure selection (DALK or PK) depends on the evaluation of deeper stroma and Descemet's membrane during the surgery. Surgeons can proceed with DALK when no hyphae and endothelial plaques are detected in the deeper stroma and Descemet's membrane. In a previous study by Dr. Gao [11], DALK was performed in a series of 23 patients with no hyphae in the posterior stroma near Descemet's

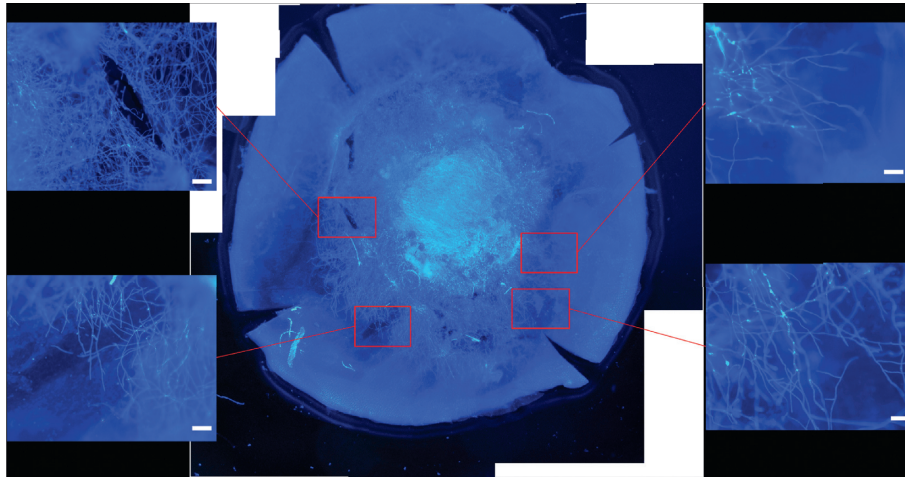


FIGURE 2: In a patient with grade 3 endothelial plaques, fungal hyphae were found in Descemet's membrane with calcofluor white stain by fluorescence microscopy (scale bar 20 μm).

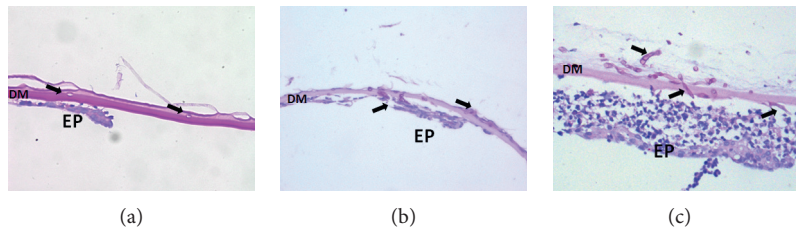


FIGURE 3: Hyphae (arrows) were found in patients with grade 1 (a), grade 2 (b), and grade 3 (c) with periodic acid-Schiff (PAS) stain. More hyphae and inflammatory cells were found in Descemet's membrane in patients with grade 3 (c) (scale bar 20 μm).

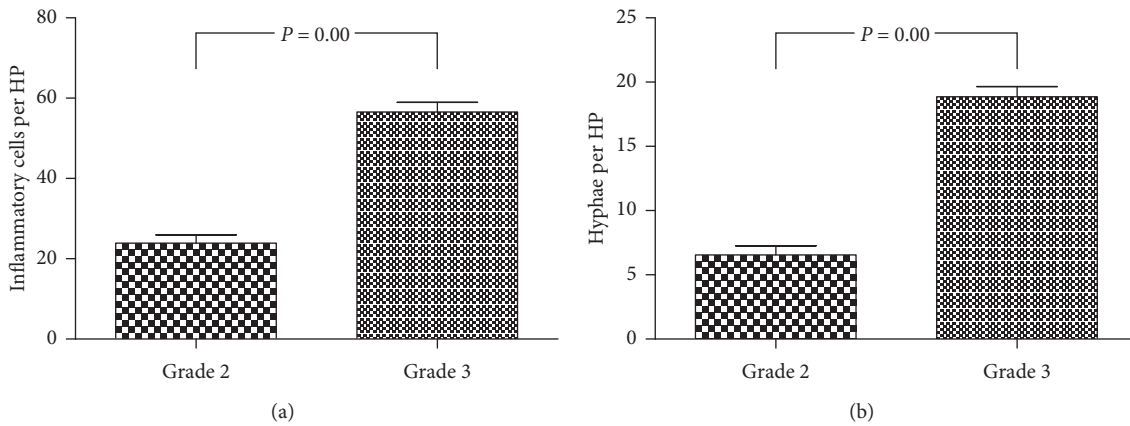


FIGURE 4: Significant differences were found between patients with grade 2 and grade 3 endothelial plaques ($P < 0.01$) including (a) the number of inflammatory cells and (b) hyphae present in Descemet's membrane per high-power field.

membrane, and recurrence of FK was found in only two patients (8.7%), much lower than the reported values [13, 19, 20].

Fusarium is still the most common pathogen of fungal keratitis, followed by *Alternaria* and *Aspergillus* species, in Shandong Province, China [11, 21–23]. However, in this study, the postoperative fungal pathogen culture of the diseased Descemet's membrane showed that 24 (63.2%) out

of the 38 positively cultured were identified as *Aspergillus* species. In addition, the cultured pathogens from the 2 patients with recurrent FK after DALK surgery were *Aspergillus* species. The main reason is that unlike *Fusarium* species with horizontally growing hyphae, most *Aspergillus* hyphae grow vertically in corneal stroma, so the deep stroma and Descemet's membrane are prone to be invaded. The rudimentary hyphae in the deep stroma and Descemet's

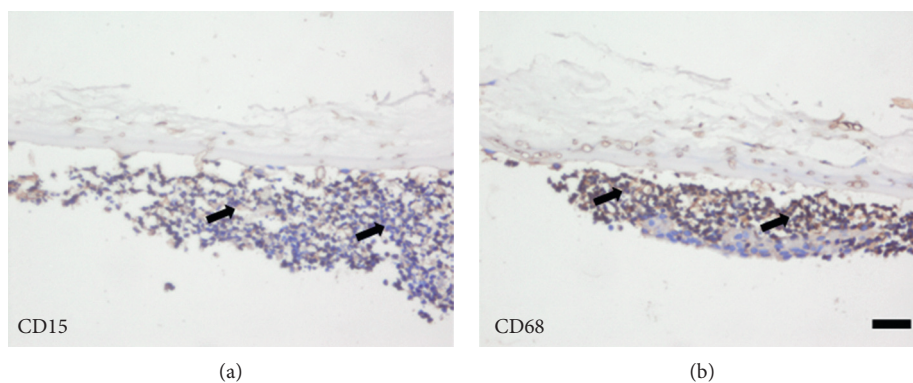


FIGURE 5: Immunohistochemical staining revealed CD15-positive neutrophils (brown color, arrowed in (a)) and CD68-positive macrophages (brown color, arrowed in (b)) accumulated in the endothelial plaques (scale bar 20 μ m).

membrane that are not cleared by DALK may cause fungal recurrence postoperatively. Hence, PK should be performed once plaques are detected in endothelium during the surgery, which means hyphae has penetrated Descemet's membrane to reduce the risk of fungal recurrence.

In conclusion, endothelial plaques are considered as a sign of hyphae infiltrating Descemet's membrane. The predominating fungal pathogens of diseased Descemet's membrane were *Aspergillus* species (63.2%). Once plaques are detected in endothelium during the surgery, PK should be performed to reduce the risk of fungal recurrence.

Data Availability

All data and material are available within the article.

Additional Points

Synopsis. Corneal endothelial plaques in FK contain a large number of bamboo-like hyphae and inflammatory cells. *Aspergillus* species is the predominating fungal pathogens capable of penetrating Descemet's membrane readily.

Ethical Approval

This study was approved by the Institutional Review Board of Shandong Eye Hospital, Jinan, China.

Conflicts of Interest

The authors declare that they have no conflicts of interest.

Authors' Contributions

Xiaolin Qi and Ting Liu contributed equally to this work.

Acknowledgments

The authors sincerely thank their colleagues at Shandong Eye Hospital for their valuable discussion and help. This study was supported by the National Natural Science Foundation of China (81870639 and 81900907), Key Project of National Natural Science Foundation of China

(81530027), Taishan Scholar Program (20150215, 201812150), and Innovation Project of Shandong Academy of Medical Sciences (2019RC009).

References

- [1] J. Sengupta, A. Khetan, S. Saha, D. Banerjee, N. Gangopadhyay, and D. Pal, "Candida keratitis," *Cornea*, vol. 31, no. 4, pp. 371–375, 2012.
- [2] A. K. Ghosh, A. Gupta, S. M. Rudramurthy, S. Paul, V. K. Hallur, and A. Chakrabarti, "Fungal keratitis in North India: spectrum of agents, risk factors, and treatment," *Mycopathologia*, vol. 181, no. 11–12, pp. 843–850, 2016.
- [3] P. Garg, A. Roy, and S. Roy, "Update on fungal keratitis," *Current Opinion in Ophthalmology*, vol. 27, no. 4, pp. 333–339, 2016.
- [4] L. Xie, W. Zhong, W. Shi, and S. Sun, "Spectrum of fungal keratitis in north China," *Ophthalmology*, vol. 113, no. 11, pp. 1943–1948, 2006.
- [5] P. A. Thomas, A. K. Leck, and M. Myatt, "Characteristic clinical features as an aid to the diagnosis of suppurative keratitis caused by filamentous fungi," *British Journal of Ophthalmology*, vol. 89, no. 12, pp. 1554–1558, 2005.
- [6] L. Xie, J. Hu, and W. Shi, "Treatment failure after lamellar keratoplasty for fungal keratitis," *Ophthalmology*, vol. 115, no. 1, pp. 33–36, 2008.
- [7] D. G. Said, M. Otri, A. Miri, A. Kailasanathan, T. Khatib, and H. S. Dua, "The challenge of fungal keratitis," *British Journal of Ophthalmology*, vol. 95, no. 12, pp. 1623–1624, 2011.
- [8] Y. Takezawa, T. Suzuki, and A. Shiraishi, "Observation of retrocorneal plaques in patients with infectious keratitis using anterior segment optical coherence tomography," *Cornea*, vol. 36, no. 36, pp. 1237–1242, 2017.
- [9] L. Xie, X. Dong, and W. Shi, "Treatment of fungal keratitis by penetrating keratoplasty," *British Journal of Ophthalmology*, vol. 85, no. 9, pp. 1070–1074, 2001.
- [10] L. Xie, W. Shi, Z. Liu, and S. Li, "Lamellar keratoplasty for the treatment of fungal keratitis," *Cornea*, vol. 21, no. 1, pp. 33–37, 2002.
- [11] H. Gao, P. Song, J. J. Echeagaray et al., "Big-bubble deep anterior lamellar keratoplasty for management of deep fungal keratitis," *Journal of Ophthalmology*, vol. 2014, Article ID 209759, 8 pages, 2014.
- [12] S.-P. Chee and A. Jap, "Immune ring formation associated with cytomegalovirus endotheliitis," *American Journal of Ophthalmology*, vol. 152, no. 3, pp. 449–453, 2011.

- [13] A. Anshu, A. Parthasarathy, J. S. Mehta, H. M. Htoon, and D. T. H. Tan, "Outcomes of therapeutic deep lamellar keratoplasty and penetrating keratoplasty for advanced infectious keratitis," *Ophthalmology*, vol. 116, no. 4, pp. 615–623, 2009.
- [14] X. Dong, W. Shi, Q. Zeng, and L. Xie, "Retracted: roles of adherence and matrix metalloproteinases in growth patterns of fungal pathogens in cornea," *Current Eye Research*, vol. 30, no. 8, pp. 613–620, 2005.
- [15] G. Galperin, M. Berra, J. Tau, G. Boscaro, J. Zarate, and A. Berra, "Treatment of fungal keratitis from *Fusarium* infection by corneal cross-linking," *Cornea*, vol. 31, no. 2, pp. 176–180, 2012.
- [16] A. Konstantopoulos, J. Kuo, D. Anderson, and P. Hossain, "Assessment of the use of anterior segment optical coherence tomography in microbial keratitis," *American Journal of Ophthalmology*, vol. 146, no. 4, pp. 534–542, 2008.
- [17] R. Shetty, H. Nagaraja, C. Jayadev, Y. Shivanna, and T. Kugar, "Collagen cross-linking in the management of advanced nonresolving microbial keratitis," *British Journal of Ophthalmology*, vol. 98, no. 8, pp. 1033–1035, 2014.
- [18] H. Kiryu, S. Yoshida, Y. Suenaga, and M. Asahi, "Invasion and survival of *Fusarium solani* in the dexamethasone-treated cornea of rabbits," *Journal of Medical and Veterinary Mycology*, vol. 29, no. 6, pp. 395–406, 1991.
- [19] S.-E. Ti, J. A. Scott, P. Janardhanan, and D. T. H. Tan, "Therapeutic keratoplasty for advanced suppurative keratitis," *American Journal of Ophthalmology*, vol. 143, no. 5, pp. 755–762, 2007.
- [20] W. Shi, T. Wang, L. Xie et al., "Risk factors, clinical features, and outcomes of recurrent fungal keratitis after corneal transplantation," *Ophthalmology*, vol. 117, no. 5, pp. 890–896, 2010.
- [21] L. Xie, H. Zhai, W. Shi, J. Zhao, S. Sun, and X. Zang, "Hyphal growth patterns and recurrence of fungal keratitis after lamellar keratoplasty," *Ophthalmology*, vol. 115, no. 6, pp. 983–987, 2008.
- [22] L. Xie, H. Zhai, J. Zhao, S. Sun, W. Shi, and X. Dong, "Antifungal susceptibility for common pathogens of fungal keratitis in Shandong Province, China," *American Journal of Ophthalmology*, vol. 146, no. 2, pp. 260–265, 2008.
- [23] Q. Wang, D. Luo, H. Chen, and X. Sun, "The distribution and drug resistance rate of 3759 cases of fungal keratitis," *Chinese Journal of Mycology*, vol. 14, pp. 16–19, 2019.

Research Article

Changes in Corneal Volume at Different Areas and Its Correlation with Corneal Biomechanics after SMILE and FS-LASIK Surgery

Pinghui Wei ^{1,2}, George PM Cheng ³, Jiamei Zhang ^{1,2}, Alex LK Ng ⁴,
Tommy CY Chan ⁵, Vishal Jhanji ⁶, and Yan Wang ^{1,2}

¹Clinical College of Ophthalmology, Tianjin Medical University, Tianjin, China

²Tianjin Eye Hospital, Tianjin Eye Institute, Tianjin Key Lab of Ophthalmology and Visual Science, Nankai University, Tianjin, China

³Hong Kong Laser Eye Center, Hong Kong, China

⁴Department of Ophthalmology, The University of Hong Kong, Hong Kong, China

⁵Department of Ophthalmology and Visual Sciences, The Chinese University of Hong Kong, Hong Kong, China

⁶UPMC Eye Center, University of Pittsburgh School of Medicine, Pittsburgh, PA, USA

Correspondence should be addressed to Yan Wang; wangyan7143@vip.sina.com

Received 14 February 2020; Accepted 6 March 2020; Published 27 April 2020

Guest Editor: Sang Beom Han

Copyright © 2020 Pinghui Wei et al. This is an open access article distributed under the Creative Commons Attribution License, which permits unrestricted use, distribution, and reproduction in any medium, provided the original work is properly cited.

Purpose. To investigate the variations of corneal volume (CV) after small incision lenticule extraction (SMILE) and femtosecond laser-assisted laser in situ keratomileusis (FS-LASIK) and analyze the influences of biomechanical properties on the changes of refraction and CV. **Methods.** Ninety-seven eyes of 97 patients undergoing SMILE and FS-LASIK were included in this retrospective study. CV was measured with Scheimpflug-based corneal topography at preoperatively and at day 1, week 1, and months 1 and 3 postoperatively. CV measured within 5 mm diameter was defined as central region volume (CV5) and between 5 mm and 10 mm diameter was defined as peripheral region volume (CV5-10). An Ocular Response Analyzer (ORA) was used to assess corneal biomechanical properties including corneal hysteresis (CH) and corneal resistant factor (CRF). The reduction of study parameters (Δ) were calculated by subtracting the preoperative value at various time points from the postoperative values. **Results.** CV had significant reduction after the SMILE and FS-LASIK procedure ($P < 0.05$). CV5 increased significantly from postoperative day 1 to month 3 ($P < 0.001$) in SMILE, while both CV5 and CV5-10 increased significantly in FS-LASIK ($P < 0.001$). The increase in CV5 after SMILE was $0.11 \pm 0.16 \text{ mm}^3$, which was significantly different from FS-LASIK ($0.20 \pm 0.13 \text{ mm}^3$, $P = 0.004$). In the SMILE group, ΔCV5 correlated with ΔCRF ($r = 0.498$, $P < 0.001$) and ΔCH ($r = 0.374$, $P = 0.007$). In the FS-LASIK group, ΔCV5 and ΔCRF had a significant correlation ($r = 0.363$, $P = 0.012$), but not with ΔCH . **Conclusions.** Dynamic changes in corneal volume were found after SMILE and FS-LASIK surgery. The central region significantly increased after SMILE, while both central and peripheral regions increased following FS-LASIK in the early postoperative period. SMILE was associated with less change in biomechanical properties per unit of reduction in CV compared with FS-LASIK.

1. Introduction

Corneal volume (CV) is one of the structural characteristics contributing to the biomechanical profile of the cornea [1]. Corneal refractive surgery involves ablation of the corneal tissue thereby leading to a reduction in the corneal volume

[2]. Several published studies use corneal thickness to evaluate the amount of tissue changed after refractive surgery and to study its relationship with refractive outcome [2, 3]. However, a change in corneal thickness does not truly reflect the actual change in the amount of corneal tissues. On the other hand, evaluation of changes in CV may be a more

comprehensive approach to study the actual amount of changes in the corneal tissue as a whole and characterize corneal morphometric changes with a single value [4].

Currently, the main applications of femtosecond laser in corneal refractive surgery include femtosecond laser-assisted laser in situ keratomileusis (FS-LASIK) and small incision lenticule extraction (SMILE). FS-LASIK creates a corneal flap with femtosecond laser followed by excimer laser ablation of the stromal tissue, while a stromal lenticule is created with femtosecond laser and then removed through a small incision in SMILE. Corneal tissue is removed and CV is reduced in both methods, which is followed by change in the corneal shape and correction of refractive errors; hence, corneal ectasia might occur [5–7]. Studies have shown a correlation between corneal volume and corneal biomechanical properties [8, 9]. However, there is still little understanding regarding the dynamic changes in the CV after SMILE and FS-LASIK [10].

To the best of our knowledge, there is no study focusing on the changes in CV at different areas of the cornea and analyzing its correlation with corneal biomechanical properties after SMILE and FS-LASIK.

2. Methods

2.1. Subjects and Examinations. This was a retrospective, comparative study that included patients with myopia and myopic astigmatism undergoing FS-LASIK and SMILE in Tianjin Eye Hospital. Inclusion criteria included age of 18 years or older, a corrected distance visual acuity (CDVA) of 20/25 or better, myopic spherical refraction from -0.50 to -10.00 diopters (D), myopic cylindrical refraction up to -3.00 D, stable refraction over 2 years, and central corneal thickness more than $480 \mu\text{m}$. All patients had stopped soft contact lens wear for at least 2 weeks and rigid lens for at least 4 weeks before the assessment. Exclusion criteria included active ocular disease, history of ocular surgery or trauma, keratoconus or suspicious corneal topography, and patients with mental disorders. The study protocol was approved by the Tianjin Eye Hospital Ethics Committee and adhered to the Declaration of Helsinki. Written informed consent was obtained from all patients before the surgery.

2.2. Measurement Methods. Clinical examinations were performed preoperatively and on postoperative day 1, week 1, month 1, and month 3. Preoperative and postoperative examinations included measurement of uncorrected visual acuity (UCVA), CDVA, eye dominance, noncontact tonometry, slit lamp biomicroscopy examination, and dilated fundus examination. All patients underwent CV measurement by Pentacam HR topography (Oculus GmbH, Wetzlar, Germany). The Pentacam was performed in a dark room, and only the scans with quality specification screen displaying “OK” were chosen for analysis. The changes in the CV before and after surgery were calculated. An ocular response analyzer (ORA, Reichert, USA) was used to measure corneal biomechanical properties including corneal

hysteresis (CH) and corneal resistance factor (CRF). Measurements below a waveform score of five were excluded due to insufficient quality.

2.3. Surgical Technique. All surgeries were performed by the same surgeon (WY) using a 500 kHz femtosecond laser machine (Visumax, Carl Zeiss Meditec AG, Germany). In FS-LASIK, the flap thickness was $110 \mu\text{m}$ and the flap diameter was 7.9–8.0 mm. The excimer laser ablation was performed with an Allegretto (Wavelight Laser Technologie AG, Germany). In SMILE, the lenticule diameter was 6.5 mm, the cap thickness was $110 \mu\text{m}$, and the incision location was at the 12 o'clock position. After the surgery, 0.3% ofloxacin (Tarivid; Santen, Inc, Japan) eye drops were administered four times a day for three days and 0.1% fluorometholone (Flumetholon; Santen, Inc, Japan) eye drops were given four times per day for the first two weeks and then decreased one time every two weeks.

2.4. Statistical Analysis. Statistical analysis was performed using SPSS (GLM UNIVARIATE, version 20, IBM). All data were tested with the Kolmogorov–Smirnov test and were normally distributed. We divided the cornea into 2 regions: central (CV5, the central 5 mm diameter region) and peripheral (CV5-10, the 5 mm to 10 mm diameter region). The reduction in the study parameters (Δ) was calculated by subtracting the preoperative value at various time points from the postoperative values. The differences in the corneal volume between the SMILE and FS-LASIK group were calculated using the independent *t*-test; the Pearson correlation test was used to evaluate the relationship between the change in corneal volume (ΔCV) and the change in spherical equivalence refraction (ΔSE), change in corneal hysteresis (ΔCH), and change in corneal resistance factor (ΔCRF). One-way repeated measures analysis of variance (ANOVA) with the post hoc Bonferroni test was applied for multiple comparisons between different time points. $P < 0.05$ was regarded as statistically significant.

3. Results

This study included 97 eyes (97 patients; 50 eyes in SMILE and 47 eyes in FS-LASIK). The average age was 24.28 ± 5.86 (range 18–41). The preoperative characteristics are shown in Table 1.

3.1. CV Changes on Postoperative Day 1, Week 1, Month 1, and Month 3. As shown in Table 2, there was a statistically significant reduction in CV5 and CV5-10 on postoperative day 1 compared with the preoperative value (all $P < 0.05$) in both groups. In SMILE, CV5-10 continued to decline at postoperative week 1 ($P = 0.039$), while a significant decrease in CV5 was observed in FS-LASIK ($P = 0.024$), when compared with postoperative day 1. Afterwards, there was a gradual increase of both CV5 and CV5-10 from postoperative week 1 until the end of 3 months.

TABLE 1: Baseline characteristics of eyes undergoing SMILE and FS-LASIK.

Parameters	SMILE	FS-LASIK	t	P value
MRSE (D)	-5.90 ± 1.33	-6.15 ± 1.72	0.804	0.423
Spherical (D)	-5.53 ± 1.36	-5.78 ± 1.69	0.814	0.418
Cylinder (D)	-0.86 ± 0.74	-0.76 ± 0.59	-0.657	0.513
Age (y)	24.56 ± 6.02	23.97 ± 5.95	0.486	0.628
CCT (μm)	545.70 ± 29.70	540.97 ± 25.21	0.841	0.402

MRSE: manifest refraction spherical equivalent, CCT: central corneal thickness.

TABLE 2: Corneal volume during postoperative visits in patients undergoing SMILE and FS-LASIK.

Parameters	Group	Preop	1 Day	1 Week	1 Month	3 Months	P value
CV5 (mm ³)	SMILE	11.56 ± 0.64	10.13 ± 0.63*	10.09 ± 0.65*	10.14 ± 0.65*	10.25 ± 0.66* [#]	<0.001
	FS-LASIK	11.47 ± 0.52	9.96 ± 0.51*	9.91 ± 0.50* [#]	9.98 ± 0.50*	10.16 ± 0.49* [#]	<0.001
CV5-10 (mm ³)	SMILE	49.69 ± 2.78	48.89 ± 2.79*	48.60 ± 2.68* [#]	48.67 ± 2.76*	49.15 ± 2.80*	<0.001
	FA-LASIK	49.17 ± 2.27	48.28 ± 2.41*	48.07 ± 2.39*	48.10 ± 2.33*	48.81 ± 2.41 [#]	<0.001

CV5: corneal volume of the central 5 mm diameter area, CV5-10: corneal volume of the peripheral 5–10 mm diameter area, P value: one-way repeated measures analysis of variance (ANOVA), *Significant difference when compared with preoperative value ($P < 0.05$), [#] Significant difference when compared with postoperative day 1 ($P < 0.05$).

3.2. Comparison of the Corneal Volume between the SMILE and FS-LASIK Group. CV5 increased significantly from postoperative day 1 to month 3 ($P < 0.001$) in SMILE, while both CV5 and CV5-10 increased significantly in FS-LASIK ($P < 0.001$). The increase in CV5 from postoperative day 1 to month 3 in the SMILE group was $0.11 \pm 0.16 \text{ mm}^3$, which was significantly different from that in the FS-LASIK group ($0.20 \pm 0.13 \text{ mm}^3$, $t = -2.917$, $P = 0.004$). The corresponding increase in the CV5-10 in SMILE and FS-LASIK group was $0.26 \pm 0.90 \text{ mm}^3$ and $0.54 \pm 0.77 \text{ mm}^3$, respectively ($t = -1.599$, $P = 0.113$).

3.3. Changes in Spherical Equivalent Refraction at Postoperative Day 1, Week 1, Month 1, and Month 3. The preoperative spherical equivalence refraction (SE) in the SMILE and FS-LASIK group was $-5.90 \pm 1.33\text{D}$ and $-6.15 \pm 1.72\text{D}$, respectively. The change in spherical equivalence refraction at postoperative month 3 (ΔSE) was $-5.82 \pm 1.29\text{D}$ and $-6.19 \pm 1.76\text{D}$, respectively, and no statistically significant difference was found between the two groups ($t = 1.153$, $P = 0.252$). The SE at postoperative day 1, week 1, month 1, and months 3 in SMILE was $-0.10 \pm 0.24\text{D}$, $-0.05 \pm 0.19\text{D}$, $-0.09 \pm 0.23\text{D}$, and $-0.07 \pm 0.18\text{D}$, respectively, and no statistically significant difference was found between these values ($P > 0.05$). The corresponding values in FS-LASIK were $0.23 \pm 0.36\text{D}$, $0.11 \pm 0.33\text{D}$, $0.06 \pm 0.33\text{D}$, and $0.04 \pm 0.27\text{D}$. There was a statistically significant difference between the SE at postoperative day 1 and all other visits ($P < 0.05$) (Figure 1).

3.4. Correlation between Change in Spherical Equivalent Refraction and Reduction in Corneal Volume. A significant correlation was found between the change in CV5 at postoperative month 3 compared with preoperative value, and the change of SE at postoperative month 3 compared with the preoperative value (SMILE group: $r = 0.746$,

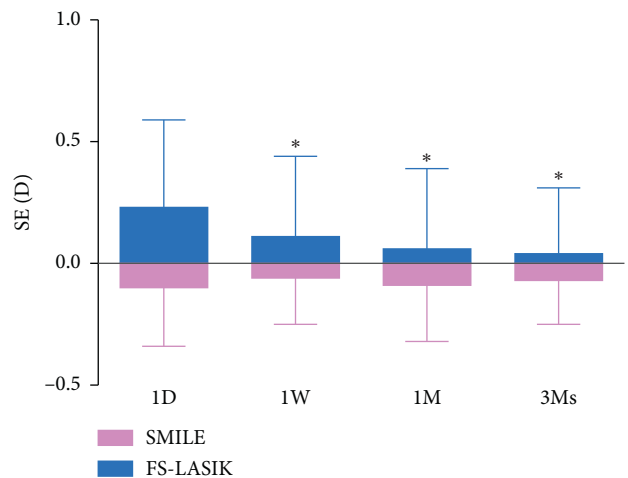


FIGURE 1: The postoperative spherical equivalence refraction (SE) at different time points. Asterisk (*): significant difference was found when compared with the postoperative day 1 value in the FS-LASIK group (post hoc Bonferroni test, ($P < 0.05$)).

$P < 0.001$; FS-LASIK group: $r = 0.798$, $P < 0.001$) (Figure 2). No correlation was found between the change in CV5 from postoperative day 1 and month 3 and change in the corresponding SE (SMILE group: $r = 0.044$, $P = 0.760$; FS-LASIK group: $r = 0.114$, $P = 0.447$).

3.5. Correlation between Change in Corneal Biomechanical Parameters and Reduction in Corneal Volume. The mean reduction of CRF and CH (ΔCRF and ΔCH) in the SMILE group was $3.58 \pm 1.02 \text{ mmHg}$ and $2.12 \pm 1.00 \text{ mmHg}$, while in the FS-LASIK group, the corresponding values were $3.96 \pm 1.07 \text{ mmHg}$ and $2.60 \pm 1.00 \text{ mmHg}$, respectively. As shown in Table 3, in the SMILE group, a statistically significant correlation was found between ΔCV5 with ΔCRF ($r = 0.498$, $P < 0.001$) and ΔCH ($r = 0.374$, $P < 0.001$) at 3

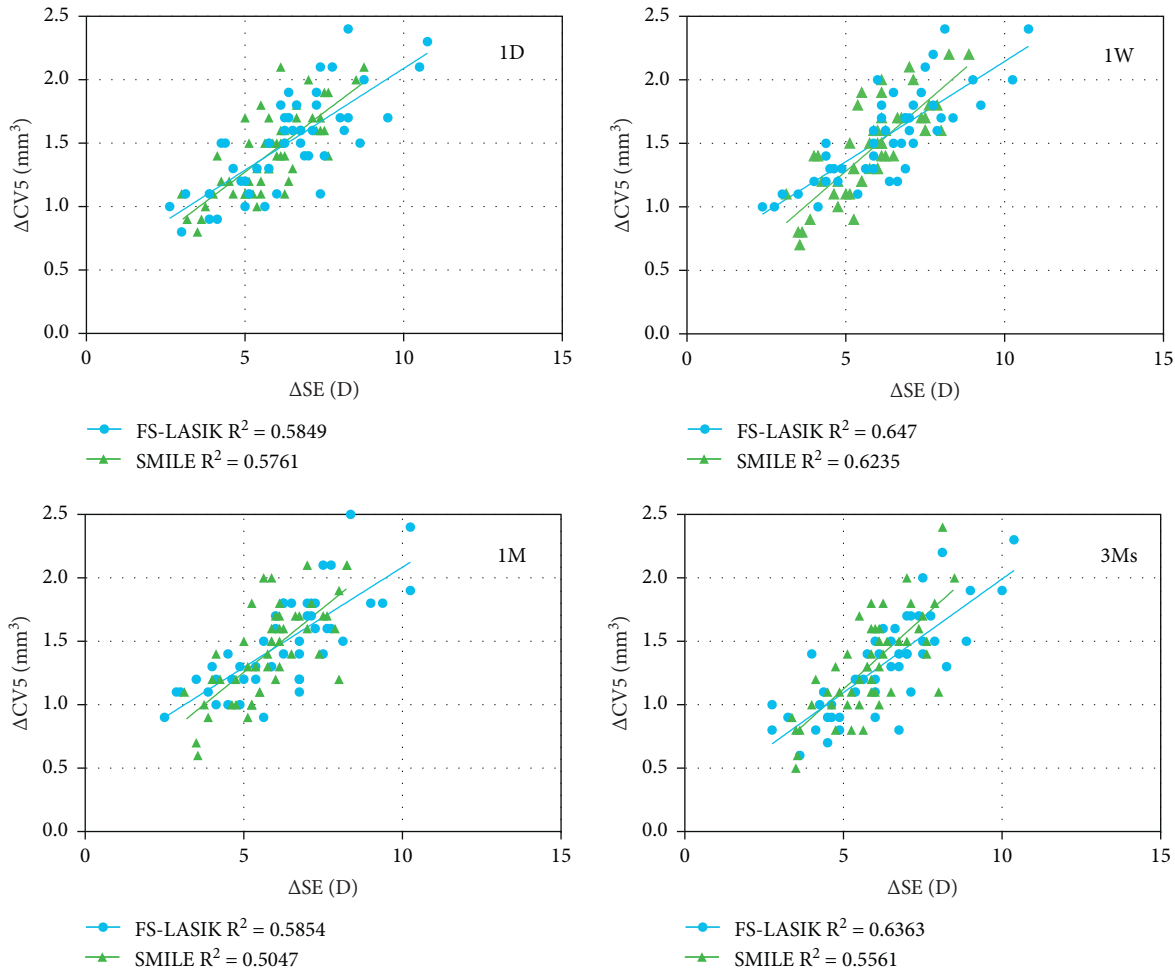


FIGURE 2: The correlation between the change in volume of the central 5 mm diameter area ($\Delta CV5$) and the change in the spherical equivalence refraction (ΔSE) at different time points.

months. In the FS-LASIK group, only $\Delta CV5$ and ΔCRF had a statistically significant correlation ($r = 0.363$, $P = 0.012$).

3.6. Correlation between the Change in Corneal Biomechanical Parameters and Change in Spherical Equivalent. As shown in Table 3, a statistically significant correlation was found between ΔSE with ΔCRF at 3 months postoperatively.

4. Discussion

Corneal volume is an important quantitative parameter for monitoring the change in the corneal tissue characteristics after surgery [11]. Precise knowledge about the actual amount of tissue ablated during surgery may help understand the predictability of the surgery. Argento et al. [12] and Pallikaris et al. [13] reported that the amount of tissue removed during surgery which is the same as the reduction in the CV could be a predicting factor for the development of corneal ectasia. CV has been used together with other parameters to improve the sensitivity and specificity for diagnosis of keratoconus [4–7]. Gatinel et al. [14] used a geometrical model to estimate the change in CV after corneal refractive surgery and found a relationship between

the change in CV with the size of optical zone and the magnitude of refractive error to be corrected. The Pentacam uses a rotating Scheimpflug camera to reconstruct the 3D image of the anterior segment and can be used to obtain corneal thickness and CV data with good repeatability and consistency [4]. The corneal thickness measurement of the Pentacam is comparable to ultrasound pachymetry [15], with good accuracy [16, 17] and high repeatability [18]. To the best of our knowledge, there are no studies that utilized Pentacam to compare the changes in CV after SMILE and FS-LASIK. CV might be more sensitive to reflect corneal profile changes than corneal thickness, since inflammatory response and corneal wound healing response after surgery would not be localized.

Our study found that for both procedures, CV changes with time. The CV5 and CV5-10 decreased in postoperative day 1 and continued to decrease at week 1, followed by a gradual increase at month 1 and month 3. From day 1 to week 1, the CV decreased in the peripheral region but not in centrally after SMILE, while following FS-LASIK, it decreased centrally not peripherally. The negative pressure suction, irrigation, and manipulation on the corneal stroma may all lead to corneal edema on postoperative day 1. Studies

TABLE 3: Correlation between the reduction of corneal volume and spherical equivalent with the change in corneal hysteresis and corneal resistance factor at 3 months.

Parameters	SMILE		FS-LASIK	
	r	P value	r	P value
$\Delta CV5$ VS ΔCRF	0.498*	<0.001	0.363*	0.012
$\Delta CV5-10$ VS ΔCRF	0.270	0.058	0.125	0.403
$\Delta CV5$ VS ΔCH	0.374*	0.007	0.264	0.073
$\Delta CV5-10$ VS ΔCH	0.116	0.420	0.098	0.512
$\Delta CV5$ VS ΔSE	-0.746*	<0.001	-0.798*	<0.001
$\Delta CV5-10$ VS ΔSE	-0.353*	0.012	-0.440*	0.002
ΔSE VS ΔCRF	-0.559*	<0.001	-0.598*	<0.001
ΔSE VS ΔCH	-0.506*	<0.001	-0.472*	0.001

CRF: corneal resistance factor, CH: corneal hysteresis, CV5: corneal volume of the central 5 mm diameter area, CV5-10: corneal volume of the peripheral 5–10 mm diameter area, SE: spherical equivalent, Δ : the reduction at postoperative month 3, * $P < 0.05$ (Pearson correlation).

have reported that the central corneal haze early after SMILE could be due to edema in the corneal stromal interface [19]. Since the flap in FS-LASIK is no longer in tension, it was more difficult to recover due to changes in the swelling pressure associated with loss of tension. In SMILE, the cap can maintain some tension after surgery and would thus be able to recover more quickly [20]. The edema usually subsides in 1 week, which explains the slight reduction in corneal volume. Afterwards, the healing response and inflammatory response in the cornea will lead to proliferation of corneal stromal collagen fibers, and this could account for the increase in CV at month 1.

The increase in CV at postoperative month 3 compared with day 1 was larger in the FS-LASIK group compared with the SMILE group. SMILE had an increase in CV centrally, while FS-LASIK showed the increase both centrally and peripherally. Both the changes of epithelial and stroma thickness may contribute to the increment of CV. Previous studies [21, 22] have shown that the epithelial thickness (ET) at postoperative day 1 and month 3 in SMILE was $53.6 \pm 3.3 \mu\text{m}$ and $58.0 \pm 3.7 \mu\text{m}$, respectively; while in the FS-LASIK group, the corresponding value was $52.43 \pm 3.1 \mu\text{m}$ and $56.42 \pm 5.6 \mu\text{m}$, respectively. The increase in ET from postoperative day 1 to month 3 in the SMILE group and FS-LASIK group was about $4.4 \mu\text{m}$ and $4 \mu\text{m}$, respectively. Such little variations seem unable to contribute to the significant differences of CV between two groups. We speculated that this difference might be related to the different corneal wound healing responses in both surgeries. A previous animal eye study has shown that when compared with LASIK, the refractive lenticule extraction (ReLEx) procedure may result in less inflammation and early extracellular matrix deposition [23]. Another study that compared early corneal wound healing and inflammatory responses between FS-LASIK and SMILE has shown that, in SMILE, there were significantly fewer Ki67-positive cells and CD11b-positive cells [24]. They also reported that SMILE induced less keratocyte apoptosis than LASIK.

We analyzed the changes in CV at different time points and their relation with SE. In SMILE, there was less change in the SE and no statistical differences existed between the SE

at each time points. In the FS-LASIK group, there was mild overcorrection at postoperative day 1. At subsequent visits, the SE showed myopic shift, and this was demonstrated by a coincidence with an increase in the corneal volume. In other words, the increase in CV at postoperative month 3 is correlated with the corresponding myopic shift. The early overcorrection and subsequent myopic shift in FS-LASIK could also be related to the postoperative changes in the corneal biomechanical properties. Our study found a close relationship between the change in CV and the biomechanical properties, and this change in the corneal structure and shape will eventually lead to change in the refraction [25]. The cornea is a heterogeneous viscoelastic biological material. Under normal circumstances, the interlamellar cohesive force, the lamellar tension, and the intraocular pressure balance out the corneal swelling pressure and maintain the biomechanical stability (Figure 3(a)). A reduction in corneal biomechanical properties has been shown after SMILE and FS-LASIK [26], but this effect was less in SMILE than in LASIK [2, 26]. We also demonstrated less change in CH and CRF for a similar change in SE in SMILE compared to FS-LASIK in the current study. We hypothesize that, in SMILE, only the collagen fibers at the side-cut region around the lenticule were cut, whereas the collagen fibers in the anterior stroma remained intact. The interlamellar cohesive force and lamellar tension in the corneal stromal interface were reduced after lenticule extraction, which decrease local resistance to corneal swelling in the interface and result in stromal thickening between the anterior cap and the residual stroma. This led to a slightly less central flattening compared to what is predicted (Figures 3(b) and 3(c)). As for FS-LASIK, the collagen fibers in the anterior stroma were cut and lamellar layers within the flap can no longer bear tension which would cause a greater change in the corneal biomechanical properties [19]. Cutting the central portion of the cornea released the lamellar tension in the peripheral corneal stroma, leading to an increase in the peripheral corneal thickness and increased the cohesive pulling force from the periphery to the central stromal region. This likely led to excess central flattening biomechanically than expected and, therefore, overcorrection early after FS-LASIK. This was also shown in our study that only central region significantly increased from postoperative day 1 to month 3 after SMILE, while both central and peripheral regions increased following FS-LASIK. Avunduk et al. [27] reported that after refractive surgery, the healing response at the keratocyte activation zone, the rearrangements of collagen fibers during corneal remodeling, and the corneal biomechanical changes may all cause changes in refraction as well as the anterior and posterior corneal curvature.

We reported that at postoperative month 3, the reduction in corneal volume at different regions in SMILE correlated with the ΔCRF and ΔCH , whereas in FS-LASIK, only the $\Delta CV5$ correlated with the ΔCRF , and no correlation was found between the corneal volume change in other regions and the reduction in corneal biomechanical properties. This is mainly due to the reduction in the amount of corneal collagen fibers and reduction of extracellular matrix components consequent to the reduction in corneal

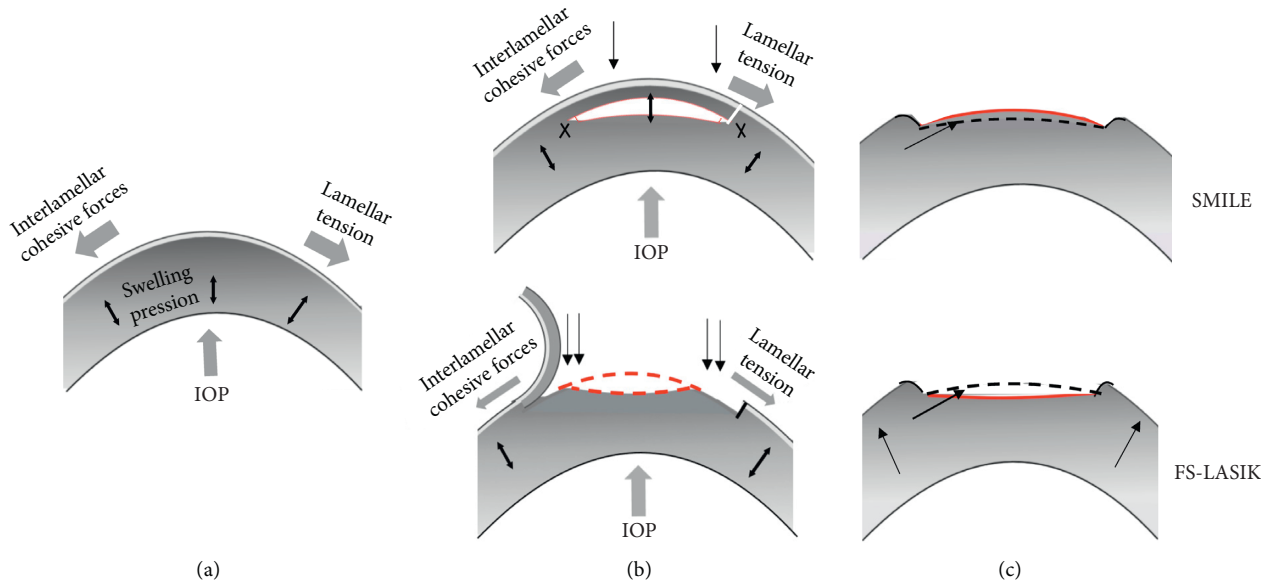


FIGURE 3: Schematic diagrams showing the effect of corneal biomechanical properties on the postoperative spherical equivalent refraction. (a) Before operation, there was a balance between the corneal swelling pressure with the interlamellar cohesive force and the lamellar tension; (b) intraoperatively, only side cuts around the lenticule were made in SMILE; in FS-LASIK, the central anterior stroma was cut, and x indicates where the collagen was cut; and (c) The black line included the simulated corneal curvature postoperatively, and the red line included the actual corneal curvature.

volume. Also, from Figure 2, we could see that SMILE had less change in biomechanical properties per unit of reduction in CV when compared with FS-LASIK. Apart from this, in both SMILE and FS-LASIK, the reduction in corneal volume had a stronger correlation with Δ CRF than with Δ CH. Chen et al. reported that after LASIK, the ablation depth correlated with the CRF parameter but not with the CH parameter, and pointed that CRF may be more useful than CH in assessing the biomechanical changes after LASIK [28].

In conclusion, there were dynamic changes in the corneal volume after SMILE and FS-LASIK during the early postoperative period. From day 1 to week 1, the CV decreased in the peripheral region but not centrally after SMILE, while following FS-LASIK, it decreased centrally not peripherally. The SMILE group had an increase in CV centrally from postoperative day 1 to month 3, while the FS-LASIK group showed the increase both centrally and peripherally. SMILE was associated with less change in biomechanical properties per unit of reduction in CV when compared with FS-LASIK. These postoperative corneal volume and biomechanics changes could be associated with the changes in the spherical equivalent. Further studies are warranted in future to confirm our findings.

Data Availability

The data that support the findings of this study are available from the corresponding author upon reasonable request.

Conflicts of Interest

The authors declare that they have no conflicts of interest.

Acknowledgments

This study has been supported by the National Natural Science Foundation of China (nos. 81670884 and 81873684).

References

- [1] D. Viswanathan, N. L. Kumar, J. J. Males, and S. L. Graham, "Relationship of structural characteristics to biomechanical profile in normal, keratoconic, and crosslinked eyes," *Cornea*, vol. 34, no. 7, pp. 791–796, 2015.
- [2] D. Z. Reinstein, T. J. Archer, and M. Gobbe, "Lenticule thickness readout for small incision lenticule extraction compared to artemis three-dimensional very high-frequency digital ultrasound stromal measurements," *Journal of Refractive Surgery*, vol. 30, no. 5, pp. 304–309, 2014.
- [3] T. H. Kim, D. Lee, and H. I. Lee, "The safety of 250 μ m residual stromal bed in preventing keratectasia after laser in situ keratomileusis (LASIK)," *Journal of Korean Medical Science*, vol. 22, no. 1, pp. 142–145, 2007.
- [4] A. Cerviño, J. M. Gonzalez-Mejome, T. Ferrer-Blasco, C. Garcia-Resua, R. Montes-Mico, and M. Parafita, "Determination of corneal volume from anterior topography and topographic pachymetry: application to healthy and keratoconic eyes," *Ophthalmic and Physiological Optics*, vol. 29, no. 6, pp. 652–660, 2009.
- [5] R. Ambrósio Jr., R. S. Alonso, A. Luz, and L. G. Coca Velarde, "Corneal-thickness spatial profile and corneal-volume distribution: tomographic indices to detect keratoconus," *Journal of Cataract & Refractive Surgery*, vol. 32, no. 11, pp. 1851–1859, 2006.
- [6] S. Emre, S. Doganay, and S. Yologlu, "Evaluation of anterior segment parameters in keratoconic eyes measured with the Pentacam system," *Journal of Cataract & Refractive Surgery*, vol. 33, no. 10, pp. 1708–1712, 2007.

- [7] L. S. Mannion, C. Tromans, and C. O'Donnell, "Reduction in corneal volume with severity of keratoconus," *Current Eye Research*, vol. 36, no. 6, pp. 522–527, 2011.
- [8] M. R. Sedaghat, M. Sharepoor, S. Hassanzadeh, and M. Abrishami, "The corneal volume and biomechanical corneal factors: is there any orrelation?" *Journal of Research in Medical Sciences*, vol. 17, no. 1, pp. 32–39, 2012.
- [9] H. S. Hwang, S. K. Park, and M. S. Kim, "The biomechanical properties of the cornea and anterior segment parameters," *BMC Ophthalmology*, vol. 13, p. 49, 2013.
- [10] C. M. Diniz, R. M. Hazarbassanov, E. Yamazaki, C. Murata, F. Mallmann, and M. Campos, "Pentacam Scheimpflug evaluation of corneal volume after LASIK," *Journal of Refractive Surgery (Thorofare, N.J.: 1995)*, vol. 26, no. 26, pp. 600–604, 2010.
- [11] H. Suzuki, H. Takahashi, J. Hori, M. Hiraoka, T. Igarashi, and T. Shiwa, "Phacoemulsification associated corneal damage evaluated by corneal volume," *American Journal of Ophthalmology*, vol. 142, no. 3, pp. 525–528, 2006.
- [12] C. Argento, M. J. Cosentino, A. Tytiun, G. Rapetti, and J. Zarate, "Corneal ectasia after laser in situ keratomileusis," *Journal of Cataract & Refractive Surgery*, vol. 27, no. 9, pp. 1440–1448, 2001.
- [13] I. G. Pallikaris, G. D. Kymionis, and N. I. Astyrakakis, "Corneal ectasia induced by laser in situ keratomileusis," *Journal of Cataract & Refractive Surgery*, vol. 27, no. 11, pp. 1796–1802, 2001.
- [14] D. Gatinel, T. Hoang-Xuan, and D. T. Azar, "Volume estimation of excimer laser tissue ablation for correction of spherical myopia and hyperopia," *Investigative Ophthalmology & Visual Science*, vol. 43, no. 43, pp. 1445–1449, 2002.
- [15] W. Wu, Y. Wang, and L. Xu, "Meta-analysis of Pentacam vs. ultrasound pachymetry in central corneal thickness measurement in normal, post-LASIK or PRK, and keratoconic or keratoconus-suspect eyes," *Graefe's Archive for Clinical and Experimental Ophthalmology*, vol. 252, no. 1, pp. 91–99, 2014.
- [16] R. Jain, G. Dilraj, and S. P. Grewal, "Repeatability of corneal parameters with Pentacam after laser in situ keratomileusis," *Indian Journal of Ophthalmology*, vol. 55, no. 5, pp. 341–347, 2007.
- [17] C. O'Donnell and C. Maldonado-Codina, "Agreement and repeatability of central thickness measurement in normal corneas using ultrasound pachymetry and the OCULUS Pentacam," *Cornea*, vol. 24, no. 8, pp. 920–924, 2005.
- [18] Y. Barkana, Y. Gerber, U. Elbaz et al., "Central corneal thickness measurement with the Pentacam Scheimpflug system, optical low-coherence reflectometry pachymeter, and ultrasound pachymetry," *Journal of Cataract & Refractive Surgery*, vol. 31, no. 9, pp. 1729–1735, 2005.
- [19] W. J. Dupps Jr. and S. E. Wilson, "Biomechanics and wound healing in the cornea," *Experimental Eye Research*, vol. 83, no. 4, pp. 709–720, 2006.
- [20] A. K. Riau, R. I. Angunawela, S. S. Chaurasia, W. S. Lee, D. T. Tan, and J. S. Mehta, "Early corneal wound healing and inflammatory responses after refractive lenticule extraction (ReLEx)," *Investigative Ophthalmology & Visual Science*, vol. 52, no. 9, pp. 6213–6221, 2011.
- [21] N. Luft, M. H. Ring, M. Dirisamer et al., "Corneal epithelial remodeling induced by small incision lenticule extraction (SMILE)," *Investigative Ophthalmology & Visual Science*, vol. 57, no. 9, pp. OCT176–183, 2016.
- [22] K. M. Rocha and R. R. Krueger, "Spectral-domain optical coherence tomography epithelial and flap thickness mapping in femtosecond laser-assisted in situ keratomileusis," *American Journal of Ophthalmology*, vol. 158, no. 2, pp. 293–301, 2014.
- [23] A. Heisterkamp, T. Mamom, O. Kermani et al., "Intrastromal refractive surgery with ultrashort laser pulses: in vivo study on the rabbit eye," *Graefe's Archive for Clinical and Experimental Ophthalmology*, vol. 241, no. 6, pp. 511–517, 2003.
- [24] Z. Dong, X. Zhou, J. Wu et al., "Small incision lenticule extraction (SMILE) and femtosecond laser LASIK: comparison of corneal wound healing and inflammation," *British Journal of Ophthalmology*, vol. 98, no. 2, pp. 263–269, 2014.
- [25] H. Dierick, "The cornea is not a piece of plastic," *Journal of Refractive Surgery*, vol. 17, no. 1, p. 76, 2001.
- [26] D. Wu, Y. Wang, L. Zhang, S. Wei, and X. Tang, "Corneal biomechanical effects: small-incision lenticule extraction versus femtosecond laser-assisted laser in situ keratomileusis," *Journal of Cataract & Refractive Surgery*, vol. 40, no. 6, pp. 954–962, 2014.
- [27] A. M. Avunduk, C. J. Senft, S. Emerah, E. D. Varnell, and H. E. Kaufman, "Corneal healing after uncomplicated LASIK and its relationship to refractive changes: a six-month prospective confocal study," *Investigative Ophthalmology & Visual Science*, vol. 45, no. 5, pp. 1334–1339, 2004.
- [28] M. C. Chen, N. Lee, N. Bourla, and R. D. Hamilton, "Corneal biomechanical measurements before and after laser in situ keratomileusis," *Journal of Cataract & Refractive Surgery*, vol. 34, no. 11, pp. 1886–1891, 2008.